MULTIDISCIPLINARY CENTER FOR EARTHQUAKE ENGINEERING RESEARCH
A National Center of Excellence in Advanced Technology Applications

ISSN 1520-295X

PB99-163693

Truss Modeling of Reinforced Concrete Shear-Flexure Behavior

by

Jang Hoon Kim and John B. Mander
University at Buffalo, State University of New York
Department of Civil, Structural and Environmental Engineering
Ketter Hall
Buffalo, New York 14260-4300

Technical Report MCEER-99-0005

March 8, 1999

This research was conducted at the University at Buffalo, State University of New York and was supported by the Federal Highway Administration under contract number DTFH61-92-C-00106.

NOTICE

This report was prepared by the University at Buffalo, State University of New York as a result of research sponsored by the Multidisciplinary Center for Earthquake Engineering Research (MCEER) through a contract from the Federal Highway Administration. Neither MCEER, associates of MCEER, its sponsors, University at Buffalo, State University of New York, nor any person acting on their behalf:

a. makes any warranty, express or implied, with respect to the use of any information, apparatus, method, or process disclosed in this report or that such use may not infringe upon privately owned rights; or

b. assumes any liabilities of whatsoever kind with respect to the use of, or the damage resulting from the use of, any information, apparatus, method, or process disclosed in this report.

Any opinions, findings, and conclusions or recommendations expressed in this publication are those of the author(s) and do not necessarily reflect the views of MCEER or the Federal Highway Administration.

50272 – 101

REPORT DOCUMENTATION PAGE	1. Report No. MCEER-99-0005	2.	3. Recipient's Accession No.

4. Title and Subtitle
Truss Modeling of Reinforced Concrete Shear-Flexure Behavior

5. Report Date
March 8, 1999

6.

7. Authors
Jang Hoon Kim and John B. Mander

8. Performing Organization Report No.

10. Project/Task/Work Unit No.
106-F-2.1

9.Performing Organization Name and Address
Department of Civil, Structural and Environmental Engineering
State University of New York at Buffalo
Ketter Hall
Buffalo, New York 14260

11. Contract(C)or Grant (G) No.
(C) DTFH61-92-C-00106

(G)

12. Sponsoring Organization Name and Address
Multidisciplinary Center for Earthquake Engineering Research
State University of New York at Buffalo
Red Jacket Quadrangle, Buffalo, NY 14261

13. Type of Report & Period Covered
Technical report

14.

15. Supplementary Notes
This research was conducted at the University at Buffalo, State University of New York and was supported by the Federal Highway Administration under contract number DTFH61-92-C-00106

16. Abstract (limit 200 words)
This reports details the development of retrofit procedures, verified by experimental testing, for reinforced concrete bridge columns and their connections. The report describes the development of a comprehensive theory for analyzing the inelastic shear force versus shear deformation behavior of columns. To achieve this, two concrete shear truss mechanisms (constant angle truss and variable angle truss) were investigated and as a result, new truss models based on numerical integration schemes were suggested and analyzed. These models will enable structural engineers to quantitatively as well as qualitatively understand the flow of forces at any instance of column deformation. They are suitable for had (design office) analysis. However, more sophisticated truss models can easily be incorporated with comprehensive computational model-based techniques (such as DRAIN-2DX).

17. Document Analysis a. Descriptors
Earthquake engineering. Reinforced concrete. Bridge columns. Beam columns. Theoretical crack angle. Modeling. Column shear analysis. Column shear strength. Stiffness analysis. Strength analysis. Truss models. Steel yielding. Concrete tensile strength. Axial load effect.

b. Identifiers/Open-Ended Terms

c. COSATI Field/Group

18. Availability Statement	19. Security Class (This Report)	21. No. of Pages
Release unlimited.	Unclassified	224
	20. Security Class (This Page)	22. Price
	Unclassified	

(see ANSI_Z39.18)

MULTIDISCIPLINARY CENTER FOR EARTHQUAKE ENGINEERING RESEARCH
A National Center of Excellence in Advanced Technology Applications

Truss Modeling of Reinforced Concrete Shear-flexure Behavior

by

Jang Hoon Kim[1] and John B. Mander[2]

Publication Date: March 8, 1999
Submittal Date: July 9, 1997

Technical Report MCEER-99-0005

Task Number 106-F-2.1

FHWA Contract Number DTFH61-92-C-00106

1 Assistant Professor, Department of Architecture, Ajou University, South Korea; former Post Doctoral Research Associate, Department of Civil, Structural and Environmental Engineering, University at Buffalo, State University of New York
2 Associate Professor, Department of Civil, Structural and Environmental Engineering, University at Buffalo, State University of New York

MULTIDISCIPLINARY CENTER FOR EARTHQUAKE ENGINEERING RESEARCH
University at Buffalo, State University of New York
Red Jacket Quadrangle, Buffalo, NY 14261

Preface

The Multidisciplinary Center for Earthquake Engineering Research (MCEER) is a national center of excellence in advanced technology applications that is dedicated to the reduction of earthquake losses nationwide. Headquartered at the University at Buffalo, State University of New York, the Center was originally established by the National Science Foundation in 1986, as the National Center for Earthquake Engineering Research (NCEER).

Comprising a consortium of researchers from numerous disciplines and institutions throughout the United States, the Center's mission is to reduce earthquake losses through research and the application of advanced technologies that improve engineering, pre-earthquake planning and post-earthquake recovery strategies. Toward this end, the Center coordinates a nationwide program of multidisciplinary team research, education and outreach activities.

MCEER's research is conducted under the sponsorship of two major federal agencies, the National Science Foundation (NSF) and the Federal Highway Administration (FHWA), and the State of New York. Significant support is also derived from the Federal Emergency Management Agency (FEMA), other state governments, academic institutions, foreign governments and private industry.

The Center's FHWA-sponsored Highway Project develops retrofit and evaluation methodologies for existing bridges and other highway structures (including tunnels, retaining structures, slopes, culverts, and pavements), and improved seismic design criteria and procedures for bridges and other highway structures. Specifically, tasks are being conducted to:

- assess the vulnerability of highway systems, structures and components;
- develop concepts for retrofitting vulnerable highway structures and components;
- develop improved design and analysis methodologies for bridges, tunnels, and retaining structures, which include consideration of soil-structure interaction mechanisms and their influence on structural response;
- review and recommend improved seismic design and performance criteria for new highway systems and structures.

Highway Project research focuses on two distinct areas: the development of improved design criteria and philosophies for new or future highway construction, and the development of improved analysis and retrofitting methodologies for existing highway systems and structures. The research discussed in this report is a result of work conducted under the existing highway structures project, and was performed within Task 106-F-2.1 "Seismic Retrofit of Shear-critical Bridge Columns" of that project as shown in the flowchart on the following page.

The overall objective of this task was to develop retrofit procedures, verified by experimental testing, for reinforced concrete bridge columns and their connections. This report describes the development of a comprehensive theory for analyzing the inelastic shear force versus shear deformation behavior of columns. To achieve this, two concrete shear truss mechanisms (constant angle truss and variable angle truss) are investigated and as a result, new truss models based on

numerical integration schemes are suggested and analyzed. These models will enable structural engineers to quantitatively as well as qualitatively understand the flow of forces at any instance of column deformation. They are suitable for hand (design office) analysis. However, more sophisticated truss models can easily be incorporated with comprehensive computational modeling-based techniques (such as DRAIN-2DX).

SEISMIC VULNERABILITY OF EXISTING HIGHWAY CONSTRUCTION
FHWA Contract DTFH61-92-C-00106

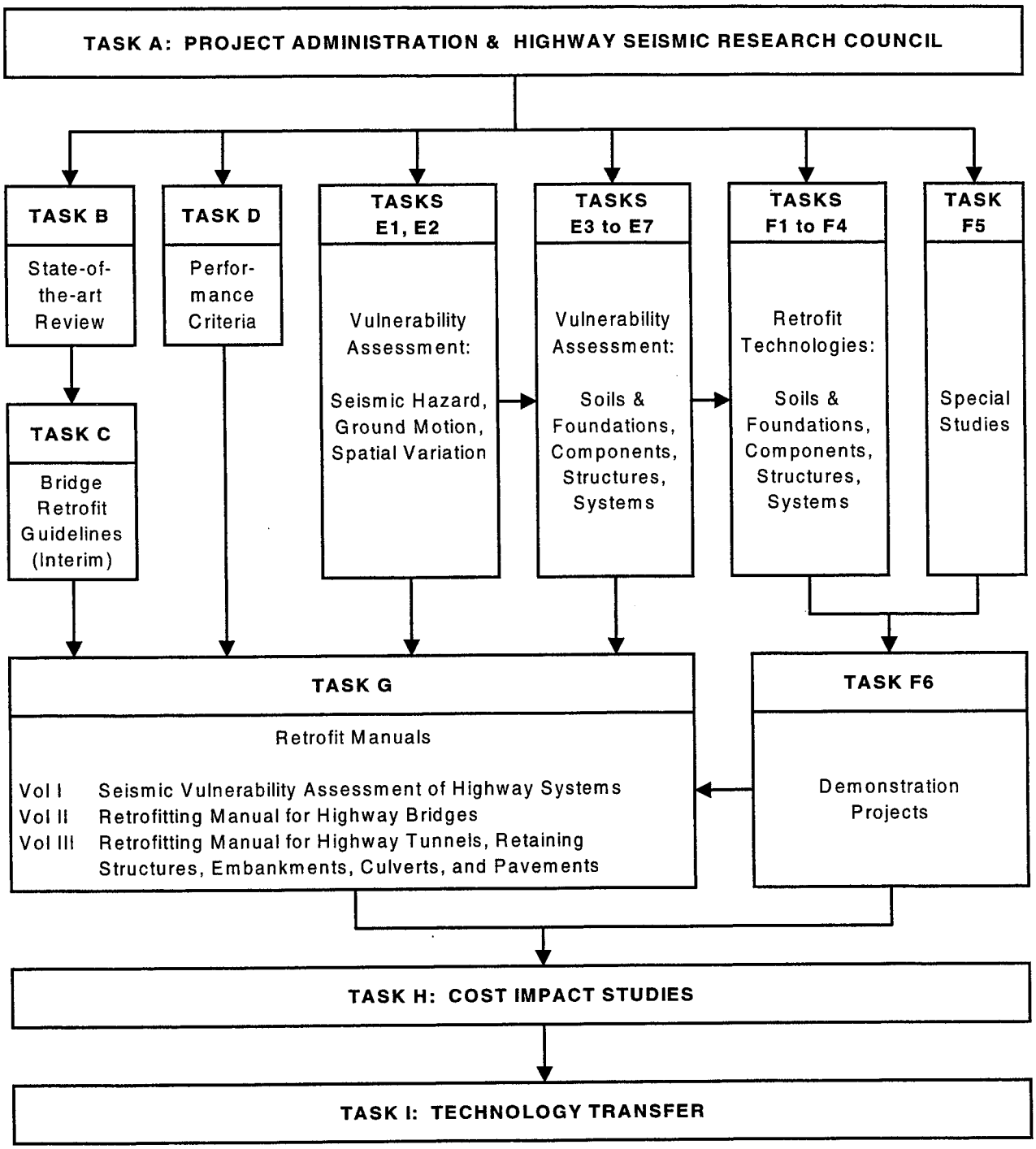

ABSTRACT

A reinforced concrete beam-column, assumed to possess a series of potential crack planes, is considered as a truss consisting of a finite number of differential truss elements and analyzed using the virtual work method to define the lateral force-deformation relationship. The differential truss is simplified using various numerical integration schemes, since the analytical integration involves the complexity. From such truss models the effects of the diagonal shear cracking can be reliably modeled and valuable information such as crack angles and the cracked elastic stiffness in both shear and flexure can be determined. An equation to estimate the theoretical crack angle is derived by considering the energy minimization on the virtual work done by shear and flexural components. Theoretical crack angles compare favorably with experimentally observed crack angles reported by previous researchers.

It is postulated that the total shear strength can be found by combining three complementary mechanisms that arise from: truss action that incorporates the transverse hoop steel; truss action that incorporates the concrete tensile strength normal to the principal diagonal crack plane; and arch action that incorporates the axial load transferring mechanism. Displacement compatibility requirements are applied when combining the three mechanisms to give the overall shear force-deformation behavior. The theory is also implemented computationally using cyclic non-linear truss elements. However, the present version of modeling technique cannot properly account for the cyclic loading effect due to the earthquake duration effect. If improved constitutive models were used to more faithfully represent concrete and steel behavior (under cyclic loading), then the overall predictions should also markedly improve.

ACKNOWLEDGEMENTS

This research was conducted under Task F-2.1 "Seismic Retrofit of Shear-Critical Bridge Columns" as part of the NCEER Highway Project. The NCEER Highway Project is funded through a contract with the Federal Highway Administration (FHWA) contract DTFH61-92-C-00106. The financial support of FHWA via NCEER is gratefully acknowledged. Much of the work presented herein formed part of the Ph.D. dissertation of the first author under the supervision of the second author.

TABLE OF CONTENTS

TABLE OF CONTENTS (cont'd)

TABLE OF CONTENTS (cont'd)

LIST OF ILLUSTRATIONS

LIST OF ILLUSTRATIONS (cont'd)

LIST OF TABLES

SECTION 1
INTRODUCTION

1.1 Overview

It is now almost a century since Ritter *(1899)* and Mörsch *(1908)* first introduced the truss concept to explain the flow of forces in a cracked reinforced concrete member. Dilger *(1966)* performed an extensive study and formulated the cracked elastic shear stiffness using a constant angle continuum truss model. Paulay *(1971a,b)* performed an extensive experimental and theoretical study on the behavior of thin webbed coupling beams. Paulay *(1971a)* was the first to utilize a variable angle truss model in defining the contribution of the truss action. Park and Paulay *(1975)* also derived the cracked elastic stiffness due to shear using the constant angle truss model and the stiffness is identical to the one derived by Dilger *(1966)*. Schlaich, et al. *(1987)* defined B- and D-regions in a structural member, in which B-region represents the beam region where Bernoulli's beam theory holds and D-region represents the disturbed region where beam theory does not hold. Vecchio and Collins *(1986)* introduced the utilization of concrete tensile strength in column shear resistance, this is referred to as the Modified Compression Field Theory (MCFT) for structural concrete. MacGregor *(1992)* extensively studied for the solution of deep beams using Strut-and-Tie models. In parallel to Collins and Mitchell *(1991)*, Hsu *(1993, 1996)* and Pang and Hsu *(1996)* developed a "softened truss theory" also based on axioms of equilibrium and compatibility.

The shear analysis of reinforced concrete beam-columns has been a contentious issue to researchers as well as structural engineers for decades. This is because there has been a general lack of comprehensive analysis tools that permit cyclic inelastic shear analysis similar to column flexural analysis *(Schlaich, et al., 1987; Collins and Mitchell, 1991; Hsu, 1993)*. As a result, analysis approaches that unify shear and flexural behavior have been difficult to achieve in a comprehensive way. Even though certain researchers have proposed some advanced analysis tools *(Collins and Mitchell, 1991; Chang and Mander, 1994; Priestley, et al., 1994a,b,c)* to overcome some of these modeling difficulties, they are still complicated in usage and limited in

applicability. This situation is the principal motivation in the present study which seeks to develop a comprehensive theory for modeling inelastic shear and flexural behavior so that a unified column analysis can be performed using hand-calculations as well as advanced computational modeling. Since flexural analysis using Bernoulli's beam theory is well established for reinforced concrete members, the focus of the present study is to advance shear analysis methods that can be amalgamated with flexure.

1.2 Background of Column Shear Analysis

In recent years there has been a resurgence in the use of truss models for the analysis of structural concrete members. Such models can be divided into two categories: (i) continuum truss models based on an extension of panel elements; and (ii) plastic truss models. The Modified Compression Field Theory (MCFT) *(Collins and Mitchell, 1991)* and the Softened Truss Model *(Hsu, 1993)* use the former and consider both equilibrium and compatibility at a critical section, while Strut-and-Tie (SAT) models use the latter and idealize an entire member as a truss but are only concerned with the equilibrium of the truss elements. Furthermore, the former is usually applied to thin webbed members such as prestressed concrete beams, whereas the latter is applied to disturbed regions in deep beams, brackets, and corbels, etc. The MCFT theory includes the concrete (tensile) component of shear resistance, but SAT models do not. The recent AASHTO LRFD code *(1994)* has implemented these two types of truss models into its provisions for shear design; the MCFT is used for beams, and SAT models for disturbed regions.

In its most general form the ultimate shear resistance given by MCFT in the LRFD code is

$$V_u = V_s + V_c + V_p \tag{1-1}$$

where V_s = contribution of the transverse reinforcement, V_c = contribution of tensile stress in the concrete, and V_p = shear carried by the axial compression. These shear resisting components are given by

$$V_s = A_{sh} f_{yh} \frac{jd}{s} \cot\theta \tag{1-2}$$

$$V_c = \beta \sqrt{f_c'}\, b_w d \cot\theta \tag{1-3}$$

$$V_p = P \tan\alpha \tag{1-4}$$

in which A_{sh} = cross section area of transverse shear reinforcement at spacing s, f_{yh} = yield strength of transverse reinforcement, jd = internal flexural lever arm at the critical section, θ = crack angle measured to the longitudinal axis of the element, β = factor depending on the tensile capacity of the concrete, f_c' = compressive strength of concrete cylinder, d = effective depth of column section, P = applied axial load, $\tan\alpha = jd/L$ = aspect ratio of the column, and L = column clear height. This form of ultimate strength of resistance is consistent with the most recent recommendations for shear analysis of Priestley et al. *(1994a,b,c)*. However, they recommend that based on the crack angles observed in their tests that $\theta = 30°$.

Thus the present shear evaluation models may be characterized as being somewhat empirical in terms of strength and deformation. Furthermore, the present models are unable to trace shear deformations that relate to the current state of shear force in the members. There are, however, several truss models found in the literature that address shear stiffness. For example, Dilger *(1966)* and Park and Paulay *(1975)* present constant angle truss models for the assessment of shear stiffness. A variable angle truss model was adopted by Paulay *(1971a)* to assess the stiffness effects of squat (fixed-fixed) coupling beams.

1.3 Background of Force-Deformation Analysis

A concrete member may be considered as a structural element of combined mechanisms as shown in figure 1-1. Therefore, the total column rotation (drift) angle can be expressed in terms of two deformation components as:

$$\Theta = \Theta_s + \Theta_f \tag{1-5}$$

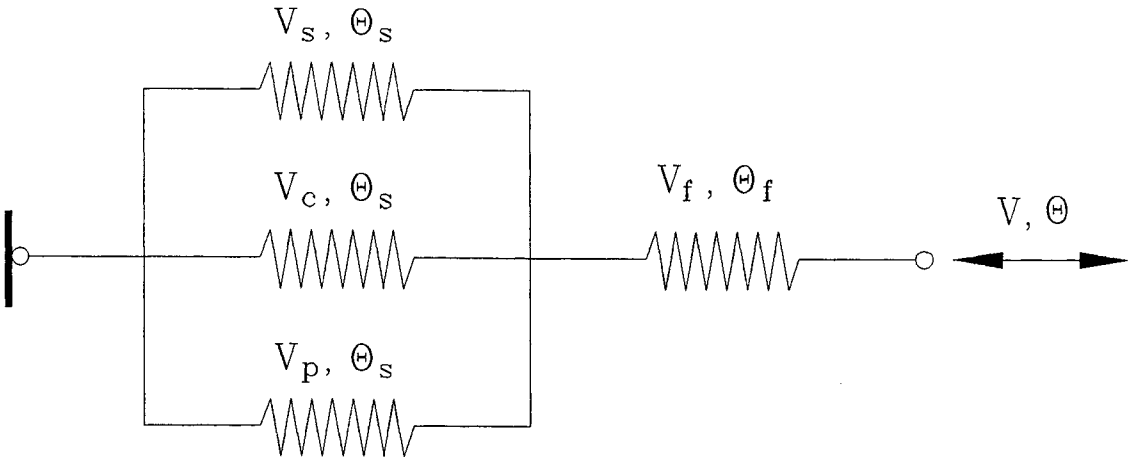

Figure 1-1. Spring analogy for combination of load transfer mechanisms.

where Θ, Θ_s and Θ_f are column total, shear and flexural rotation (drift) angles, respectively. Then, the resultant lateral resistance of the column should be the lesser of

$$V = V_u = V_s + V_c + V_p \tag{1-6a}$$

and

$$V = V_f = \frac{M_s + M_c}{L} \tag{1-6b}$$

where V_f= shear resisted by flexural mechanism, M_s= moment capacity due to longitudinal steel, and M_c= moment capacity due to eccentric concrete stress block. Using equations (1-5) and (1-6), the complete relationship of column force and deformation can be obtained. In order to maintain the deformation compatibility and equilibrium conditions between load transferring mechanisms, it is assumed that the column cross section is proportioned to the ratio of component strength to the total strength. Thus

$$A_{vs} = b_{ws}\, jd\,; \quad A_{vc} = b_{wc}\, jd\,; \quad A_{vp} = b_{wp}\, jd \tag{1-7}$$

where A_{vs}, A_{vc} and A_{vp} are respectively effective shear areas for V_s, V_c and V_p mechanisms and b_{ws}, b_{wc} and b_{wp} are respectively effective column width for V_s, V_c and V_p mechanisms which are estimated as

$$\frac{b_{ws}}{b_w} = \frac{V_s}{V_u}\ ; \quad \frac{b_{wc}}{b_w} = \frac{V_c}{V_u}\ ; \quad \frac{b_{wp}}{b_w} = \frac{V_p}{V_u} \tag{1-8}$$

It is noted that $b_w = b_{ws} + b_{wc} + b_{wp}$ as shown in figure 1-2 and $A_v = A_{vs} + A_{vc} + A_{vp} = b_w\, jd$ in which A_v is the total shear area of a concrete column.

1.4 Scope of This Report

In order to develop a comprehensive theory for analyzing the inelastic shear force - shear deformation behavior of columns, two truss mechanisms (constant angle truss and variable angle truss) are investigated in Section 2 and as a result, new truss models based on numerical integration schemes are suggested and analyzed. In Section 3, a piece-wise linear elastic analysis

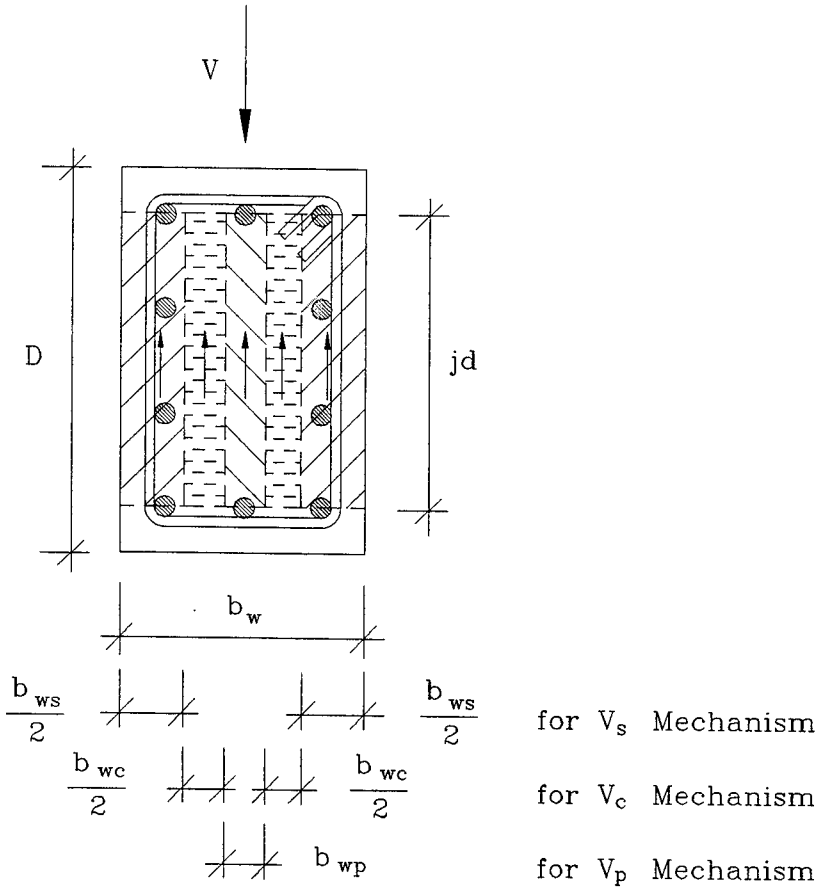

Figure 1-2. Proportioning of column section for load transfer mechanisms.

for shear and flexure is introduced using the analysis results of the proposed truss models. The analysis method is advanced by employing the material constitutive law for steel. The effect of concrete tensile strength on column shear strength is discussed in Section 4. The axial load effect on column lateral strength via arch action is discussed in Section 5. In Section 6, the load transfer mechanisms developed in the foregoing sections are combined together to produce some analysis procedures useful for engineering design practice. Also presented in the same section is the verification of the theory using the experimental results reported by previous investigators in the literature. Demonstration of the CIST (Cyclic Inelastic Strut-and-Tie) modeling technique is also made in this section. Finally, conclusions and suggestions for further research are presented in Section 7.

SECTION 2
STIFFNESS ANALYSIS OF CONCRETE COLUMNS

The purpose of this section is to investigate unifying attributes of strut-and-tie (SAT) models in order to solve combined shear force and deformation problems due to the truss mechanism (V_s) and flexural mechanism (V_f) for concrete columns. The effect of other shear components such as tensile stress in the concrete (V_c) and column axial compression (V_p) will be discussed later in the following sections.

2.1 Pre-Cracked Elastic Stiffness

The elastic stiffness for shear and flexure of a concrete column before the formation of cracks can be formulated using the principles of elasticity. The modulus of elasticity in shear is obtained from the well-known relationship

$$G = \frac{E_c}{2(1+\nu)} \tag{2-1}$$

where $E_c = 4700\sqrt{f_c'}\ (MPa)$ is the modulus of elasticity for normal weight concrete and ν = Poisson's ratio. If $\nu = 0.25$, then $G = 0.4E_c$, thus the shear rotational stiffness of an uncracked column section may be expressed by

$$K_s \approx 0.4\,E_c A_v \tag{2-2}$$

where A_v = area contributing shear stiffness.

The uncracked elastic flexural stiffness of a column for the applied shear force with respect to the drift angle may be determined using the well-known moment-area theorem, that is,

$$K_{f\theta} = \frac{12\,E\,I_g}{L^2} \qquad \textit{for fixed-fixed column} \tag{2-3a}$$

$$K_{f\theta} = \frac{3EI_g}{L^2} \qquad \textit{for fixed-pinned column} \tag{2-3b}$$

where I_g = moment of inertia of a column gross cross section and L = column clear height.

2.2 Post-Cracked Elastic Stiffness

After concrete cracking, the member stiffness drops dramatically as a new internal force transfer mechanism develops. The shear resistance is formed by a series of concrete struts, aggregate interlock and dowel action. Park and Paulay *(1975)* show that the latter contribute little in terms of strength and stiffness, and it is principally truss or arch action that provides the post-cracked strength and stiffness. Truss analogies will now be discussed in what follows.

2.2.1 Introduction to the Truss Analogy

It has long been recognized that the behavior of reinforced concrete beam-columns after the onset of cracking can be analyzed using an appropriate truss model *(Ritter, 1899; Mörsch, 1908; Dilger, 1966; Paulay, 1971a,b; Park and Paulay, 1975; Schlaich, et al., 1987; Collins and Mitchell, 1991; MacGregor, 1992; Hsu, 1993, 1996; and Pang and Hsu, 1996)*. In truss analogies, longitudinal reinforcement is represented by the longitudinal chords of a truss while transverse hoop steel is represented by the transverse tensile ties. The effect of concrete in flexural compression may be considered as a part of the longitudinal compression chord member. The longitudinal chords and the transverse tensile ties are internally stabilized by the diagonal struts which model the concrete compressive stress field. The inclination of the diagonal struts should coincide with the probable diagonal crack direction. For simplicity, the longitudinal chords, transverse tensile ties and diagonal struts are assumed to be joined together through rigid nodes.

Schlaich, et al. *(1987)* defined two standard regions in structural concrete elements. Behavior in these regions is either governed by beam action or is disturbed, and are respectively referred to as B- and D-regions. In the B-region the Bernoulli's hypothesis of *plane sections*

remaining plane is assumed valid while in the D-region the strain distribution of a section is disturbed and may be significantly non-linear. Near concentrated loads, corners, bends, openings and other discontinuities are included in the D-region. Figure 2-1 shows the concept of the structural B- and D-regions in reinforced concrete beam-columns in terms of crack patterns.

Based on these considerations two truss mechanisms are investigated in the present study: (i) constant angle truss; and (ii) variable angle truss. Constant angle truss models should be used for the undisturbed region (B-region) of a column which can be defined as "long". This generally means that the shear span of the column ($L = M/V$) should be longer than the length defined by crack angle, that is, $L > jd\cot\theta$. The analysis of shear deformation of a "short" column or the disturbed region (D-region) of the "long" column that has regions of disturbance that affect the entire length of the column can be achieved using a variable angle truss (when $\alpha > \theta$).

2.2.2 Constant Angle Truss

Figure 2-2 shows the shear transfer mechanism for undisturbed regions (B-regions) in a diagonally-cracked "long" beam/column member. From the overall member shown in figure 2-2(a) a "differential" portion of truss with prismatic members having finite depths can be extracted for analysis purposes as shown in figure 2-2(b). In this representation, it is assumed that the transverse steel is uniformly distributed over the length of the member. Consider this single differential truss subjected to the differential shear force dV_s. Member forces of the differential truss can easily be found by static equilibrium as shown in figure 2-2(c). The shear deformation of a differential truss due to the applied differential shear force can be calculated using the principles of Virtual Work method of analysis. Rigid longitudinal chords are assumed in this calculation in order to negate the effect of flexural deformation. The analysis using this method is presented in table 2-1. It should be noted that under constant shear the deformation of each differential truss is the same over the entire constant angle truss.

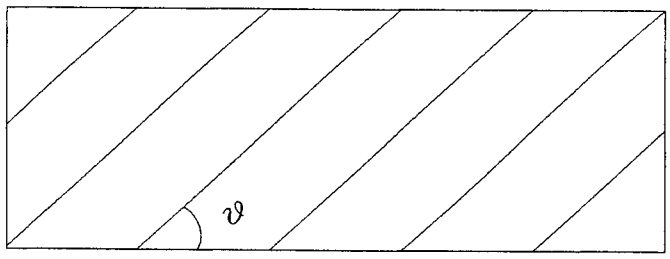

(a) B−type

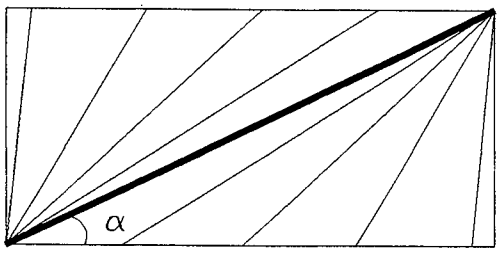

(b) D−type

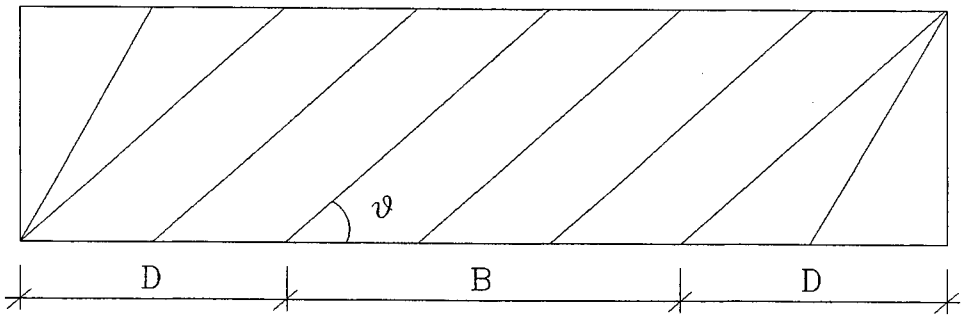

(c) Combined type

Figure 2-1. Postulated diagonal crack patterns in concrete columns.

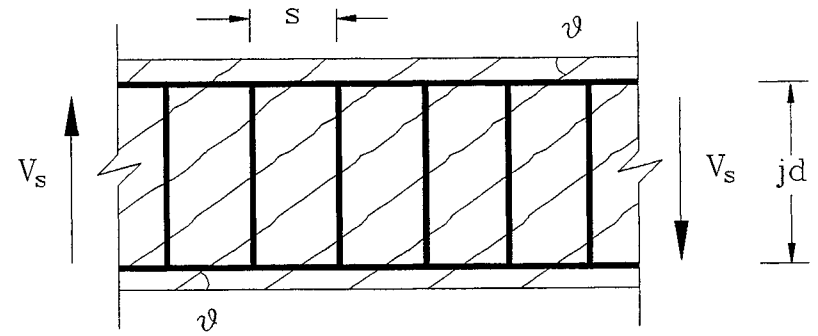

(a) Undisturbed region of a "long" cracked beam–column

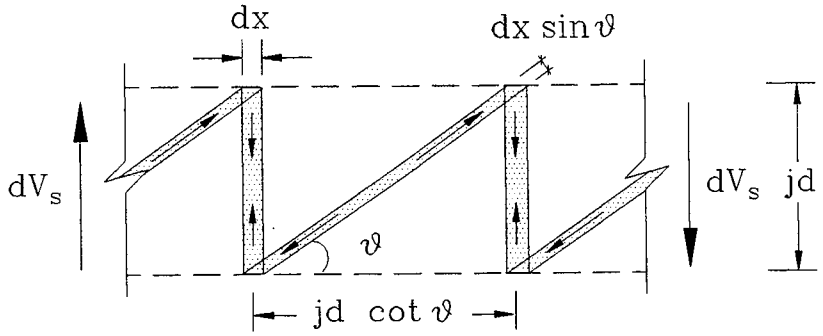

(b) A differential element of a constant angle truss

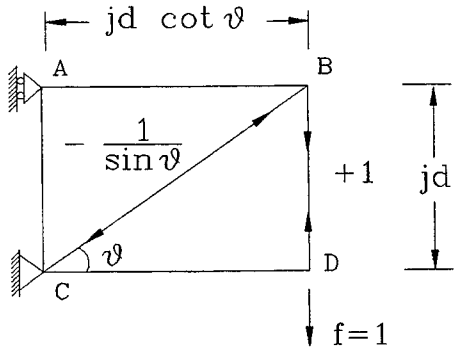

(c) Member forces for a unit load

Figure 2-2. Constant angle truss model.

Table 2-1. Virtual work done on a differential portion of a constant angle truss.

Member	Force F	Unit Load f	Length l	Rigidity EA	Strain $\varepsilon = F/EA$	Deformation $\frac{Ffl}{EA}$
B-D	$+dV_s$	$+1$	jd	$E_s A_{sh}\frac{dx}{s}$	$\frac{+\,s\,dV_s}{E_s A_{sh} dx}$	$\frac{jd\,s\,dV_s}{E_s A_{sh} dx}$
B-C	$-\frac{dV_s}{\sin\theta}$	$-\frac{1}{\sin\theta}$	$\frac{jd}{\sin\theta}$	$E_c b_{ws} \sin\theta\, dx$	$\frac{-\,dV_s}{E_c b_{ws} \sin^2\theta\, dx}$	$\frac{jd\,dV_s}{E_c b_{ws} \sin^4\theta\, dx}$

Note: Refer to figure 2-2.

The shear deformation of a differential truss is contributed by a transverse tie and a strut, thus,

$$\Delta_s = \sum \frac{Ffl}{EA} = \frac{jd\,dV_s}{E_c b_w dx}\left(\frac{s\,b_w}{\frac{E_s}{E_c}A_{sh}} + \frac{1}{\left(\frac{b_{ws}}{b_w}\right)\sin^4\theta}\right) \qquad \text{(2-4a)}$$

Rearranging,

$$\Delta_s = \frac{jd\,dV_s}{E_c b_w dx}\left(\frac{1}{\rho_v n} + \frac{1}{\left(\frac{b_{ws}}{b_w}\right)\sin^4\theta}\right) \qquad \text{(2-4b)}$$

where $jd =$ internal lever arm of the section, $A_{sh} =$ cross section area of transverse shear reinforcement at spacing s, $\rho_v =$ volumetric ratio of shear reinforcement content, $n = E_s/E_c$ which is the modular ratio and b_{ws}/b_w is given in equation (1-8). The internal lever arm may be idealized as the distance between the outermost layer of the longitudinal steel as shown in figure 2-3. The volumetric ratio of transverse steel content is given by

$$\rho_v = \frac{A_{sh}}{b_w s} \quad \textit{for a rectangular column} \qquad \text{(2-5a)}$$

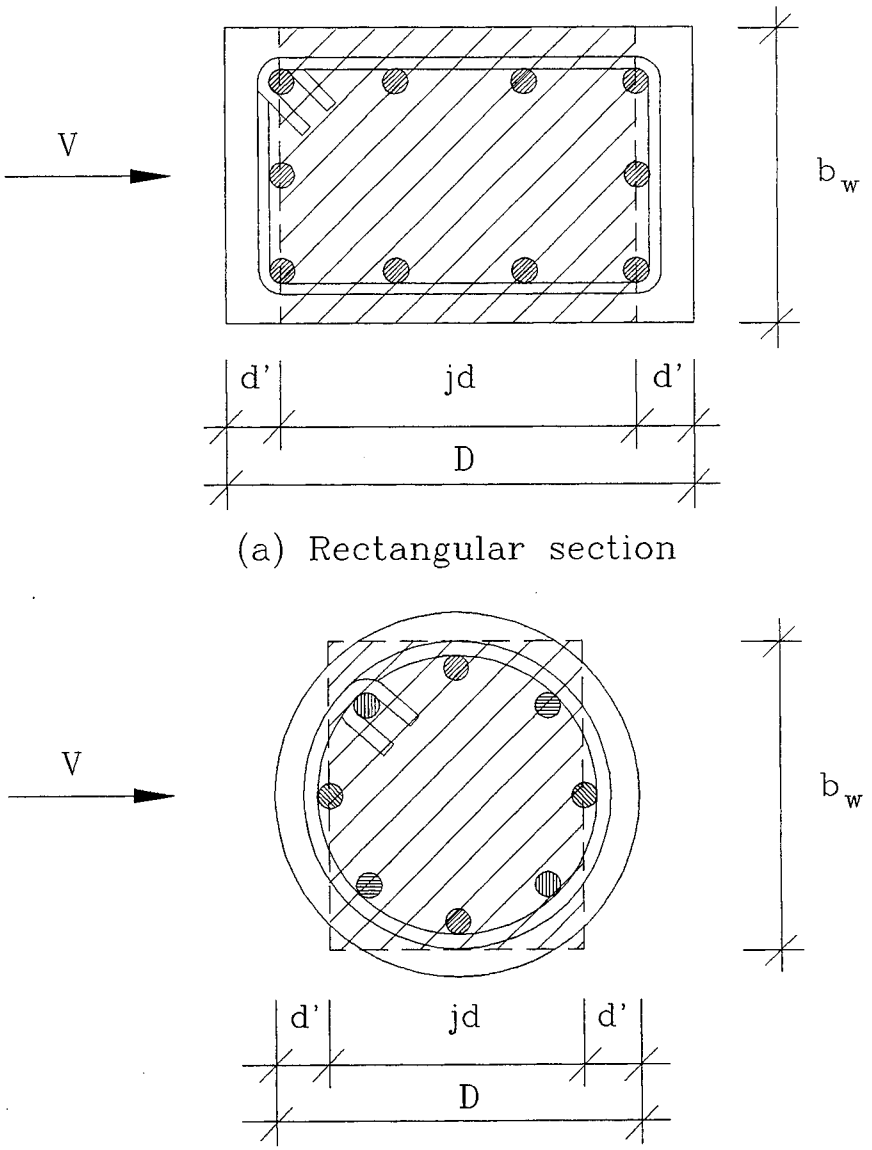

Figure 2-3. Definition of column shear area.

$$\rho_v = \frac{\rho_s}{2} = \frac{2A_b}{d_c s} \quad \textit{for a circular column} \tag{2-5b}$$

where A_b = section area of a single leg of a transverse hoop and d_c = center-to-center diameter of the transverse reinforcement in a circular column.

The corresponding shear strain (or rotation) is then determined by dividing equation (2-4b) by the unit length of a single crack ($jd\cot\theta$), thus

$$\Theta_s = \frac{\Delta_s}{jd\cot\theta} = \frac{dV_s}{E_c b_w \cot\theta\, dx}\left(\frac{1}{\rho_v n} + \frac{1}{\left(\frac{b_{ws}}{b_w}\right)\sin^4\theta}\right) \tag{2-6}$$

Therefore, the shear stiffness of a differential truss element is

$$dK_s = \frac{dV_s}{\Theta_s} = \frac{E_c b_w \cot\theta\, dx}{\left(\frac{1}{\rho_v n} + \frac{1}{\left(\frac{b_{ws}}{b_w}\right)\sin^4\theta}\right)} \tag{2-7}$$

The total shear stiffness of a cracked concrete member due to the constant angle truss mechanism is derived by integrating equation (2-7) through the unit length ($jd\cot\theta$):

$$K_s = \int dK_s = \int_0^{jd\cot\theta} \frac{E_c b_w \cot\theta}{\left(\frac{1}{\rho_v n} + \frac{1}{\left(\frac{b_{ws}}{b_w}\right)\sin^4\theta}\right)} dx \tag{2-8a}$$

Carrying out the integration gives:

$$K_s = \frac{\rho_v n \cot^2\theta}{1 + \rho_v n\left(\frac{b_w}{b_{ws}}\right)\operatorname{cosec}^4\theta} E_c A_v \tag{2-8b}$$

where $A_v = b_w jd =$ shear area of a column section defined in figure 2-3. When $b_{ws}/b_w = 1$, this expression is identical to the equation developed for 90° transverse steel ties by Dilger *(1966)* and Park and Paulay *(1975)*.

2.2.3 Variable Angle Truss Theory

A variable angle truss shown in figure 2-4(a) can appropriately represent a diagonally cracked short column where the disturbed regions prevail. As mentioned previously, Paulay *(1971a,b)* extensively investigated the variable angle truss. For ease of integrating, Paulay determined the stiffness of his variable angle truss model by assuming a quadratic distribution of transverse tie forces over the length of a squat coupling beam. A more rigorous integration procedure is now investigated.

In a manner similar to the solution of the constant angle truss mechanism, consider a single differential truss element subjected to the differential shear force dV_s in figure 2-4(b). Unlike in the constant angle truss, the differential shear force dV_s is not uniform over the longitudinal axis of the variable angle truss. Note that a differential truss consists of an idealized steel tie with a finite depth Ldx and two tapered diagonal concrete struts, where x is a non-dimensionalized parameter varying from 0 to 1. A tapered diagonal concrete strut is idealized as a prismatic strut with the average depth. Assuming rigid longitudinal chords to eliminate the effects of flexural deformation, the shear deformation of the differential truss can be calculated by the Virtual Work method of analysis using the member forces shown in figure 2-4(c). Since the differential truss element is statically determinate, the member forces can easily be determined by static equilibrium. The determination of the member deformations of a differential portion of a variable angle truss is presented in table 2-2. Again, the displacement compatibility requires that the deformation of each differential truss element be the same as the overall shear deformation of the whole variable angle truss.

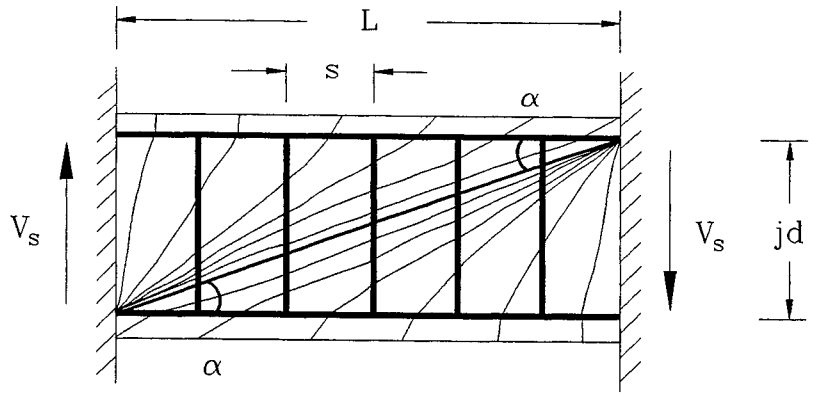

(a) Variable angle crack pattern of a "squat" beam–column

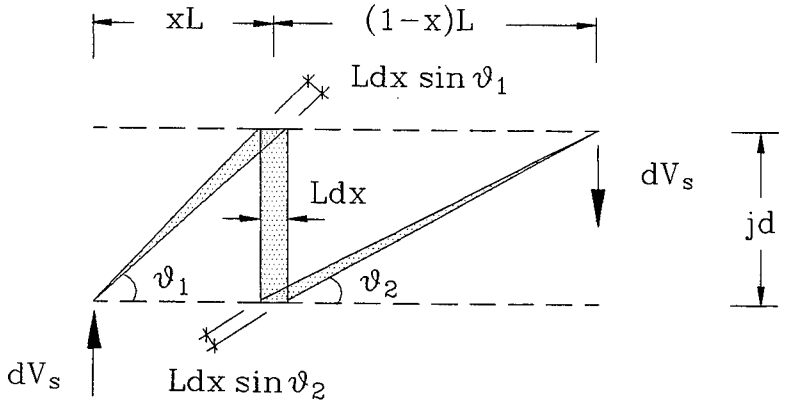

(b) A differential element of a variable angle truss

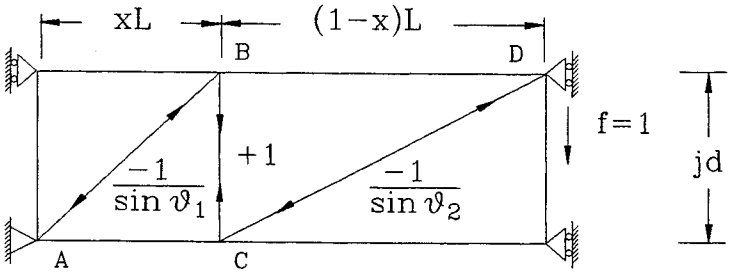

(c) Member forces for a unit load

Figure 2-4. Variable angle truss model.

Table 2-2. Shear deformation of a differential element in a variable angle truss.

Member	Force F	Load f	Length l	Rigidity EA	Strain $\varepsilon = F/EA$	Deformation $\frac{Ffl}{EA}$
B-C	$+dV_s$	$+1$	jd	$E_s A_{sh}\frac{L}{s}dx$	$\frac{+s\,dV_s}{E_s A_{sh} L\,dx}$	$\frac{s\,jd\,dV_s}{E_s A_{sh} L\,dx}$
A-B	$\frac{-dV_s}{\sin\theta_1}$	$\frac{-1}{\sin\theta_1}$	$\frac{jd}{\sin\theta_1}$	$\frac{E_c b_{ws} L \sin\theta_1\,dx}{2}$	$\frac{-2\,dV_s}{E_c b_{ws} L \sin^2\theta_1\,dx}$	$\frac{2\,jd\,dV_s}{E_c b_{ws} L \sin^4\theta_1\,dx}$
C-D	$\frac{-dV_s}{\sin\theta_2}$	$\frac{-1}{\sin\theta_2}$	$\frac{jd}{\sin\theta_2}$	$\frac{E_c b_{ws} L \sin\theta_2\,dx}{2}$	$\frac{-2\,dV_s}{E_c b_{ws} L \sin^2\theta_2\,dx}$	$\frac{2\,jd\,dV_s}{E_c b_{ws} L \sin^4\theta_2\,dx}$

Note: Refer to figure 2-4.

$$\sin\theta_1 = \frac{\left(\frac{jd}{L}\right)}{\sqrt{x^2 + \left(\frac{jd}{L}\right)^2}} \quad ; \quad \sin\theta_2 = \frac{\left(\frac{jd}{L}\right)}{\sqrt{(1-x)^2 + \left(\frac{jd}{L}\right)^2}}$$

The shear deformation of a differential truss is the sum of the component deformations of a tie and two struts, thus

$$\Delta_s = \sum \frac{Ffl}{EA} = \frac{jd\,dV_s}{E_c b_w L dx}\left(\frac{s b_w}{\frac{E_s}{E_c}A_{sh}} + \frac{2\left\{1 + x^2\left(\frac{L}{jd}\right)^2\right\}^2}{\left(\frac{b_{ws}}{b_w}\right)} + \frac{2\left\{1 + (1-x)^2\left(\frac{L}{jd}\right)^2\right\}^2}{\left(\frac{b_{ws}}{b_w}\right)}\right) \qquad \textbf{(2-9)}$$

where b_{ws}/b_w is the ratio of effective column width for the steel truss mechanism given in equation (1-8). Recalling that $\cot\alpha = L/jd$, $\rho_v = A_{sh}/b_w s$, $A_v = b_w jd$ and $n = E_s/E_c$, equation (2-9) can be rewritten as

$$\Delta_s = \frac{jd\,dV_s}{E_c A_v \cot\alpha\,dx}\left[\frac{1}{\rho_v n} + 2\left(\frac{b_w}{b_{ws}}\right)\left(\left\{1 + x^2\cot^2\alpha\right\}^2 + \left\{1 + (1-x)^2\cot^2\alpha\right\}^2\right)\right] \qquad \textbf{(2-10)}$$

where α = corner-to-corner diagonal angle of the variable angle truss. Then, the end-to-end rotation (drift) angle is determined by dividing the shear displacement by the column length $L = jd\cot\alpha$, thus

$$\Theta_s = \frac{dV_s}{E_c A_v \cot^2\alpha \, dx}\left[\frac{1}{\rho_v n} + 2\left(\frac{b_w}{b_{ws}}\right)\left(\{1 + x^2\cot^2\alpha\}^2 + \{1 + (1-x)^2\cot^2\alpha\}^2\right)\right] \tag{2-11}$$

Therefore, the shear stiffness of a differential portion of the variable angle truss is

$$dK_s = \frac{dV_s}{\Theta_s} = \frac{E_c A_v \cot^2\alpha \, dx}{\frac{1}{\rho_v n} + 2\left(\frac{b_w}{b_{ws}}\right)\left(\{1 + x^2\cot^2\alpha\}^2 + \{1 + (1-x)^2\cot^2\alpha\}^2\right)} \tag{2-12}$$

The elastic shear stiffness of a cracked concrete column due to the variable angle truss mechanism can be obtained by integrating equation (2-12) over the entire length of the variable angle truss, thus

$$K_s = \int dK_s = \int_0^1 \frac{\rho_v n E_c A_v \cot^2\alpha}{1 + 2\rho_v n\left(\frac{b_w}{b_{ws}}\right)\left[\{1 + x^2\cot^2\alpha\}^2 + \{1 + (1-x)^2\cot^2\alpha\}^2\right]} dx \tag{2-13}$$

A closed-form analytical solution to this equation has not been found. However, it is possible to use an appropriate numerical integration scheme instead. Such schemes are investigated in the following subsections.

2.2.4 Numerical Solution to Find The Stiffness of A Variable Angle Truss

Several efficient numerical integration schemes such as Gauss quadrature and Newton-Cotes closed formulas may be employed for solving equation (2-13). The numerical schemes investigated in this study are two-point and three-point Gauss-Legendre formulas for Gauss quadrature, and Simpson's 1/3 rule and Boole's rule for the Newton-Cotes family. Details of these numerical integration schemes may be found in any numerical analysis text such as Hornbeck *(1975)* and Chapra and Canale *(1988)*. Using those numerical schemes, the cracked elastic shear stiffness of the variable angle truss in equation (2-13) can be expressed as

$$K_s = \sum_{i=1}^{N} \frac{\omega_i \rho_v n \cot^2 \alpha}{1 + 2\rho_v n \left(\frac{b_w}{b_{ws}}\right)\left[\left\{1 + x_i^2 \cot^2\alpha\right\}^2 + \left\{1 + (1 - x_i)^2 \cot^2\alpha\right\}^2\right]} E_c A_v \qquad (2\text{-}14)$$

where N = number of numerical integration points considered, ω_i = numerical weight factor, and x_i = normalized coordinate of i^{th} numerical point. The values of these parameters with the truncation error for each numerical integration scheme are presented in table 2-3.

Table 2-3. Numerical scheme parameter values for cracked elastic column shear stiffness due to variable angle truss model for the steel mechanism.

Numerical Scheme	N	i	x_i	ω_i	Truncation Error
Two-Point Gauss	2	1	0.2113249	0.5	$\frac{1}{135} f^{(4)}(\xi)$
		2	0.7886751	0.5	
Three-Point Gauss	3	1	0.11270171	5/18	
		2	0.5	8/18	$\frac{1}{15750} f^{(6)}(\xi)$
		3	0.88729829	5/18	
Simpson's 1/3 Rule	3	1	0.0	1/6	
		2	0.5	4/6	$-\frac{1}{2880} f^{(4)}(\xi)$
		3	1.0	1/6	
Boole's Rule	5	1	0.0	7/90	
		2	0.25	32/90	
		3	0.5	12/90	$-\frac{1}{1935360} f^{(6)}(\xi)$
		4	0.75	32/90	
		5	1.0	7/90	

Figure 2-5 compares the stiffness of the constant angle truss given by equation (2-8b) with the variable angle truss stiffness given by equation (2-14) when $b_{ws}/b_w = 1$ and also compares the sensitivity of the numerical integration schemes for the variable angle truss. For this purpose, it is necessary to put $\alpha = \theta$ which denotes that the steepest crack angle to the longitudinal axis of the fan-shaped cracks at the disturbed region of the column will be equal to the constant crack angle at the undisturbed region. The shear stiffness due to the variable angle truss in figure 2-5(a) represents the "exact" solution of the variable angle truss in figure 2-5(b).

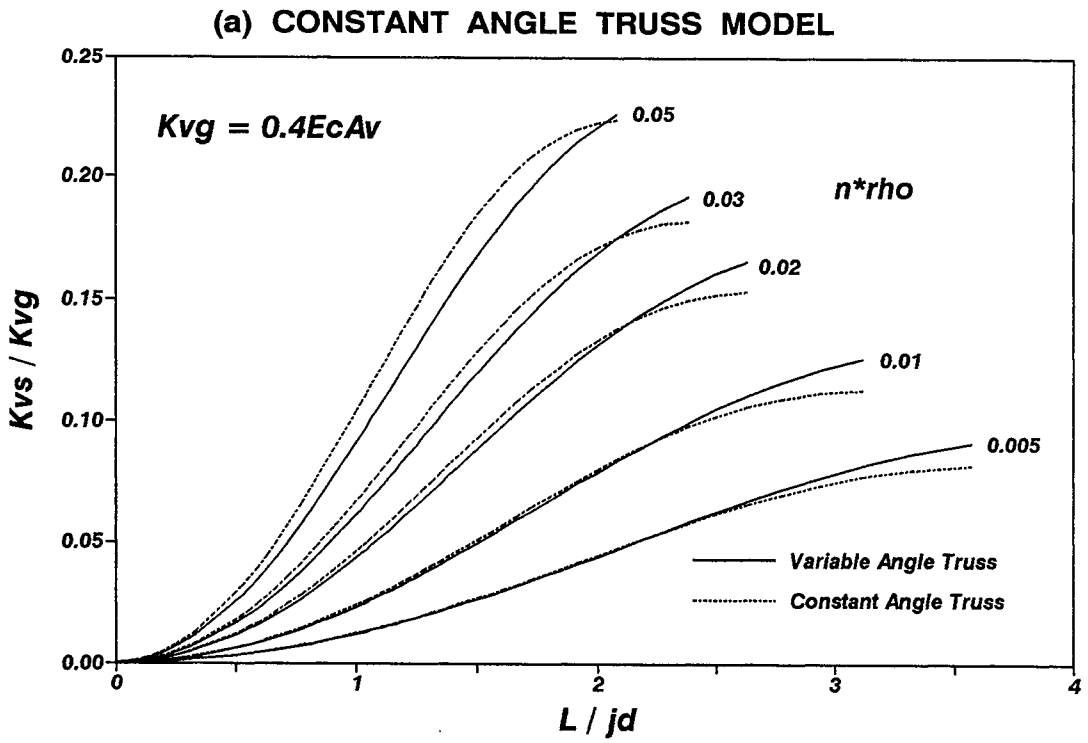

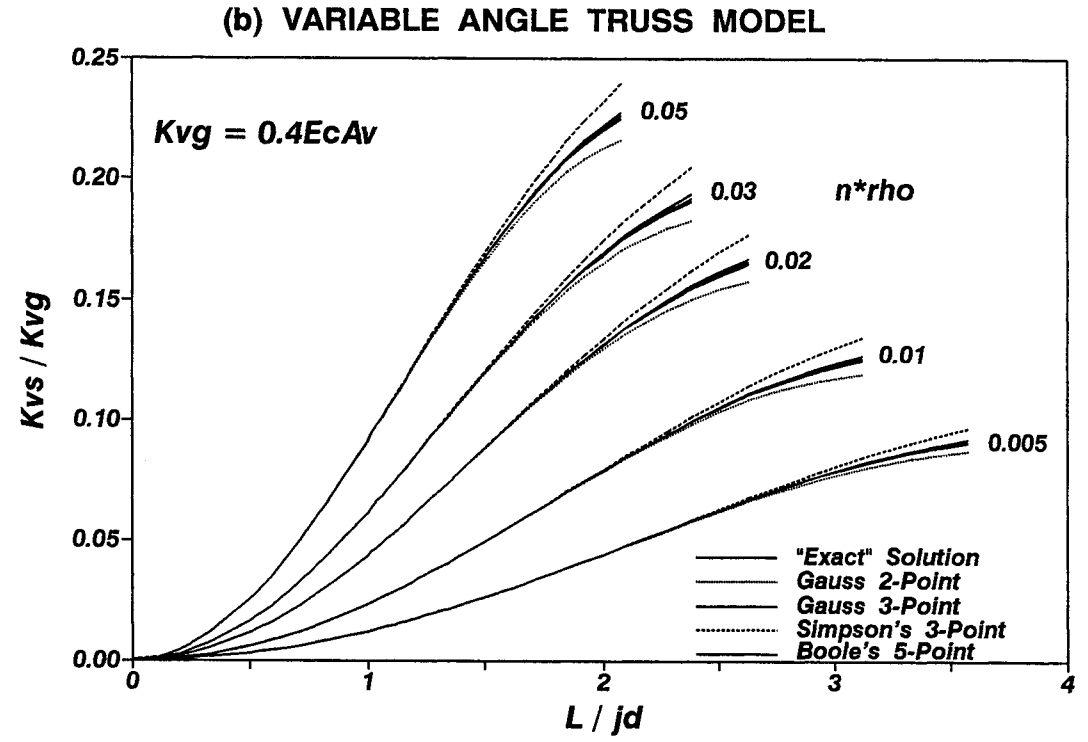

Figure 2-5. Comparison of shear stiffnesses between truss mechanism models.

The "exact" solution of the variable angle truss was calculated using 20-segment Simpson's 1/3 rule. It is of interest to note that:

1) All methods give similar results so that either of constant angle modeling or variable angle modeling may be satisfactory for determining shear stiffness over the length of the member.
2) The shear stiffnesses calculated by three-point Gauss quadrature and Boole's rule are closest to the exact solution of the variable angle truss mechanism.
3) For squat columns where shear is generally critical (small L/jd), there is virtually no difference in stiffness calculations between numerical schemes.

Since equation (2-14) with numerical parameter values in table 2-3 gives a lengthy solution, a convenient simplified solution may be obtained from the following approximation:

$$K_s = \frac{\rho_v n \cot^2 \alpha}{1 + 4 \rho_v n \left(\frac{b_w}{b_{ws}}\right)(1 + 0.39 \cot^2 \alpha)^2} E_c A_v \qquad \text{(2-15)}$$

This approximate solution (equation 2-15) is plotted and compared to the exact solution (equation 2-14) for the variable angle truss in figure 2-6 for $b_{ws}/b_w = 1$. It is evident that the agreement between the approximation and the exact solution is very close.

2.2.5 Implementation of Numerical Schemes into Truss Modeling and Dimensioning

Using equation (2-14) with numerical integration weights given in table 2-3 implies that the variable angle truss model shown in figure 2-4 can be physically simplified with reasonable accuracy. Consider the compound truss in figure 2-7. The compound truss consists of a series of lumped transverse hoops allocated by weight factor ω_i at numerical coordinate x_i. Then, the behavior of the compound truss can be determined by the sum of responses of the individual strut-and-tie linkages, that is, $V_s = \Sigma \phi_i V_s$ in which ϕ_i = distribution factor of shear resistance for i^{th} linkage. It should be noted that for the statically indeterminate truss model, usually $\phi_i \neq \omega_i$.

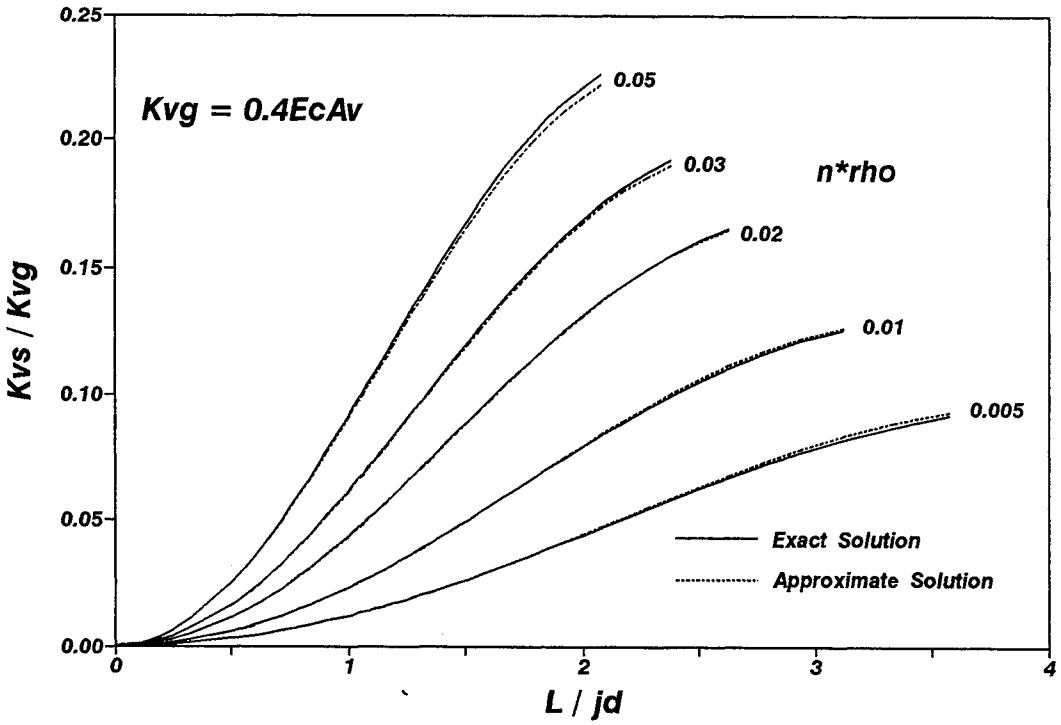

Figure 2-6. Approximation of shear stiffness due to variable angle truss model.

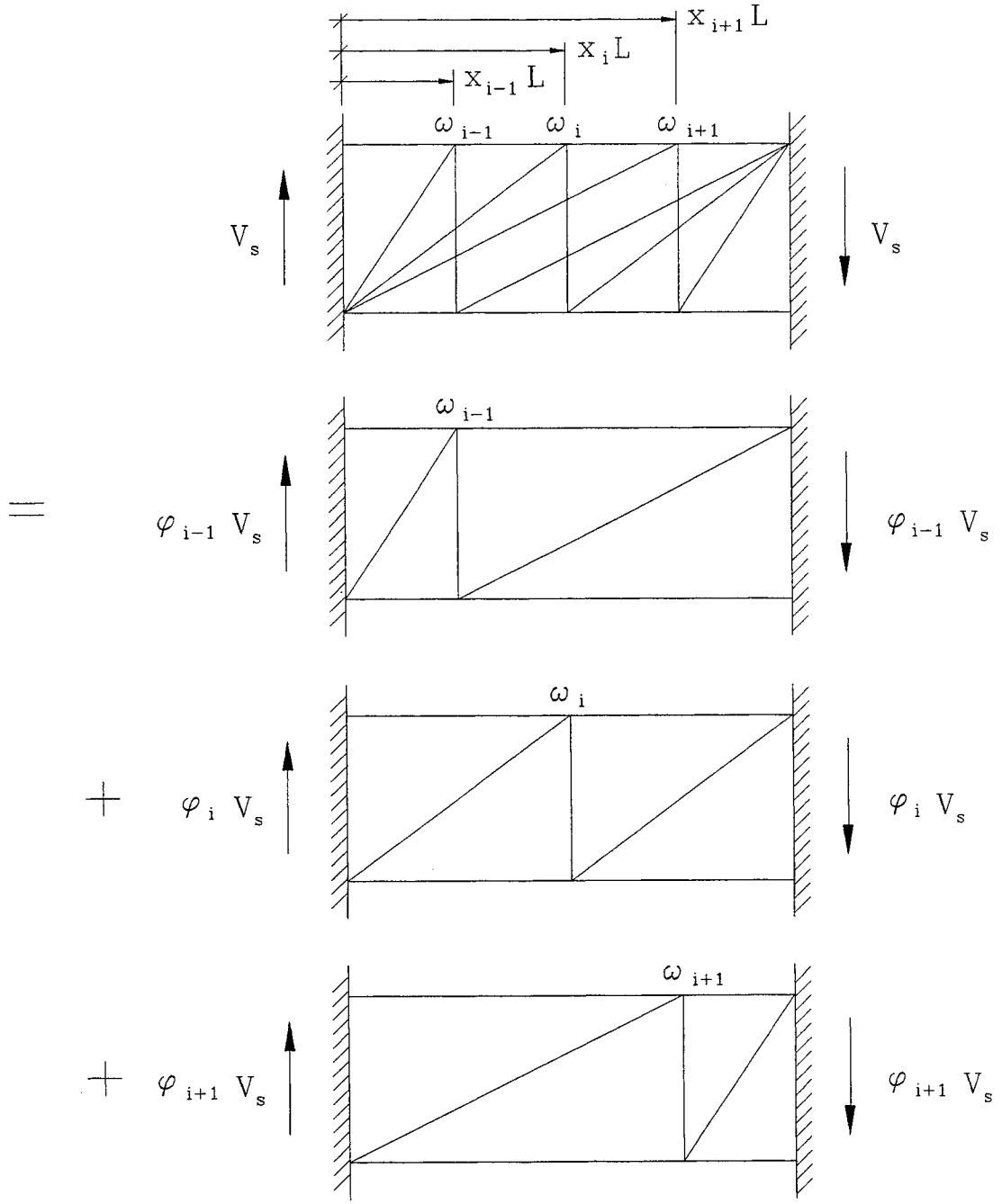

Figure 2-7. A compound truss model due to numerical integration schemes.

These simplified truss models may not only be used to determine the force-displacement relationship of concrete columns subjected to applied shear forces, but can also be imbedded within advanced computational modeling techniques.

The simplified truss model with two-point and three-point Gauss quadratures will now be used to determine the forces of longitudinal and transverse truss elements in order to establish the overall deformation/stiffness of combined shear and flexure. Two-point Gauss truss model leads to a simpler expression of force-deformation relationship in shear and flexure while three-point Gauss truss model gives more accurate relationship of shear force - strain for the transverse ties. Boundary conditions considered are fixed-fixed and fixed-pinned ends. In order to assess truss member deformations, the sectional dimensions of the elements should first be determined.

The location and size of transverse ties are readily determined by the numerical coordinates and weight factors of the two-point and three-point Gauss quadrature schemes presented in table 2-3. Therefore, the axial rigidity of a transverse tie at each numerical point in figures 2-8 and 2-9 can be expressed as

$$(EA)_{Ti} = \omega_i E_s A_{sh} \frac{L}{s} \qquad (2\text{-}16)$$

where ω_i = numerical weights at i^{th} Gauss point.

For longitudinal chord members, a distinction should be made between tension and compression member stiffnesses. For tension members, the concrete will naturally be cracked and not contribute significantly to the axial stiffness of those members. For the compression members, however, in addition to the stiffness contribution of the steel, an allowance should be made for concrete compression. Flexure causes linear compression strain profile in the concrete over a depth c from the neutral axis to the extreme compression fiber. Thus, the effective area of concrete in compression may be taken as $0.5\,c\,b_w$ or $0.5\,\frac{c}{D}A_g$. Paulay *(1971a)* has shown that for cracked squat/deep members with fixed-fixed ends, the longitudinal reinforcement may behave in tension over its entire length. Thus, the longitudinal chord members can be modeled

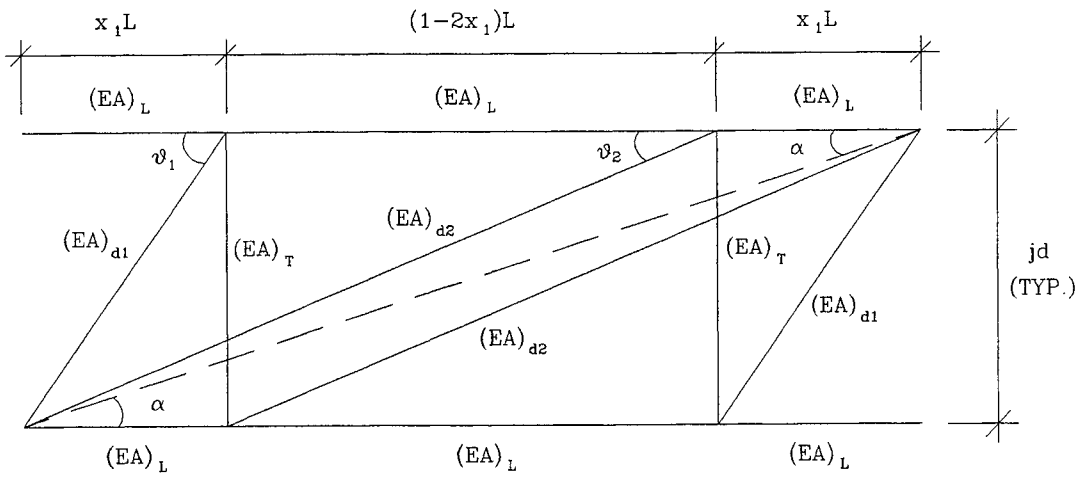

(a) Notations for truss members

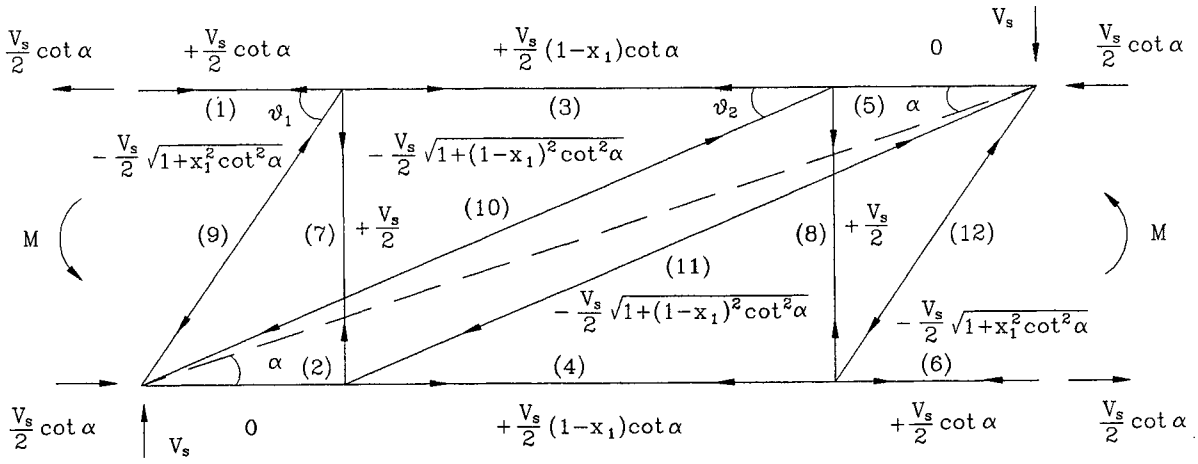

(b) Member forces in a fixed–fixed column

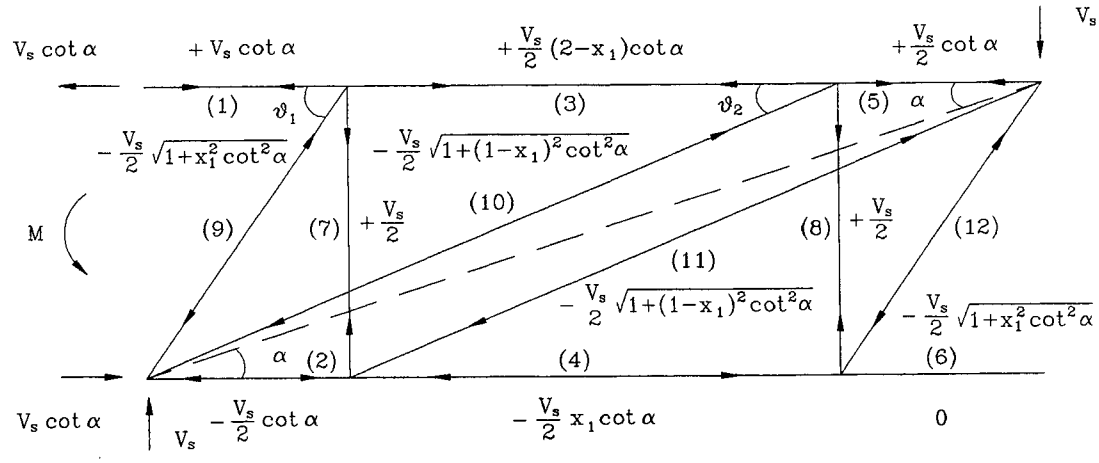

(c) Member forces in a fixed–pinned column

Figure 2-8. Member forces in a truss model by two-point Gauss quadrature.

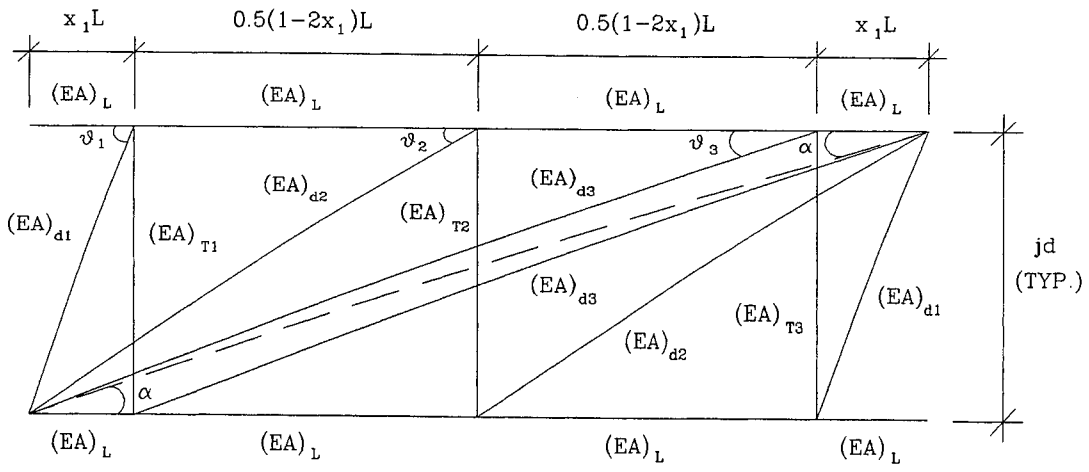

(a) Notations for truss members

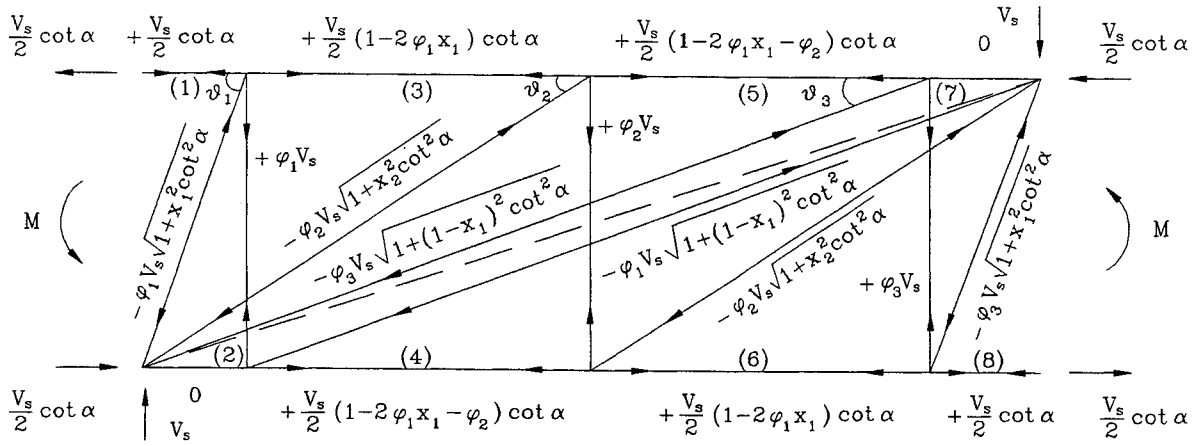

(b) Member forces in a fixed−fixed column

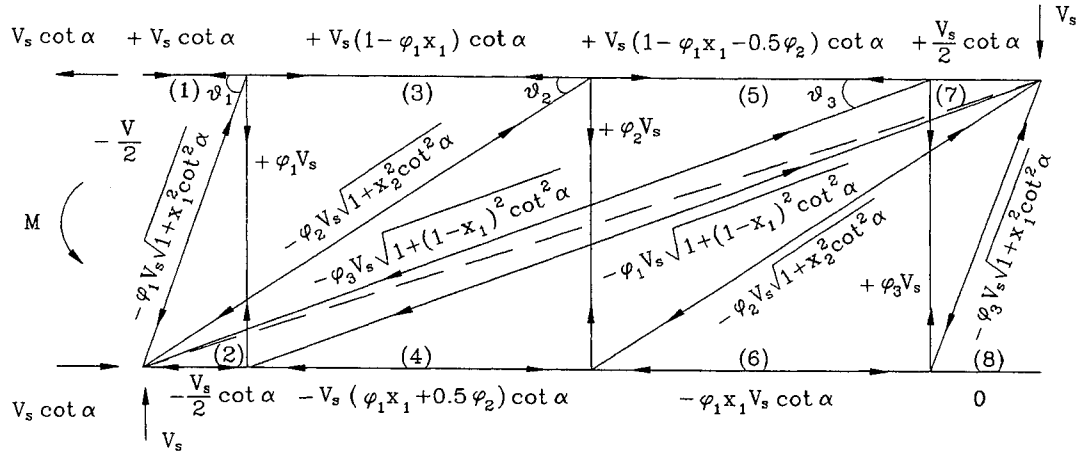

(c) Member forces in a fixed−pinned column

Figure 2-9. Member forces in a truss model by three-point Gauss quadrature.

with one half of column longitudinal steel content with the distance of the column section flexural lever arm *jd* over the length of the column. The axial rigidity of a longitudinal tension chord member in figure 2-8(a) is thus given by

$$(EA)_L = 0.5\,E_s A_{st} = 0.5\,E_c A_g\,\rho_t n \tag{2-17a}$$

where A_{st} = section area of total longitudinal steel in a column section. For more heavily loaded column members or columns with fixed-pinned ends, where compression exists in the longitudinal chords, the following axial rigidity should be used:

$$(EA)_L = 0.5\left(\frac{c}{D} + \rho_t(n-1)\right)E_c A_g \tag{2-17b}$$

This equation may be used in dimensioning the longitudinal chord members of a truss model for rigorous computer analysis. However, the difference in resultant column stiffness between two equations is negligible. Therefore, equation (2-17a) will be used for all longitudinal chord members of the Gauss trusses for simplicity in the present investigation.

The sectional dimensions of diagonal struts can be determined by comparing the truss solution to the numerical solution. The rigidities of diagonal struts shown in figures 2-8 and 2-9 use the following expression with unknown parameters until they are determined:

$$(EA)_{di} = a_i E_c A_v \tag{2-18}$$

where a_i = effective sectional area factors of diagonal struts at i^{th} numerical point. It is assumed that the behavior of concrete diagonal struts is linear elastic.

2.2.6 Analysis of A Truss Model with Two-Point Gauss Quadrature

2.2.6.1 Shear Deformation

Consider a truss model shown in figures 2-8(b) and 2-8(c). Also shown are the member forces determined by static equilibrium at each joint. Note that the two-point Gauss truss model is statically determinate. Comparing member forces in between fixed-fixed and fixed-pinned

columns, it is noted that the shear transfer mechanism causes the same member forces in transverse ties and diagonal struts. Thus the shear stiffnesses of the truss models with fixed-fixed and fixed-pinned ends should be the same. The shear deformation of the truss model is determined using the Virtual Work method of analysis on the transverse ties and diagonal struts. The analysis is presented in table 2-4.

Table 2-4. Virtual work done on transverse ties and diagonal struts of the two-point Gauss truss model.

Member	Force F	Unit Load f	Length l	Rigidity EA	Strain $\varepsilon = F/EA$	Deformation $\frac{Ffl}{EA}$
(7),(8)	$+\frac{V_s}{2}$	$+\frac{1}{2}$	jd	$\frac{E_s A_{sh} L}{2s}$	$\frac{V_s s}{E_s A_{sh} L}$	$\frac{V_s jd s}{2E_s A_{sh} L}$
(9),(12)	$\frac{-V_s}{2\sin\theta_1}$	$\frac{-1}{2\sin\theta_1}$	$\frac{jd}{\sin\theta_1}$	$a_1 E_c A_v$	$\frac{-V_s}{2a_1 E_c A_v \sin\theta_1}$	$\frac{V_s jd}{4a_1 E_c A_v \sin^3\theta_1}$
(10),(11)	$\frac{-V_s}{2\sin\theta_2}$	$\frac{-1}{2\sin\theta_2}$	$\frac{jd}{\sin\theta_2}$	$a_2 E_c A_v$	$\frac{-V_s}{2a_2 E_c A_v \sin\theta_2}$	$\frac{V_s jd}{4a_2 E_c A_v \sin^3\theta_2}$

Note:
1. Refer to figure 2-8(b) for member forces.
2. Refer to equations (2-16) and (2-18) for rigidities.

$$\sin\theta_1 = \frac{1}{\sqrt{1 + x_1^2 \cot^2\alpha}} \; ; \quad \sin\theta_2 = \frac{1}{\sqrt{1 + (1 - x_1)^2 \cot^2\alpha}}$$

The shear deformation of the simple truss model with two-point Gauss quadrature is the sum of the deformation components. Recalling that $\cot\alpha = L/jd$ and $\rho_v = A_{sh}/b_w s$,

$$\Delta_s = \sum_{i=7}^{12} \frac{Ffl}{EA} = \frac{V_s}{E_c A_v}\left(\frac{jd\{1 + x_1^2\cot^2\alpha\}^2}{2a_1\sqrt{1 + x_1^2\cot^2\alpha}} + \frac{jd\{1 + (1-x_1)^2\cot^2\alpha\}^2}{2a_2\sqrt{1 + (1-x_1)^2\cot^2\alpha}} + \frac{jd}{\rho_v n \cot\alpha}\right) \qquad (2\text{-}19)$$

The shear strain (rotation) is then determined by dividing the shear displacement by the length of the truss model, thus

$$\theta_s = \frac{V_s}{E_c A_v}\left(\frac{\{1+x_1^2\cot^2\alpha\}^2}{2a_1\cot\alpha\sqrt{1+x_1^2\cot^2\alpha}} + \frac{\{1+(1-x_1)^2\cot^2\alpha\}^2}{2a_2\cot\alpha\sqrt{1+(1-x_1)^2\cot^2\alpha}} + \frac{1}{\rho_v n\cot^2\alpha}\right) \tag{2-20}$$

Therefore, the shear stiffness of the truss model with two-point Gauss quadrature can be given by

$$K_s = \frac{\rho_v n\cot^2\alpha}{1 + 2\rho_v n\left(\frac{\cot\alpha\{1+x_1^2\cot^2\alpha\}^2}{4a_1\sqrt{1+x_1^2\cot^2\alpha}} + \frac{\cot\alpha\{1+(1-x_1)^2\cot^2\alpha\}^2}{4a_2\sqrt{1+(1-x_1)^2\cot^2\alpha}}\right)} E_c A_v \tag{2-21}$$

The cracked elastic shear stiffness of concrete columns given by equation (2-14) using two-point Gauss quadrature is

$$K_s = \frac{\rho_v n\cot^2\alpha}{1 + 2\rho_v n\left(\frac{b_w}{b_{ws}}\right)\left(\{1+x_1^2\cot^2\alpha\}^2 + \{1+(1-x_1)^2\cot^2\alpha\}^2\right)} E_c A_v \tag{2-22}$$

By comparing equations (2-21) and (2-22), the effective sectional area factors for diagonal struts can be obtained. That is,

$$a_i = \frac{\cot\alpha}{4\sqrt{1 + x_i^2\cot\alpha}}\left(\frac{b_{ws}}{b_w}\right) \tag{2-23}$$

The axial rigidities of the diagonal struts of the truss model in figure 2-8(a) are then determined by

$$(EA)_{di} = \frac{0.5\,\omega_i}{\sqrt{x_i^2+\tan^2\alpha}} E_c A_v\left(\frac{b_{ws}}{b_w}\right) = \frac{0.25\,E_c A_v}{\sqrt{x_i^2+\tan^2\alpha}}\left(\frac{b_{ws}}{b_w}\right) \tag{2-24}$$

where $\omega_1 = \omega_2 = 0.5$, $x_2 = 1-x_1$ and $A_v = b_w jd$. The values of x_i and ω_i for two-point Gauss quadrature are available in table 2-3. The section areas of diagonal struts can alternatively be

obtained by measuring the depth of the diagonal struts along the truss center line on the scaled sketch of the truss as shown in figure 2-10(a). However, equation (2-24) provides the simpler and more accurate way in determining axial rigidities of diagonal struts. For more complex section shapes (eg., non-prismatic members) the graphical determination of diagonal strut sizes should suffice. The corresponding compressive axial stress in i^{th} diagonal strut is obtained from table 2-4, thus

$$f_{cdi} = E_c \varepsilon_{cdi} = \frac{-2V_s\left\{1 + x_i^2 \cot^2\alpha\right\}}{A_v\left(\frac{b_{ws}}{b_w}\right)\cot\alpha} \qquad (2\text{-}25)$$

Note that the location of i^{th} diagonal strut is depicted in figure 2-8(a). It is assumed that diagonal struts of the truss model behave linear-elastically. Therefore, the magnitude of axial stress in the diagonal struts should be checked over the column response.

The average tensile strain of the transverse hoops in the two-point Gauss truss model is readily available in table 2-4, thus

$$\varepsilon_T = \frac{\Delta_T}{jd} = \frac{sV_s}{E_s A_{sh} L} = \frac{V_s}{E_c A_v \rho_v n \cot\alpha} \qquad (2\text{-}26)$$

where Δ_T = transverse elongation of the truss member (7) or (8) in figures 2-8(b) and (c). It should be noted that the tensile strain given by equation (2-26) is only the numerical average of the transverse steel strain over the length of the concrete column. Note that if it is important to assess the maximum transverse hoop strain that occurs at the center of the column, then it is necessary to use a numerical integration scheme that has an integration point at the center of the truss. Therefore, the more realistic transverse steel strain distribution over the column length can be captured by truss modeling with higher order of numerical integration schemes such as three-point Gauss quadrature and Boole's rule.

2.2.6.2 Flexural Deformation

Consider a truss model with fixed-fixed ends shown in figure 2-8(b). It is of interest to

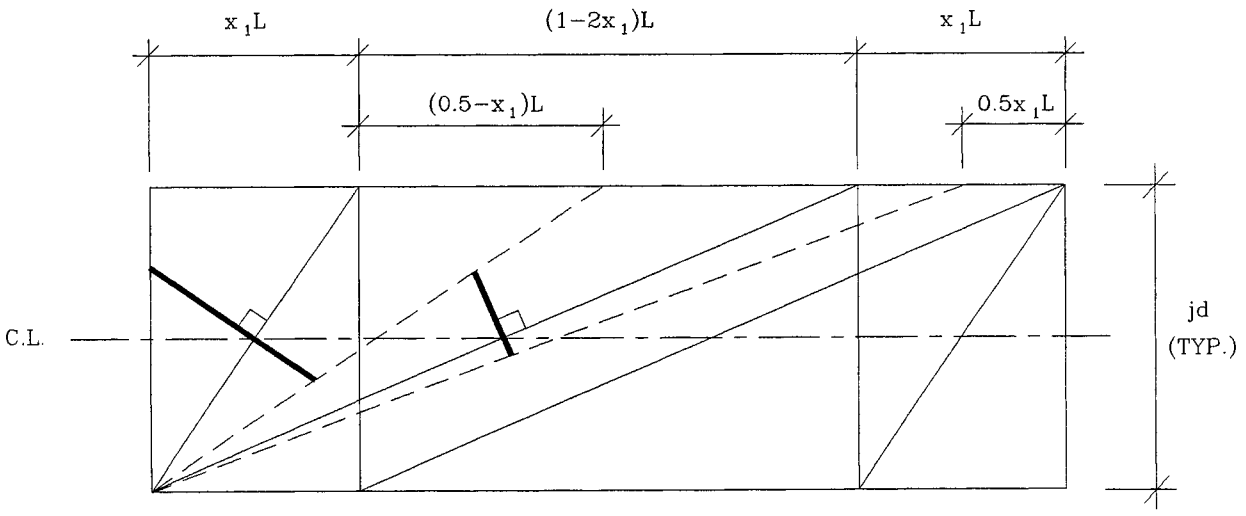

(a) Truss model with two-point Gauss quadrature

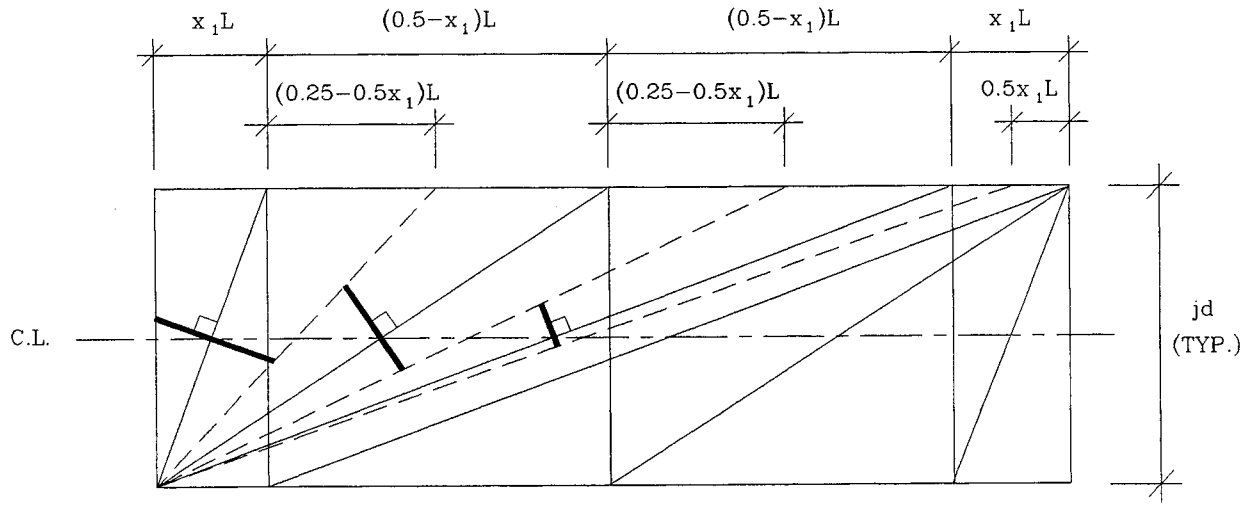

(b) Truss model with three-point Gauss quadrature

Figure 2-10. Determination of diagonal strut size by measurement.

note that no compression forces are generated in longitudinal chord members over the entire length of the model. As mentioned above, this same phenomenon was also observed by Paulay both theoretically and experimentally *(1971a,b)*. Note that this is contrary to the Bernoulli beam theory where a column always has compression and tension parts. The flexural deformation of the truss model can be determined using the Virtual Work method of analysis considering only the longitudinal chord members in figure 2-8(b). This analysis is presented in table 2-5.

Table 2-5. Virtual work done on longitudinal chord members of the two-point Gauss truss model with fixed-fixed ends.

Member	Force F	Unit Load f	Length l	Rigidity EA	Strain $\varepsilon = F/EA$	Deformation $\frac{Ffl}{EA}$
(1), (6)	$\frac{+V_s}{2\tan\alpha}$	$\frac{+1}{2\tan\alpha}$	$x_1 L$	$\frac{E_s A_{st}}{2}$	$\frac{+V_s\cot\alpha}{E_s A_{st}}$	$\frac{V_s x_1 L\cot^2\alpha}{2E_s A_{st}}$
(2), (5)	0	0	$x_1 L$	$\frac{E_s A_{st}}{2}$	0	0
(3), (4)	$\frac{+V_s Q_1}{2\tan\alpha}$	$\frac{+Q_1}{2\tan\alpha}$	$Q_2 L$	$\frac{E_s A_{st}}{2}$	$\frac{+V_s Q_1\cot\alpha}{E_s A_{st}}$	$\frac{V_s Q_1^2 Q_2 L}{2E_s A_{st}\tan^2\alpha}$

Note: Refer to figure 2-8(b) for member forces.
where $Q_1 = 1 - x_1$; $Q_2 = 1 - 2x_1$

The flexural deformation of the truss is the sum of the component deformations taking the value of $x_1 = 0.2113249$ (see table 2-3 for two-point Gauss quadrature), thus

$$\Delta_f = \sum_{i=1}^{6} \frac{Ffl}{EA} = \zeta \frac{V_s L\cot^2\alpha}{E_s A_{st}} \qquad (2\text{-}27)$$

where $\zeta = x_1 + (1-x_1)^2(1-2x_1) = 0.5704$. The flexural drift angle is then determined by dividing the flexural displacement by the length of the truss model, thus

$$\theta_f = \frac{\Delta_f}{L} = \zeta \frac{V_s \cot^2 \alpha}{E_s A_{st}} \tag{2-28}$$

Therefore, the elastic flexural stiffness of a cracked concrete column about drift angle due to the variable angle truss model with fixed-fixed ends is

$$K_{f\theta} = \zeta^{-1} E_s A_{st} \tan^2 \alpha \tag{2-29}$$

where $\zeta^{-1} = 1.753$.

It is of interest to compare this result with Bernoulli beam theory. Considering the longitudinal steel only, the flexural stiffness in terms of drift angle for a fixed-fixed beam is

$$K_{f\theta} = \frac{12EI}{L^2} = \frac{12 E_s A_{st} \frac{(jd)^2}{4}}{L^2} = 3 E_s A_{st} \tan^2 \alpha \tag{2-30}$$

Thus, by using a truss model there is a 40% reduction in flexural stiffness for a fixed-fixed column.

The corresponding tensile strain of the longitudinal chord at the critical region can be determined by the average strain over the chord length of $x_1 L$ in figure 2-8(b) and is readily available in table 2-5. Thus

$$\varepsilon_L = \frac{\Delta_L}{x_1 L} = \frac{V_s \cot \alpha}{E_s A_{st}} \tag{2-31}$$

where Δ_L = longitudinal elongation of truss member (1) or (6) in figure 2-8(b).

Consider a truss model with fixed-pinned ends shown in figure 2-8(c). The flexural deformation of the truss model can be determined by the Virtual Work method of analysis on the longitudinal chord members in figure 2-8(c). The analysis is presented in table 2-6.

In a manner similar to the fixed-fixed column, the flexural deformation of the simplified truss model with fixed-pinned end is the sum of the component deformations taking the value

of numerical coordinate x_1 from table 2-3, thus

$$\Delta_f = \sum_{i=1}^{6} \frac{Ffl}{EA} = \zeta \frac{V_s L \cot^2 \alpha}{E_s A_{st}} \tag{2-32}$$

where $\zeta = 2 - 3x_1 + 5x_1^2 - 2x_1^3 = 1.5704$. The flexural drift angle is then determined by dividing the flexural displacement by the length of the truss model, thus

$$\theta_f = \frac{\Delta_f}{L} = \zeta \frac{V_s \cot^2 \alpha}{E_s A_{st}} \tag{2-33}$$

Table 2-6. Virtual work done on longitudinal chord members of two-point Gauss truss model with fixed-pinned ends.

Member	Force F	Unit Load f	Length l	Rigidity EA	Strain $\varepsilon = F/EA$	Deformation $\frac{Ffl}{EA}$
(1)	$\frac{+V_s}{\tan\alpha}$	$\frac{+1}{\tan\alpha}$	$x_1 L$	$\frac{E_s A_{st}}{2}$	$\frac{+2\,V_s \cot\alpha}{E_s A_{st}}$	$\frac{2\,V_s x_1 L}{E_s A_{st} \tan^2\alpha}$
(2)	$\frac{-V_s}{2\tan\alpha}$	$\frac{-1}{2\tan\alpha}$	$x_1 L$	$\frac{E_s A_{st}}{2}$	$\frac{-V_s \cot\alpha}{E_s A_{st}}$	$\frac{V_s x_1 L \cot^2\alpha}{2 E_s A_{st}}$
(3)	$\frac{+V_s Q_1}{2\tan\alpha}$	$\frac{+Q_1}{2\tan\alpha}$	$Q_2 L$	$\frac{E_s A_{st}}{2}$	$\frac{+V_s Q_1}{E_s A_{st} \tan\alpha}$	$\frac{V_s Q_1^2 Q_1 L}{2 E_s A_{st} \tan^2\alpha}$
(4)	$\frac{-V_s x_1}{2\tan\alpha}$	$\frac{-x_1}{2\tan\alpha}$	$Q_2 L$	$\frac{E_s A_{st}}{2}$	$\frac{-V_s x_1}{E_s A_{st} \tan\alpha}$	$\frac{V_s x_1^2 Q_2 L}{2 E_s A_{st} \tan^2\alpha}$
(5)	$\frac{+V_s}{2\tan\alpha}$	$\frac{+1}{2\tan\alpha}$	$x_1 L$	$\frac{E_s A_{st}}{2}$	$\frac{+V_s \cot\alpha}{E_s A_{st}}$	$\frac{V_s x_1 L \cot^2\alpha}{2 E_s A_{st}}$
(6)	0	0	$x_1 L$	$\frac{E_s A_{st}}{2}$	0	0

Note: Refer to figure 2-8(c) for member forces.
where $Q_1 = 2 - x_1$; $Q_2 = 1 - 2x_1$.

Therefore, the elastic flexural stiffness of a cracked concrete column about the drift angle due

to the variable angle truss model with fixed-pinned ends is

$$K_{f\theta} = \zeta^{-1} E_s A_{st} \tan^2 \alpha \tag{2-34}$$

where $\zeta^{-1} = 0.6368$.

Compare now this result with Bernoulli beam theory. Considering the longitudinal steel only, the flexural stiffness in terms of drift angle for a fixed-pinned beam is

$$K_{f\theta} = \frac{3EI}{L^2} = \frac{3 E_s A_{st} \frac{(jd)^2}{4}}{L^2} = 0.75 E_s A_{st} \tan^2 \alpha \tag{2-35}$$

Thus, by using a truss model there is a 15% reduction in flexural stiffness for a fixed-pinned column.

The corresponding tensile strain of the longitudinal chord at the critical region can be determined by the average strain over the chord length of $x_1 L$ in figure 2-8(c) and is readily available in table 2-6. Thus

$$\varepsilon_L = \frac{\Delta_L}{x_1 L} = \frac{2 V_s \cot \alpha}{E_s A_{st}} \tag{2-36}$$

where Δ_L = longitudinal elongation of truss member (1) in figure 2-8(c).

2.2.7 Analysis of A Truss Model with Three-Point Gauss Quadrature

2.2.7.1 Shear Deformation

The simplified truss model with three-point Gauss quadrature is investigated to determine the forces and deformations in the transverse ties of the truss model. As mentioned previously, the compound truss due to three-point Gauss quadrature in figure 2-9 can be decoupled into three truss linkages as shown in figure 2-11. Unlike the flexural force transfer mechanism, the shear transfer mechanism between the fixed-fixed and fixed-pinned columns causes the same member forces in transverse ties and diagonal struts. This means that the shear stiffnesses of the truss

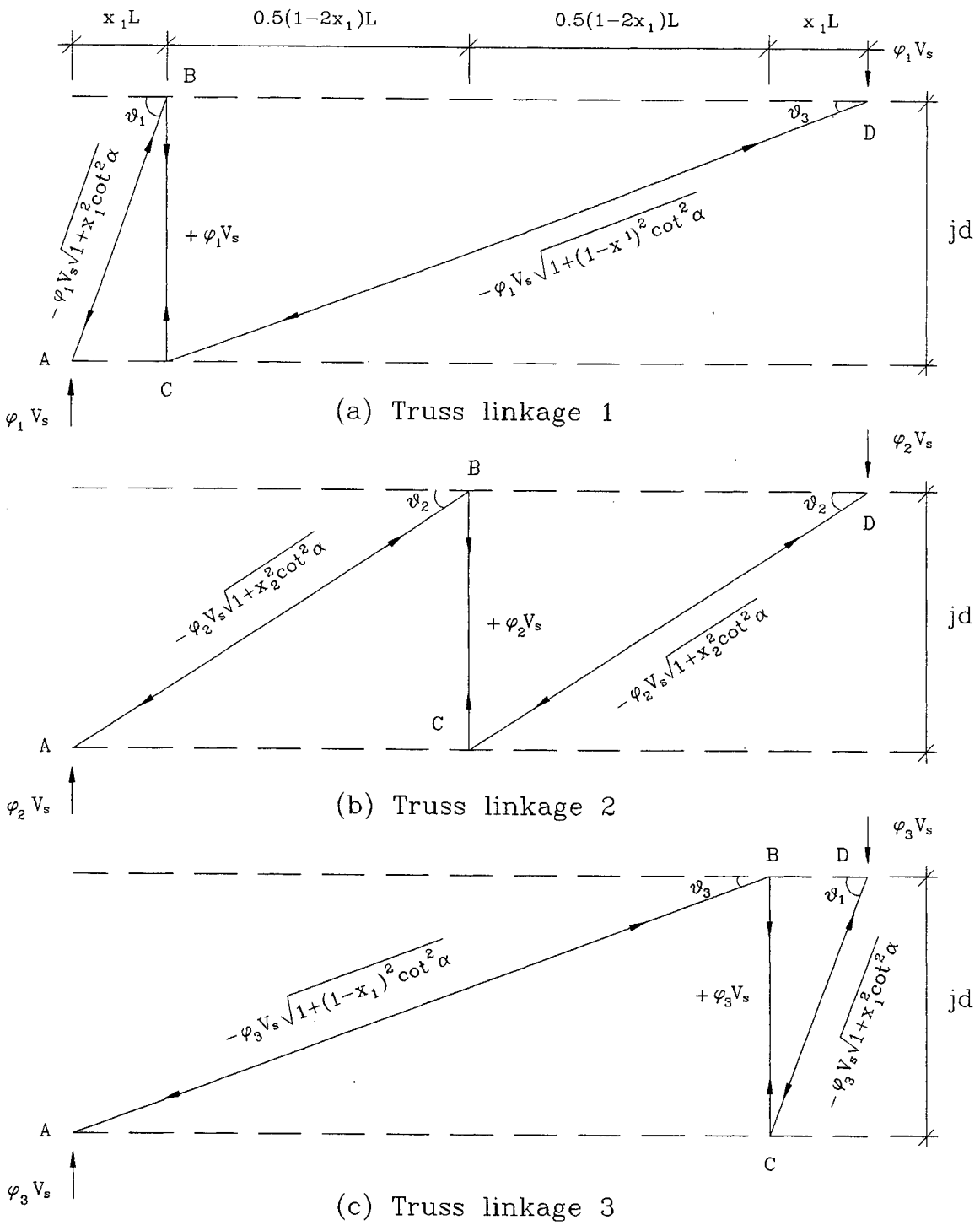

Figure 2-11. Decoupled linkages of three-point Gauss truss model.

model with fixed-fixed and fixed-pinned ends should be the same. Therefore, it can be said that the boundary conditions of the column do not affect the features of column shear. The distribution factors ϕ_i of the shear force V_s for each truss linkage in figures 2-9 and 2-11 are not clearly defined at present because the truss model due to three-point Gauss quadrature is statically indeterminate. Those unknown factors will be defined using the geometry and displacement compatibility at ends of the truss model in what follows.

First, consider the truss linkage 1 with member forces in figure 2-11(a). The shear deformation of the truss linkage 1 is determined using the Virtual Work method of analysis. The analysis is presented in table 2-7.

Table 2-7. Virtual work done on the truss linkage 1 of the three-point Gauss truss model.

Mem	Force F	Unit Load f	Length l	Rigidity EA	Strain $\varepsilon = F/EA$	Deformation $\frac{Ffl}{EA}$
B-C	$+\phi_1 V_s$	$+1$	jd	$\omega_1 E_s A_{sh} \frac{L}{s}$	$\frac{+\phi_1 V_s s}{\omega_1 E_s A_{sh} L}$	$\frac{\phi_1 V_s jd s}{\omega_1 E_s A_{sh} L}$
A-B	$\frac{-\phi_1 V_s}{\sin\theta_1}$	$\frac{-1}{\sin\theta_1}$	$\frac{jd}{\sin\theta_1}$	$a_1 E_c A_v$	$\frac{-\phi_1 V_s}{a_1 E_c A_v \sin\theta_1}$	$\frac{\phi_1 jd V_s}{a_1 E_c A_v \sin^3\theta_1}$
C-D	$\frac{-\phi_1 V_s}{\sin\theta_3}$	$\frac{-1}{\sin\theta_3}$	$\frac{jd}{\sin\theta_3}$	$a_3 E_c A_v$	$\frac{-\phi_1 V_s}{a_3 E_c A_v \sin\theta_3}$	$\frac{\phi_1 jd V_s}{a_3 E_c A_v \sin^3\theta_3}$

Note:
1. Refer to figure 2-11(a) for member forces.
2. Refer to equations (2-16) and (2-18) for member rigidities.

$$\sin\theta_1 = \frac{1}{\sqrt{1 + x_1^2 \cot^2\alpha}} \; ; \quad \sin\theta_3 = \frac{1}{\sqrt{1 + (1 - x_1)^2 \cot^2\alpha}}$$

The shear deformation of the truss linkage 1 is the sum of the deformation components. Recalling that $\cot\alpha = L/jd$ and $\rho_v = A_{sh}/b_w s$, the shear deformation is

$$\Delta_s = \sum \frac{Ffl}{EA}$$

$$= \frac{\phi_1 V_s jd \tan\alpha}{E_c A_v \omega_1 \rho_v n}\left(1 + \frac{\omega_1 \rho_v n\left\{1 + x_1^2 \cot^2\alpha\right\}^2}{a_1 \tan\alpha \sqrt{1 + x_1^2 \cot^2\alpha}} + \frac{\omega_1 \rho_v n\left\{1 + (1 - x_1)^2 \cot^2\alpha\right\}^2}{a_3 \tan\alpha \sqrt{1 + (1 - x_1)^2 \cot^2\alpha}}\right) \quad (2\text{-}37)$$

The shear strain (rotation) is then determined by dividing the shear displacement by the length of the truss linkage, thus

$$\Theta_s = \frac{\Delta_s}{L}$$

$$= \frac{\phi_1 V_s \tan^2\alpha}{E_c A_v \omega_1 \rho_v n}\left(1 + \frac{\omega_1 \rho_v n\left\{1 + x_1^2 \cot^2\alpha\right\}^2}{a_1 \tan\alpha \sqrt{1 + x_1^2 \cot^2\alpha}} + \frac{\omega_1 \rho_v n\left\{1 + (1 - x_1)^2 \cot^2\alpha\right\}^2}{a_3 \tan\alpha \sqrt{1 + (1 - x_1)^2 \cot^2\alpha}}\right) \quad (2\text{-}38)$$

Therefore, the shear stiffness of truss linkage 1 for the applied shear force $\phi_1 V_s$ is obtained as

$$K_{s1} = \frac{\omega_1 \rho_v n \cot^2\alpha}{1 + \frac{\omega_1 \rho_v n\left\{1 + x_1^2 \cot^2\alpha\right\}^2}{a_1 \tan\alpha \sqrt{1 + x_1^2 \cot^2\alpha}} + \frac{\omega_1 \rho_v n\left\{1 + (1 - x_1)^2 \cot^2\alpha\right\}^2}{a_3 \tan\alpha \sqrt{1 + (1 - x_1)^2 \cot^2\alpha}}} E_c A_v \quad (2\text{-}39)$$

It should be noted that the unknown factor ϕ_1 for the distribution of shear force V_s due to indeterminacy of the truss model is no more included in equation (2-39).

Next, consider the truss linkage 2 with member forces in figure 2-11(b). The shear deformation of the truss linkage 2 is then determined using the Virtual Work method of analysis. The analysis is presented in table 2-8.

The shear deformation of the truss linkage 2 is the sum of the deformation components. Recalling that $\cot\alpha = L/jd$ and $\rho_v = A_{sh}/b_w s$, the shear deformation is given by

$$\Delta_s = \sum \frac{Ffl}{EA} = \frac{\phi_2 V_s jd}{E_c A_v \omega_2 \rho_v n \cot\alpha}\left(1 + \frac{2\omega_2 \rho_v n \cot\alpha\left\{1 + x_2^2 \cot^2\alpha\right\}^2}{a_2 \sqrt{1 + x_2^2 \cot^2\alpha}}\right) \quad (2\text{-}40)$$

Table 2-8. Virtual work done on the truss linkage 2 of the three-point Gauss truss model.

Member	Force F	Unit Load f	Length l	Rigidity EA	Strain $\varepsilon = F/EA$	Deformation $\frac{Ffl}{EA}$
B-C	$+\phi_2 V_s$	$+1$	jd	$\omega_2 E_s A_{sh} \frac{L}{s}$	$\frac{+\phi_2 V_s s}{\omega_2 E_s A_{sh} L}$	$\frac{\phi_2 V_s jd s}{\omega_2 E_s A_{sh} L}$
A-B, C-D	$\frac{-\phi_2 V_s}{\sin\theta_2}$	$\frac{-1}{\sin\theta_2}$	$\frac{jd}{\sin\theta_2}$	$a_2 E_c A_v$	$\frac{-\phi_2 V_s}{a_2 E_c A_v \sin\theta_2}$	$\frac{\phi_2 V_s jd}{a_2 E_c A_v \sin^3\theta_2}$

Note:
1. Refer to figure 2-11(b) for member forces.
2. Refer to equations (2-16) and (2-18) for member rigidities.

$$\sin\theta_2 = \frac{1}{\sqrt{1 + x_2^2 \cot^2\alpha}}$$

The shear strain (rotation) is then determined by dividing the shear displacement by the length of the truss linkage 2, thus

$$\Theta_s = \frac{\Delta_s}{L} = \frac{\phi_2 V_s}{E_c A_v \omega_2 \rho_v n \cot^2\alpha}\left(1 + \frac{2\omega_2 \rho_v n \cot\alpha \left\{1 + x_2^2 \cot^2\alpha\right\}^2}{a_2 \sqrt{1 + x_2^2 \cot^2\alpha}}\right) \qquad (2\text{-}41)$$

Therefore, the shear stiffness of the truss linkage 2 for the applied shear force $\phi_2 V_s$ is obtained by

$$K_{s2} = \frac{\omega_2 \rho_v n \cot^2\alpha}{1 + \frac{2\omega_2 \rho_v n \cot\alpha \left\{1 + x_2^2 \cot^2\alpha\right\}^2}{a_2 \sqrt{1 + x_2^2 \cot^2\alpha}}} E_c A_v \qquad (2\text{-}42)$$

Now, the geometrical symmetry of the truss model of three-point Gauss quadrature requires that the shear resistances of truss linkages 1 and 3 are the same, that is, $\phi_1 = \phi_3$ (see figures 2-9 and 2-11). Therefore, the total shear force resisted by the truss mechanism can be expressed as

$$V_s = (\phi_1 + \phi_2 + \phi_3) V_s = (2\phi_1 + \phi_2) V_s \tag{2-43}$$

in which $2\phi_1 + \phi_2 = 1$. Using this relationship, the total combined shear stiffness of the concrete column represented by the simplified truss model can be obtained as

$$K_s = 2K_{s1} + K_{s2} \tag{2-44}$$

Substituting equations (2-39) and (2-42) into equation (2-44) and rearranging,

$$K_s = \frac{2\omega_1 \rho_v n \cot^2\alpha}{1 + 2\rho_v n \left(\frac{\omega_1 \cot\alpha \left\{1 + x_1^2 \cot^2\alpha\right\}^2}{2a_1\sqrt{1 + x_1^2 \cot^2\alpha}} + \frac{\omega_1 \cot\alpha \left\{1 + (1 - x_1)^2 \cot^2\alpha\right\}^2}{2a_3\sqrt{1 + (1 - x_1)^2 \cot^2\alpha}} \right)} E_c A_v$$

$$+ \frac{\omega_2 \rho_v n \cot^2\alpha}{1 + 4\rho_v n \dfrac{\omega_2 \cot\alpha \left\{1 + x_2^2 \cot^2\alpha\right\}^2}{2a_2\sqrt{1 + x_2^2 \cot^2\alpha}}} E_c A_v \tag{2-45}$$

The cracked elastic shear stiffness of concrete columns given by equation (2-14) for three-point Gauss quadrature is

$$K_s = \frac{2\omega_1 \rho_v n \cot^2\alpha}{1 + 2\rho_v n \left(\frac{b_w}{b_{ws}} \right) \left(\left\{1 + x_1^2 \cot^2\alpha\right\}^2 + \left\{1 + (1 - x_1)^2 \cot^2\alpha\right\}^2 \right)} E_c A_v$$

$$+ \frac{\omega_2 \rho_v n \cot^2\alpha}{1 + 4\rho_v n \left(\frac{b_w}{b_{ws}} \right) \left\{1 + x_2^2 \cot^2\alpha\right\}^2} E_c A_v \tag{2-46}$$

The stiffnesses given by equations (2-45) and (2-46) should be the same. Therefore, the effective section area factors for diagonal struts can be obtained by comparing equations (2-45) and (2-46), thus,

$$a_i = \frac{0.5\,\omega_i \cot\alpha}{\sqrt{1 + x_i^2 \cot^2\alpha}} \left(\frac{b_{ws}}{b_w} \right) \tag{2-47}$$

The axial rigidities of the diagonal struts of the truss model in figures 2-9 and 2-11 are determined by

$$(EA)_{di} = \frac{0.5\,\omega_i}{\sqrt{x_i^2 + \tan^2\alpha}} E_c A_v \left(\frac{b_{ws}}{b_w}\right) \tag{2-48}$$

in which $x_3 = 1 - x_1$, $\omega_3 = \omega_1$ and $A_{vs} = b_{ws} jd$. The values of numerical coordinates x_i and weighting factors ω_i for three-point Gauss quadrature are defined in table 2-3. As mentioned previously, the section areas of diagonal struts can alternatively be obtained by measuring the depth of the diagonal struts along the truss center line on the scaled drawing as shown in figure 2-10(b). However, equation (2-48) provides the simpler and more accurate way in determining axial rigidities of diagonal struts in normal cases. Note that equations (2-24) and (2-48) are identical, which means that the axial rigidities of the diagonal struts of the truss model with any numerical integration scheme can be simply determined using equation (2-48) and the corresponding parameter values are available in table 2-3. The corresponding compressive axial stress in ith diagonal strut is obtained from tables 2-7 and 2-8, thus

$$f_{cdi} = E_c \varepsilon_{cdi} = \frac{-4\,\phi_i V_s \left\{1 + x_i^2 \cot^2\alpha\right\}}{A_v \left(\frac{b_{ws}}{b_w}\right) \cot\alpha} \tag{2-49}$$

The location of ith diagonal strut is depicted in figure 2-9(a).

The distribution factor ϕ_i of shear force V_s is now investigated. Consider the compound truss in figures 2-9 and 2-11. Then, the displacement compatibility at both ends of the truss requires that the shear displacement of truss linkages be the same all the time, that is,

$$(\Delta_s)_{Linkage1} = (\Delta_s)_{Linkage2} = (\Delta_s)_{Linkage3} \tag{2-50}$$

Therefore, by equating equations (2-37) and (2-40) with a_i determined by equation (2-48) the relationship between ϕ_1 and ϕ_2 can be obtained as

$$\phi_1 = \frac{\frac{\omega_1}{\omega_2}\left(1 + 4\,\rho_v n\left(\frac{b_w}{b_{ws}}\right)\left\{1 + x_2^2\cot^2\alpha\right\}^2\right)}{1 + 2\,\rho_v n\left(\frac{b_w}{b_{ws}}\right)\left(\left\{1 + x_1^2\cot^2\alpha\right\}^2 + \left\{1 + (1-x_1)^2\cot^2\alpha\right\}^2\right)}\,\phi_2 \qquad (2\text{-}51)$$

where $\phi_1 = \phi_3$. Relating this equation to equation (2-43), the shear force distribution factor ϕ_i can be defined as

$$\phi_1 = \phi_3 = \frac{1}{2 + \frac{1 + 2\,\rho_v n\left(\frac{b_w}{b_{ws}}\right)\left(\left\{1 + x_1^2\cot^2\alpha\right\}^2 + \left\{1 + (1-x_1)^2\cot^2\alpha\right\}^2\right)}{0.625\left(1 + 4\,\rho_v n\left(\frac{b_w}{b_{ws}}\right)\left\{1 + x_2^2\cot^2\alpha\right\}^2\right)}} \qquad (2\text{-}52a)$$

$$\phi_2 = \frac{1}{1 + \frac{1.25\left(1 + 4\,\rho_v n\left(\frac{b_w}{b_{ws}}\right)\left\{1 + x_2^2\cot^2\alpha\right\}^2\right)}{1 + 2\,\rho_v n\left(\frac{b_w}{b_{ws}}\right)\left(\left\{1 + x_1^2\cot^2\alpha\right\}^2 + \left\{1 + (1-x_1)^2\cot^2\alpha\right\}^2\right)}} \qquad (2\text{-}52b)$$

The tensile strains of the transverse ties of the truss model are readily available in tables 2-7 and 2-8, that is

$$\varepsilon_{Ti} = \frac{\Delta_{Ti}}{jd} = \frac{V_s}{E_c A_v \rho_v n \cot\alpha}\left(\frac{\phi_i}{\omega_i}\right) \qquad (2\text{-}53)$$

where ε_{Ti} = tensile strain of the transverse ties and Δ_T = axial deformation of the transverse ties of the truss model and the transverse tie strains at linkages 1 and 3 are the same. It should be noted that the tensile strain is the maximum at the center of the member as shown in figure 2-12. Whereas, the transverse hoop strain given by the two-point Gauss truss model is the overall average for the column. Therefore, the ratio of the maximum transverse hoop strain to the minimum in the three-point Gauss truss model can be obtained from equation (2-53):

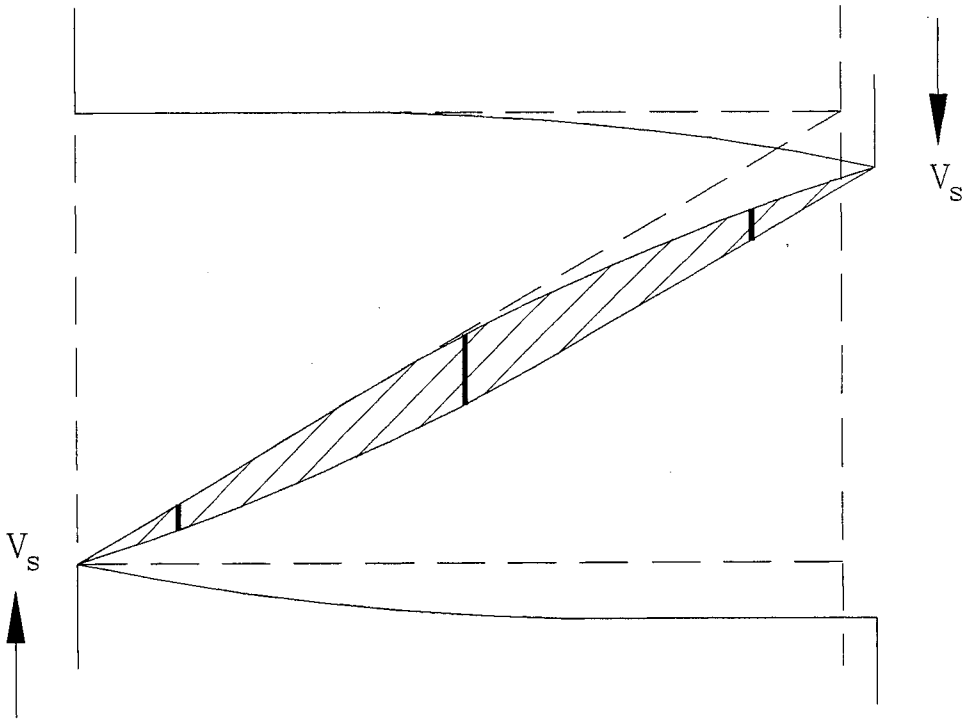

Figure 2-12. Elongation of transverse ties across a diagonally cracked zone.

$$\frac{\varepsilon_{T\text{-max}}}{\varepsilon_{T\text{-min}}} = \frac{\varepsilon_{T2}}{\varepsilon_{T1}} = \left(\frac{\phi_2}{\phi_1}\right)\left(\frac{\omega_1}{\omega_2}\right) = 0.625\,\frac{\phi_2}{\phi_1} \tag{2-54}$$

where values of ω_i are defined in table 2-3. Compared to the average tensile strain of the transverse hoops in the two-point Gauss truss model given by equation (2-26), the ratio of the maximum and minimum transverse hoop strain to the average is respectively given by

$$\frac{\varepsilon_{T\text{-max}}}{\varepsilon_{T\text{-avg}}} = \frac{\varepsilon_{T2}}{\varepsilon_{T\text{-avg}}} = \frac{\phi_2}{\omega_2} \tag{2-55a}$$

$$\frac{\varepsilon_{T\text{-min}}}{\varepsilon_{T\text{-avg}}} = \frac{\varepsilon_{T1}}{\varepsilon_{T\text{-avg}}} = \frac{\phi_1}{\omega_1} \tag{2-55b}$$

2.2.7.2 Flexural Deformation

Consider a truss model with fixed-fixed ends shown in figure 2-9(b). As in the truss model with two-point Gauss quadrature, no compression forces are generated over the entire length of the model. The flexural deformation of the truss model can be determined using the Virtual Work method of analysis on the longitudinal chord members. The analysis is presented in table 2-9.

The flexural deformation of the simplified truss model is the sum of the component deformations, thus

$$\Delta_f = \sum_{i=1}^{8} \frac{Ffl}{EA} = \zeta \frac{V_s L \cot^2 \alpha}{E_s A_{st}} \tag{2-56}$$

where $\zeta = x_1 + (1-2x_1)\left\{2\phi_1^2(1-x_1)^2 + 0.5(1-2\phi_1 x_1)^2\right\}$. The flexural drift angle is then determined by dividing the flexural displacement by the length of the truss model, thus

$$\Theta_f = \frac{\Delta_f}{L} = \zeta \frac{V_s \cot^2 \alpha}{E_s A_{st}} \tag{2-57}$$

Table 2-9. Virtual work done on longitudinal chord members of three-point Gauss truss model with fixed-fixed ends.

Member	Force F	Unit Load f	Length l	Rigidity EA	Strain $\varepsilon = F/EA$	Deformation $\frac{Ffl}{EA}$
(1)(8)	$\frac{+V_s}{2\tan\alpha}$	$\frac{+1}{2\tan\alpha}$	$x_1 L$	$\frac{E_s A_{st}}{2}$	$\frac{+V_s\cot\alpha}{E_s A_{st}}$	$\frac{V_s x_1 L\cot^2\alpha}{2E_s A_{st}}$
(2)(7)	0	0	$x_1 L$	$\frac{E_s A_{st}}{2}$	0	0
(3)(6)	$\frac{+V_s Q_1}{2\tan\alpha}$	$\frac{+Q_1}{2\tan\alpha}$	$\frac{Q_3 L}{2}$	$\frac{E_s A_{st}}{2}$	$\frac{+V_s Q_1}{E_s A_{st}\tan\alpha}$	$\frac{V_s Q_1^2 Q_3 L}{4E_s A_{st}\cot^2\alpha}$
(4)(5)	$\frac{+V_s Q_2}{2\tan\alpha}$	$\frac{+Q_2}{2\tan\alpha}$	$\frac{Q_3 L}{2}$	$\frac{E_s A_{st}}{2}$	$\frac{+V_s Q_2}{E_s A_{st}\tan\alpha}$	$\frac{V_s Q_2^2 Q_3 L}{4E_s A_{st}\cot^2\alpha}$

Refer to figure 2-10(b) for member forces.

where $Q_1 = 1 - 2\phi_1 x_1$; $Q_2 = 1 - 2\phi_1 x_1 - \phi_2$; $Q_3 = 1 - 2x_1$.

Therefore, the elastic flexural stiffness of a cracked concrete column about drift angle due to the variable angle truss model with fixed-fixed ends is

$$K_{f\theta} = \zeta^{-1} E_s A_{st}\tan^2\alpha \tag{2-58}$$

The corresponding tensile strain of the longitudinal chord at the critical region can be determined by the average strain over the chord length of $x_1 L$ in figure 2-9(b) and is readily available in table 2-9. Thus

$$\varepsilon_L = \frac{\Delta_L}{x_1 L} = \frac{V_s\cot\alpha}{E_s A_{st}} \tag{2-59}$$

where Δ_L = longitudinal elongation of truss member (1) or (8) in figure 2-9(b).

Consider a truss model with fixed-pinned ends shown in figure 2-9(c). The flexural deformation of the truss model can be determined by the Virtual Work method of analysis on the longitudinal chord members in figure 2-9(c). The analysis is presented in table 2-10.

Table 2-10. Virtual work done on longitudinal chord members of three-point Gauss truss model with fixed-pinned ends

Member	Force F	Unit Load f	Length l	Rigidity EA	Strain $\varepsilon = F/EA$	Deformation $\frac{Ffl}{EA}$
(1)	$\frac{+V_s}{\tan\alpha}$	$\frac{+1}{\tan\alpha}$	$x_1 L$	$\frac{E_s A_{st}}{2}$	$\frac{+2\,V_s \cot\alpha}{E_s A_{st}}$	$\frac{2\,V_s x_1 L \cot^2\alpha}{E_s A_{st}}$
(2)	$\frac{-V_s}{2\tan\alpha}$	$\frac{-1}{2\tan\alpha}$	$x_1 L$	$\frac{E_s A_{st}}{2}$	$\frac{-V_s \cot\alpha}{E_s A_{st}}$	$\frac{V_s x_1 L \cot^2\alpha}{2 E_s A_{st}}$
(3)	$\frac{+V_s Q_1}{\tan\alpha}$	$\frac{+Q_1}{\tan\alpha}$	$\frac{Q_4 L}{2}$	$\frac{E_s A_{st}}{2}$	$\frac{+2\,V_s Q_1}{E_s A_{st}\tan\alpha}$	$\frac{V_s Q_1^2 Q_4 L}{E_s A_{st}\tan^2\alpha}$
(4)	$\frac{-V_s Q_2}{\tan\alpha}$	$\frac{-Q_2}{\tan\alpha}$	$\frac{Q_4 L}{2}$	$\frac{E_s A_{st}}{2}$	$\frac{-2\,V_s Q_2}{E_s A_{st}\tan\alpha}$	$\frac{V_s Q_2^2 Q_4 L}{E_s A_{st}\tan^2\alpha}$
(5)	$\frac{+V_s Q_3}{\tan\alpha}$	$\frac{+Q_3}{\tan\alpha}$	$\frac{Q_4 L}{2}$	$\frac{E_s A_{st}}{2}$	$\frac{+2\,V_s Q_3}{E_s A_{st}\tan\alpha}$	$\frac{V_s Q_3^2 Q_4 L}{E_s A_{st}\tan^2\alpha}$
(6)	$\frac{-\phi_1 x_1 V_s}{\tan\alpha}$	$\frac{-\phi_1 x_1}{\tan\alpha}$	$\frac{Q_4 L}{2}$	$\frac{E_s A_{st}}{2}$	$\frac{-2\,V_s \phi_1 x_1}{E_s A_{st}\tan\alpha}$	$\frac{V_s \phi_1^2 x_1^2 Q_4 L}{E_s A_{st}\tan^2\alpha}$
(7)	$\frac{+V_s}{2\tan\alpha}$	$\frac{+1}{2\tan\alpha}$	$x_1 L$	$\frac{E_s A_{st}}{2}$	$\frac{+V_s \cot\alpha}{E_s A_{st}}$	$\frac{V_s x_1 L \cot^2\alpha}{2 E_s A_{st}}$
(8)	0	0	$x_1 L$	$\frac{E_s A_{st}}{2}$	0	0

Note: Refer to figure 2-9(c) for member forces.

where $Q_1 = 1 - \phi_1 x_1$; $Q_2 = \phi_1 x_1 + \frac{1}{2}\phi_2$; $Q_3 = 1 - \phi_1 x_1 - \frac{1}{2}\phi_2$; $Q_4 = 1 - 2x_1$.

The flexural deformation of the simplified truss model is the sum of the component deformations taking the value of numerical coordinate x_1 from table 2-3, thus

$$\Delta_f = \sum_{i=1}^{8} \frac{Ffl}{EA} = \zeta \frac{V_s L \cot^2 \alpha}{E_s A_{st}} \tag{2-60}$$

where $\zeta = 3x_1 + (1-2x_1)\{(1-\phi_1 x_1)^2 + (1-\phi_1 x_1 - \phi_2 x_2)^2 + (\phi_1 x_1 + \phi_2 x_2)^2 + \phi_1^2 x_1^2\}$. The flexural drift angle is then determined by dividing the flexural displacement by the length of the truss model, thus

$$\theta_f = \frac{\Delta_f}{L} = \zeta \frac{V_s \cot^2 \alpha}{E_s A_{st}} \tag{2-61}$$

Therefore, the elastic flexural stiffness of a cracked concrete column about the drift angle due to the variable angle truss model with fixed-pinned ends is

$$K_{f\theta} = \zeta^{-1} E_s A_{st} \tan^2 \alpha \tag{2-62}$$

The corresponding tensile strain of the longitudinal chord at the critical region can be determined by the average strain over the chord length of $x_1 L$ in figure 2-9(c) and is readily obtained from table 2-10. Thus,

$$\varepsilon_L = \frac{\Delta_L}{x_1 L} = \frac{2 V_s \cot \alpha}{E_s A_{st}} \tag{2-63}$$

where Δ_L = longitudinal elongation of truss member (1) in figure 2-9(c).

2.3 Determination of Crack Angle θ

2.3.1 Theoretical Basis from Energy Considerations

As noted previously, the crack angle in a structural concrete member is very important as it affects both the strength (equations 1-2 and 1-3) and stiffness (equations 2-8 and 2-14) of the member. The theoretical determination of the crack angle θ was first attempted by Dilger *(1966)*. However, this was for a constant angle truss mechanism and concerned only the shear component of displacement.

It is believed in this study that the crack angle in a concrete member depends on both flexure and shear components of displacement and will occur at an orientation that requires the minimum amount of energy.

The external work done on the member due to a unit shear force ($V_s = 1$) is the same as the total drift angle, thus

$$EWD = \Theta_1 = \Theta_{s,1} + \Theta_{f,1} \tag{2-64}$$

The shear rotation of a column subjected to a unit shear force using the constant angle truss mechanism is obtained from equation (2-8b) for $b_{ws}/b_w = 1$ as

$$\Theta_{s,1} = \frac{1 + \rho_v n \operatorname{cosec}^4\theta}{E_c A_v \rho_v n \cot^2\theta} \tag{2-65}$$

Recalling that $n = E_s/E_c$ and $\rho_t = A_{st}/A_g$ and letting $\alpha = \theta$, the flexural drift angle of a squat column subjected to lateral loading may be obtained by rearranging equations (2-28) and (2-33) as

$$\Theta_{f,1} = \frac{\zeta \cot^2\theta}{E_c A_g \rho_t n} \tag{2-66}$$

where ζ is a boundary condition constant and may be taken as 0.5704 for a fixed-fixed column and 1.5704 for a fixed-pinned column in which the analysis results of two-point Gauss truss are used for simplicity. Therefore, the external work given by equation (2-64) can be rewritten as

$$EWD = \frac{1 + \rho_v n \operatorname{cosec}^4\theta}{E_c A_v \rho_v n \cot^2\theta} + \frac{\zeta \cot^2\theta}{E_c A_g \rho_t n} \tag{2-67}$$

Thus by differentiating equation (2-67) with respect to θ and minimizing the external work done leads to the crack angle causing the minimum energy:

$$\frac{d(EWD)}{d\theta} = 0 \tag{2-68}$$

Carrying out the differentiation of equation (2-68) leads to the following solution for the crack angle θ:

$$\theta = \tan^{-1}\left(\frac{\rho_v n + \zeta \frac{\rho_v}{\rho_t}\frac{A_v}{A_g}}{1 + \rho_v n}\right)^{\frac{1}{4}} \qquad (2\text{-}69)$$

The crack angle given by equation (2-69) denotes the steepest crack angle measured to the longitudinal axis of the fan-shaped cracks at the disturbed region of the column and the constant crack angle at the undisturbed region.

2.3.2 Validation with Experimental Observations

It is considered important to validate the theoretical crack angle with cracks observed in previous experimental investigations. Unfortunately, there is a paucity of data with good photographic documentation of crack distribution to be found in the literature. Table 2-11 presents a comparison of experimentally observed crack angles with crack angles computed using equation (2-69). This table gives results of columns with a light amount of transverse reinforcement as well as more highly confined columns. The comparison is also made in figure 2-13 by visualizing the data in table 2-11. It is evident that the theoretical results using equation (2-69) compare very favorably with the experimentally observed crack angle. It is considered that this finding is of particular significance as it shows the dependence of the crack angle on the quantity of longitudinal and transverse reinforcement. Thus it is clearly evident that the crack angle of 45° that has been traditionally assumed in the ACI 318 code *(1995)* for many decades as well as the newly suggested $\theta = 30°$ recommended by Priestley, et al. *(1994a,b,c)* that has been recently incorporated into the FHWA Seismic Retrofit Manual *(Buckle and Friedland, 1995)* both lead to a faulty prediction of shear strength.

2.4 Parametric Studies

In this subsection, parametric studies for the boundary condition constant ζ of three-point Gauss truss model, its effect on the theoretical determination of crack angle θ, distribution of tensile strain at transverse steel over the length of a cracked column, and the effective stiffnesses of concrete beam-columns are presented.

Table 2-11. Crack angle comparison between theory and experiment.

Specimen	Boundary	n	ρ_t	ρ_v	A_v/A_g	θ_{theory}	$\theta_{exp.}$
A) 1/3 Pier Model[a]	F-F	5.7	0.0186	0.00147	0.756	24.3°	26°
B) Prototype[a]	F-P	6.3	0.0186	0.00115	0.746	27.9°	26°
C) 1/3 Model[b]	F-P	6.0	0.0102	0.00492	0.701	40.7°	39°
D) Column - A[c]	F-P	7.8	0.0156	0.00785	0.405	37.8°	36°
E) Column - C[c]	F-P	7.9	0.0156	0.01178	0.405	40.4°	39°
F) Column - D[c]	F-P	7.9	0.0156	0.00785	0.405	37.8°	33°
G) Circular - C1[d]	F-F	7.2	0.0254	0.00089	0.852	21.3°	22°
H) Rectangular - R2[d]	F-F	7.2	0.0255	0.00102	0.901	22.2°	23°
I) Unit_9[e]	F-P	7.8	0.032	0.00518	0.828	35.0°	35°
J) Unit_13[e]	F-P	7.1	0.032	0.00518	0.828	34.9°	35°
K) Unit_14[e]	F-P	7.3	0.0324	0.00259	0.828	30.5°	31°
L) Unit_16[e]	F-P	7.4	0.032	0.00259	0.828	30.6°	32°
M) 2R10-60u[f]	F-P	7.8	0.032	0.00727	0.81	37.1°	38°
N) 4R6-65u[f]	F-P	7.8	0.032	0.00239	0.828	30.1°	26°
O) 4R10-60u[f]	F-P	7.8	0.032	0.00727	0.81	37.1°	36°
P) 0R6-80b[f]	F-P	7.8	0.032	0.00194	0.828	28.9°	29°
Q) 2R6-60b[f]	F-P	7.8	0.032	0.00259	0.828	30.6°	30°
R) R1A[g]	F-F	6.9	0.025	0.00123	0.881	23.0°	24°
S) R3A[g]	F-F	7.2	0.025	0.00123	0.881	23.1°	24°
T) R5A[g]	F-F	7.5	0.025	0.00123	0.881	23.1°	22°

[a]Niagara Parkway bridge pier circular column tested by Mander, et al. *(1996a,b)*.

[b]Seismically designed circular column tested by Mander and Cheng *(1995)*.

[c]Square hollow-core columns tested by Mander et al. *(1984)*.

[d]Specimens tested by Chai, et al. *(1990)*.

[e]Circular columns tested by Ang, et al. *(1989)*.

[f]Circular columns tested by Wong *(1990)*.

[g]Rectangular columns tested by Priestley, et al. *(1994a,b)*.

F-F: Fixed-fixed ends.

F-P: Fixed-pinned ends.

Note: Comparison is also made in figure 2-13.

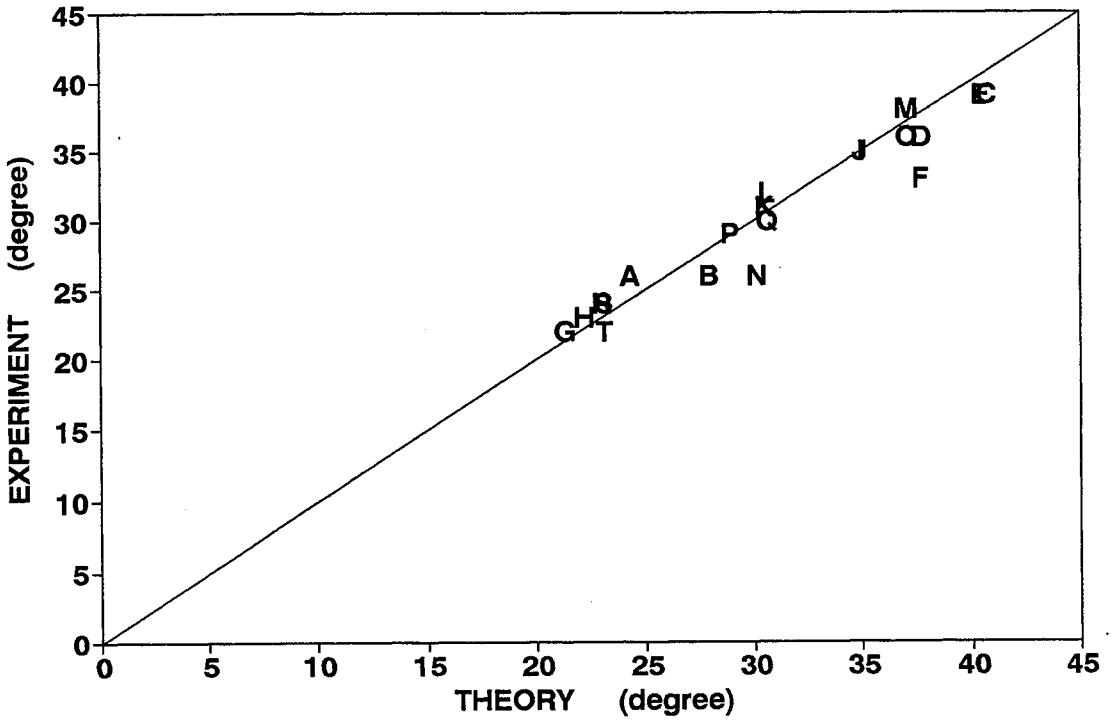

Figure 2-13. Crack angle comparison between theory and experiment (Note: letters define data points and refer to table 2-11).

2.4.1 Boundary Condition Constants of Three-Point Gauss Truss Model

It is of interest to quantify the boundary condition coefficient ζ shown in equations (2-56) through (2-62) given for cracked elastic flexural deformation determined by three-point Gauss truss model so that it can be compared with the results of two-point Gauss truss model as well as Bernoulli's beam theory. Table 2-12 presents the values of boundary condition constant ζ for those specimens that have been also used for the crack angle calculation in table 2-11. Those experimental specimens show the wide range of transverse steel contents. It is noted that the corner-to-corner angle α was set to be equal to the constant crack angle θ and $b_{ws}/b_w = 1$ for the calculation of shear force distribution factor ϕ_1 and ϕ_2. It is also noted at a glance that the boundary condition constants ζ determined by the three-point Gauss truss model analysis tend to be approximately 0.54 for fixed-fixed ends and 1.54 for fixed-pinned ends no matter what the transverse and longitudinal steel contents are. These results are close to those determined by the two-point Gauss truss model which are 0.5704 for fixed-fixed ends and 1.5704 for fixed-pinned ends. It is found from the present study that $\zeta(\textit{fixed-fixed}) = \zeta(\textit{fixed-pinned}) + 1$ in both two-point and three-point Gauss truss models. Moreover, the results show that the boundary condition constants are almost constant along the wide range of transverse steel contents. Therefore, it is concluded that the two-point Gauss truss model is sufficient to determine the post-cracked elastic flexural stiffness of beam-columns.

2.4.2 Crack Angle Determination Using Three-Point Gauss Truss Model

Determination of the theoretical crack angle θ based on energy minimization has been demonstrated in table 2-11. For this purpose, the shear deformation of the constant angle truss model and the flexural deformation of the variable angle truss represented by two-point Gauss truss model, both subjected to a unit shear force, were considered. The components of shear and flexural contribution are included in equation (2-69). The effect of three-point Gauss truss model on determination of the theoretical crack angle can be investigated by using the corresponding boundary condition constants determined previously. As expected, there is no

Table 2-12. Coefficients for elastic flexural stiffness of cracked concrete columns determined by three-point Gauss truss model.

Specimen	n	ρ_v	ϕ_1	ϕ_2	ζ $(F\text{-}F)$	ζ $(F\text{-}P)$
A) 1/3 Pier Model[a]	5.7	0.00147	0.25315	0.49370	0.535225	1.535225
B) Prototype[a]	6.3	0.00115	0.26456	0.47088	0.540553	1.540553
C) 1/3 Model[b]	6.0	0.00492	0.26773	0.46454	0.542092	1.542092
D) Column - A[c]	7.8	0.00785	0.25539	0.48922	0.536245	1.536245
E) Column - C[c]	7.9	0.01178	0.25516	0.48969	0.536138	1.536138
F) Column - D[c]	7.9	0.00785	0.25518	0.48964	0.536149	1.536149
G) Circular - C1[d]	7.2	0.00089	0.24640	0.50720	0.532224	1.532224
H) Rectangular - R2[d]	7.2	0.00102	0.24713	0.50575	0.532542	1.532542
I) Unit_9[e]	7.8	0.00518	0.25551	0.48890	0.536319	1.536319
J) Unit_13[e]	7.1	0.00518	0.25680	0.48641	0.536893	1.536893
K) Unit_14[e]	7.3	0.00259	0.25685	0.48630	0.536917	1.536917
L) Unit_16[e]	7.4	0.00259	0.25695	0.48611	0.536961	1.536961
M) 2R10-60u[f]	7.8	0.00727	0.25511	0.48979	0.536115	1.536115
N) 4R6-65u[f]	7.8	0.00239	0.25629	0.48743	0.536657	1.536657
O) 4R10-60u[f]	7.8	0.00727	0.25511	0.48979	0.536115	1.536115
P) 0R6-80b[f]	7.8	0.00194	0.25651	0.48699	0.536758	1.536758
Q) 2R6-60b[f]	7.8	0.00259	0.25620	0.48759	0.536619	1.536619
R) R1A[g]	6.9	0.00123	0.24760	0.50481	0.532748	1.532748
S) R3A[g]	7.2	0.00123	0.24679	0.50642	0.532395	1.532395
T) R5A[g]	7.5	0.00123	0.24627	0.50747	0.532165	1.532165
Average			0.2545	0.4909	0.5359	1.5359

[a]Niagara Parkway bridge pier circular column tested by Mander, et al. *(1996a,b)*.

[b]Seismically designed circular column tested by Mander and Cheng *(1995)*.

[c]Square hollow-core columns tested by Mander et al. *(1984)*.

[d]Specimens tested by Chai, et al. *(1990)*.

[e]Circular columns tested by Ang, et al. *(1989)*.

[f]Circular columns by Wong *(1990)*.

[g]Rectangular columns tested by Priestley, et al. *(1994a,b)*.

F-F: Fixed-fixed ends.

F-P: Fixed-pinned ends.

significant difference in theoretically determined crack angle between two-point and three-point Gauss truss models because of closeness of the boundary condition constants.

2.4.3 Strains at Transverse Steel

It is of interest to compare the maximum and minimum tensile strains of the transverse steel in a cracked concrete column. As previously mentioned, the tensile strain of the transverse ties in the two-point Gauss truss model given by equation (2-26) represents the average ($\varepsilon_{T\text{-}avg}$) of the transverse steel strain over the length of the concrete column. That is,

$$\varepsilon_{T\text{-}avg} = \frac{V_s}{E_c A_v \rho_v n \cot\alpha} \tag{2-26}$$

In the three-point Gauss truss model, the transverse tie strain at linkage 1 represents the minimum tensile strain ($\varepsilon_{T\text{-min}}$) while the transverse tie strain at linkage 2 represents the maximum tensile strain ($\varepsilon_{T\text{-max}}$) as given by equation (2-53) of the transverse hoop steel for the applied shear force. It is noted that the minimum strain occurs at near ends while the maximum strain occurs at the center of a cracked column as shown in figure 2-12.

By examining values of ϕ_1 and ϕ_2 in table 2-12, these parameters can be approximated so that $\phi_1 \approx 0.25$ and $\phi_2 \approx 0.5$ no matter what the transverse and longitudinal steel contents are. Using these values and the values for ω_1 and ω_2 in table 2-3 for equation (2-53), the minimum and maximum tensile strains of transverse steel can be obtained as

$$\varepsilon_{T\text{-min}} = \frac{0.9 V_s}{E_c A_v \rho_v n \cot\alpha} \tag{2-70a}$$

$$\varepsilon_{T\text{-max}} = \frac{1.125 V_s}{E_c A_v \rho_v n \cot\alpha} \tag{2-70b}$$

Therefore, the ratio of maximum tensile strain to the minimum is $\varepsilon_{T\text{-max}} / \varepsilon_{T\text{-min}} = 1.25$ which means that the tensile strain of the transverse steel at the middle will be larger than that at near ends of a cracked column by 25%. Equation (2-54) also gives the same ratio. Also noted is

that the ratio of the maximum tensile strain to the average is $\varepsilon_{T\text{-}max}/\varepsilon_{T\text{-}avg} = 1.125$ while the ratio of the minimum tensile strain to the average is $\varepsilon_{T\text{-}min}/\varepsilon_{T\text{-}avg} = 0.9$ as given by equation (2-55). Figure 2-14 describes the distribution of the tensile strain of the transverse steel over the length of a cracked column.

2.4.4 Effective Stiffness Ratios

The effective stiffness in this study is defined as the total combined stiffness in shear and flexure of reinforced concrete beam-columns and can be obtained by taking the inverse of the total combined flexibility. The total combined flexibility is expressed referring to equation (2-64) as

$$\Theta_1 = \Theta_{s,1} + \Theta_{f,1} \tag{2-71}$$

where $\Theta_{s,1}$ and $\Theta_{f,1}$ are the flexibility in shear and flexure, respectively. The effective stiffness ratio is defined as the ratio of the effective flexural stiffness to the uncracked elastic flexural stiffness of a reinforced concrete beam-column and obtained by the ratio of the effective flexural rigidity EI_{eff} to the rigidity of the uncracked gross section EI_g. The effective flexural flexibility with respect to the drift angle can be expressed referring to equation (2-3) as

$$\Theta_{eff,1} = \frac{\zeta L^2}{EI_{eff}} \tag{2-72}$$

where ζ is the boundary condition constant for uncracked beam-columns and is taken as 1/12 for fixed-fixed ends and 1/3 for fixed-pinned ends. The effective stiffness ratio of a reinforced concrete beam-column can be obtained by equating equations (2-71) and (2-72), that is,

$$\frac{EI_{eff}}{EI_g} = \frac{\zeta L^2}{(\Theta_{s,1} + \Theta_{f,1})EI_g} \tag{2-73}$$

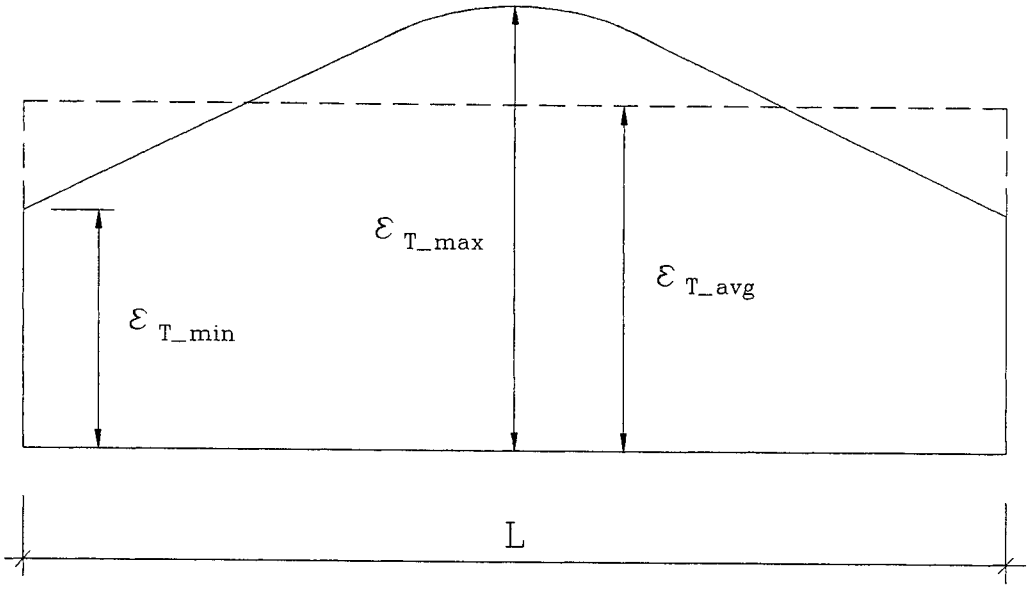

Figure 2-14. Tensile strain at transverse steel over the length of a cracked column.

2.4.4.1 Pre-Cracked Stage

The shear flexibility of a uncracked concrete beam-column is obtained by taking the inverse of equation (2-2). Expressing it more rigorously by including the form factor f_f,

$$\Theta_{s,1} = \frac{2.5 f_f}{E_c A_v} \tag{2-74}$$

where f_f may be taken as 1.2 for rectangular, 1.1 for circular and A_g/A_{web} for hollow-core or I sections. In a manner similar to shear, the flexural flexibility of a uncracked concrete beam-column with respect to the drift angle is obtained by taking the inverse of equation (2-3), that is,

$$\Theta_{f,1} = \frac{\zeta L^2}{EI_g} \tag{2-75}$$

Substituting equations (2-74) and (2-75) into equation (2-73), the effective stiffness ratio of uncracked concrete beam-columns can be obtained as

$$\frac{EI_{eff}}{EI_g} = \frac{1}{1 + \lambda_{un}} \tag{2-76}$$

The parameter λ_{un} for uncracked stage is obtained by section shapes and boundary conditions such that:

$\lambda_{un} = 3\left(\frac{D}{L}\right)^2$ for fixed-fixed rectangular column;
$\lambda_{un} = 0.75\left(\frac{D}{L}\right)^2$ for fixed-pinned rectangular column;
$\lambda_{un} = \frac{33}{16}\left(\frac{D}{L}\right)^2$ for fixed-fixed circular column;
$\lambda_{un} = \frac{33}{64}\left(\frac{D}{L}\right)^2$ for fixed-pinned circular column;
$\lambda_{un} = 5\left[\left(\frac{D}{L}\right)^2 + \left(\frac{D}{L} - 2\frac{t}{L}\right)^2\right]$ for fixed-fixed square hollow-core column; and
$\lambda_{un} = 1.25\left[\left(\frac{D}{L}\right)^2 + \left(\frac{D}{L} - 2\frac{t}{L}\right)^2\right]$ for fixed-pinned square hollow-core column

in which D is the overall depth of a section; L is the column length; and t is the wall thickness of a square hollow-core section.

2.4.4.2 Post-Cracked Stage

The shear flexibility of a cracked elastic concrete beam-column is obtained by taking the inverse of equation (2-8b) which is the expression for column shear stiffness for $b_{ws}/b_w = 1$, that is,

$$\Theta_{s,1} = \frac{1 + \rho_v n \operatorname{cosec}^4\theta}{\rho_v n \cot^2\theta \, E_c A_v} \tag{2-77}$$

The flexural flexibility of a cracked elastic concrete beam-column is obtained directly from equations (2-28), (2-33), (2-57), and (2-61) by putting $V_s = 1$, that is,

$$\Theta_{f,1} = \frac{\zeta \cot^2\alpha}{E_s A_{st}} \tag{2-78}$$

where ζ is the boundary condition constant for two-point Gauss truss model and may be taken as 0.5704 for fixed-fixed column and 1.5704 for fixed-pinned column. Substituting equations (2-77) and (2-78) into equation (2-73) and recalling that $\rho_v = A_{sh}/b_w s$, $\rho_t = A_{st}/A_g$ and $n = E_s/E_c$ and putting $\alpha = \theta$, the effective stiffness ratio of cracked elastic concrete beam-columns can be obtained as

$$\frac{EI_{eff}}{EI_g} = \frac{\lambda_{cr} \rho_t n \left(\frac{jd}{D}\right)^2}{\zeta + \left(\frac{\rho_t}{\rho_v}\right)\left(\frac{A_g}{A_v}\right)\tan^4\theta + \rho_t n \left(\frac{A_g}{A_v}\right)\sec^4\theta} \tag{2-79}$$

The parameter λ_{cr} is determined by section shapes and boundary conditions such that:

$\lambda_{cr} = 1$ for fixed-fixed rectangular column;

$\lambda_{cr} = 4$ for fixed-pinned rectangular column;

$\lambda_{cr} = \frac{4}{3}$ for fixed-fixed circular column;

$\lambda_{cr} = \frac{16}{3}$ for fixed-pinned circular column;

$\lambda_{cr} = \left[1 + \left(1 - 2\frac{t}{D}\right)^2\right]^{-1}$ for fixed-fixed square hollow-core column; and

$\lambda_{cr} = 4\left[1 + \left(1 - 2\frac{t}{D}\right)^2\right]^{-1}$ for fixed-pinned square hollow-core column

in which t is the wall thickness of a square hollow-core section; and D is the overall depth of a section.

2.4.4.3 Worked Examples

Table 2-13 presents a series of worked examples for the effective stiffness ratio using those columns used for the calculation of crack angles in table 2-11. Evidently the effective stiffness ratio of a cracked section to an uncracked section ranges from 0.07 through 0.28 in most cases. Also note that the longitudinal steel content affects the "effective stiffness ratio" more than the transverse steel content. The effective stiffness obtained by the suggested equation can be used for the evaluation of the natural period of structures before and after cracking.

2.5 Summary and Conclusions of Elastic Truss Representation of R.C. Columns

The present study on the stiffness analysis of post-cracked reinforced concrete beam-columns draws the following conclusions:

1. Caveats in this analysis are: i) tensile part of concrete is not considered, concrete is assumed to already be cracked and mostly ineffective; and ii) corner-to-corner strut that is important for heavily loaded columns is not considered.

2. Either of constant angle modeling or variable angle modeling is satisfactory for determining shear stiffness over the length of the beam-column. However, the shear stiffness calculated by three-point Gauss quadrature and Boole's rule are closer to the exact solution of the variable angle truss mechanism.

3. Numerical integration schemes employed for the solution of the variable angle truss are also used for physical simplification of the truss model. Two-point Gauss truss model provides a simple and sufficiently accurate tool to determine the post-cracked stiffness in shear and flexure. However, using three-point Gauss truss model, a more realistic distribution of tensile

Table 2-13. Effective Stiffness Ratios of Reinforced Concrete Beam-Columns.

Specimen	L (mm)	λ_{un}	λ_{cr}	Stiffness Ratio (EI_{eff}/EI_g)		EI_{cr}/EI_{un}
				Pre-Cracked	Post-Cracked	
A) 1/3 Pier Model[a]	1844	0.0473	1.3333	0.95479	0.06517	0.06826
B) Prototype[a]	2012	0.0895	5.3333	0.91784	0.11869	0.12932
C) 1/3 Model[b]	641	0.0979	5.3333	0.91087	0.05936	0.06517
D) Column - A[c]	3225	0.0989	2.7352	0.91003	0.06863	0.07542
E) Column - C[c]	3225	0.0989	2.7352	0.91003	0.06827	0.07502
F) Column - D[c]	3225	0.0989	2.7352	0.91003	0.06952	0.07640
G) Circular - C1[d]	2438	0.1289	1.3333	0.88581	0.11915	0.13451
H) Rectangular - R2[d]	2921	0.1875	1.0	0.84211	0.09504	0.11286
I) Unit_9[e]	1000	0.0825	5.3333	0.92379	0.24268	0.26270
J) Unit_13[e]	800	0.1289	5.3333	0.88581	0.22520	0.25422
K) Unit_14[e]	800	0.1289	5.3333	0.88581	0.22771	0.25707
L) Unit_16[e]	800	0.1289	5.3333	0.88581	0.23717	0.26774
M) 2R10-60u[f]	800	0.1289	5.3333	0.88581	0.22724	0.25653
N) 4R6-65u[f]	800	0.1289	5.3333	0.88581	0.24803	0.280
O) 4R10-60u[f]	800	0.1289	5.3333	0.88581	0.22724	0.25653
P) 0R6-80b[f]	800	0.1289	5.3333	0.88581	0.24926	0.28139
Q) 2R6-60b[f]	800	0.1289	5.3333	0.88581	0.24752	0.27943
R) R1A[g]	2438	0.1875	1.0	0.84211	0.08651	0.102726
S) R3A[g]	2438	0.1875	1.0	0.84211	0.089425	0.106192
T) R5A[g]	1829	0.3333	1.0	0.75	0.091347	0.121796

[a]Niagara Parkway bridge pier circular column tested by Mander, et al. *(1996a,b)*.

[b]Seismically designed circular column tested by Mander and Cheng *(1995)*.

[c]Square hollow-core columns tested by Mander et al. *(1984)*.

[d]Specimens tested by Chai, et al. *(1990)*.

[e]Circular columns tested by Ang, et al. *(1989)*.

[f]Circular columns tested by Wong *(1990)*.

[g]Rectangular columns tested by Priestley, et al. *(1994a,b)*

F-F: Fixed-fixed ends.

F-P: Fixed-pinned ends.

strain in the transverse ties can be obtained. This may be an important factor when modeling the non-linear (post-yield) behavior of columns which are lightly reinforced transversely and may eventually lead to premature failure at column mid-height due to corner-to-corner diagonal cracking (refer to figure 2-12).

4. A theoretical foundation for computing the principal crack angle has been formulated using energy considerations in which the combined external work done by both shear plus flexure is minimized. Comparison of the theoretical crack angles with those observed experimentally showed very favorable agreement.

5. The ratio of maximum to minimum tensile strain at the transverse steel over the length of a cracked column has been found by the analysis of three-point Gauss truss model. The tensile strain of the transverse steel at the middle of a column is larger than that at near ends by 25% and the average strain by 12.5%.

6. The effective stiffness ratio of a cracked section to a uncracked section may range between 0.07 through 0.28 in most cases, where it may be observed that the longitudinal steel content has a more pronounced effect on the ratio EI_{eff}/EI_g than the transverse steel contents.

SECTION 3
STRENGTH ANALYSIS OF TRUSS MODELS - EFFECT OF STEEL YIELDING

The purpose of this section is to generate a comprehensive shear force-deformation relationship for reinforced concrete beam-columns using the truss models described in the previous subsection. Two analytical approaches will be discussed: one is the piece-wise linear elastic analysis, while the other is an advanced strength method of analysis using the material constitutive law. These analyses will still be limited to the contribution of transverse and longitudinal reinforcement and diagonal compression struts in the concrete.

3.1 Piece-Wise Linear Elastic Analysis

A piece-wise linear elastic analysis is one way to generate the force-deformation relationship of truss models for reinforced concrete members by hand-analysis. In this analysis approach, the response of a structural member is built up by connecting the nearest events with straight lines, in which the event is termed for a point where the stiffness changes. Using the foregoing equations resulting from the truss model analyses, this analysis approach can readily produce the combined shear and flexural response of reinforced concrete members. However, because of the linearity, this analysis approach is more proper for thin-webbed squat members such as coupling beams where the effect of concrete in tension is minimal.

3.1.1 Total Stiffness of a Cracked Member

The total drift angle of a cracked concrete column for a unit shear force ($V_s = 1$) is shown in equation (2-64) to be the sum of shear rotation and flexural drift angle. For the general column lateral force V due to the contribution of transverse reinforcement, the expression becomes

$$\Theta = \Theta_s + \Theta_f \tag{3-1}$$

In terms of stiffness, the equation can be rewritten as

$$\Theta = \left(\frac{1}{K_s} + \frac{1}{K_{f\theta}}\right) V \tag{3-2}$$

in which K_s and $K_{f\theta}$ are shear and flexural stiffness, respectively, about column drift angle. Therefore, the combined total stiffness of a member is

$$K_\theta = \frac{1}{\frac{1}{K_s} + \frac{1}{K_{f\theta}}} \tag{3-3}$$

As previously discussed, the three-point Gauss truss model provides a suitable numerical representation as it models well the real distribution of the tensile strains in the transverse ties while the two-point Gauss truss model gives an overall average transverse tensile strain. The three-point model which gives the user more information is slightly more accurate but being more complex to use lends itself to computer analysis, whereas the two-point model being statically determinate lends itself to hand-analysis. Thus both truss models will be discussed to investigate the combined total stiffness of reinforced concrete beam-columns in what follows.

3.1.1.1 Two-Point Gauss Truss Model

As the tensile strain in the transverse ties in this model represents the overall average, then the relationship between the applied shear force and shear strain of the two-point Gauss truss model can be expressed as a function of one variable, the average transverse tie strain. Since equation (2-15) has one simple term that gives good accuracy, the cracked elastic shear stiffness of a concrete column can be expressed by putting $\alpha = \theta$, thus

$$K_s = \frac{\rho_v n \cot^2\theta}{1 + 4\rho_v n\left(\frac{b_w}{b_{ws}}\right)(1 + 0.39\cot^2\theta)^2} E_c A_v \tag{3-4}$$

Rearranging equations (2-29) and (2-34), the flexural stiffness of a cracked column in terms of drift angle is found to be

$$K_{f\theta} = \frac{\rho_t n}{\zeta \cot^2\alpha}\left(\frac{A_g}{A_v}\right)E_c A_v \tag{3-5}$$

in which ζ is a boundary condition constant and may be taken as 0.57 for a fixed-fixed ends and 1.57 for fixed-pinned ends. Note that the corner-to-corner angle α has not been converted to the crack angle θ in equation (3-5) because unlike the shear transfer mechanism, the flexural mechanism should be considered with the shear span M/V rather than the unit length defined by a single crack ($jd\cot\theta$). Substituting equations (3-4) and (3-5) into equation (3-3), the combined total stiffness of a member due to the two-point Gauss truss model is expressed as

$$K_\theta = \frac{E_c A_v}{\dfrac{1+4\rho_v n\left(\dfrac{b_w}{b_{ws}}\right)(1+0.39\cot^2\theta)^2}{\rho_v n\cot^2\theta} + \dfrac{\zeta\cot^2\alpha}{\rho_t n}\left(\dfrac{A_v}{A_g}\right)} \tag{3-6}$$

The corresponding lateral force-deformation relationship becomes

$$V = K_\theta \Theta = \frac{E_c A_v \Theta}{\dfrac{1+4\rho_v n\left(\dfrac{b_w}{b_{ws}}\right)(1+0.39\cot^2\theta)^2}{\rho_v n\cot^2\theta} + \dfrac{\zeta\cot^2\alpha}{\rho_t n}\left(\dfrac{A_v}{A_g}\right)} \tag{3-7}$$

3.1.1.2 Three-Point Gauss Truss Model

Unlike the two-point Gauss truss model, the maximum and minimum tensile strains in the transverse ties can be obtained from the three-point Gauss truss model. As mentioned previously and shown in figure 2-12, the maximum and minimum tensile strains at transverse ties occur in the middle (linkage 2) and near ends (linkages 1 and 3) of the truss model, respectively. Therefore, the relationship between the applied shear force and shear strain of the three-point Gauss truss model should be expressed as a function of two variables, the maximum and minimum tensile strains at transverse ties. For this purpose, the cracked elastic shear stiffness given by equation (2-46) with $\alpha = \theta$ should be used, since the equation has two terms

in which the first is for linkages 1 and 3 and the second is for linkage 2. Thus,

$$K_s = \frac{2\,\omega_1\,\rho_v\,n\cot^2\theta}{1+2\,\rho_v\,n\left(\frac{b_w}{b_{ws}}\right)\left(\left\{1+x_1^2\cot^2\theta\right\}^2+\left\{1+(1-x_1)^2\cot^2\theta\right\}^2\right)}E_c A_v + \frac{\omega_2\,\rho_v\,n\cot^2\theta}{1+4\,\rho_v\,n\left(\frac{b_w}{b_{ws}}\right)\left\{1+x_2^2\cot^2\theta\right\}^2}E_c A_v \tag{3-8}$$

Introducing the shear force distribution factor ϕ_i given by equation (2-52), the expression for shear stiffness given in equation (3-8) by the three-point Gauss truss quadrature can be reduced to

$$K_s = \frac{\omega_2\,\rho_v\,n\cot^2\theta}{\phi_2\left(1+4\,\rho_v\,n\left(\frac{b_w}{b_{ws}}\right)\left\{1+x_2^2\cot^2\theta\right\}^2\right)}E_c A_v \tag{3-9}$$

Rearranging equations (2-58) and (2-62), the flexural stiffness of a cracked column about drift angle is

$$K_{f\theta} = \frac{\rho_t\,n}{\zeta\cot^2\alpha}\left(\frac{A_g}{A_v}\right)E_c A_v \tag{3-10}$$

in which ζ is a boundary condition constant taken as:

$\zeta = x_1+(1-2x_1)\left\{2\phi_1^2(1-x_1)^2+0.5(1-2\phi_1 x_1)^2\right\}$ for fixed-fixed ends; and

$\zeta = 3x_1+(1-2x_1)\left\{(1-\phi_1 x_1)^2+(1-\phi_1 x_1-\phi_2 x_2)^2+(\phi_1 x_1+\phi_2 x_2)^2+\phi_1^2 x_1^2\right\}$ for fixed-pinned ends.

The numerical coordinates x_i for three-point Gauss quadrature are available in table 2-3. Again, as noted previously, the corner-to-corner angle α has not been converted to the crack angle θ in equation (3-10). Substituting equations (3-9) and (3-10) into equation (3-3), the combined total stiffness of a member due to the three-point Gauss truss model becomes

$$K_\theta = \frac{E_c A_v}{\dfrac{\phi_2\left(1+4\,\rho_v\,n\left(\frac{b_w}{b_{ws}}\right)\left\{1+x_2^2\cot^2\theta\right\}^2\right)}{\omega_2\,\rho_v\,n\cot^2\theta}+\dfrac{\zeta\cot^2\alpha}{\rho_t\,n}\left(\dfrac{A_v}{A_g}\right)} \tag{3-11}$$

Therefore, the column lateral force related to the deformation of the truss mechanism is expressed as

$$V = K_\Theta \Theta = \frac{E_c A_v \Theta}{\dfrac{\phi_2 \left(1 + 4\,\rho_v n \left(\dfrac{b_w}{b_{ws}}\right)\left\{1 + x_2^2 \cot^2\theta\right\}^2\right)}{\omega_2\,\rho_v n \cot^2\theta} + \dfrac{\zeta \cot^2\alpha}{\rho_t n}\left(\dfrac{A_v}{A_s}\right)} \tag{3-12}$$

3.1.2 Post-Yield Stiffness

All that is necessary to obtain the post-yield stiffness is to use the appropriate modular ratio n in the foregoing stiffness formulations. By respectively defining the transverse and longitudinal modular ratios as $n_T = E_{sT}/E_c$ and $n_L = E_{sL}/E_c$, the expressions for stiffness and strength should apparently include the modified modular ratios. Prior to yielding of any reinforcement, $n_T = n_L = E_s/E_c$. If the transverse steel yields, then $n_T = E_{sp}/E_c$, or if the longitudinal steel yields, then $n_L = E_{sp}/E_c$ where E_{sp} is the post-yield plastic modulus of reinforcement. For this purpose, the material properties of concrete in compression and reinforcing steel are idealized as shown in figure 3-1. The stress-strain relation of concrete in compression is idealized as a straight line passing through the stress-strain curve at $0.4f_c'$. This secant modulus E_c is given as $4700\sqrt{f_c'\ (MPa)}$ for normal weight concrete in ACI 318 *(1995)*. It is assumed that concrete in compression behaves linear-elastically up to the stress of $0.85f_c'$. For reinforcing steel, the modulus of elasticity E_s is assumed to be $200\,GPa$ and the post-yield ascending branch of the simplified trilinear model was built up as suggested by Hsu *(1993)* considering the average stress - average strain of rebar imbedded in the cracked concrete. Therefore, the post-yield plastic modulus of reinforcing steel for the trilinear model is given by

$$E_{sp} = \frac{f_{0.05} - f_y}{0.05 - \varepsilon_{sh}} \tag{3-13}$$

where $f_{0.05}$ is the stress of steel at strain of 0.05 and f_y is yield stress and ε_y is the yield strain. For convenience, this may be taken as 25% of the measured strain-hardening modulus E_{sh} or 0.5% of the modulus of elasticity E_s. Therefore, diagonal struts will behave in a linear elastic

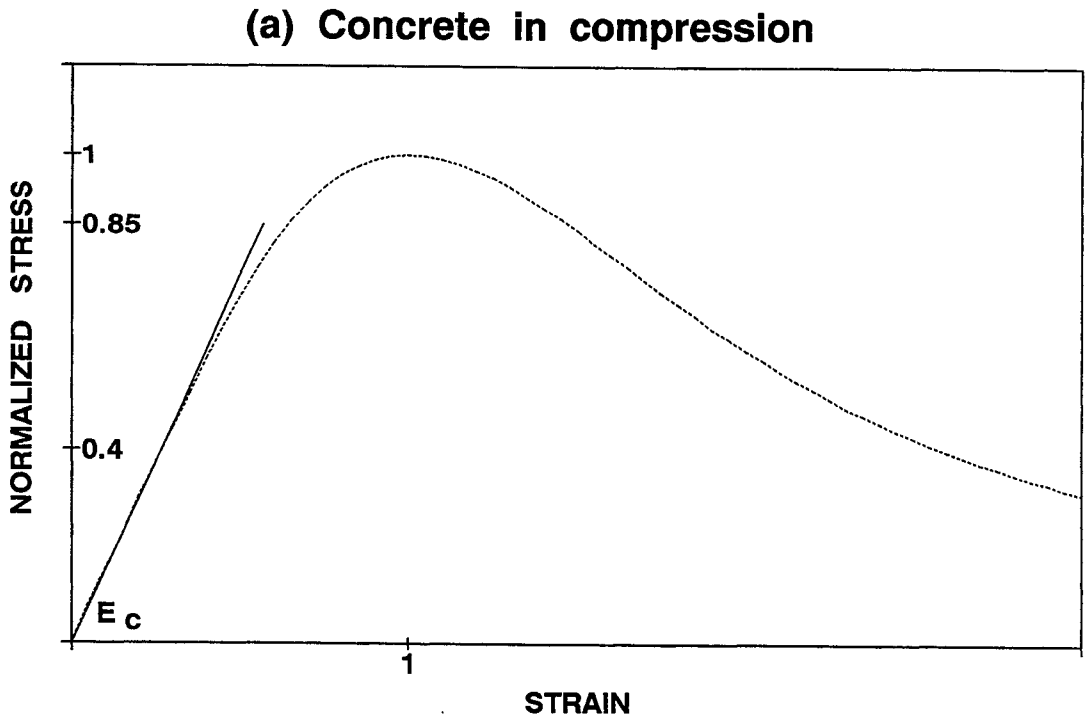

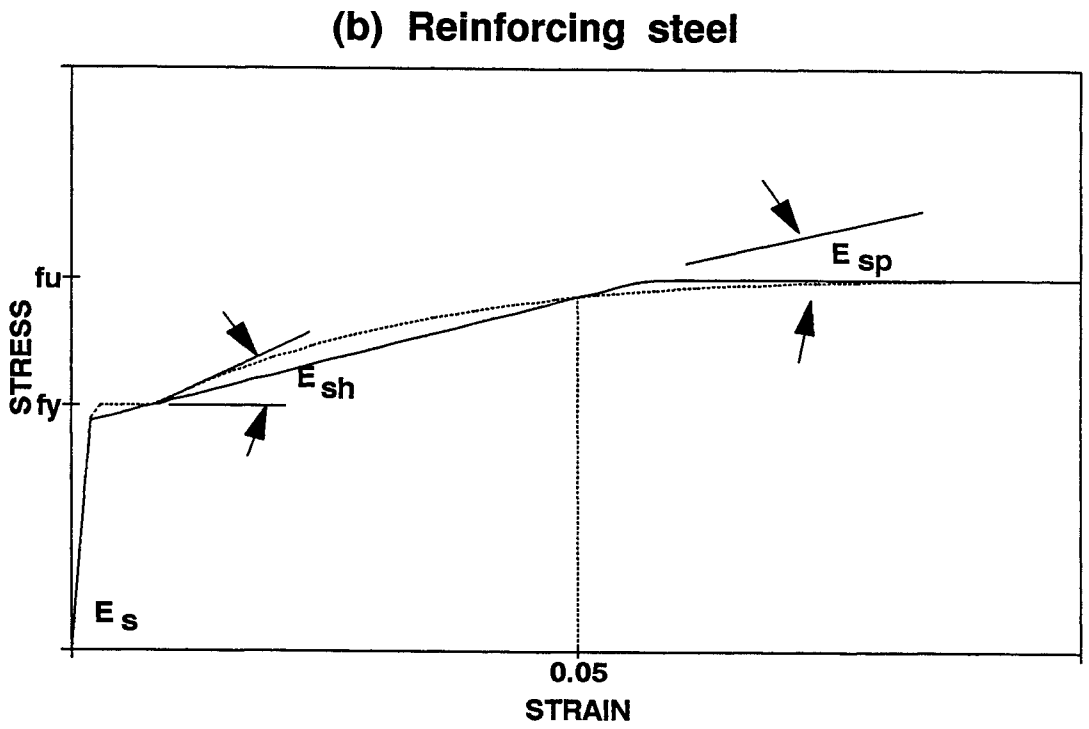

Figure 3-1. Idealized properties of materials for piece-wise linear elastic analysis.

manner through the entire response while transverse ties and longitudinal chords will work trilinearly.

3.1.2.1 Two-Point Gauss Truss Model

With the modified modular ratios, the combined total stiffness of a member due to two-point Gauss truss model given by equation (3-6) becomes

$$K_\theta = \frac{E_c A_v}{\dfrac{1 + 4\,\rho_v n_T \left(\dfrac{b_w}{b_{ws}}\right)(1 + 0.39\cot^2\theta)^2}{\rho_v n_T \cot^2\theta} + \dfrac{\zeta \cot^2\alpha}{\rho_t n_L}\left(\dfrac{A_v}{A_g}\right)} \tag{3-14}$$

The corresponding column lateral force-deformation relationship becomes

$$V = \frac{E_c A_v \Theta}{\dfrac{1 + 4\,\rho_v n_T \left(\dfrac{b_w}{b_{ws}}\right)(1 + 0.39\cot^2\theta)^2}{\rho_v n_T \cot^2\theta} + \dfrac{\zeta \cot^2\alpha}{\rho_t n_L}\left(\dfrac{A_v}{A_g}\right)} \tag{3-15}$$

3.1.2.2 Three-Point Gauss Truss Model

The combined total stiffness of a member given in equation (3-11) becomes

$$K_\theta = \frac{E_c A_v}{\dfrac{\phi_2\left(1 + 4\,\rho_v n_{T2}\left(\dfrac{b_w}{b_{ws}}\right)\left\{1 + x_2^2\cot^2\theta\right\}^2\right)}{\omega_2\,\rho_v n_{T2}\cot^2\theta} + \dfrac{\zeta \cot^2\alpha}{\rho_t n_L}\left(\dfrac{A_v}{A_g}\right)} \tag{3-16}$$

Using the modified modulus ratios, the shear force distribution factor ϕ_i given in equation (2-52) becomes

$$\phi_1 = \phi_3 = \frac{1}{2 + \dfrac{1 + 2\rho_v n_{T1}\left(\dfrac{b_w}{b_{ws}}\right)\left(\left\{1 + x_1^2\cot^2\theta\right\}^2 + \left\{1 + (1-x_1)^2\cot^2\theta\right\}^2\right)}{\dfrac{\omega_1}{\omega_2}\dfrac{n_{T1}}{n_{T2}}\left(1 + 4\rho_v n_{T2}\left(\dfrac{b_w}{b_{ws}}\right)\left\{1 + x_2^2\cot^2\theta\right\}^2\right)}} \tag{3-17a}$$

$$\phi_2 = \frac{1}{1 + \dfrac{2\dfrac{\omega_1}{\omega_2}\dfrac{n_{T1}}{n_{T2}}\left(1 + 4\rho_v n_{T2}\left(\dfrac{b_w}{b_{ws}}\right)\left\{1 + x_2^2\cot^2\theta\right\}^2\right)}{1 + 2\rho_v n_{T1}\left(\dfrac{b_w}{b_{ws}}\right)\left(\left\{1 + x_1^2\cot^2\theta\right\}^2 + \left\{1 + (1-x_1)^2\cot^2\theta\right\}^2\right)}} \tag{3-17b}$$

where n_{T1} and n_{T2} are the modified transverse modulus ratios for truss linkages 1 and 2, respectively. Note that n_{T1} is also used for truss linkage 3. The expression in equation (3-12) given for the relationship between column lateral force and deformation of the three-point Gauss truss model becomes

$$V = \frac{E_c A_v \Theta}{\dfrac{\phi_2\left(1 + 4\rho_v n_{T2}\left(\dfrac{b_w}{b_{ws}}\right)\left\{1 + x_2^2\cot^2\theta\right\}^2\right)}{\omega_2 \rho_v n_{T2}\cot^2\theta} + \dfrac{\zeta\cot^2\alpha}{\rho_t n_L}\left(\dfrac{A_v}{A_g}\right)} \tag{3-18}$$

It is of interest to investigate how much the boundary condition constant ζ is influenced by yielding of the transverse tie at truss linkage 2 which is critical. For this purpose, the experimental specimens shown in table 2-12 for the cracked elastic stage are used taking $E_{sp} = 0.005E_s$ for n_{T2} in equation (3-17). The calculated results are presented in table 3-1. It is noted that after yielding of the transverse tie at linkage 2 the boundary condition constants ζ determined by the three-point Gauss truss model analysis are approximately 0.72 for fixed-fixed ends and 1.72 for fixed-pinned ends no matter what the transverse and longitudinal steel contents are. These values are quite close to those determined by the two-point Gauss truss model (0.57 for fixed-fixed ends and 1.57 for fixed-pinned ends) as well as those determined by the three-point Gauss truss model at cracked elastic stage (0.54 for fixed-fixed ends and 1.54 for fixed-pinned ends). Therefore, it is concluded that the boundary condition constants determined by the two-point Gauss truss model analysis may be used in all cases for simplicity. However, the

Table 3-1. Coefficients for cracked concrete columns determined by three-point Gauss truss model after yield of transverse tie at linkage 2.

Specimen	n	ρ_v	ϕ_1	ϕ_2	ζ $(F\text{-}F)$	ζ $(F\text{-}P)$
A) 1/3 Pier Model[a]	5.7	0.00147	0.49731	0.00538	0.719685	1.719685
B) Prototype[a]	6.3	0.00115	0.497585	0.00483	0.719976	1.719976
C) 1/3 Model[b]	6.0	0.00492	0.497415	0.005171	0.719796	1.719796
D) Column - A[c]	7.8	0.00785	0.496528	0.006945	0.718858	1.718858
E) Column - C[c]	7.9	0.01178	0.496099	0.007801	0.718406	1.718406
F) Column - D[c]	7.9	0.00785	0.496503	0.006993	0.718832	1.718832
G) Circular - C1[d]	7.2	0.00089	0.497144	0.005712	0.719509	1.719509
H) Rectangular - R2[d]	7.2	0.00102	0.497144	0.005711	0.71951	1.71951
I) Unit_9[e]	7.8	0.00518	0.496814	0.006372	0.719161	1.719161
J) Unit_13[e]	7.1	0.00518	0.496917	0.006167	0.719269	1.719269
K) Unit_14[e]	7.3	0.00259	0.497178	0.00661	0.719537	1.719537
L) Unit_16[e]	7.4	0.00259	0.497172	0.00657	0.719539	1.719539
M) 2R10-60u[f]	7.8	0.00727	0.496574	0.006852	0.718907	1.718907
N) 4R6-65u[f]	7.8	0.00239	0.497156	0.005688	0.719522	1.719522
O) 4R10-60u[f]	7.8	0.00727	0.496574	0.006852	0.718907	1.718907
P) 0R6-80b[f]	7.8	0.00194	0.497218	0.005564	0.719588	1.719588
Q) 2R6-60b[f]	7.8	0.00259	0.497129	0.005741	0.719494	1.719494
R) R1A[g]	6.9	0.00123	0.497135	0.005729	0.7195	1.7195
S) R3A[g]	7.2	0.00123	0.4971	0.0058	0.719463	1.719463
T) R5A[g]	7.5	0.00123	0.497076	0.005847	0.719438	1.719438

[a]Niagara Parkway bridge pier circular column tested by Mander, et al. *(1996a,b)*.

[b]Seismically designed circular column tested by Mander and Cheng *(1995)*.

[c]Square hollow-core columns tested by Mander et al. *(1984)*.

[d]Specimens tested by Chai, et al. *(1990)*.

[e]Circular columns tested by Ang, et al. *(1989)*.

[f]Circular columns by Wong *(1990)*.

[g]Rectangular columns tested by Priestley, et al. *(1994a,b)*.

F-F: Fixed-fixed ends.

F-P: Fixed-pinned ends.

shear force distribution factors ϕ_1 and ϕ_2 are affected a lot by transverse steel yielding. It is noted that after the critical transverse steel yields, linkages 1 and 3 resist virtually all of the applied shear force.

3.1.3 Strength Analysis

In order to generate the shear force-deformation relationship, it is necessary to relate the local truss member strain to the global truss deformation.

3.1.3.1 Yield of Transverse Ties

Two-Point Gauss Truss Model

Consider the average force in transverse hoops of the two-point Gauss truss model in figure 2-8. Rearranging equation (2-26) with $\alpha = \theta$, the column lateral force at the average tensile yield strain of transverse hoops is

$$(V_y)_T = (\varepsilon_y)_T E_c A_v \rho_v n_T \cot\theta \tag{3-19}$$

where $(\varepsilon_y)_T$ is the average yield strain of transverse hoop/stirrup steel. Substituting equation (3-19) into equation (3-7) and rearranging, the drift angle corresponding to the yield of transverse ties can be obtained as

$$(\Theta_y)_T = \frac{(V_y)_T}{E_c A_v}\left(\frac{1 + 4\,\rho_v n_T\left(\frac{b_w}{b_{ws}}\right)(1 + 0.39\cot^2\theta)^2}{\rho_v n_T \cot^2\theta} + \frac{\zeta\cot^2\alpha}{\rho_t n_L}\left(\frac{A_v}{A_g}\right)\right) \tag{3-20}$$

Three-Point Gauss Truss Model

Consider truss linkages of the three-point Gauss truss model in figures 2-9 and 2-11. Although the tensile strain of the transverse tie of truss linkage 2 located at the column middle

is the critical one as shown in figure 2-12, it is necessary to investigate the tensile strains of transverse ties at all linkages for global force-deformation plotting. Again, by introducing the modified modular ratios n_{T1} and n_{T2} and $\alpha = \theta$, the expressions for the tensile strains of transverse ties given in equation (2-53) can be rearranged to obtain the shear force when the transverse ties yield as follows

$$(V_y)_{T1} = \left(\frac{\omega_1}{\phi_1}\right)(\varepsilon_y)_{T1} E_c A_v \rho_v n_{T1} \cot\theta \qquad \text{(3-21a)}$$

$$(V_y)_{T2} = \left(\frac{\omega_2}{\phi_2}\right)(\varepsilon_y)_{T2} E_c A_v \rho_v n_{T2} \cot\theta \qquad \text{(3-21b)}$$

where $(V_y)_{T1}$ and $(V_y)_{T2}$ are respectively column lateral forces at yield of transverse ties at linkages 1 and 2, and $(\varepsilon_y)_{T1}$ and $(\varepsilon_y)_{T2}$ are respectively yield strains of transverse ties at linkages 1 and 2. Therefore, column end-to-end rotation (drift angle) when transverse ties yield is found by relating equation (3-21) to equation (3-18) to be

$$(\Theta_y)_{T1} = \frac{(V_y)_{T1}}{E_c A_v}\left(\frac{\phi_2\left(1 + 4\,\rho_v n_{T2}\left(\frac{b_w}{b_{ws}}\right)\left\{1 + x_2^2\cot^2\theta\right\}^2\right)}{\omega_2\,\rho_v n_{T2}\cot^2\theta} + \frac{\zeta\cot^2\alpha}{\rho_t n_L}\left(\frac{A_v}{A_g}\right)\right) \qquad \text{(3-22a)}$$

$$(\Theta_y)_{T2} = \frac{(V_y)_{T2}}{E_c A_v}\left(\frac{\phi_2\left(1 + 4\,\rho_v n_{T2}\left(\frac{b_w}{b_{ws}}\right)\left\{1 + x_2^2\cot^2\theta\right\}^2\right)}{\omega_2\,\rho_v n_{T2}\cot^2\theta} + \frac{\zeta\cot^2\alpha}{\rho_t n_L}\left(\frac{A_v}{A_g}\right)\right) \qquad \text{(3-22b)}$$

where $(\Theta_y)_{T1}$ and $(\Theta_y)_{T2}$ are respectively column rotation angle at yield of transverse ties of linkages 1 and 2.

3.1.3.2 Yield of Longitudinal Chords

Two-Point Gauss Truss Model

The strain at the critical longitudinal chord given by equations (2-31) and (2-36) can be

rearranged with the modified modulus ratio n_L to obtain the expression for column lateral force V when the longitudinal chord at the critical section yields as follows

$$(V_y)_L = (\varepsilon_y)_L E_c A_g \rho_t n_L \tan\alpha \qquad \textit{for fixed-fixed ends} \qquad \textbf{(3-23a)}$$

$$(V_y)_L = 0.5(\varepsilon_y)_L E_c A_g \rho_t n_L \tan\alpha \qquad \textit{for fixed-pinned ends} \qquad \textbf{(3-23b)}$$

where $(V_y)_L$ is shear force at yield of the critical longitudinal chord and $(\varepsilon_y)_L$ is the corresponding yield strain. It is noted that the corner-to-corner angle α is used for the flexural strength, since the flexural mechanism should be considered with the shear span M/V rather than the unit length defined by the crack angle ($jd\cot\theta$). As expected for the column lateral force V, the critical longitudinal strain of a fixed-pinned column is twice that of a fixed-fixed column. Therefore, column end-to-end rotation (drift angle) corresponding to yielding of the longitudinal chord at the critical section is found by relating equations (3-15) and (3-23) to be

$$(\Theta_y)_L = \frac{(V_y)_L}{E_c A_v}\left(\frac{1 + 4\,\rho_v n_T\left(\frac{b_w}{b_{ws}}\right)(1 + 0.39\cot^2\theta)^2}{\rho_v n_T \cot^2\theta} + \frac{\zeta\cot^2\alpha}{\rho_t n_L}\left(\frac{A_v}{A_g}\right)\right) \qquad \textbf{(3-24)}$$

Three-Point Gauss Truss Model

The strain at the critical longitudinal chord given in equations (2-59) and (2-63) can be rearranged by introducing the modified modular ratio n_L for shear force V_s. Note that equations are exactly the same between the two-point and three-point Gauss truss models. Therefore, the expressions given in equation (3-23) for column lateral force when the longitudinal chord at the critical section yield in the two-point Gauss truss model can also be used for the three-point Gauss truss model. Thus the column end-to-end rotation (drift angle) when the longitudinal chord at the critical section yield is found by relating equations (3-18) and (3-23) to be

$$(\Theta_y)_L = \frac{(V_y)_L}{E_c A_v}\left(\frac{\phi_2\left(1 + 4\,\rho_v n_{T2}\left(\frac{b_w}{b_{ws}}\right)\left\{1 + x_2^2\cot^2\theta\right\}^2\right)}{\omega_2\,\rho_v n_{T2}\cot^2\theta} + \frac{\zeta\cot^2\alpha}{\rho_t n_L}\left(\frac{A_v}{A_g}\right)\right) \qquad \textbf{(3-25)}$$

3.2 Advanced Strength Analysis Using A Material Constitutive Law

In the previous subsections, the piece-wise linear elastic analysis method using the idealized linear model for concrete diagonal struts and trilinear model for longitudinal chords and transverse ties in Gauss truss models was introduced. That simple and comprehensive analysis method enables the strength analysis of reinforced concrete beam-columns to be performed by hand-calculation. In the present subsection, the analysis method is advanced by implementing a non-linear material model for reinforcing steel. In performing this advanced analysis method, any spreadsheet type computer software may be suitable for automating the calculations. It is noted that the discussion is still limited to the truss mechanism. For the purpose of simple analysis method, only Gauss 2-point truss model will be considered in the present study.

3.2.1 Material Model for Reinforcing Steel

Chang and Mander *(1994)* suggested a steel model (stress-strain relationship) for reinforcing steel by modifying the Menegotto-Pinto equation *(1973)* and the expression is

$$f_s = \frac{E_s \varepsilon_s}{\left[1 + \left(\frac{E_s \varepsilon_s}{f_y}\right)^{20}\right]^{0.05}} + \left(\frac{1 + sign(\varepsilon_s - \varepsilon_{sh})}{2}\right)(f_{su} - f_y)\left(1 - \left|\frac{\varepsilon_{su} - \varepsilon_s}{\varepsilon_{su} - \varepsilon_{sh}}\right|^p\right) \qquad \text{(3-26)}$$

where $$p = E_{sh}\left(\frac{\varepsilon_{su} - \varepsilon_{sh}}{f_{su} - f_y}\right) \quad \text{and} \quad E_{sh} \cong 0.02\, E_S$$

$sign(\varepsilon_s - \varepsilon_{sh}) = -1$ for $\varepsilon_s < \varepsilon_{sh}$ and $sign(\varepsilon_s - \varepsilon_{sh}) = 1$ for $\varepsilon_s \geq \varepsilon_{sh}$, and notations for other parameters are described in figure 3-2. This equation fits very accurately experimental results of steel coupon tests. However, as previously mentioned, the study conducted by Hsu *(1993)* indicates that the average stress - average strain relationship should be used for the reinforcing steel embedded in the cracked concrete. Considering this effect, the steel model given in equation (3-26) is modified as

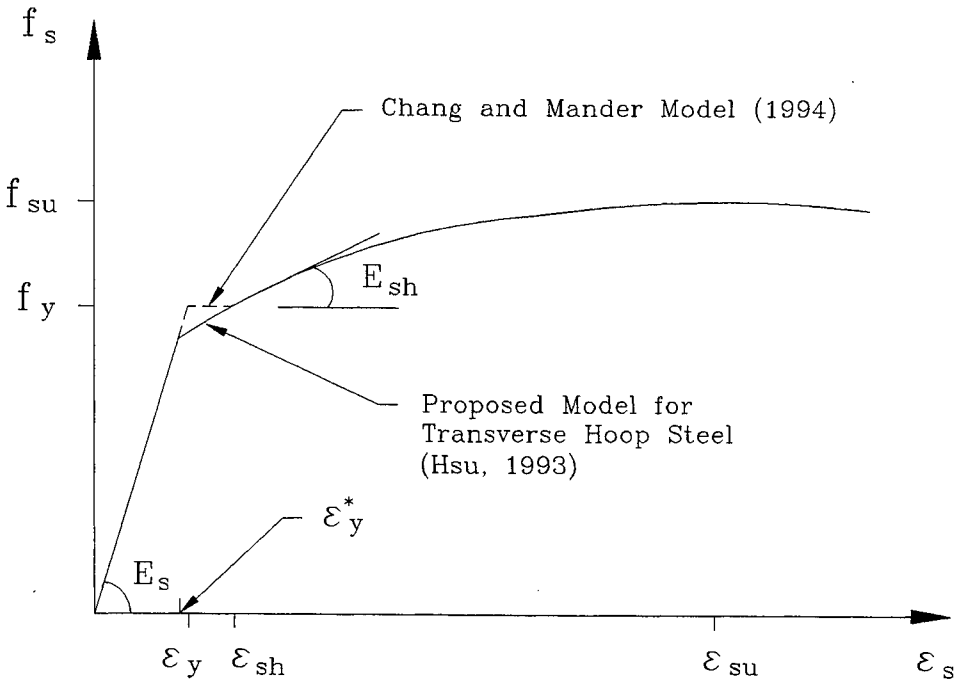

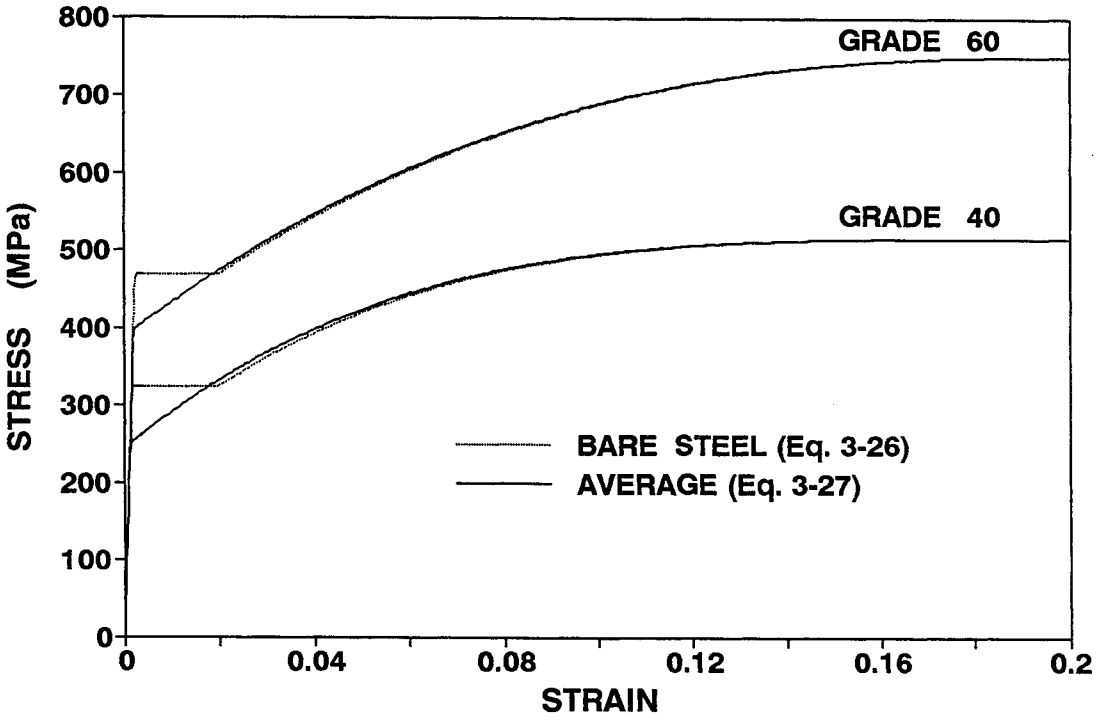

Figure 3-2. Proposed model for reinforcing steel.

$$f_s = \frac{E_s \varepsilon_s}{\left(1 + \left(\frac{\varepsilon_s}{\varepsilon_y^*}\right)^{20}\right)^{0.05}} + \left(\frac{1 + sign\left(\varepsilon_s - \varepsilon_y^*\right)}{2}\right)\left(f_{su} - E_s \varepsilon_y^*\right)\left(1 - \left|\frac{\varepsilon_{su} - \varepsilon_s}{\varepsilon_{su} - \varepsilon_y^*}\right|^p\right) \qquad (3\text{-}27)$$

where $$\varepsilon_y^* = \frac{f_y - E_{sh}\varepsilon_{sh}}{E_s - E_{sh}}$$

and other parameters are defined in equation (3-26) and figure 3-2. The parameter ε_y^* is the average strain of transverse hoop steel at imminent yielding. Figure 3-2 gives a comparison between steel models given by equations (3-26) and (3-27) for Grades 40 and 60.

It is noted that the strain amplitude in longitudinal steel at the critical column section is localized, while the one in transverse hoop steel is considered quite evenly distributed. Therefore, it is recommended that equation (3-26) be used for longitudinal reinforcing steel and equation (3-27) be used for transverse hoop steel.

3.2.2 Force-Deformation Relationship of Gauss 2-Point Truss due to Shear

The average transverse tie strain is used in evaluation of column shear force and deformation relationship for this truss model. The column shear strength V_s can be expressed in terms of transverse tie strain ε_T or stress f_T by rearranging equation (2-26) with $\rho_v = A_{sh}/b_w s$ and $\alpha = \theta$. Thus

$$V_s = E_s \varepsilon_T A_v \rho_v \cot\theta \qquad (3\text{-}28a)$$

$$V_s = f_T A_v \rho_v \cot\theta \qquad (3\text{-}28b)$$

The column shear deformation can also be arranged in terms of average transverse tie strain using the information available in table 2-4, that is,

$$\Delta_s = \varepsilon_1 jd + \frac{2V_s jd}{E_c A_v \left(\frac{b_{ws}}{b_w}\right)\cot\theta}\left(\left[1+x_1^2\cot^2\theta\right]^2 + \left[1+(1-x_1)^2\cot^2\theta\right]^2\right) \tag{3-29}$$

Note that the diagonal concrete struts are assumed to be linear elastic. The corresponding column shear rotation (drift) angle can be obtained by dividing the displacement in equation (3-29) by the shear unit length $jd\cot\theta$, thus

$$\Theta_s = \varepsilon_1 \tan\theta + \frac{2V_s \tan^2\theta}{E_c A_v \left(\frac{b_{ws}}{b_w}\right)}\left(\left[1+x_1^2\cot^2\theta\right]^2 + \left[1+(1-x_1)^2\cot^2\theta\right]^2\right) \tag{3-30}$$

Substituting equation (3-28b) for V_s into equation (3-30),

$$\Theta_s = \varepsilon_T \tan\theta + \frac{2f_T \rho_v T^*(\theta)}{E_c\left(\frac{b_{ws}}{b_w}\right)\cot\theta} \tag{3-31}$$

where $T^*(\theta) = \left[1+x_1^2\cot^2\theta\right]^2 + \left[1+(1-x_1)^2\cot^2\theta\right]^2$. Substituting equation (3-27) for f_T into equation (3-31) and rearranging, the column shear rotation Θ_s becomes

$$\Theta_s = \varepsilon_T\left[\tan\theta + \frac{2\rho_v n T^*(\theta)}{\left(\frac{b_{ws}}{b_w}\right)\cot\theta}\left\{\left(1+\left(\frac{\varepsilon_T}{\varepsilon_y^*}\right)^{20}\right)^{-0.05} + \frac{\left\{1+sign\left(\varepsilon_T-\varepsilon_y^*\right)\right\}}{2E_s\varepsilon_T}\left(f_{su}-E_s\varepsilon_y^*\right)\left[1-\left|\frac{\varepsilon_{su}-\varepsilon_T}{\varepsilon_{su}-\varepsilon_y^*}\right|^p\right]\right\}\right] \tag{3-32}$$

in which parameters are defined in equations (3-26) and (3-27). Rearranging equation (3-32), the transverse tie strain ε_T for a given column rotation Θ_s becomes

$$\varepsilon_T = \frac{\Theta_s \cot\theta}{1+\frac{2\rho_v n T^*(\theta)}{\left(\frac{b_{ws}}{b_w}\right)}\left(\left(1+\left(\frac{\varepsilon_T}{\varepsilon_y^*}\right)^{20}\right)^{-0.05} + \frac{\left\{1+sign\left(\varepsilon_T-\varepsilon_y^*\right)\right\}}{2E_s\varepsilon_T}\left(f_{su}-E_s\varepsilon_y^*\right)\left[1-\left|\frac{\varepsilon_{su}-\varepsilon_T}{\varepsilon_{su}-\varepsilon_y^*}\right|^p\right]\right)} \tag{3-33}$$

By substituting ε_T calculated by equation (3-33) into equation (3-27) the transverse tie stress f_T can be obtained. Solution of equation (3-33) may require some iterative process since ε_T is a

function of itself. By rearranging equation (3-28b) with $A_v = b_w jd$ and $\rho_v = A_{sh}/b_w s$, the column shear strength V_s can also be expressed as

$$V_s = A_{sh} f_T \frac{jd}{s} \cot\theta \qquad (3\text{-}34)$$

This equation is the same expression as the traditionally accepted formula *(Dilger, 1966; Park and Paulay, 1975)* as well as the expression for the transverse steel contribution of the recently highlighted MCFT *(Collins and Mitchell, 1991)*.

The solution strategy for the force and deformation relationship of Gauss 2-point truss model due to shear is summarized as follows:

Step 1 Choose column shear strain (rotation) Θ_s.

Step 2 Determine the ratio of effective column width b_{ws}/b_w.

Step 3 Calculate the transverse tie strain ε_T for a given column shear strain (rotation)Θ_s using equation (3-33). Repeat this step until converged.

Step 4 Calculate the transverse tie stress f_T using equation (3-27).

Step 5 Calculate the column shear resistance V_s due to the transverse steel mechanism using equation (3-34).

Step 6 Return to step 2 until converged.

Step 7 Repeat steps 1-6 for increasing values of Θ_s.

Step 8 Plot Θ_s vs. V_s and ε_T vs. f_T.

3.2.3 Force-Deformation Relationship of Gauss 2-Point Truss due to Flexure

The tensile strain of the longitudinal chord at the critical region of the truss model is used in evaluation of the column flexural force and deformation relationship. The column flexural strength V_f can be expressed in terms of the critical longitudinal chord strain ε_L or stress f_L by rearranging equations (2-31) and (2-36). Thus,

for a column with fixed-fixed ends,

$$V_f = E_s \varepsilon_L A_{st} \tan\alpha \quad \text{(3-35a)}$$

$$V_f = f_L A_{st} \tan\alpha \quad \text{(3-35b)}$$

for a column with fixed-pinned ends,

$$V_f = 0.5 E_s \varepsilon_L A_{st} \tan\alpha \quad \text{(3-36a)}$$

$$V_f = 0.5 f_L A_{st} \tan\alpha \quad \text{(3-36b)}$$

Note that the corner-to-corner diagonal angle α is used for flexure rather than the crack angle θ. Substituting equations (3-35a) and (3-36a) for V_f into equation (2-28) and (2-33) and rearranging, the column drift angle Θ_f is expressed as

for a column with fixed-fixed ends,

$$\Theta_f = \zeta \varepsilon_L \cot\alpha \quad \text{(3-37a)}$$

for a column with fixed-pinned ends,

$$\Theta_f = 0.5 \zeta \varepsilon_L \cot\alpha \quad \text{(3-37b)}$$

in which ζ is a boundary condition constant and may be taken as 0.57 for a column with fixed-fixed ends and 1.57 for a column with fixed-pinned ends. Therefore, the longitudinal chord strain ε_L at the critical region for a given column drift angle Θ_f is obtained as:

for a column with fixed-fixed ends,

$$\varepsilon_L = 1.753 \Theta_f \tan\alpha \quad \text{(3-38a)}$$

for a column with fixed-pinned ends,

$$\varepsilon_L = 1.274 \Theta_f \tan\alpha \quad \text{(3-38b)}$$

The solution strategy for the force and deformation relationship of Gauss 2-point truss model due to flexure is summarized as follows:

Step 1 Choose a column drift angle Θ_f.

Step 2 Calculate the longitudinal chord strain ε_L at the critical region for a given drift angle Θ_f using equation (3-38).

Step 3 Calculate the corresponding longitudinal chord stress f_L using equations (3-26).

Step 4 Calculate the column flexural strength V_f using equations (3-35b) and (3-36b) for a column with fixed-fixed ends and with fixed-pinned ends, respectively.

Step 5 Repeat steps 1-4 for increasing values of Θ_f.

Step 6 Plot Θ_f vs. V_f and ε_L vs. f_L.

3.3 Supplementary Flexural Analysis

Even though the cracked effective stiffness can reasonably be predicted, the flexural response obtained by the truss model analysis may have some shortfall because:

1) When dimensioning for truss model in subsection 2.2.5, it is assumed that the longitudinal chord members in the truss model can be modeled by one half of longitudinal steel content with the distance of flexural lever arm *jd* over the column length;
2) Also assumed is that involvement of concrete compressive stress block has been ignored for simplicity; and
3) Externally applied column axial load is not considered.

In order to overcome the probable shortfall in flexural response due to the mentioned assumption for truss modeling, the column flexural force-deformation response can be determined by the moment-curvature relationship rather than the truss model analysis. The moment-curvature analysis can be performed by any suitable computer program, such as: COLUMN *(Mander, et al., 1984)*; RESPONSE *(Collins and Mitchell, 1991)*; and UB-COLA

(Chang and Mander, 1994a). Mander et al. *(1984)* suggested the idealized plastic curvature distribution as shown in figure 3-3. Then, the elastic portion of the curvature can be extrapolated using the curvature at first yield moment, that is,

$$\phi_e = \phi_y' \frac{M_{max}}{M_y} \tag{3-39}$$

where M_y and ϕ_y' are respectively the first yield moment and the corresponding curvature and M_{max} is the moment at the critical column section. Utilizing moment area method, the elastic portion of column end-to-end rotation can be calculated as

$$\Theta_f^e = \frac{1}{2} \phi_e L_c \tag{3-40}$$

where $L_c = M/V$. The plastic portion of column end-to-end rotation angle is calculated by

$$\Theta_f^p = (\phi - \phi_e)\left(\frac{1}{3} L_{pc} + L_{py}\right) \tag{3-41}$$

where $L_{pc} = L_c\left(1 - \frac{M_y}{M_{max}}\right)$ and $L_{py} = 32\sqrt{d_b\ (mm)}$.

Then, the column end-to-end rotation (drift) angle is the sum of elastic and plastic portions:

$$\Theta_f = \Theta_f^e + \Theta_f^p \tag{3-42}$$

Plotting V_f and Θ_f gives the column flexural force-deformation response. If the joint where the fixation is provided to the column end is expected to rotate due to the flexibility of cab beam or foundation beam, the effect can also be accounted for. Consider column-beam subassemblage shown in figure 3-4. Using the moment-area theorem, the flexibility of the connected beam is calculated by

for T-shaped beam-column,

$$f_b = \frac{L_b}{12 E I_b} \tag{3-43a}$$

for L-shaped beam-column,

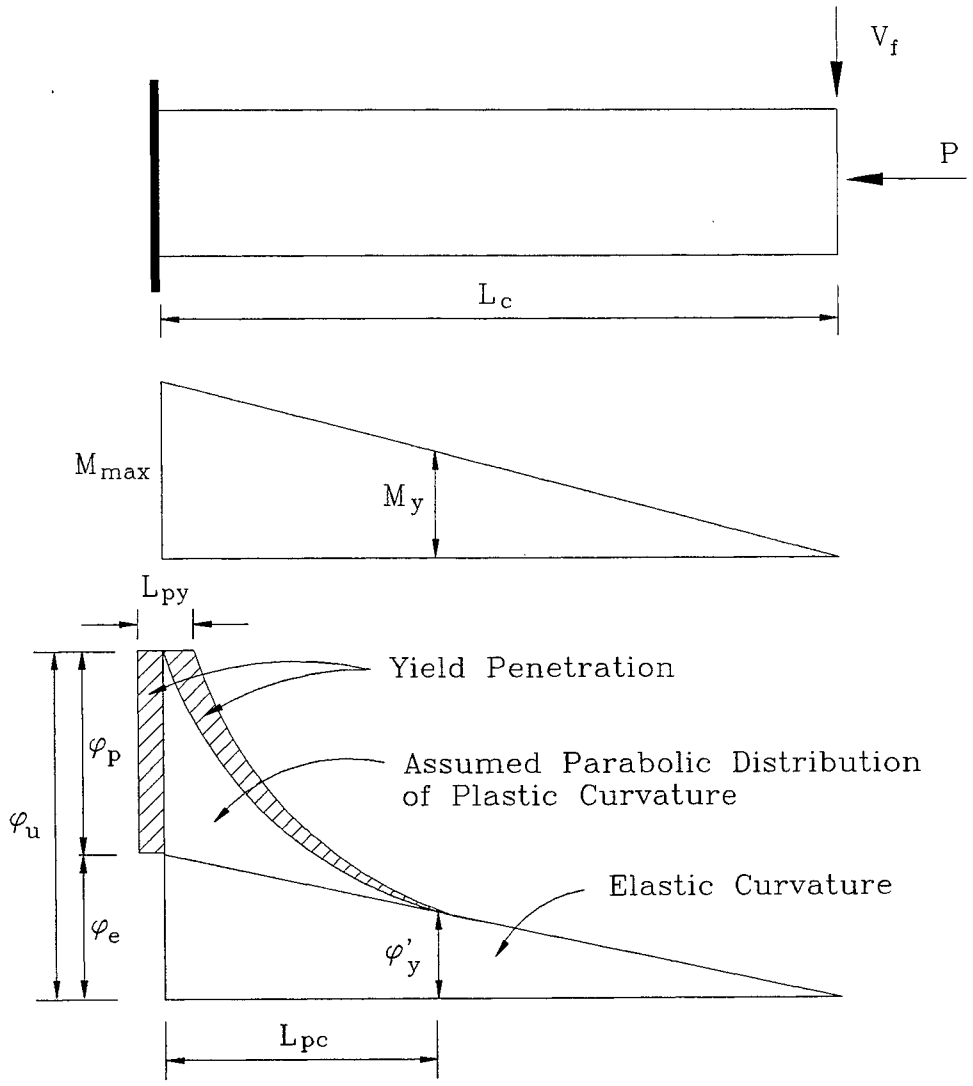

Figure 3-3. Moment-curvature relationship after Mander, et al. *(1984)*.

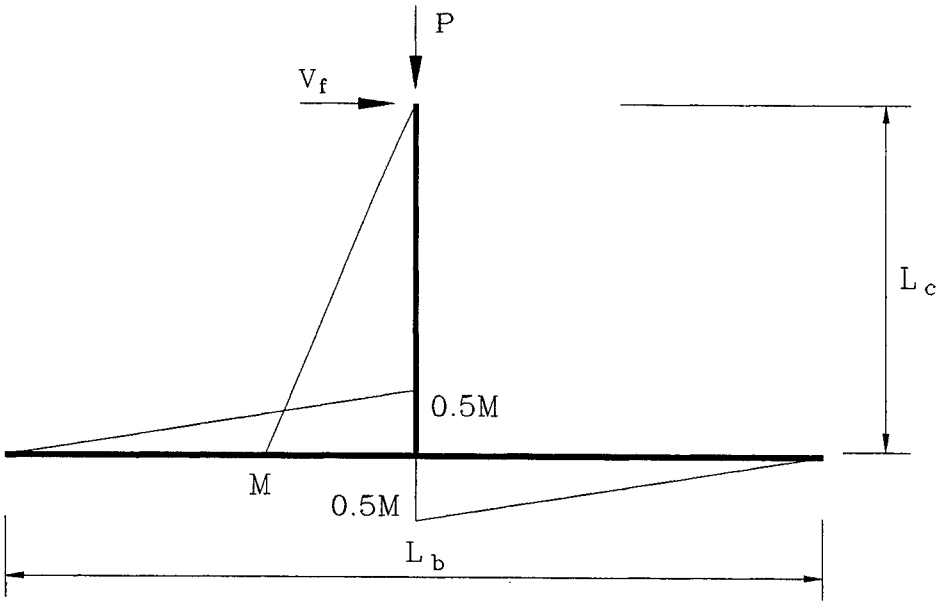

(a) T-shaped beam-column subassemblage

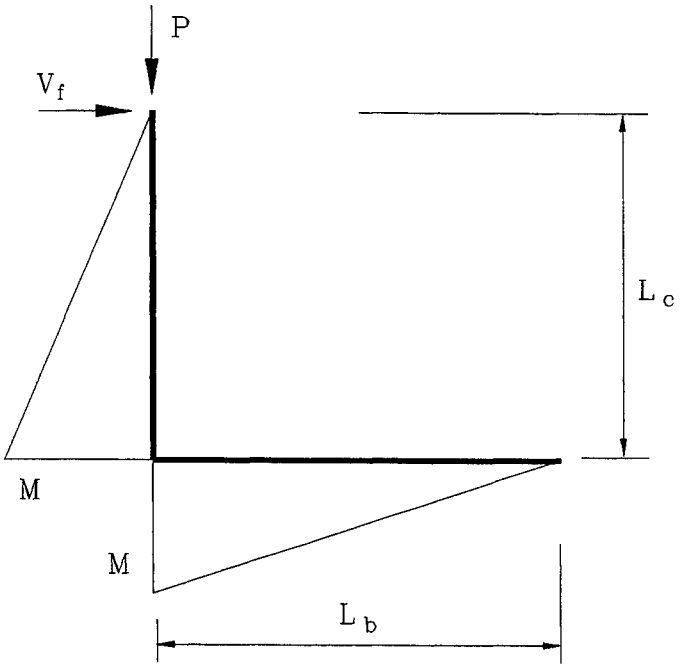

(b) L-shaped beam-column subassemblage

Figure 3-4. Consideration of beam-column joint flexibility.

$$f_b = \frac{L_b}{3EI_b} \tag{3-43b}$$

in which f_b is flexibility of a beam, L_b is shear span of the beam and I_b is the moment of inertia of the beam section. Considering joint rotation, the total column end-to-end rotation due to flexure will be

$$\Theta_f = \Theta_f^e + \Theta_f^p + f_b M \tag{3-44}$$

3.4 Combined Response of Shear and Flexure

Once shear and flexure responses are defined, they should be combined together to obtain the total response as shown in the previous subsections for the piece-wise linear elastic analysis. Since the discussion for shear so far has been limited to the truss mechanism only, the combined total response will be discussed after concrete and arch (axial load) mechanisms are defined in the following sections.

3.5 Evaluation of Effective Section Area of Shear Steel in Circular Columns

It is important to properly evaluate the effective section area of transverse shear reinforcement A_{sh} at spacing s in equations (3-28) through (3-34) for the calculation of shear strength V_s of circular columns. In prismatic sections such as square, rectangular and square hollow-core columns, the section area of transverse shear reinforcement can be straightforwardly obtained, that is, the multiplication of the section area of a single leg by the number of transverse steel legs across the cracked plane. However, in circular columns since the fraction of stress intensity along the circular hoop steel in the loading direction varies as shown in figure 3-5, special care should be used in the evaluation of the effective section area of transverse shear reinforcement of circular columns. Ang *(1985)* and Ang, et al. *(1989)* suggest a reasonable approach in assessing the effective section area of transverse shear reinforcement of circular reinforced concrete columns. Their idea is supplemented and extended to a more general form of equation in the present subsection.

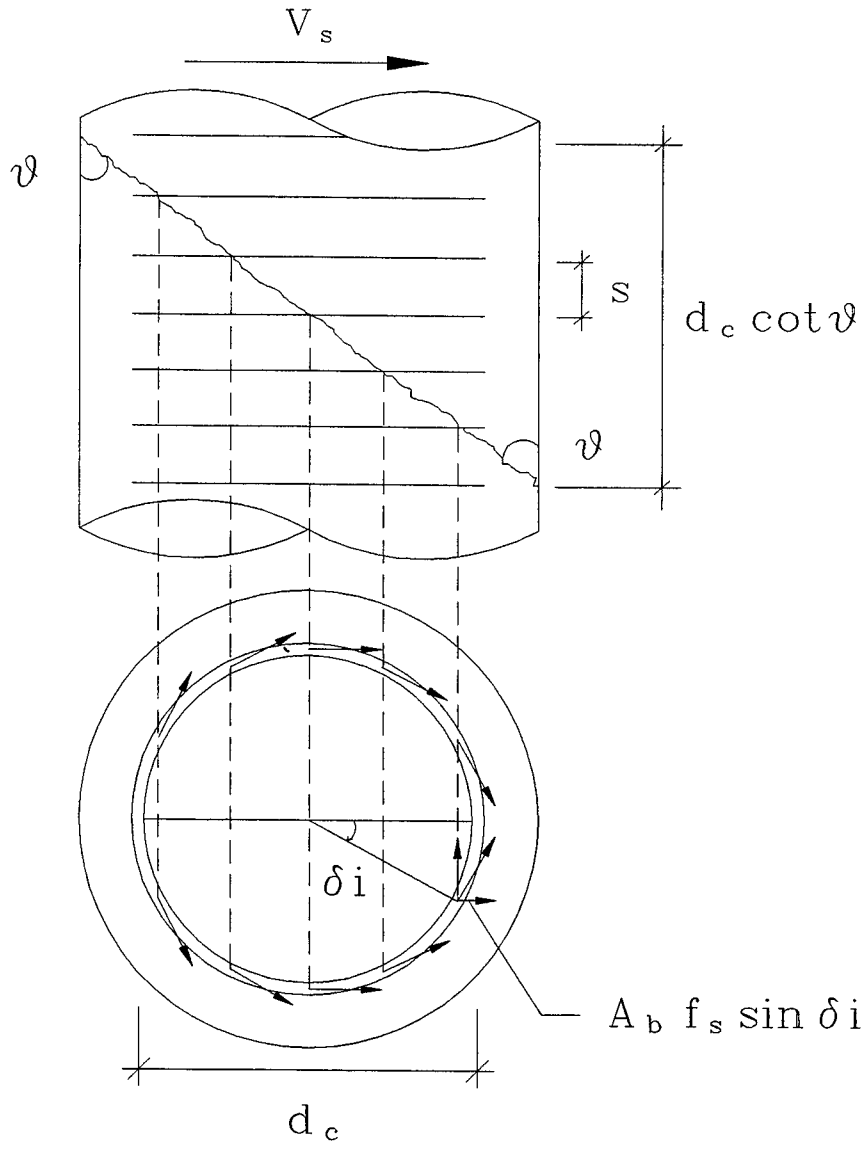

Figure 3-5. Shear resisted by transverse hoops of circular columns after Ang, et al. *(1989)*.

Consider a potential diagonal failure plane defined by the crack angle θ measured to the column longitudinal axis in figure 3-5. Then, the shear force V_s is resisted by the summation of the fractions of forces generated along the circular hoops across the failure plane in the loading direction. Using the average transverse steel strain approach in which it is assumed that the considered transverse hoops develop the same amplitude of stress and strain, the shear force resisted by the transverse hoop steel is calculated by

$$V_s = \sum_{i=1}^{N} 2 A_b f_T \sin\delta i = 2 A_b f_T N (\sin\delta i)_{avg} \tag{3-45}$$

where N is the number of transverse hoops across the cracked plane and A_b is the section area of a single leg of a transverse hoop. Then the average of $\sin\delta i$ is calculated by

$$(\sin\delta i)_{avg} = \frac{1}{N} \sum_{i=1}^{N} \sin\delta i \tag{3-46}$$

where $\delta = \pi/(N+1)$. Performing the summation of the series of constants in equation (3-46),

$$(\sin\delta i)_{avg} = \frac{1}{N} \frac{\sin\left(\frac{\pi}{2}\frac{N}{N+1}\right)}{\sin\left(\frac{\pi}{2}\frac{1}{N+1}\right)} \tag{3-47}$$

where $N = d_c \cot\theta / s$. Substituting equation (3-47) into equation (3-45) gives

$$V_s = \frac{1}{N} \frac{\sin\left(\frac{\pi}{2}\frac{N}{N+1}\right)}{\sin\left(\frac{\pi}{2}\frac{1}{N+1}\right)} 2 A_b f_T \frac{d_c}{s} \cot\theta \tag{3-48}$$

where d_c is the center-to-center diameter of the transverse hoop reinforcement in a circular column. Equation (3-48) can be expressed in resemblance of equation (3-34), thus

$$V_s = A_{sh} f_T \frac{d_c}{s} \cot\theta \tag{3-49}$$

Since $d_c \approx jd$, this equation is considered identical to equation (3-34) itself. Now, the effective section area of transverse shear reinforcement A_{sh} for <u>circular</u> columns is obtained as

$$A_{sh} = \frac{2}{N} \frac{\sin\left(\frac{\pi}{2}\frac{N}{N+1}\right)}{\sin\left(\frac{\pi}{2}\frac{1}{N+1}\right)} A_b \qquad (3\text{-}50)$$

where A_b = area of the spiral or circular hoop bar. Substituting $N = jd\cot\theta/s$ into equation (3-50), the expression can also be

$$A_{sh} = 2\left(\frac{s}{jd}\tan\theta\right) \frac{\sin\left(\frac{\pi/2}{1+\frac{s}{jd}\tan\theta}\right)}{\sin\left(\frac{\pi/2}{1+\frac{jd}{s}\cot\theta}\right)} A_b \qquad (3\text{-}51)$$

This equation can be interpreted in the way that the effective section area of transverse shear reinforcement for a circular column is the summation of the effective number of section areas of single legs of a transverse hoop. The effective number of single legs of a transverse hoop depends on the number of transverse hoops N across the cracked plane as presented in figure 3-6 where equation (3-50) is plotted. It is noted from the figure that the range of the effective section area of a transverse hoop for circular columns is from $A_{sh} = 2A_b$ through $A_{sh} = \frac{4}{\pi}A_b$. This means that the effective section area of a transverse hoop for a circular column varies with the number of transverse hoops provided within the unit length defined by the crack angle ($jd\cot\theta$). Therefore, when a single transverse hoop is placed in the middle of the unit length defined by the crack angle, the effective section area of a transverse hoop is the full section of the transverse hoop reinforcement ($2A_b$). When $N \to \infty$ which is for the case of circular steel jacketing, the effective section area of transverse shear reinforcement is reduced to $\frac{4}{\pi}A_b$ in which $A_b = t_j^2$ where t_j is the thickness of the steel jacket. The present study indicates some insufficient aspect on the shear resisted by transverse reinforcement of circular columns suggested by Ang *(1985)* and Ang, et al. *(1989)*, Chai, et al. *(1991)* and Priestley, et al. *(1994a)*. In their study, they used a single constant parameter $\frac{\pi}{2}A_b$ for the effective section area of transverse shear reinforcement in all cases. This may not do serious harm to the evaluation of shear strength for circular columns with non-seismically designed transverse hoop reinforcement, since the parameter $\frac{\pi}{2}A_b$ gives slightly conservative results. However, for well-

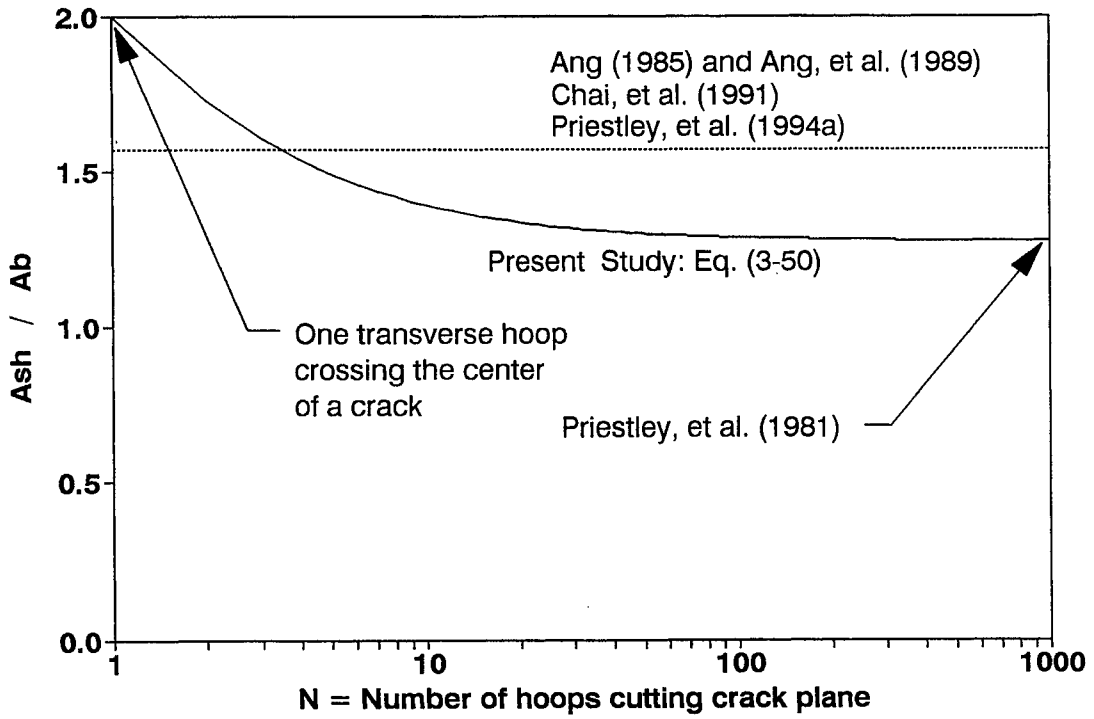

Figure 3-6. Effective section area of transverse shear steel for circular columns.

confined circular columns with close spacing, the parameter $\frac{\pi}{2}A_b$ gives unconservative results. For circular steel jacketing as an extreme case, it gives about a 20% overestimation of the shear capacity. In reality, this measure of unconservatism may be compensated for by the fact that the transverse steel yields and strain-hardens. However, it is recommended that equation (3-49) continued to be used for analyzing circular columns, but A_{sh} be determined specifically from equation (3-50) or (3-51).

3.6 Conclusions Arising from Strength (V_s) Analysis of Truss Mechanism

In this subsection a discussion has been presented for the strength and deformation analysis of a Gauss truss model. The following conclusions are drawn:

1. The piece-wise linear elastic analysis method using the idealized linear model for concrete diagonal struts and trilinear model for longitudinal chords and transverse ties offers a simple and comprehensive analysis tool for shear and flexure that can be performed by hand-calculation.

2. The present study shows that the analysis method can be advanced by implementing a non-linear material model for reinforcing steel which can still be performed by hand-analysis.

3. Yielding of critical transverse steel does not seriously affect the boundary condition constants of the three-point Gauss truss model which are close to those of the two-point Gauss truss model. Therefore, the boundary condition constants determined by the two-point Gauss truss model analysis may be used in all cases.

4. Yielding of critical transverse steel influences the shear force distribution factors for truss linkages of the three-point Gauss truss model. This makes hand analysis implementation a protracted process, but lends itself to a computer-based implementation.

5. The effective section area of transverse shear reinforcement for circular columns is affected by diameter of column section, crack angle and transverse hoop spacing. This indicates

that the widely accepted constant $\pi/2$ used for the calculation of shear strength of circular columns due to transverse steel is not universally applicable, but strictly only applicable when approximately four circular transverse hoops pass through the diagonal crack. Instead, the constant should range between 2 and $4/\pi$, the former being applicable when only one circular transverse hoop cuts the crack and the latter when the circular transverse hoops are very closely spaced or if a steel tube is used for confinement.

SECTION 4

MODELING THE EFFECT OF CONCRETE TENSILE STRENGTH ON COLUMN SHEAR STRENGTH

The truss analogy for the analysis of beam-columns subjected to shear and flexure discussed so far has been limited to the contribution of transverse and longitudinal steel and diagonal concrete compression struts. It should be noted that even though the behavior of reinforced concrete beam-columns after cracking can be modeled with the truss analogy, they are not perfect trusses but still structural elements with a measure of continuity provided by a diagonal tension field. The mere notion of compression field denotes that there should be some tension field coexisting perpendicularly to the compression field. The compression field is assumed to form parallel to the crack plane that forms under combined flexure and shear. Therefore, the concrete tension field may be defined as a mechanism existing across the crack and resisting crack opening. In the present section, the effect of concrete tensile properties on the shear strength and stiffness of reinforced concrete beam-columns is discussed using the Gauss two-point truss model.

4.1 Modeling the Cracked Concrete in Tension (Strain-Softening)

There is a common misconception that concrete having limited tensile strength behaves in a brittle fashion *(Barnard, 1964)*. This misconception has arisen over the years mostly because there is only limited number of references available describing the tensile behavioral characteristics of concrete *(ACI, 1982; Carreira and Chu, 1986; Vecchio and Collins, 1986; Yankelevsky and Reinhardt, 1987; Collins and Mitchell, 1991; Hsu, 1993)*. In fact concrete stress and strain characteristics when normalized with respect to the peak stress and strain are similar in both tension and compression. Such tensile behavior can play a vital role in the shear resistance mechanism of structural elements. Therefore, it is important to utilize the tensile as well as compressive characteristics of concrete in estimating the shear strength and stiffness of reinforced concrete beam-columns. However, it should be noted that following cracking the effect of concrete tensile strength on column shear strength lessens as the deformations increase. Moreover, the scale of concrete tensile strain is considered as about one tenth of concrete

compression strain, which denotes that the effect of concrete tensile strength will be mostly exhausted within a small to moderate deformation range if the column behavior is governed by shear.

4.1.1 Nonlinear Descending Branch Model

Collins and Mitchell *(1991)* suggested the experimentally verified monotonic tensile stress-strain relationship by modifying the equation recommended by Vecchio and Collins *(1986)* to take tensile stresses in concrete between the cracks into account using the average stress-average strain relationship for the cracked concrete. That is,

$$f_t = E_c \varepsilon_t \quad for \quad \varepsilon_t \le \varepsilon_t' \tag{4-1a}$$

$$f_t = \frac{\alpha_1 \alpha_2 f_t'}{1 + \sqrt{500\,\varepsilon_t}} \quad for \quad \varepsilon_t > \varepsilon_t' \tag{4-1b}$$

where f_t = average concrete tensile stress, ε_t = average concrete tensile strain, ε_t' = strain at peak tensile stress, α_1 and α_2 = factors accounting for bond characteristics of reinforcement and sustained or repeated loading, respectively, and f_t' = concrete tensile strength. Collins and Mitchell *(1991)* recommended to take the following as the concrete tensile strength

$$f_t' = 0.333\sqrt{f_c'\ (MPa)} = 4\sqrt{f_c'\ (psi)} \tag{4-2}$$

where f_c' is the concrete cylinder compressive strength. This formulation implicitly assumes that the average concrete stress between diagonal cracks is about two thirds of the maximum given by Carreira and Chu *(1986)*. When the crack opens widely, the shear transfer capacity of the member calculated using equation (4-1) for the average stress – average strain of the cracked concrete may be limited by local variations along the crack plane. The principal local variations are known to be the dowel action and aggregate interlock mechanisms. Paulay *(1971a,b)* theoretically and experimentally showed that the effect of dowel action on the shear behavior is small. To avoid crack slipping failure due to loss of aggregate interlock, the descending branch of the average stress-average strain relationship given in equation (4-1b) needs to be limited by

$$f_t \le \frac{0.6\sqrt{f_c'}}{1 + \dfrac{80\, s_{m\theta}\, \varepsilon_t}{d_a + 16}} \quad (MPa \text{ and } mm) \tag{4-3}$$

where $s_{m\theta}$ = average spacing of the diagonal cracks and d_a = maximum aggregate size. Refer to Vecchio and Collins *(1986)* and Collins and Mitchell *(1991)* for a description of this limitation. However, Hsu *(1996)* and Pang and Hsu *(1996)* have recently pointed out that this is a theoretical fallacy as shear can not coexist in the direction of principal tension strains. Their so-called "softened truss" model neglects this effect.

According to Carreira and Chu *(1986)*, the shape of the monotonic tensile stress-strain curve has been shown to have a descending branch similar to that of monotonic compression. Thus they proposed the use of an equation by Popovics *(1973)* for modeling cracked concrete in tension. The suggested Popovics equation for concrete tensile stress-strain relationship is

$$f_t = \frac{f_t'\, r \left(\dfrac{\varepsilon_t}{\varepsilon_t'}\right)}{r - 1 + \left(\dfrac{\varepsilon_t}{\varepsilon_t'}\right)^r} \tag{4-4}$$

where

$$r = \frac{E_c}{E_c - E_{sec}} \quad , \quad E_{sec} = \frac{f_t'}{\varepsilon_t'} \quad and \quad E_c = 5000\sqrt{f_c'} \ \ (MPa).$$

One advantage in using Popovics' equation is that the equation contains the ascending as well as descending branches in a single expression. For f_c' = 30 *MPa*, ε_t' = 0.0002, $s_{m\theta}$ = 450 *mm* and d_a = 20 *mm*, figure 4-1 presents the normalized stress-strain curves of concrete in tension suggested by Collins and Mitchell *(1991)* and using Popovics equation. Note the closeness of two curves to each other. Furthermore, Chang and Mander *(1994)* concluded that considerable experimental data scattering for the descending branch of concrete in tension given by Vecchio and Collins *(1986)* makes the choice of any simple equation justifiable. This is a very important

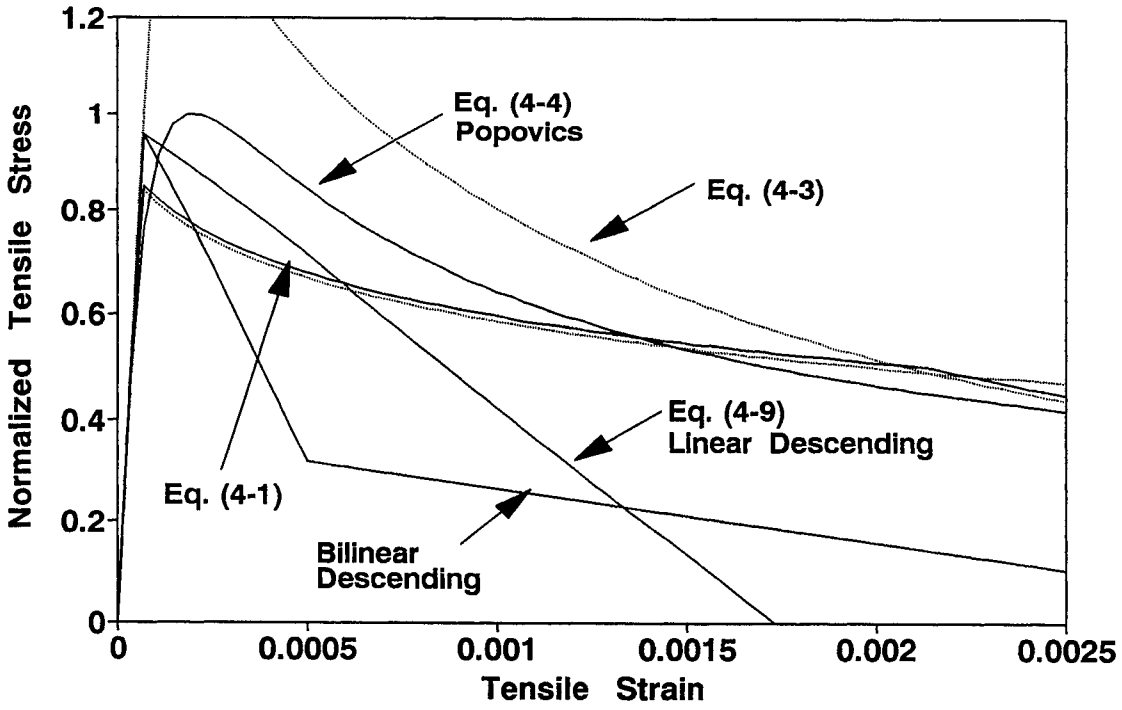

Figure 4-1. Concrete tensile stress curves considered for concrete mechanism.

conclusion. Therefore, Popovics equation will be adopted herein for concrete tensile characteristics in the following discussion.

4.1.2 Linear Descending Branch Model

The previously mentioned concrete tensile stress curves can be further simplified by using the straight line descending branch. The simplified model can then be implemented into computational modeling of concrete mechanism for shear resistance using a general purpose nonlinear inelastic structural analysis program. In the simplified model with the linear descending branch, it is very important to properly determine the ultimate tensile strain at which tensile stress can no longer be transferred. For this purpose, the fracture energy of concrete is considered so that the equivalent amount of energy can be dissipated by concrete rupture between the nonlinear and linear descending branch models.

For the consideration of fracture energy of concrete in the present study, references are made to Rots, et al. *(1985)* and Morcos and Bjorhovde *(1995)*. The fracture energy G_f is defined as the amount of energy required to create one unit of area of a continuous crack and calculated by the area under the tensile stress - cracking opening softening diagram as shown in figure 4-2. Therefore, the fracture energy G_f can be expressed as

$$G_f = h g_f = h \int_{\varepsilon_t'}^{\varepsilon_u} \sigma \, d\varepsilon_t \tag{4-5}$$

where g_f = area under the stress-strain softening diagram, $\varepsilon_t' = f_t'/E_c$ and ε_u = ultimate strain where stress can no longer be transferred. The discrete crack model can be related to the smeared crack model by the relationship of

$$w = h \varepsilon_1 \tag{4-6}$$

where w = crack opening displacement due to crack strain over the crack band width h within the finite element and ε_1 = average crack normal strain over the band width h in the direction of the maximum tensile stress. Based on studies undertaken by Bažant and Oh *(1983)*, the crack band width h is dependent on the aggregate size, they found:

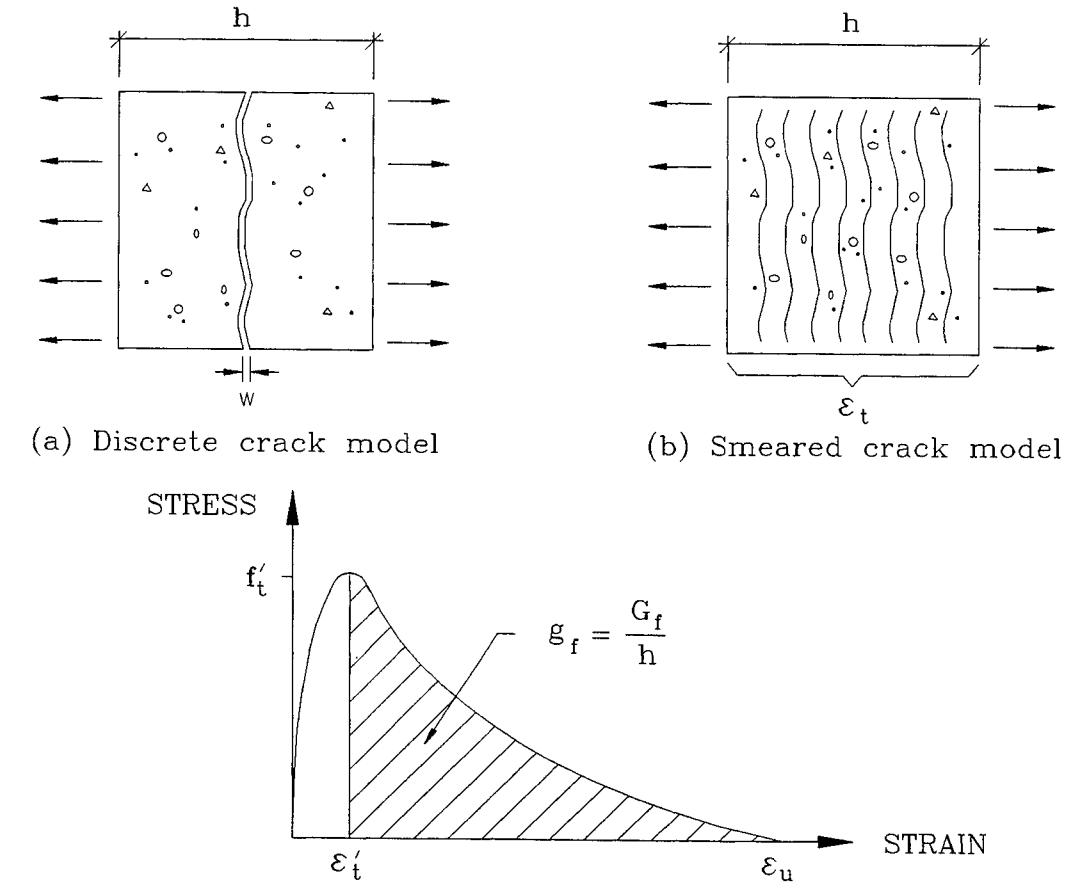

Figure 4-2. Crack models and definition of fracture energy of concrete.

$$h = 3 d_a \tag{4-7}$$

where d_a = maximum aggregate size. Referring to figure 4-2 and using equations (4-5) and (4-7), the ultimate tensile strain ε_u for the straight line descending branch model is obtained by

$$\varepsilon_u = \varepsilon_t' + \frac{G_f}{1.5\, d_a\, f_t'} = \varepsilon_t' + \frac{2\, G_f}{f_t'\, h} \tag{4-8a}$$

Note that the inelastic portion of ultimate strain given by equation (4-8) is identical to the one proposed by Rots, et al. *(1985)*. Petersson *(1980)* found from the experimental study that typical values of the fracture energy of normal-weight concrete are in the range of 60 - 100 N/m. As an example, for G_f = 100 *N/m*, d_a = 20 *mm*, f_t' = 2 *MPa* (f_c' = 30 *MPa*) and ε_t' = 0.000067, then the ultimate strain becomes ε_u = 0.00173 which is $26\,\varepsilon_t'$. Rots, et al. *(1985)* also proposes a bilinear descending branch model as shown in figure 4-2(e). The ultimate strain ε_u is given by

$$\varepsilon_u = \frac{18}{5} \frac{G_f}{f_t'\, h} \tag{4-8b}$$

The bilinear representation of the stress-strain relation for concrete in tension can be achieved using the Menegotto-Pinto equation, thus

$$f_t = E_c \varepsilon_t \left[Q + \frac{1 - Q}{\left\{ 1 + \left(\frac{E_c \varepsilon_t}{f_t'} \right)^{20} \right\}^{0.05}} \right] \tag{4-9}$$

where

$$Q = \frac{-f_t'}{E_c (\varepsilon_u - \varepsilon_t')} \quad .$$

Using the previously presented parameter values, the resultant bilinear behavior of concrete in tension is shown in figure 4-1 together with previously discussed models. Also shown in figure 4-1 is the behavior of bilinear softening diagram. From the comparison it is noted that the fracture energy-based model shows much more rapid descending branch than the other models.

4.2 Variable Angle Truss for Concrete Only Mechanism - Theory

A variable angle truss shown in figure 4-3 is considered for the effect of concrete continuum acting across the representative corner-to-corner crack plane on the shear strength of a short column. In a similar way to the solution of the variable angle truss mechanism for transverse steel contribution discussed in subsection 2.2.3, consider a single differential truss element subjected to the differential shear force dV_c in figure 4-3. The differential shear force dV_c depends on the concrete tensile stress-crack opening relation and varies along the column length. Note that a differential truss consists of an idealized concrete tie with a finite depth $d_x \cos\alpha$ inclined by corner-to-corner angle α from the transverse direction of the column and two tapered diagonal concrete struts. A tapered diagonal concrete strut is idealized as a prismatic strut with the average depth. Assuming rigid longitudinal chords to negate the effects of flexural deformation, the contribution of concrete only mechanism to the column shear resistance can be considered. The shear deformation of the differential truss can then be calculated by the Virtual Work method of analysis using the member forces shown in figure 4-3. Since the differential truss element is statically determinate, the member forces can easily be determined by static equilibrium. The determination of the member deformations of a differential portion of a variable angle truss is presented in table 4-1. Displacement compatibility requires that the deformation of each differential truss element be the same as the overall shear deformation of the short column.

The axial strain and stress of truss member B-C are respectively considered as the principal strain ε_1 and stress f_1 acting across the crack plane. Using this notion, the component shear deformation due to the contribution of truss member B-C can also be expressed as

$$\Delta_{B-C} = \left(\frac{Ffl}{EA}\right)_{B-C} = \varepsilon_1 fL = \varepsilon_1 jd \sec^2\alpha \qquad (4\text{-}10)$$

The shear deformation of a differential truss is the sum of the component deformations of a tie and two struts, thus

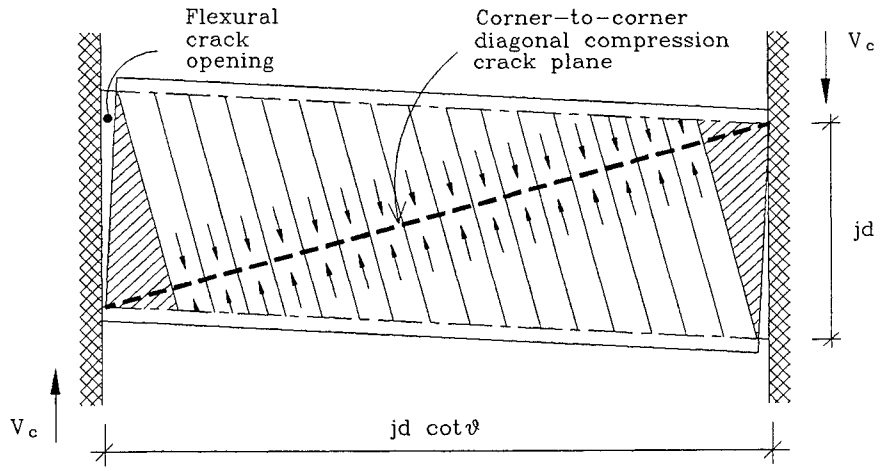

(a) Tension field in concrete continuum

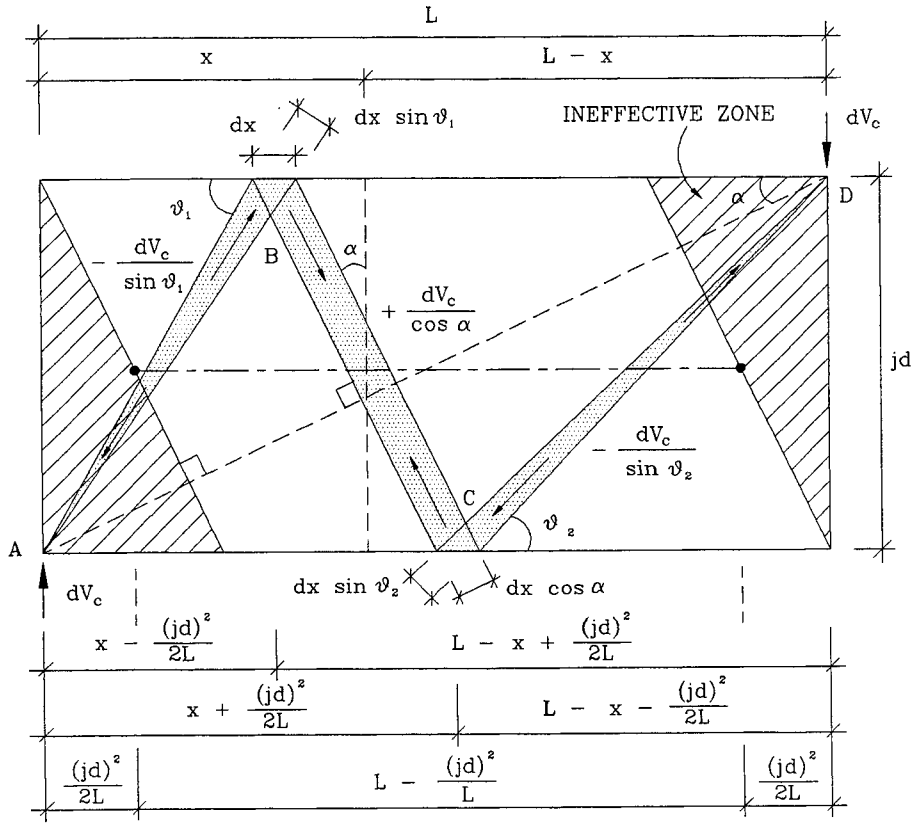

(b) A differential truss mechanism

Figure 4-3. Variable angle truss model for concrete only mechanism.

Table 4-1. Shear deformation of a differential element in a variable angle truss.

Member	Force F	Unit Load f	Length l	Rigidity EA	Strain $\varepsilon = F/EA$	$\frac{Ffl}{EA}$
A-B	$\frac{-dV_c}{\sin\theta_1}$	$\frac{-1}{\sin\theta_1}$	$\frac{jd}{\sin\theta_1}$	$\frac{E_{cc}b_{wc}dx\sin\theta_1}{2}$	$\frac{-2dV_c/dx}{E_{cc}b_{wc}\sin^2\theta_1}$	$\frac{2jd\,dV_c/dx}{E_{cc}b_{wc}\sin^4\theta_1}$
B-C	$\frac{+dV_c}{\cos\alpha}$	$\frac{+1}{\cos\alpha}$	$\frac{jd}{\cos\alpha}$	$E_{ct}b_w dx\cos\alpha$	$\frac{+dV_c/dx}{E_{ct}b_w\cos^2\alpha}$	$\frac{jd\,dV_c/dx}{E_{ct}b_w\cos^4\alpha}$
C-D	$\frac{-dV_c}{\sin\theta_2}$	$\frac{-1}{\sin\theta_2}$	$\frac{jd}{\sin\theta_2}$	$\frac{E_{cc}b_{wc}dx\sin\theta_2}{2}$	$\frac{-2dV_c/dx}{E_{cc}b_{wc}\sin^2\theta_2}$	$\frac{2jd\,dV_c/dx}{E_{cc}b_{wc}\sin^4\theta_2}$

Note: Refer to figure 4-3.

$$\sin\theta_1 = \frac{\left(\frac{jd}{L}\right)}{\sqrt{\left[\frac{x}{L} - \frac{1}{2}\left(\frac{jd}{L}\right)^2\right]^2 + \left(\frac{jd}{L}\right)^2}} \quad ; \quad \sin\theta_2 = \frac{\left(\frac{jd}{L}\right)}{\sqrt{\left[1 - \frac{x}{L} - \frac{1}{2}\left(\frac{jd}{L}\right)^2\right]^2 + \left(\frac{jd}{L}\right)^2}}$$

$$\Delta_s = \sum \frac{Ffl}{EA}$$

$$= \frac{2jd\left(\frac{L}{jd}\right)^4}{E_{cc}b_{wc}} \frac{dV_c}{dx}\left\{\left[\left(\frac{x}{L} - \frac{1}{2}\left(\frac{jd}{L}\right)^2\right)^2 + \left(\frac{jd}{L}\right)^2\right]^2 + \left[\left(1 - \frac{x}{L} - \frac{1}{2}\left(\frac{jd}{L}\right)^2\right)^2 + \left(\frac{jd}{L}\right)^2\right]^2\right\} + \varepsilon_1 jd\sec^2\alpha \tag{4-11}$$

where E_{cc} = modulus of elasticity of concrete in compression and b_{wc} = portion of column width contributing to struts for the concrete only mechanism. Note that the same shear deformation Δ_s should be imposed on the concrete truss mechanism as well as the steel truss mechanism. Recalling that $\cot\alpha = L/jd$, equation (4-11) can be rearranged as:

$$\Delta_s = \frac{2jd\cot^4\alpha}{E_{cc}b_{wc}} \frac{dV_c}{dx}\left\{\left[\left(\frac{x}{L} - \frac{1}{2}\tan^2\alpha\right)^2 + \tan^2\alpha\right]^2 + \left[\left(1 - \frac{x}{L} - \frac{1}{2}\tan^2\alpha\right)^2 + \tan^2\alpha\right]^2\right\} \tag{4-12}$$

$$+ \varepsilon_1 jd(1 + \tan^2\alpha)$$

where α = corner-to-corner diagonal angle of the variable angle truss. Then, the column end-to-end rotation (drift) angle is determined by dividing the shear displacement Δ_s by the column

length L, thus

$$\Theta_s = \frac{2\cot^3\alpha}{E_{cc}b_{wc}}\frac{dV_c}{dx}\left\{\left[\left(\frac{x}{L}-\frac{1}{2}\tan^2\alpha\right)^2+\tan^2\alpha\right]^2+\left[\left(1-\frac{x}{L}-\frac{1}{2}\tan^2\alpha\right)^2+\tan^2\alpha\right]^2\right\} \quad (4\text{-}13)$$

$$+\varepsilon_1\tan\alpha(1+\tan^2\alpha)$$

Referring to table 4-1 for the axial strain of truss member B-C, dV_c/dx can be expressed as:

$$\frac{dV_c}{dx} = \varepsilon_1 E_{ct} b_w \cos^2\alpha = f_1 b_w \cos^2\alpha \quad (4\text{-}14)$$

where ε_1 and f_1 are the principal tensile strain and stress, respectively. It is noted that the full width of column section (b_w) is used in equation (4-14) for concrete tensile tie member B-C because cracking over the full width ($b_{ws} + b_{wc} + b_{wp}$) should be considered for the contribution of concrete tensile strength. However, only a portion of column width (b_{wc}) is considered in equations (4-11) to (4-13) for concrete struts (members A-B and C-D) for equilibrium and compatibility conditions in compression struts between different mechanisms. The significance of b_{ws}, b_{wc} and b_{wp} has been mentioned in Section 1. Substituting the expression for dV_c/dx into equation (4-13), the shear deformation can be expressed in terms of stress-strain relation, thus

$$\Theta_s = \frac{2f_1\cos^2\alpha\cot^3\alpha}{E_{cc}\left(\frac{b_{wc}}{b_w}\right)}\left\{\left[\left(\frac{x}{L}-\frac{1}{2}\tan^2\alpha\right)^2+\tan^2\alpha\right]^2+\left[\left(1-\frac{x}{L}-\frac{1}{2}\tan^2\alpha\right)^2+\tan^2\alpha\right]^2\right\} \quad (4\text{-}15)$$

$$+\varepsilon_1\tan\alpha(1+\tan^2\alpha)$$

Rearranging equation (4-15), a convenient constant can be defined as

$$C = \Theta_s\cot\alpha\cos^2\alpha$$

$$= \frac{2f_1\cos^4\alpha\cot^4\alpha}{E_{cc}\left(\frac{b_{wc}}{b_w}\right)}\left\{\left[\left(\frac{x}{L}-\frac{1}{2}\tan^2\alpha\right)^2+\tan^2\alpha\right]^2+\left[\left(1-\frac{x}{L}-\frac{1}{2}\tan^2\alpha\right)^2+\tan^2\alpha\right]^2\right\}+\varepsilon_1 \quad (4\text{-}16)$$

It is noted from the first term of equation (4-16) that the constant C for the given shear deformation is independent on coordinate x. Therefore, the relation of stress f_1 and strain ε_1

for concrete in tension acting across and along the crack plane can be defined for the given constant C. Furthermore, the constant C, as a function of f_1 and ε_1, can be used to determine the shear deformation Θ_s. That is, from equation (4-16):

$$\Theta_s = C \tan\alpha \sec^2\alpha \tag{4-17}$$

It is also noted in equations (4-15) and (4-16) that the ratio of column width b_{wc}/b_w is introduced. When the column is reinforced only with longitudinal reinforcement and there is no axial load which means that $\rho_v = 0.0$ and $P = 0.0$, the full range of column width becomes effective, that is, $b_{wc}/b_w = 1.0$. In all other cases, the ratio b_{wc}/b_w should change instantaneously with shear deformation in proportion to V_c/V_u to maintain the equilibrium and compatibility conditions, in which $V_u = V_s + V_c + V_p$. In defining the column shear force and deformation relationship due to the contribution of concrete only mechanism, two equations are considered for concrete tensile stress-strain relationship: Popovics equation for the nonlinear descending branch model and Menegotto-Pinto equation for the linear descending branch model. The analysis can be performed by hand-calculation using the spreadsheet or implemented into the advanced computer analysis program.

4.2.1 Nonlinear Descending Branch Model

Substituting Popovics equation given in equation (4-4) into equation (4-16) for f_1 and rearranging,

$$C = \varepsilon_1 \left[1 + \frac{2\cos^4\alpha \cot^4\alpha \left\{ \left[\left(\frac{x}{L} - \frac{1}{2}\tan^2\alpha \right)^2 + \tan^2\alpha \right]^2 + \left[\left(1 - \frac{x}{L} - \frac{1}{2}\tan^2\alpha \right)^2 + \tan^2\alpha \right]^2 \right\}}{\left(\frac{b_{wc}}{b_w} \right) \left\{ 1 + \left(\frac{E_{cc}}{E_{sec}} - 1 \right) \left(\frac{\varepsilon_1}{\varepsilon_t'} \right)^r \right\}} \right] \tag{4-18}$$

in which $E_{cc} = E_c$ is the modulus of elasticity of concrete struts and r and E_{sec} are defined in equation (4-4). The concrete tensile strain profile along the crack plane is then obtained from equation (4-18) in terms of the longitudinal coordinate x, thus

$$\varepsilon_1 = \frac{C}{1 + \dfrac{2\cos^4\alpha\cot^4\alpha\left\{\left[\left(\frac{x}{L} - \frac{1}{2}\tan^2\alpha\right)^2 + \tan^2\alpha\right]^2 + \left[\left(1 - \frac{x}{L} - \frac{1}{2}\tan^2\alpha\right)^2 + \tan^2\alpha\right]^2\right\}}{\left(\frac{b_{wc}}{b_w}\right)\left\{1 + \left(\frac{E_{cc}}{E_{sec}} - 1\right)\left(\frac{\varepsilon_1}{\varepsilon_t'}\right)^r\right\}}} \tag{4-19}$$

Since for a given shear deformation, C is constant through the column length [see equation (4-16)], C can be determined by any value of x. Taking $x/L = 0.5$ where the maximum concrete tensile strain is expected (see figure 2-12), C can be defined in terms of the maximum strain ε_1^{max}, that is,

$$C = \varepsilon_1^{max}\left[1 + \frac{4\cos^4\alpha\cot^4\alpha\left[\frac{1}{4}(1-\tan^2\alpha)^2 + \tan^2\alpha\right]^2}{\left(\frac{b_{wc}}{b_w}\right)\left\{1 + \left(\frac{E_{cc}}{E_{sec}} - 1\right)\left(\frac{\varepsilon_1^{max}}{\varepsilon_t'}\right)^r\right\}}\right] \tag{4-20}$$

Substituting the constant C in equation (4-20) into equation (4-19), the ratio of the concrete tensile strain ε_1 of any location x to the maximum concrete tensile strain ε_1^{max} at column center can be calculated as

$$\frac{\varepsilon_1}{\varepsilon_1^{max}} = \frac{1 + \dfrac{4\cos^4\alpha\cot^4\alpha\left[\frac{1}{4}(1-\tan^2\alpha)^2 + \tan^2\alpha\right]^2}{\left(\frac{b_{wc}}{b_w}\right)\left\{1 + \left(\frac{E_{cc}}{E_{sec}} - 1\right)\left(\frac{\varepsilon_1^{max}}{\varepsilon_t'}\right)^r\right\}}}{1 + \dfrac{2\cos^4\alpha\cot^4\alpha\left\{\left[\left(\frac{x}{L} - \frac{1}{2}\tan^2\alpha\right)^2 + \tan^2\alpha\right]^2 + \left[\left(1 - \frac{x}{L} - \frac{1}{2}\tan^2\alpha\right)^2 + \tan^2\alpha\right]^2\right\}}{\left(\frac{b_{wc}}{b_w}\right)\left\{1 + \left(\frac{E_{cc}}{E_{sec}} - 1\right)\left(\frac{\varepsilon_1}{\varepsilon_t'}\right)^r\right\}}} \tag{4-21}$$

Therefore, for a chosen ε_1^{max}, the principal tensile strain profile ε_1 along the column length can be determined. However, some iterative procedure is required since ε_1 is also a function of itself.

4.2.2 Linear Descending Branch Model

Substituting Menegotto-Pinto equation given in equation (4-9) into equation (4-16) for f_1 and rearranging,

$$C = \varepsilon_1 \left\{ 1 + \frac{2\cos^4\alpha \cot^4\alpha}{\left(\frac{b_{wc}}{b_w}\right)} \left[Q + \frac{1-Q}{\left[1 + \left(\frac{E_{cc}\varepsilon_1}{f_t'} \right)^R \right]^{\frac{1}{R}}} \right] \left(\left[\left(\frac{x}{L} - \frac{1}{2}\tan^2\alpha \right)^2 + \tan^2\alpha \right]^2 + \left[\left(1 - \frac{x}{L} - \frac{1}{2}\tan^2\alpha \right)^2 + \tan^2\alpha \right]^2 \right) \right\} \tag{4-22}$$

in which $E_{cc} = E_c$ is the modulus of elasticity of concrete struts and Q is defined in equation (4-9). The concrete tensile strain profile along the crack plane is then obtained from equation (4-22) in terms of the longitudinal coordinate x, thus

$$\varepsilon_1 = \frac{C}{1 + \frac{2\cos^4\alpha\cot^4\alpha}{\left(\frac{b_{wc}}{b_w}\right)} \left[Q + \frac{1-Q}{\left[1 + \left(\frac{E_{cc}\varepsilon_1}{f_t'} \right)^R \right]^{\frac{1}{R}}} \right] \left(\left[\left(\frac{x}{L} - \frac{1}{2}\tan^2\alpha \right)^2 + \tan^2\alpha \right]^2 + \left[\left(1 - \frac{x}{L} - \frac{1}{2}\tan^2\alpha \right)^2 + \tan^2\alpha \right]^2 \right)} \tag{4-23}$$

Taking $x/L = 0.5$ where the maximum concrete tensile strain is expected (see figure 2-12), the constant C can be defined in terms of the maximum strain ε_1^{max}, that is,

$$C = \varepsilon_1^{max} \left\{ 1 + \frac{4\cos^4\alpha\cot^4\alpha}{\left(\frac{b_{wc}}{b_w}\right)} \left[Q + \frac{1-Q}{\left[1 + \left(\frac{E_{cc}\varepsilon_1^{max}}{f_t'} \right)^R \right]^{\frac{1}{R}}} \right] \left[\frac{1}{4}(1 - \tan^2\alpha)^2 + \tan^2\alpha \right]^2 \right\} \tag{4-24}$$

Substituting the constant C in equation (4-24) into equation (4-23), the ratio of concrete tensile strain ε_1 of any location x to the maximum concrete tensile strain ε_1^{max} at column center can be calculated as

$$\frac{\varepsilon_1}{\varepsilon_1^{max}} = \frac{1 + \frac{4\cos^4\alpha\cot^4\alpha}{\left(\frac{b_{wc}}{b_w}\right)} \left[Q + \frac{1-Q}{\left[1 + \left(\frac{E_{cc}\varepsilon_1^{max}}{f_t'} \right)^R \right]^{\frac{1}{R}}} \right] \left[\frac{1}{4}(1 - \tan^2\alpha)^2 + \tan^2\alpha \right]^2}{1 + \frac{2\cos^4\alpha\cot^4\alpha}{\left(\frac{b_{wc}}{b_w}\right)} \left[Q + \frac{1-Q}{\left[1 + \left(\frac{E_{cc}\varepsilon_1}{f_t'} \right)^R \right]^{\frac{1}{R}}} \right] \left(\left[\left(\frac{x}{L} - \frac{1}{2}\tan^2\alpha \right)^2 + \tan^2\alpha \right]^2 + \left[\left(1 - \frac{x}{L} - \frac{1}{2}\tan^2\alpha \right)^2 + \tan^2\alpha \right]^2 \right)} \tag{4-25}$$

4.2.3 Solution Strategy

Equations derived through subsections 4.2.1 and 4.2.2 are to build up the profiles of concrete tensile strain and stress acting across and along the corner-to-corner diagonal crack plane. The following calculation steps are introduced for this purpose:

Step 1 Choose ε_1^{max}.

Step 2 For all locations of x, calculate $\varepsilon_1/\varepsilon_1^{max}$ using equation (4-21) for nonlinear descending branch model; equation (4-25) for linear descending branch model.

Step 3 Calculate $\varepsilon_1(x)$ for all locations of x, where $\varepsilon_1 = \varepsilon_1^{max}\left(\varepsilon_1/\varepsilon_1^{max}\right)$.

Step 4 Return to Step 2 until converged.

Step 5 Calculate $f_1(\varepsilon_1(x))$ for all locations of x using equation (4-4) for nonlinear descending branch model; equation (4-9) for linear descending branch model.

Step 6 Repeat Steps 1-5 for increasing values of ε_1^{max}.

Step 7 Plot ε_1 vs. f_1 for a given α.

Figures 4-4 and 4-5 present the concrete tensile strain and stress profiles for nonlinear and linear descending branch models, respectively, with value of $b_{wc}/b_w = 1.0$, acting across and along the diagonal crack plane. As an example, $f_c' = 30\ MPa$, $f_t' = 2\ MPa$, $\varepsilon_t' = 0.0002$, and $\cot\alpha = L/jd = 2$ (*i.e.*, $\alpha = 26.6°$) are used for the nonlinear descending branch model. For linear descending branch model $\varepsilon_t' = 0.000067$ and $\varepsilon_u = 0.00173$ are used. The maximum principal strains ε_1^{max} at column center is chosen as 0.0002, 0.0004, 0.0006, 0.0008 and 0.001 for demonstration. The increasing ε_1^{max} denotes the increasing column shear deformation Θ_s. It is noted that the principal strain and stress profiles are changing as ε_1^{max} changes. Principal strain and stress profiles are symmetrical about column center along the column longitudinal axis. Also noted is that the peak stresses are moving outward as ε_1^{max} increases. Note that the similarity of the principal strain and stress profiles between nonlinear descending branch model in figure 4-4 and linear descending branch model in figure 4-5. Principal stresses of the linear descending branch model degrade more rapidly than those of the nonlinear descending branch model as expected from the concrete tensile stress curves presented in figure 4-1. Because of the effect of

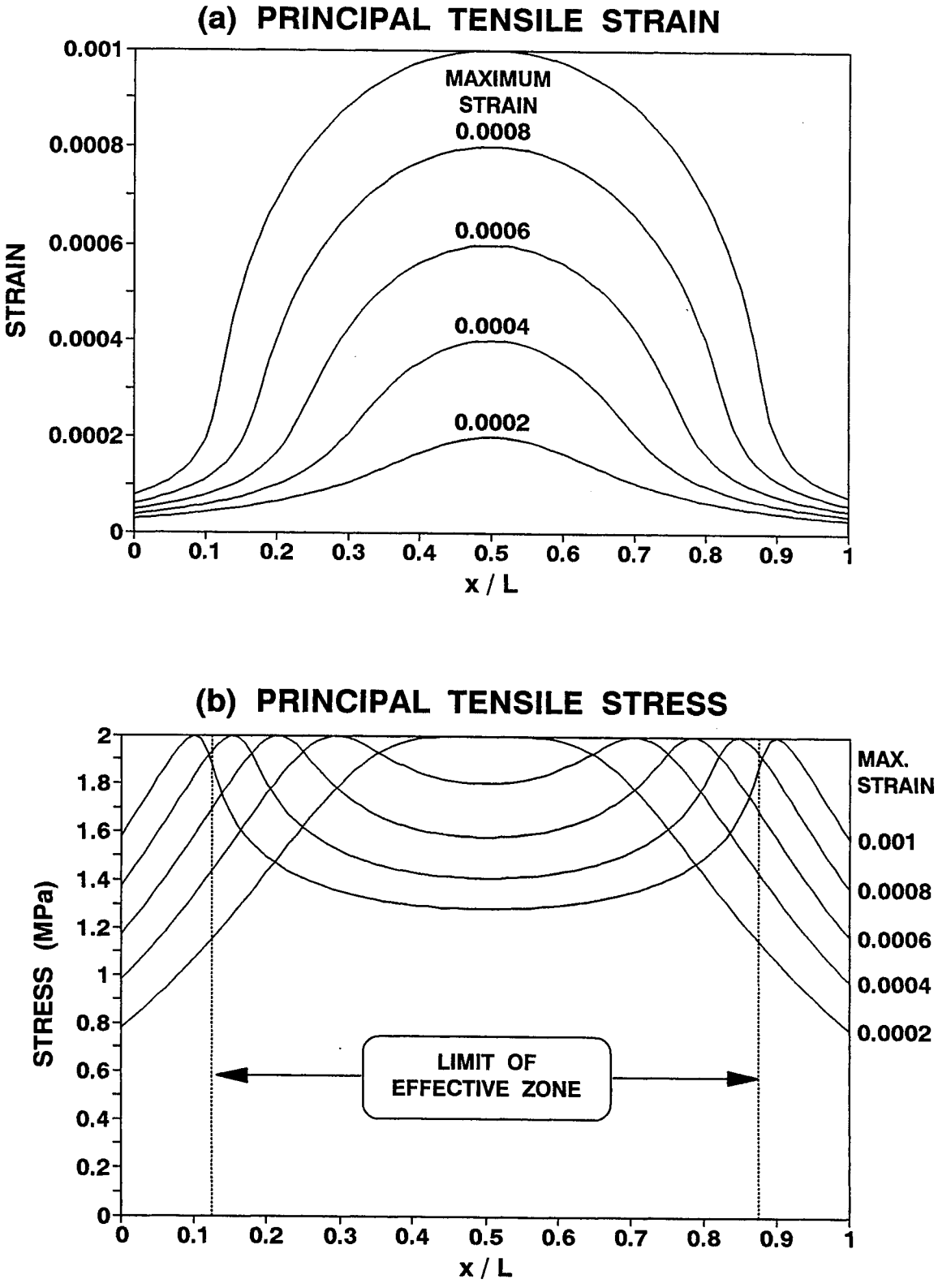

Figure 4-4. Concrete tensile strain and stress profiles using nonlinear softening model for $f_t' = 2\ MPa$, $\varepsilon_t' = 0.0002$, $L/jd = 2$ and $b_{wc}/b_w = 1.0$.

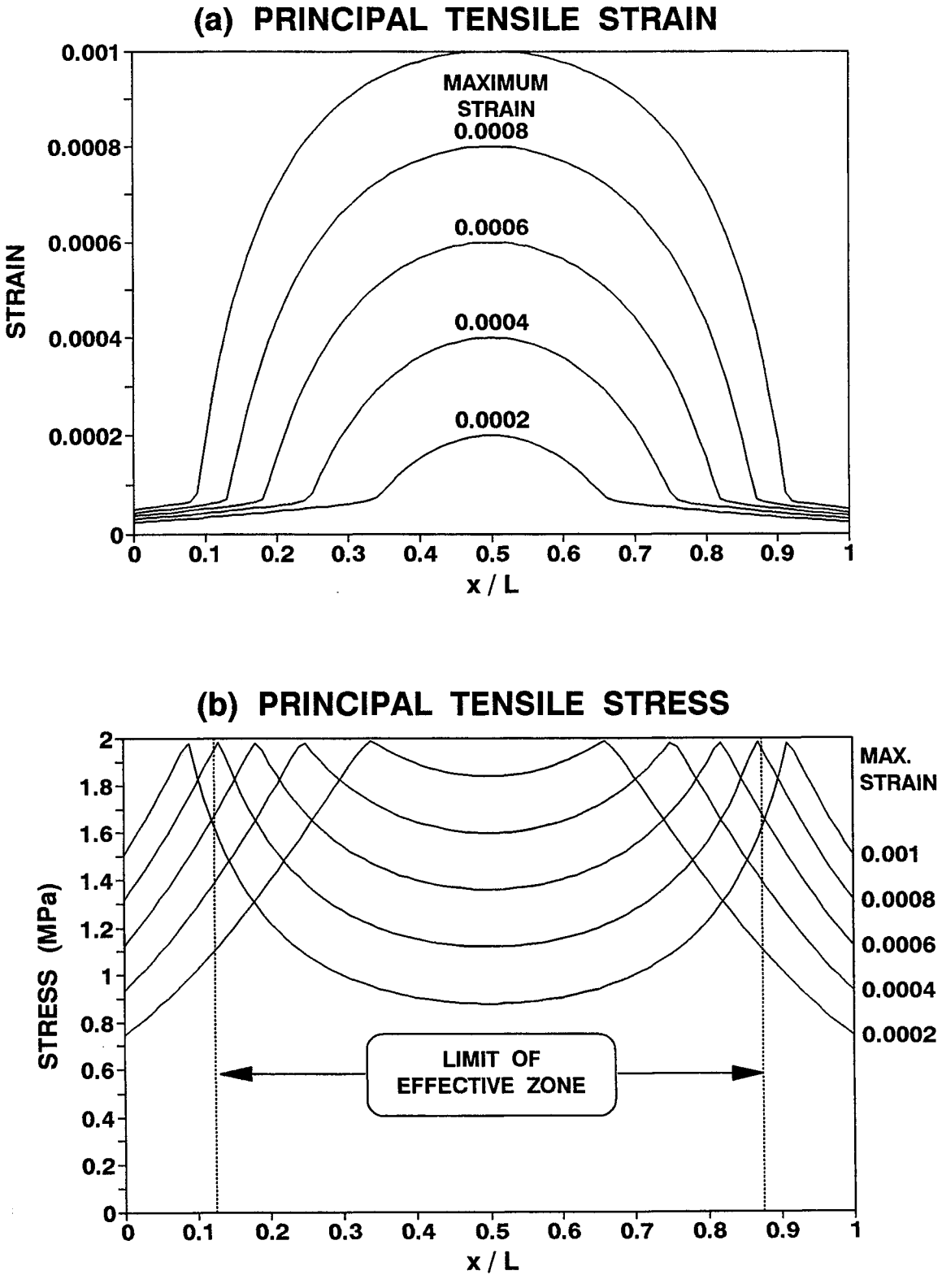

Figure 4-5. Concrete tensile strain and stress profiles using linear softening model for $f_t' = 2\ MPa$, $\varepsilon_t' = 0.0002$, $L/jd = 2$ and $b_{wc}/b_w = 1.0$.

exponential parameter in equation (4-9), the peak stresses of the linear descending branch model are slightly less than f_t'. Also noted is that the strains at peak stresses between two descending branch models are different from each other.

The limit of effective zone noted in figures 4-4 and 4-5 is introduced to consider the effect of flexural cracking at the critical region which is usually the disturbed region (so-called D-region). There are shaded triangular parts in a column at both ends shown in figure 4-3. If concrete tie member B-C is located within this region, it is considered that because of flexural cracking along the column end, there will be no proper anchorage existing to maintain the concrete tie strength. The same problem is expected to exist at the free end zone, too. Those shaded triangular end regions, either of fixed or free, become ineffective on the strength of concrete only mechanism. Therefore, the only effective zone will be considered for the column shear resistance in the following discussion. By the column geometry and corner-to-corner diagonal angle α, the effective zone is estimated as

$$L_{eff} = jd(\cot\alpha - \tan\alpha) = L(1 - \tan^2\alpha) \tag{4-26}$$

4.3 Numerical Solution of A Variable Angle Truss for Concrete Only Mechanism

To obtain the column shear strength V_c due to concrete tensile strength effect, it is necessary to integrate the principal stress profiles shown in figures 4-4 and 4-5 over the effective length of the column given in equation (4-26). For this purpose, equation (4-13) is rearranged for differential shear force dV_c:

$$dV_c = \frac{\dfrac{E_{cc}\, b_{wc}}{2\cot^3\alpha}\left\{\Theta_s - \varepsilon_1(x)\tan\alpha\,(1+\tan^2\alpha)\right\}}{\left[\left(\dfrac{x}{L} - \dfrac{1}{2}\tan^2\alpha\right)^2 + \tan^2\alpha\right]^2 + \left[\left(1 - \dfrac{x}{L} - \dfrac{1}{2}\tan^2\alpha\right)^2 + \tan^2\alpha\right]^2} dx \tag{4-27}$$

The column shear strength V_c is then calculated by integrating equation (4-27) along the effective region of the column length. Normalizing x with respect to column length $L = jd\cot\alpha$,

$$V_c = \int_{0.5\tan^2\alpha}^{1-0.5\tan^2\alpha} \frac{\frac{E_{cc}\, b_{wc}\, jd}{2\cot^2\alpha}\left\{\Theta_s - \varepsilon_1(x)\tan\alpha\,(1+\tan^2\alpha)\right\}}{\left[\left(x-\frac{1}{2}\tan^2\alpha\right)^2+\tan^2\alpha\right]^2+\left[\left(1-x-\frac{1}{2}\tan^2\alpha\right)^2+\tan^2\alpha\right]^2}\,dx \qquad (4\text{-}28)$$

Using the numerical integration schemes such as Gauss quadrature or Newton-Cotes closed formulas discussed in subsection 2.2.4 for the solution of a variable angle truss due to steel mechanism, the column shear strength V_c given in equation (4-28) can be expressed as

$$V_c = \sum_{i=1}^{N} \frac{0.5\,\bar{\omega}_i\, E_{cc}\, b_{wc}\, jd\tan^2\alpha\left\{\Theta_s - \varepsilon_1(\bar{x}_i)\tan\alpha\,(1+\tan^2\alpha)\right\}}{\left[\left(\bar{x}_i-\frac{1}{2}\tan^2\alpha\right)^2+\tan^2\alpha\right]^2+\left[\left(1-\bar{x}_i-\frac{1}{2}\tan^2\alpha\right)^2+\tan^2\alpha\right]^2} \qquad (4\text{-}29)$$

where N = number of numerical integration points considered, $\bar{\omega}_i$ = numerical weight factor and $\bar{x}_i$ = normalized coordinate of i^{th} numerical point for concrete only mechanism. The values of these parameters with the truncation error for each numerical integration scheme are presented in table 4-2. It is noted in tables 2-3 and 4-2 that the numerical coordinates (x_i and $\bar{x}_i$) and weight factors (ω_i and $\bar{\omega}_i$) between steel mechanism and concrete only mechanism are not coincided with each other.

4.4 Analysis of A Truss Model with Two-Point Gauss Quadrature

Since the two-point Gauss quadrature is reasonably accurate and simple enough to handle as discussed in Sections 2 and 3, the generation of column shear force and deformation relationship due to the contribution of concrete tensile strength can be accomplished using this numerical integration scheme. The column shear force given in equation (4-29) can be rewritten for the two-point Gauss quadrature, thus

$$V_c = \frac{0.5\, E_{cc}\, b_{wc}\, jd\tan^2\alpha\,(1-\tan^2\alpha)\left\{\Theta_s - \varepsilon_1(\bar{x}_1)\tan\alpha\,(1+\tan^2\alpha)\right\}}{\left[(1-\tan^2\alpha)^2 x_1^2+\tan^2\alpha\right]^2+\left[(1-\tan^2\alpha)^2(1-x_1)^2+\tan^2\alpha\right]^2} \qquad (4\text{-}30)$$

Rearranging equation (4-30) with respect to Θ_s,

Table 4-2. Numerical scheme parameter values for column shear strength due to a variable angle truss model for concrete only mechanism.

Numerical Schemes	N	i	$\bar{x}_i$	$\bar{\omega}_i$	Truncation Error
Gauss 2-Point	2	1	$x_1 + (0.5 - x_1)\tan^2\alpha$	$0.5(1 - \tan^2\alpha)$	$\frac{1}{135} f^{(4)}(\xi)$
		2	$1 - x_1 - (0.5 - x_1)\tan^2\alpha$	$0.5(1 - \tan^2\alpha)$	
Gauss 3-Point	3	1	$x_1 + (0.5 - x_1)\tan^2\alpha$	$5(1 - \tan^2\alpha)/18$	
		2	0.5	$8(1 - \tan^2\alpha)/18$	$\frac{1}{15750} f^{(6)}(\xi)$
		3	$1 - x_1 - (0.5 - x_1)\tan^2\alpha$	$5(1 - \tan^2\alpha)/18$	
Simpson's 1/3 Rule	3	1	$0.5\tan^2\alpha$	$(1 - \tan^2\alpha)/6$	
		2	0.5	$4(1 - \tan^2\alpha)/6$	$-\frac{1}{2880} f^{(4)}(\xi)$
		3	$1 - 0.5\tan^2\alpha$	$(1 - \tan^2\alpha)/6$	
Boole's Rule	5	1	$0.5\tan^2\alpha$	$7(1 - \tan^2\alpha)/90$	
		2	$0.25 + 0.25\tan^2\alpha$	$32(1 - \tan^2\alpha)/90$	
		3	0.5	$12(1 - \tan^2\alpha)/90$	$-\frac{1}{1935360} f^{(6)}(\xi)$
		4	$0.75 - 0.25\tan^2\alpha$	$32(1 - \tan^2\alpha)/90$	
		5	$1 - 0.5\tan^2\alpha$	$7(1 - \tan^2\alpha)/90$	

Note: $x_1 = 0.2113249$ is the first numerical integration point of Gauss truss for steel mechanism. Refer to table 2-3.

$$\Theta_s = \varepsilon_1(\bar{x}_1)\tan\alpha\,(1 + \tan^2\alpha) + \frac{2V_c\cot^2\alpha}{E_{cc}\,b_{wc}\,jd\,(1 - \tan^2\alpha)}\left\{\left[(1 - \tan^2\alpha)^2 x_1^2 + \tan^2\alpha\right]^2 + \left[(1 - \tan^2\alpha)^2 (1 - x_1)^2 + \tan^2\alpha\right]^2\right\} \quad (4\text{-}31)$$

in which $\varepsilon_1(\bar{x}_1)$ is the principal tensile strain of column concrete at coordinate $\bar{x}_1$ in the two-point Gauss quadrature which denotes the <u>average</u> tensile strain ε_1^{avg} over the diagonal crack plane.

4.4.1 Average Strain and Average Stress of Concrete in Tension

The average principal strain and stress may be calculated by integrating the strain and stress profiles shown in figures 4-4 and 4-5 over the effective column length as presented in figure 4-6. Thus

$$\varepsilon_1^{avg} = \frac{1}{1-\tan^2\alpha}\int_{0.5\tan^2\alpha}^{1-0.5\tan^2\alpha} \varepsilon_1(x)\,dx \tag{4-32}$$

$$f_1^{avg} = \frac{1}{1-\tan^2\alpha}\int_{0.5\tan^2\alpha}^{1-0.5\tan^2\alpha} f_1(\varepsilon_1(x))\,dx \tag{4-33}$$

where x is the normalized coordinate along the column longitudinal axis. The solution strategy of equations (4-32) and (4-33) is readily available in subsection 4.2.3. The calculated average principal strain and stress profiles are presented with solid straight lines in figures 4-7 and 4-8 by overlapping over the original profiles shown in dashed curves which are identical to those profiles presented in figures 4-4 and 4-5.

4.4.2 Gauss 2-Point Truss Model with Inclined Ties

The average principal strain and stress can also be obtained by performing the analysis of Gauss 2-point truss model. Also obtainable using the analysis results is the column shear force and deformation relationship due to concrete only mechanism. For this purpose, consider a truss model with inclined ties and corresponding struts shown in figure 4-9(a). The truss model is proportioned according to the two-point Gauss quadrature and the effective zone only is considered. Member forces determined by the static equilibrium at each joint are also presented. The inclined ties represent the concrete tension field lumped at the modified Gauss points $\bar{x}_1$ and $\bar{x}_2$, due to ineffective zone, where the average component responses are expected. The diagonal struts represent the concrete compression field stabilizing the truss model. Also important is to maintain the equilibrium and compatibility conditions in diagonal struts between steel mechanism and concrete only mechanism. For this purpose, the effective column width b_{wc} for concrete only mechanism is used and is expected to change instantaneously in proportion

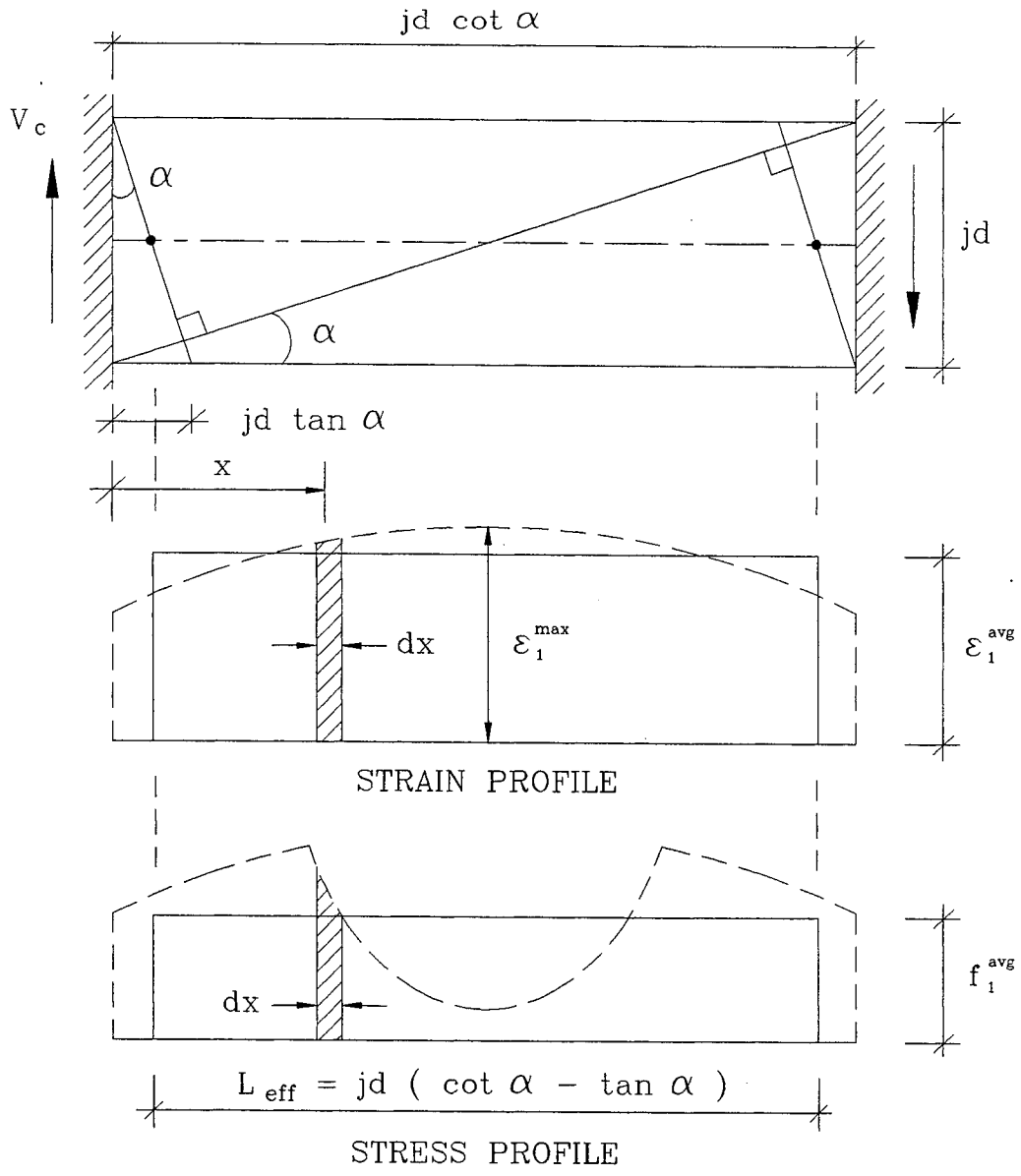

Figure 4-6. Estimation of average principal strain and stress across crack plane along the column length.

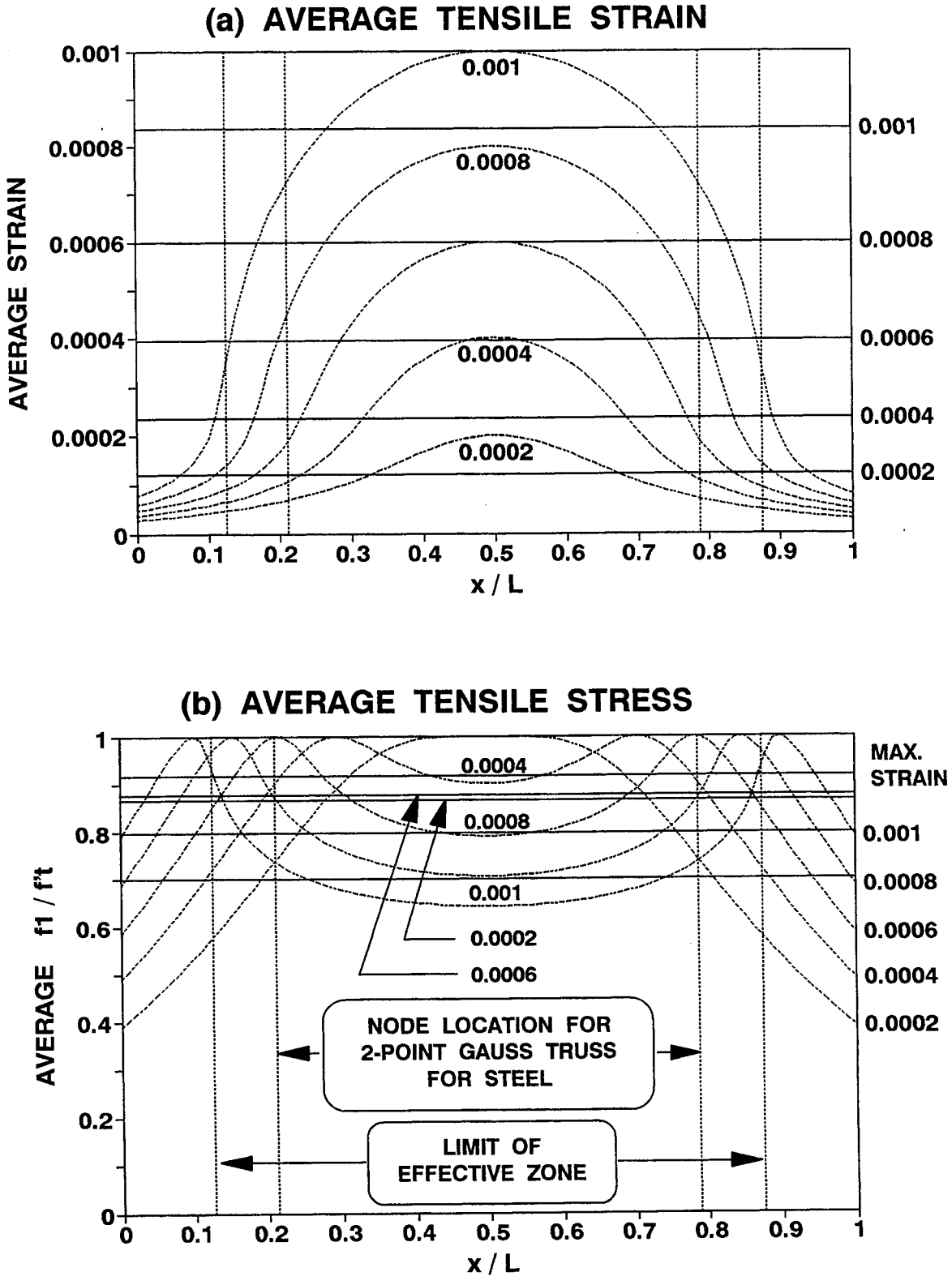

Figure 4-7. Average tensile strain and stress profiles using nonlinear softening model for $f_t' = 2\ MPa$, $\varepsilon_t' = 0.0002$, $L/jd = 2$ and $b_{wc}/b_w = 1.0$.

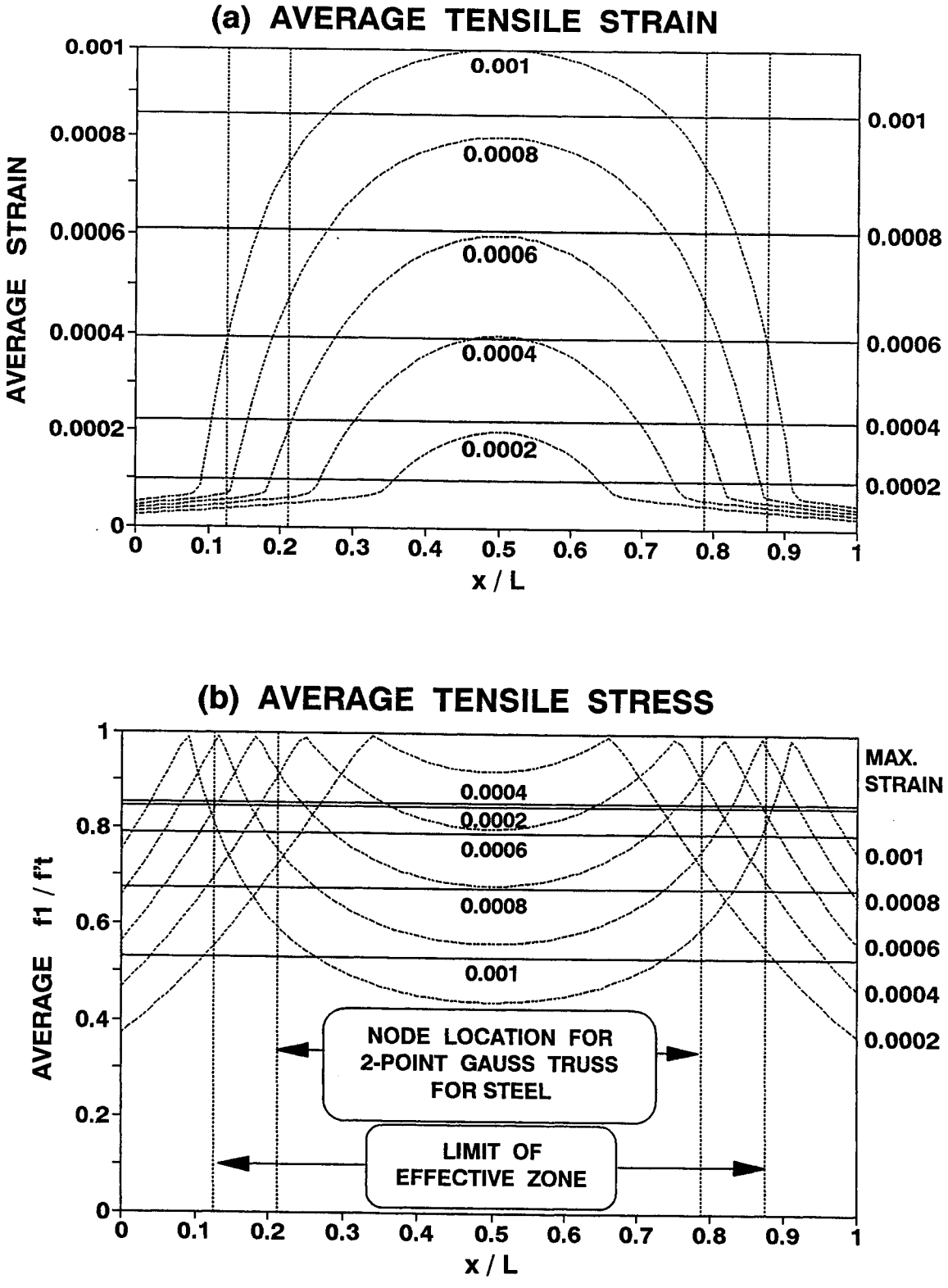

Figure 4-8. Average tensile strain and stress profiles using linear softening model for $f_t' = 2\ MPa$, $\varepsilon_t' = 0.0002$, $L/jd = 2$ and $b_{wc}/b_w = 1.0$.

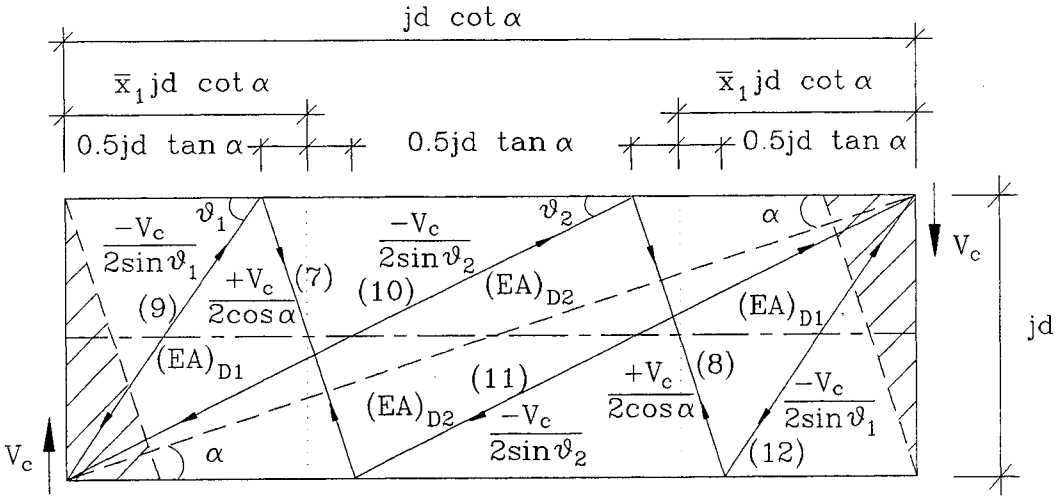

(a) Truss model with inclined concrete ties.

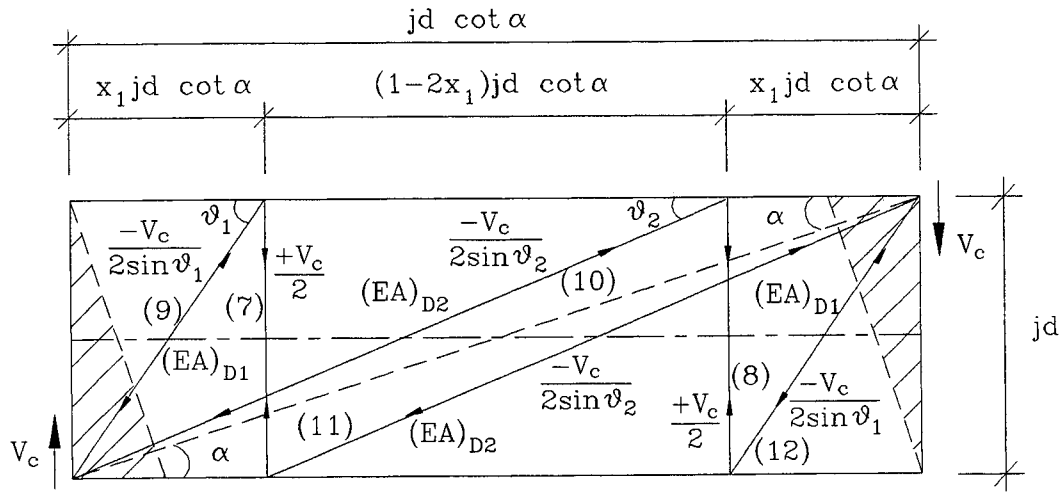

(b) Truss model with perpendicular concrete ties.

Figure 4-9. Gauss 2-point truss models for the concrete tensile strength mechanism.

to the ratio of V_c / V_u in which $V_u = V_s + V_c + V_p$. For consistency, struts and ties are numbered in the same fashion as the two-point Gauss truss model with perpendicular ties for steel mechanism shown in figure 2-8. It is thought that the effect of concrete tensile ties on the longitudinal flexural elements is less than that of transverse steel since concrete in tension has the descending branch and the anchorage of concrete tensile ties will degrade as deformation increases. As noted in Section 2 for the Gauss 2-point truss for steel mechanism, the shear transfer mechanism is not affected by column end condition. The shear deformation of the truss model with inclined ties is determined using the Virtual Work method and the analysis is presented in table 4-3. Strut sizes are not yet known so that they are expressed with unknown factors a_1 and a_2, but they will be determined later.

Table 4-3. Shear deformation of the Gauss two-point truss model with inclined ties for concrete only mechanism.

Member	Force F	Unit f	Length l	Rigidity EA	Strain $\varepsilon = F/EA$	$\frac{Ffl}{EA}$
(7) (8)	$\frac{+V_c}{2\cos\alpha}$	$\frac{+1}{2\cos\alpha}$	$\frac{jd}{\cos\alpha}$	$\left(\frac{1-2\sin^2\alpha}{2\sin\alpha}\right)E_{ct}A_v$	$\frac{+V_c\tan\alpha}{E_{ct}A_v(1-2\sin^2\alpha)}$	$\frac{V_c\tan\alpha}{2E_{ct}b_w\cos^2\alpha(1-2\sin^2\alpha)}$
(9) (12)	$\frac{-V_c}{2\sin\theta_1}$	$\frac{-1}{2\sin\theta_1}$	$\frac{jd}{\sin\theta_1}$	$a_1E_{cc}A_v$	$\frac{-V_c}{2a_1E_{cc}A_v\sin\theta_1}$	$\frac{V_c}{4E_{cc}b_{wc}a_1\sin^3\theta_1}$
(10) (11)	$\frac{-V_c}{2\sin\theta_2}$	$\frac{-1}{2\sin\theta_2}$	$\frac{jd}{\sin\theta_2}$	$a_2E_{cc}A_v$	$\frac{-V_c}{2a_2E_{cc}A_v\sin\theta_2}$	$\frac{V_c}{4E_{cc}b_{wc}a_2\sin^3\theta_2}$

Note: Refer to figure 4-9(a).

$$\sin\theta_1 = \frac{\tan\alpha}{\sqrt{(1-\tan^2\alpha)^2 x_1^2 + \tan^2\alpha}} \quad ; \quad \sin\theta_2 = \frac{\tan\alpha}{\sqrt{(1-\tan^2\alpha)^2 (1-x_1)^2 + \tan^2\alpha}}$$

The shear deformation of the Gauss 2-point truss model with inclined ties is the sum of component deformations. Recalling that $\cot\alpha = L/jd$, the column shear deformation is

$$\Delta_s = \sum_{i=7}^{12} \frac{Ffl}{EA}$$

$$= \varepsilon_1^{avg} \frac{jd}{\cos^2\alpha} + \frac{V_c jd \cot^3\alpha}{2E_{cc}A_v}\left(\frac{\left[(1-\tan^2\alpha)^2 x_1^2 + \tan^2\alpha\right]^2}{a_1\sqrt{(1-\tan^2\alpha)^2 x_1^2 + \tan^2\alpha}} + \frac{\left[(1-\tan^2\alpha)^2(1-x_1)^2 + \tan^2\alpha\right]^2}{a_2\sqrt{(1-\tan^2\alpha)^2(1-x_1)^2 + \tan^2\alpha}}\right) \quad (4\text{-}34)$$

in which the average strain ε_1^{avg} is used for the strain of the inclined ties located at two Gauss points $\overline{x_1}$ and $\overline{x_2}$. The shear strain (rotation) is then determined by dividing the shear displacement by the length of the truss model. Rearranging the resultant equation in a form similar to equation (4-31),

$$\theta_s = \varepsilon_1^{avg}\tan\alpha\,(1+\tan^2\alpha)$$

$$+ \frac{2V_c\cot^2\alpha}{E_{cc}A_v(1-\tan^2\alpha)}\left(\frac{(1-\tan^2\alpha)\left[(1-\tan^2\alpha)^2 x_1^2 + \tan^2\alpha\right]^2}{4a_1\sqrt{(1-\tan^2\alpha)^2 x_1^2 + \tan^2\alpha}} + \frac{(1-\tan^2\alpha)\left[(1-\tan^2\alpha)^2(1-x_1)^2 + \tan^2\alpha\right]^2}{4a_2\sqrt{(1-\tan^2\alpha)^2(1-x_1)^2 + \tan^2\alpha}}\right) \quad (4\text{-}35)$$

By comparing equations (4-31) and (4-35), the effective sectional area factors a_i for diagonal struts can be obtained. Thus

$$a_i = \frac{1 - \tan^2\alpha}{4\sqrt{(1-\tan^2\alpha)^2 x_i^2 + \tan^2\alpha}}\left(\frac{b_{wc}}{b_w}\right) \quad (4\text{-}36)$$

where x_i is the Gauss node location for steel mechanism defined in table 2-3. Then, the axial rigidities of the diagonal struts of the Gauss 2-point truss model with inclined ties in figure 4-9(a) are determined by

$$(EA)_{di} = \frac{0.5\,\overline{\omega}_i}{\sqrt{(\overline{x}_i - 0.5\tan^2\alpha)^2 + \tan^2\alpha}} E_{cc}A_v\left(\frac{b_{wc}}{b_w}\right) = \frac{0.25\,(1-\tan^2\alpha)}{\sqrt{(1-\tan^2\alpha)^2 x_i^2 + \tan^2\alpha}} E_c A_v\left(\frac{b_{wc}}{b_w}\right) \quad (4\text{-}37)$$

where $\overline{x}_i$ and $\overline{\omega}_i$ are the Gauss node location and weighting factor for concrete mechanism available in table 4-2. The corresponding compressive stress in i^{th} diagonal strut is obtained from table 4-3, thus

$$f_{cdi} = E_c \varepsilon_{cdi} = \frac{-2 V_c \left\{(1 - \tan^2\alpha)^2 x_i^2 + \tan^2\alpha\right\}}{A_v \left(\frac{b_{wc}}{b_w}\right) \tan\alpha \,(1 - \tan^2\alpha)} \tag{4-38}$$

Note that the location of i[th] diagonal strut is depicted in figure 4-9(a). It is assumed that diagonal struts of the truss model behave linear-elastically. Therefore, the amplitude of axial stress in the diagonal should be checked over the column response.

Note from table 4-3 that the average strain ε_1^{avg} in the inclined ties is expressed as

$$\varepsilon_1^{avg} = \frac{V_c \tan\alpha}{E_{ct} A_v (1 - 2\sin^2\alpha)} \tag{4-39}$$

Substituting a_i and ε_1^{avg} into equation (4-35) and rearranging, the cracked elastic stiffness of the concrete mechanism can be calculated, that is,

$$K_{sc} = \frac{\cos^4\alpha \cot^2\alpha \,(1 - \tan^2\alpha)\, E_c A_v}{1 + 2\cos^4\alpha \cot^4\alpha \left(\frac{b_w}{b_{wc}}\right) \left\{\left[(1 - \tan^2\alpha)^2 x_1^2 + \tan^2\alpha\right]^2 + \left[(1 - \tan^2\alpha)^2 (1 - x_1)^2 + \tan^2\alpha\right]^2\right\}} \tag{4-40}$$

in which $E_{ct} = E_{cc} = E_c$ is assumed within the elastic range and $1 - 2\sin^2\alpha = \cos^2\alpha\,(1 - \tan^2\alpha)$.

Using equation (4-39) the column shear force can be expressed in terms of the average strain ε_1^{avg} as well as the corresponding stress f_1^{avg} in the inclined ties, thus, recalling that $A_v = b_w jd$,

$$V_c = E_{ct} \varepsilon_1^{avg} A_v \cot\alpha \cos 2\alpha \tag{4-41}$$

$$V_c = f_1^{avg} A_v \cot\alpha \cos 2\alpha \tag{4-42}$$

Substituting V_c given in equation (4-42) into equation (4-31) and replacing $\varepsilon_1(\bar{x}_1)$ with ε_1^{avg}, the column shear deformation becomes

$$\Theta_s = \varepsilon_1^{avg} \tan\alpha \left(1 + \tan^2\alpha\right) + \frac{2 f_1^{avg} \cot^3\alpha \cos^2\alpha}{E_{cc}\left(\frac{b_{wc}}{b_w}\right)} \left\{\left[\left(1 - \tan^2\alpha\right)^2 x_1^2 + \tan^2\alpha\right]^2 + \left[\left(1 - \tan^2\alpha\right)^2 \left(1 - x_1\right)^2 + \tan^2\alpha\right]^2\right\} \quad (4\text{-}43)$$

Now, the average principal strain and stress relationship is readily obtained. Two different material models are investigated in what follows.

4.4.2.1 Nonlinear Descending Branch Model

Substituting Popovics equation given in equation (4-4) into equation (4-43) for f_1^{avg} and rearranging for ε_1^{avg},

$$\varepsilon_1^{avg} = \frac{\Theta_s \cot\alpha \cos^2\alpha}{1 + \dfrac{2\,T(\alpha) \cos^4\alpha \cot^4\alpha}{\left(\dfrac{b_{wc}}{b_w}\right)\left\{1 + \left(\dfrac{E_{cc}}{E_{sec}} - 1\right)\left(\dfrac{\varepsilon_1^{avg}}{\varepsilon_t'}\right)^r\right\}}} \quad (4\text{-}44)$$

in which $T(\alpha) = \left[\left(1 - \tan^2\alpha\right)^2 x_1^2 + \tan^2\alpha\right]^2 + \left[\left(1 - \tan^2\alpha\right)^2 \left(1 - x_1\right)^2 + \tan^2\alpha\right]^2$ and parameters such as E_{sec} and r are defined in equation (4-4). The corresponding average stress can be obtained by equating equations (4-30) and (4-42), thus

$$f_1^{avg} = \frac{0.5 E_{cc}}{T(\alpha)}\left(\frac{b_{wc}}{b_w}\right) \tan^3\alpha \left(1 + \tan^2\alpha\right)\left\{\Theta_s - \varepsilon_1^{avg} \tan\alpha \left(1 + \tan^2\alpha\right)\right\} \quad (4\text{-}45)$$

Substituting ε_1^{avg} into equation (4-4) is expected to give the same result as equation (4-45). It is noted that the solution of equation (4-44) requires some iterative process since ε_1^{avg} is a function of itself.

4.4.2.2 Linear Descending Branch Model

Substituting the Menegotto-Pinto equation given in equation (4-9) into equation (4-43) for f_1^{avg} and rearranging for ε_1^{avg},

$$\varepsilon_1^{avg} = \frac{\Theta_s \cot\alpha \cos^2\alpha}{1 + \dfrac{2\,T(\alpha)\cos^4\alpha \cot^4\alpha}{\left(\dfrac{b_{wc}}{b_w}\right)}\left[Q + \dfrac{1-Q}{\left\{1 + \left(\dfrac{E_{cc}\varepsilon_1^{avg}}{f_t'}\right)^R\right\}^{\frac{1}{R}}}\right]} \tag{4-46}$$

in which constant $T(\alpha)$ is defined in equation (4-44) and parameter Q is defined in equation (4-9). The corresponding average stress f_1^{avg} can be obtained by equation (4-9) or (4-45). Equation (4-46) requires some iterative process for solution.

4.4.3 Conversion into Gauss 2-point Truss Model with Perpendicular Ties

The Gauss 2-point truss model with inclined ties discussed for concrete only mechanism can be converted to the one with perpendicular ties by modifying properties of the concrete ties. This enables the steel mechanism (V_s) and concrete only mechanism (V_c) for shear resistance to be considered together using the geometrically identical truss model, which allows combined computational modeling of reinforced concrete columns for shear to be feasible. For this purpose, consider the Gauss 2-point truss model shown in figure 4-9(b). This truss model is identical to the one shown in figure 2-8 used for the steel mechanism with the exception of rigidity of transverse ties and applied shear force. The column shear force V_c instead of V_s is applied and transverse ties represent the lumped concrete tension field projected from the principal direction instead of the lumped transverse steel. Considering the effective zone only [equation (4-26)], the shear deformation of the truss model with perpendicular ties is determined using the Virtual Work analysis method as presented in table 4-4.

Table 4-4. Shear deformation of the Gauss two-point truss model with perpendicular ties for concrete only mechanism.

member	Force F	Unit f	Leng. l	Rigidity EA	Strain $\varepsilon = F/EA$	$\frac{Ffl}{EA}$
(7) (8)	$+\frac{V_c}{2}$	$+\frac{1}{2}$	jd	$\frac{E_{ct}A_v(\cot\alpha - \tan\alpha)}{2}$	$\frac{+V_c}{E_{ct}A_v(\cot\alpha - \tan\alpha)}$	$\frac{V_c\, jd}{2E_{ct}A_v(\cot\alpha - \tan\alpha)}$
(9) (12)	$\frac{-V_c}{2\sin\theta_1}$	$\frac{-1}{2\sin\theta}$	$\frac{jd}{\sin\theta_1}$	$\frac{0.25E_{cc}b_{wc}jd}{\sqrt{x_1^2 + \tan^2\alpha}}$	$-\frac{2V_c\sqrt{x_1^2 + \tan^2\alpha}}{E_{cc}b_{wc}jd\sin\theta_1}$	$\frac{V_c jd\sqrt{x_1^2 + \tan^2\alpha}}{E_{cc}b_{wc}jd\sin^3\theta_1}$
(10) (11)	$\frac{-V_c}{2\sin\theta_2}$	$\frac{-1}{2\sin\theta}$	$\frac{jd}{\sin\theta_2}$	$\frac{0.25E_{cc}b_{wc}jd}{\sqrt{(1-x_1)^2 + \tan^2\alpha}}$	$-\frac{2V_c\sqrt{(1-x_1)^2 + \tan^2\alpha}}{E_{cc}b_{wc}jd\sin\theta_2}$	$\frac{V_c jd\sqrt{(1-x_1)^2 + \tan^2\alpha}}{E_{cc}b_{wc}jd\sin^3\theta_2}$

Note: Refer to figure 4-9(b).

$$\sin\theta_1 = \frac{1}{\sqrt{1 + x_1^2\cot^2\alpha}} \quad ; \quad \sin\theta_2 = \frac{1}{\sqrt{1 + (1-x_1)^2\cot^2\alpha}}$$

The shear deformation of the Gauss 2-point truss model with perpendicular ties is the sum of component deformations. Thus

$$\begin{aligned}\Delta_s^* &= \sum_{i=7}^{12} \frac{Ffl}{EA} \\ &= \varepsilon_1^* jd + \frac{2V_c}{E_{cc}b_{wc}\cot\alpha}\left\{\left[1 + x_1^2\cot^2\alpha\right]^2 + \left[1 + (1-x_1)^2\cot^2\alpha\right]^2\right\}\end{aligned} \tag{4-47}$$

where the asterisk mark (*) in superscript denotes that the corresponding response is for the converted Gauss 2-point truss model with perpendicular ties. The shear strain (rotation) is then determined by dividing the shear displacement by the length of the truss model. Recalling that $L = jd\cot\alpha$,

$$\Theta_s^* = \frac{\Delta_s^*}{L}$$

$$= \varepsilon_1^* \tan\alpha + \frac{2V_c}{E_{cc}A_v\left(\frac{b_{wc}}{b_w}\right)\cot^2\alpha}\left\{\left[1+x_1^2\cot^2\alpha\right]^{\frac{1}{2}} + \left[1+(1-x_1)^2\cot^2\alpha\right]^{\frac{1}{2}}\right\} \quad (4\text{-}48)$$

From table 4-4, the column shear force can be expressed in terms of the average strain ε_1^* and the corresponding stress f_1^* in the perpendicular ties, that is, recalling that $A_v = b_w jd$,

$$V_c = E_{ct}\varepsilon_1^* A_v \cot\alpha\,(1-\tan^2\alpha) \quad (4\text{-}49)$$

$$V_c = f_1^* A_v \cot\alpha\,(1-\tan^2\alpha) \quad (4\text{-}50)$$

Substituting V_c given in equation (4-50) into equation (4-48), the column shear deformation becomes

$$\Theta_s^* = \varepsilon_1^* \tan\alpha + \frac{2f_1^*\tan\alpha\,(1-\tan^2\alpha)}{E_{cc}\left(\frac{b_{wc}}{b_w}\right)}\left\{\left[1+x_1^2\cot^2\alpha\right]^{\frac{1}{2}} + \left[1+(1-x_1)^2\cot^2\alpha\right]^{\frac{1}{2}}\right\} \quad (4\text{-}51)$$

In order to compare the behavior of the truss model with perpendicular ties to the truss model with inclined ties due to concrete mechanism, the stiffness must be the best measure. From equation (4-49) the average strain of the perpendicular tie is obtained as

$$\varepsilon_1^* = \frac{V_c}{E_{ct}A_v\cot\alpha\,(1-\tan^2\alpha)} \quad (4\text{-}52)$$

Substituting ε_1^* into equation (4-48) and rearranging with $E_{ct} = E_{cc} = E_c$, the cracked elastic stiffness of the truss model with perpendicular ties due to concrete mechanism can be calculated, that is,

$$K_{sc}^{*} = \frac{\cot^2\alpha\,(1-\tan^2\alpha)\;\; E_c A_v}{1+2(1-\tan^2\alpha)\left(\frac{b_w}{b_{wc}}\right)\left\{\left[1+x_1^2\cot^2\alpha\right]^2+\left[1+(1-x_1)^2\cot^2\alpha\right]^2\right\}} \tag{4-53}$$

For the comparison, normalizing K_{sc}^{*} to K_{sc} in equation (4-40) gives the ratio of cracked elastic stiffness of the truss model with perpendicular ties to the one with inclined ties, that is,

$$\frac{K_{sc}^{*}}{K_{sc}} = \frac{1+2\cos^4\alpha\,\cot^4\alpha\left(\frac{b_w}{b_{wc}}\right)\left\{\left[(1-\tan^2\alpha)^2 x_1^2+\tan^2\alpha\right]^2+\left[(1-\tan^2\alpha)^2(1-x_1)^2+\tan^2\alpha\right]^2\right\}}{\left[1+2(1-\tan^2\alpha)\left(\frac{b_w}{b_{wc}}\right)\left\{\left[1+x_1^2\cot^2\alpha\right]^2+\left[1+(1-x_1)^2\cot^2\alpha\right]^2\right\}\right]\;\cos^4\alpha} \tag{4-54}$$

The stiffness ratio K_{sc}^{*}/K_{sc} given in equation (4-54) is plotted in figure 4-10 taking $\alpha = \theta$ for b_{wc}/b_w = 0.25, 0.5, 0.75 and 1.0. It is noted that the amplitude b_{wc}/b_w does not seriously affect the stiffness ratio. That is, for the range of practical crack angle considered to be 15°-35°, the stiffness ratio shows very narrow difference over largely varied values of b_{wc}/b_w. However, it is noted that within this variation of crack angle, the cracked elastic stiffness ratio varies between 0.7 and 1.0. This denotes that the two-point Gauss truss model with inclined ties for concrete only mechanism can not be perfectly converted to the one with perpendicular ties. Therefore, when the truss model with perpendicular ties should be used, it should be used with caution.

4.4.4 Solution Strategy for Column Shear Force and Deformation Relationship

The generation of column shear force and deformation relationship is readily obtainable but is limited to the truss model with inclined ties discussed in subsection 4.4.2. Note that the corner-to-corner diagonal angle α is usually not the same as the crack angle θ. Therefore, for shear analysis, the crack angle θ should be used for α in equations. The step-by-step solution procedure is as follows:

Step 1 Calculate the crack angle θ using equation (2-69) and put $\alpha = \theta$.

Step 2 Choose column shear deformation Θ_s.

Step 3 Calculate the ratio of effective column width b_{wc}/b_w.

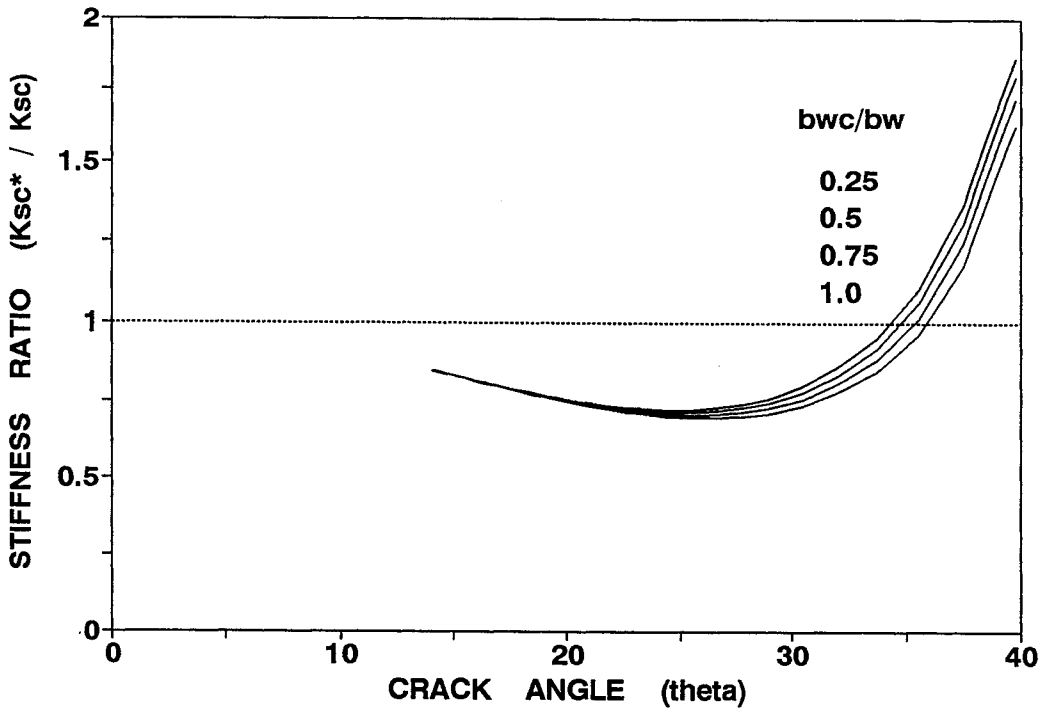

Figure 4-10. Stiffness ratio between the two-point Gauss truss model with inclined ties and perpendicular ties in terms of crack angle.

Step 4 Calculate the average principal strain ε_1^{avg} using equation (4-44) for the nonlinear descending branch model; and equation (4-46) for the linear descending branch model. Repeat this step until converged.

Step 5 Calculate the average principal stress f_1^{avg} using equation (4-45).

Step 6 Calculate column shear strength V_c using equation (4-42).

Step 7 Return to Step 3 until converged.

Step 8 Repeat Steps 2-7 for increasing values of Θ_s.

Step 9 Plot Θ_s vs. V_c and ε_1^{avg} vs. f_1^{avg}.

4.5 Conclusions

The effect of concrete tensile strength on column shear force and deformation relationship has been discussed in the present section and the findings from the study are summarized in the following:

1. Concrete tensile stress and strain relationship has been formulated using the Popovics equation for the nonlinear descending branch model and a softening bilinear form of the Menegotto-Pinto equation for the linear descending branch model. For the linear descending branch model, the ultimate tensile strain at which no more concrete tensile strength can be expected has been determined by considering the fracture energy capacity. As a result, the corresponding column response shows more brittle property as compared to the nonlinear descending branch model.

2. A variable angle truss model may be used for the concrete only mechanism from which the concrete principal tensile strain and stress profiles along the diagonal crack plane have been obtained. The average values of principal tensile strain and stress can be obtained by integrating those profiles within the effective region of the column length. The effective region has been defined by consideration of flexural cracking at the critical section.

3. The solution of the variable angle truss model has been achieved by several numerical integration schemes. Among them, the two-point Gauss-Legendre quadrature and the corresponding simplified truss model with inclined ties have been extensively investigated. The location of Gauss points for the truss model with inclined ties are different from those for the truss model with perpendicular ties used for transverse steel mechanism. Using the Gauss two-point truss model with inclined ties, the concrete average principal tensile strain and stress as well as column shear force and deformation relationship have been obtained. It has been shown that for convenience in analysis, the Gauss truss model with inclined ties can be converted to the truss model with perpendicular ties with an acceptable degree of accuracy. However, the column shear strength due to concrete truss mechanism may be properly accounted for by adjusting concrete tensile strength proportionally based on the stiffness ratio shown in figure 4-10.

SECTION 5
AXIAL LOAD EFFECT ON COLUMN SHEAR STRENGTH

5.1 Introduction

The column axial load is considered to be transferred from the corner of one end of the column to the corner of the other end through a compression field formed along the corner-to-corner diagonal when the column is subjected to the lateral displacement as shown in figure 5-1(a). This phenomenon can also be observed by performing the ACI style *(ACI, 1995)* flexural analysis on column sections along the length of the column. The axial load transferring action through the corner-to-corner concrete strut is termed as the "arch action" or "strut action".

There are some examples utilizing this mechanism in estimation of the member shear strength. Paulay *(1971a,b)* and Watanabe and Ichinose *(1992)* used the arch action mechanism in calculation of beam shear capacity. Paulay, in particular, attempted to relate the shear force and deformation due to the arch action. However, Paulay's arch action was not for the axial load transfer mechanism but resisted against the lateral deformation of coupling beams by the axial deformation of the corner-to-corner diagonal strut. Priestley et al. *(1994c)* showed the enhancement of column shear strength with the column axial load via the arch action using a Watanabe and Ichinose-like model. However, these previous models do not provide an overtly clear understanding for the corner-to-corner diagonal strut mechanism and the relationship of shear force and deformation due to arch action.

The corner-to-corner diagonal compression field can be idealized as a concrete diagonal strut presented in figure 5-1(b) for columns with fixed-fixed and fixed-pinned ends. The shape and dimension of the diagonal strut has been determined based on the postulated compression field in figure 5-1(a) and Paulay's assumption for his coupling beam study *(1971a,b)*. The axial load P is assumed to apply to the flexural compression block at the fixed end of the laterally deformed column while $0.5P$ is to be evenly applied to both sides of the pinned end. Note that there is no way in the arch action mechanism to relate the corner-to-corner diagonal angle α to

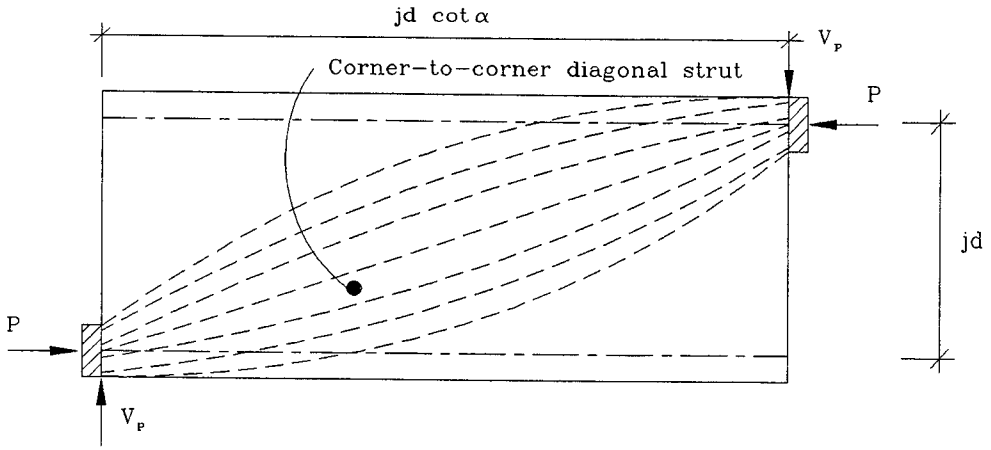

(a) Corner-to-corner diagonal compression field

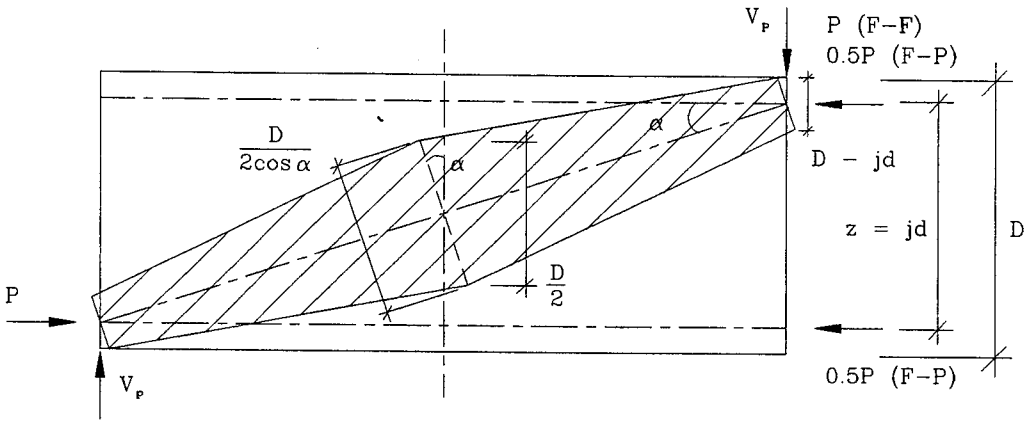

(b) Idealized single diagonal strut

Figure 5-1. Axial load transferring mechanism - arch action.

the crack angle θ.

There may be two possible approaches in modeling the axial load transfer mechanism through the corner-to-corner diagonal strut: i) V_p only mechanism; and ii) $V_p + V_c$ combined mechanism, in which V_p is a portion of column shear resistance due to the applied axial load and V_c is due to the effect of concrete tensile strength. The V_p only mechanism consists of a single corner-to-corner diagonal strut and hand-analysis is feasible for this mechanism. The $V_p + V_c$ combined mechanism (which is discussed in more detail in subsection 5.3) includes a tie element to take the effect of concrete tensile strength into account and the calculation of member forces are complicate enough to have to use computer analysis. In the present study, the V_p only mechanism is extensively investigated to obtain the column shear force and deformation relationship.

5.2 Analysis of V_p Only Mechanism

The mean section area of the corner-to-corner diagonal strut in figure 5-1(b) can be estimated by

$$A_D = \frac{A_v}{2\cos\alpha}\left(\frac{b_{wp}}{b_w}\right)\left(1.5\frac{D}{jd} - 1\right) \qquad (5\text{-}1)$$

where b_{wp} given in equation (1-8) is a portion of column width effective for shear resistance due to the axial load transfer mechanism and α is the corner-to-corner diagonal angle. There may be three stages in defining the action of the corner-to-corner diagonal strut: i) initial stage; ii) loading stage; and iii) rocking (releasing) stage.

5.2.1 Initial Stage

The initial stage is represented by the state that no lateral deformation is yet imposed which means that $V_p = 0$. The axial load P at this stage is supported exclusively by the column longitudinal elements only. Figure 5-2(a) describes the state of the initial stage. It is noted that the axial load P is assumed to evenly distributed to both sides of the column section.

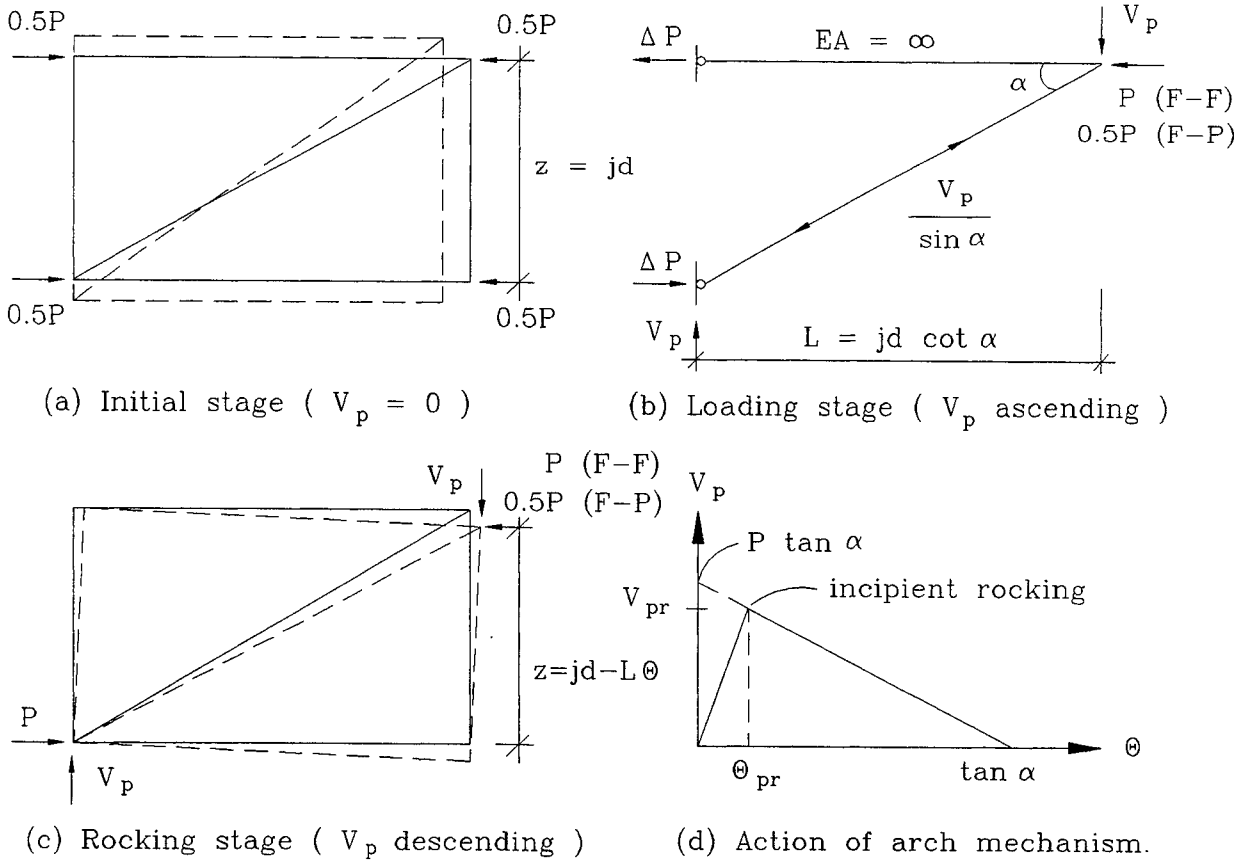

Figure 5-2. Action of column axial load transfer mechanism (V_p).

5.2.2 Loading Stage

In the loading stage the shear resistance V_p increases up to the incipient rocking stage in which the theoretically possible maximum V_p is

$$(V_p)_{max} = P \tan\alpha \qquad \textit{for fixed-fixed ends} \tag{5-2a}$$

$$(V_p)_{max} = 0.5\, P \tan\alpha \qquad \textit{for fixed-pinned ends} \tag{5-2b}$$

The increase of V_p is attained by the axial deformation of the corner-to-corner diagonal strut. The column response at the loading stage can be estimated by performing the Virtual Work analysis method on a single strut truss model shown in figure 5-2(b). The rigidity of longitudinal member is assumed to be infinity to remove any possible interaction with flexure. Then, assuming the linear elastic behavior of the strut, the lateral displacement of the column using the truss model is calculated by

$$\Delta_s = \frac{Ffl}{EA} = \frac{\left(\frac{V_p}{\sin\alpha}\right)\left(\frac{1}{\sin\alpha}\right)\left(\frac{L}{\cos\alpha}\right)}{E_c A_D} = \frac{2\,V_p L}{E_c A_v \left(\frac{b_{wp}}{b_w}\right)\left(1.5\,\frac{D}{jd} - 1\right)\sin^2\alpha} \tag{5-3}$$

in which the strut section area A_D is given by equation (5-1). The corresponding column shear rotation (drift) angle is

$$\Theta_s = \frac{\Delta_s}{L} = \frac{2\,V_p}{E_c A_v \left(\frac{b_{wp}}{b_w}\right)\left(1.5\,\frac{D}{jd} - 1\right)\sin^2\alpha} \tag{5-4}$$

Then, the shear stiffness for rotation due to column axial load transfer action is

$$K_{p\theta} = \frac{V_p}{\Theta_s} = 0.5\, E_c A_v \left(\frac{b_{wp}}{b_w}\right)\left(1.5\,\frac{D}{jd} - 1\right)\sin^2\alpha \tag{5-5}$$

At this juncture it is appropriate to determine the incipient rocking point in figure 5-2(d). The column shear resistance at the moment of incipient rocking is calculated by

$$V_{pr} = K_{p\theta}\,\Theta_{pr} \tag{5-6}$$

in which V_{pr} and Θ_{pr} are the column shear resistance and deformation at incipient rocking. The same shear resistance should be obtained by consideration of overturning moment equilibrium, that is,

$$V_{pr} = P\left(\tan\alpha - \Theta_{pr}\right) \quad \textit{for fixed-fixed ends} \tag{5-7a}$$

$$V_{pr} = 0.5\,P\left(\tan\alpha - \Theta_{pr}\right) \quad \textit{for fixed-pinned ends} \tag{5-7b}$$

The column shear strain at the moment of incipient rocking can be obtained by equating equations (5-6) and (5-7), thus

$$\Theta_{pr} = \frac{\tan\alpha}{1 + \dfrac{K_{p\theta}}{P}} \quad \textit{for fixed-fixed ends} \tag{5-8a}$$

$$\Theta_{pr} = \frac{\tan\alpha}{1 + \dfrac{2K_{p\theta}}{P}} \quad \textit{for fixed-pinned ends} \tag{5-8b}$$

Substituting equation (5-5) for $K_{\theta p}$ into equation (5-8) and rearranging,

$$\Theta_{pr} = \frac{\tan\alpha}{1 + \dfrac{0.5\,E_c A_v\left(1.5\dfrac{D}{jd} - 1\right)\sin^2\alpha}{P}\left(\dfrac{b_{wp}}{b_w}\right)} \quad \textit{for fixed-fixed ends} \tag{5-9a}$$

$$\Theta_{pr} = \frac{\tan\alpha}{1 + \dfrac{E_c A_v\left(1.5\dfrac{D}{jd} - 1\right)\sin^2\alpha}{P}\left(\dfrac{b_{wp}}{b_w}\right)} \quad \textit{for fixed-pinned ends} \tag{5-9b}$$

It is usual that the column axial load P can be expressed in the relationship:

$$P = \psi f_c' A_g \tag{5-10}$$

where $A_g = b_w D$ is the column gross section area. It is noted that $\psi \leq 0.2$ in most short to medium span bridge pier columns. Generally, the modulus of elasticity of concrete E_c can be approximated by

$$E_c = 1000 f_c' \tag{5-11}$$

Thus substituting equations (5-10) and (5-11) into equation (5-9) and recalling that $A_{vp} = b_{wp} jd$, the column shear deformation at the moment of incipient rocking becomes

$$\Theta_{pr} = \frac{\tan\alpha}{1 + \left(\frac{500}{\psi}\right)\sin^2\alpha \left(\frac{A_v}{A_g}\right)\left(\frac{b_{wp}}{b_w}\right)\left(1.5\frac{D}{jd} - 1\right)} \quad \textit{for fixed-fixed ends} \tag{5-12a}$$

$$\Theta_{pr} = \frac{\tan\alpha}{1 + \left(\frac{1000}{\psi}\right)\sin^2\alpha \left(\frac{A_v}{A_g}\right)\left(\frac{b_{wp}}{b_w}\right)\left(1.5\frac{D}{jd} - 1\right)} \quad \textit{for fixed-pinned ends} \tag{5-12b}$$

5.2.3 Rocking Stage

In the rocking stage, the axial stress stored in the corner-to-corner diagonal strut is released. Accordingly, the column shear resistance V_p also decreases down until $V_p = 0$ as column shear deformation Θ_s increases. This can be achieved by reduction of the distance z as shown in figure 5-2(c). Therefore, the column shear resistance at this stage is calculated by

$$V_p = P(\tan\alpha - \Theta_s) \quad \textit{for fixed-fixed ends} \tag{5-13a}$$

$$V_p = 0.5P(\tan\alpha - \Theta_s) \quad \textit{for fixed-pinned ends} \tag{5-13b}$$

Figure 5-2(d) presents the whole response due to the action of arch mechanism for the axial load transfer. When $\Theta_s = \tan\alpha$, there will be no more shear resistance due to arch action.

5.2.4 Analytical Model for V_p Only Mechanism

Since the action of arch mechanism shown in figure 5-2(d) is bilinear, it can be expressed

using the Menegotto-Pinto equation. Thus

$$V_p = K_{p\theta}\,\theta_s\left[Q + \frac{1-Q}{\left\{1+\left(\frac{\theta_s}{\theta_{pr}}\right)^{20}\right\}^{0.05}}\right] \tag{5-14}$$

where $K_{p\theta} = \dfrac{V_{pr}}{\theta_{pr}}$ and $Q = \dfrac{-\theta_{pr}}{\tan\alpha - \theta_{pr}}$.

Note that the increase of V_p also causes the axial stress in the corner-to-corner diagonal strut to increase at the loading stage. Therefore, it is necessary to make sure that the diagonal strut has an appropriate section size to successfully transfer the applied column axial load P. The compressive axial stress in the corner-to-corner diagonal strut is calculated by

$$f_{cd} = \frac{V_p/\sin\alpha}{A_D} = \frac{-2\,V_p\cot\alpha}{A_v\left(\frac{b_{wp}}{b_w}\right)\left(1.5\,\frac{D}{jd}-1\right)} \tag{5-15}$$

5.3 $V_p + V_c$ Combined Mechanism

Figure 5-3 presents the $V_p + V_c$ combined mechanism model. This model consists of one longitudinal element, diagonal struts and inclined tie(s). This model is considered most adequate for the analysis of transversely unreinforced concrete members in which $V_s = 0$. However, the calculation of member forces at each column deformation step is difficult to perform by hand-analysis. Moreover, since this model includes several load transfer mechanisms together, computational modeling may be required and further study is necessary.

5.4 Conclusions Arising from the Analysis of V_p Mechanism

The axial load effect on column shear force and deformation relationship has been discussed in the present subsection and the findings from the study are summarized in the following:

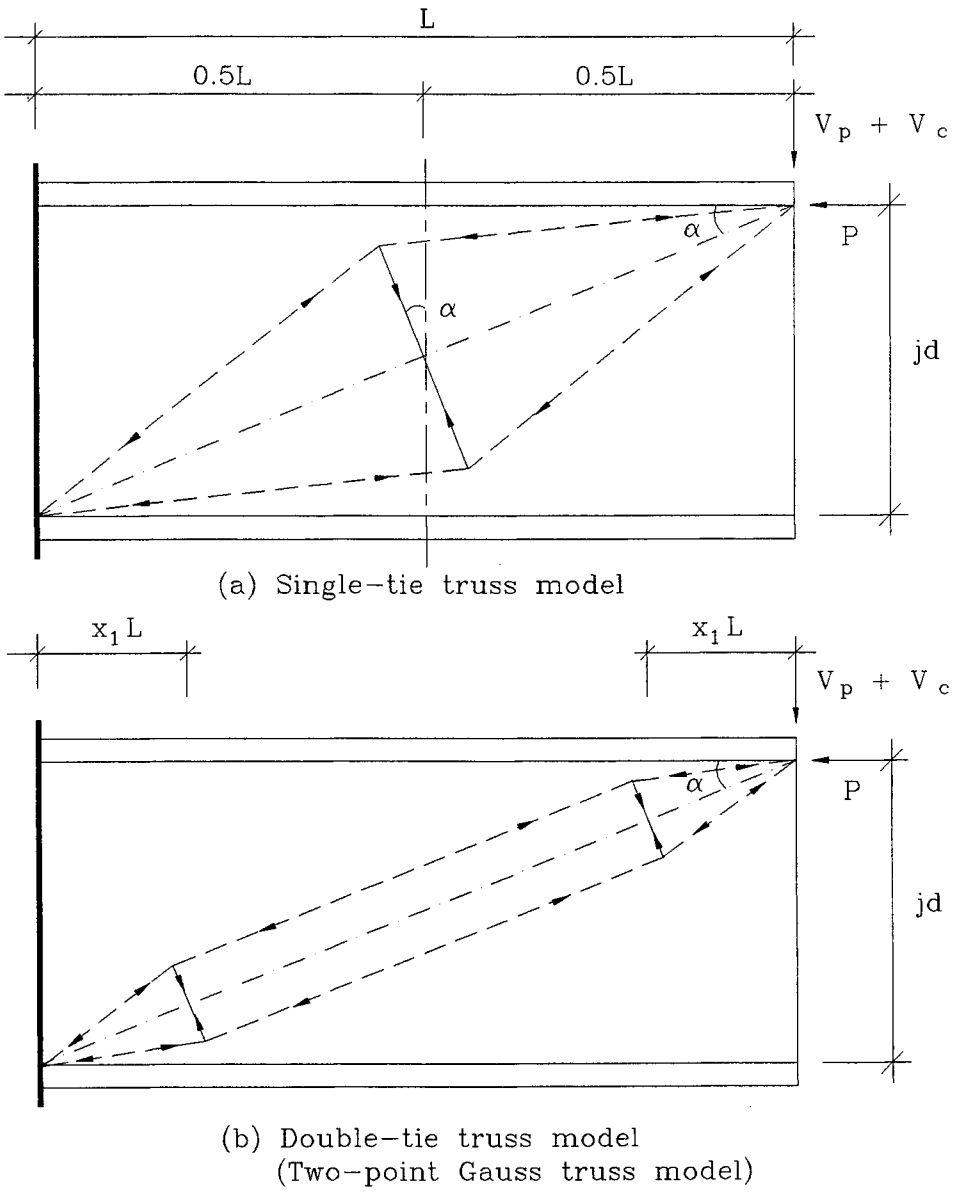

Figure 5-3. $V_p + V_c$ combined mechanism for computational modeling.

1. The mean section area of the corner-to-corner diagonal strut has been determined based on the postulated compression field. It is noted that the arch action mechanism for column axial load transfer has little to do with the crack angle.

2. The strength of arch action mechanism is governed by the amplitude of applied column axial load and load transfer capacity of the diagonal strut. The column shear resistance increases up to the moment of incipient rocking by axial deformation of the diagonal strut and then, decreases with rocking. For this, the linear elastic behavior of the diagonal strut is assumed.

3. Since the action of arch mechanism is bilinear, it may simply be simulated by the Menegotto-Pinto equation.

SECTION 6
COMBINATION OF RESPONSES DUE TO SHEAR AND FLEXURE

6.1 Introduction

It has been postulated in Section 1 that the full range of column shear strength is generated by three mechanisms: i) a transverse steel truss mechanism (V_s); ii) a truss mechanism that utilizes the tensile strength of concrete (V_c); and iii) a corner-to-corner arch mechanism that transmits axial load through a diagonal compression field (V_p). At the same time, the column lateral strength is also affected by the flexural mechanism (V_f) which provides moment resistance from two sources: i) moment from the longitudinal steel couple (M_s); and ii) moments provided by the eccentric concrete stress block (M_c). These two lateral force resisting mechanisms (shear and flexure) are depicted in figure 1-1 using the spring analogy which is helpful in gaining an understanding of overall behavior through the combination of the individual mechanisms. Thus the full range of column shear strength V_u can be obtained by summing V_s, V_c and V_p for the various values of shear deformation Θ_s. Then, the total column strength (V) is determined by the weaker mechanism of flexure (V_f) and shear (V_u), and the total column deformation (Θ) is determined by the sum of flexural (Θ_f) and shear (Θ_s) deformations as given in equation (1-5) after adjusted for $V = V_f = V_u$.

When combining flexure and shear, an overall column failure mode can be approximately expected by comparing the strengths of shear mechanisms with the flexural strength. Column responses may be classified in a conservative sense as follows:

(i) Brittle Shear-Critical;

$$[V_s + V_c + V_p]_{max} < V_f^y \qquad (6\text{-}1)$$

(ii) Semi-Ductile Shear-Critical;

$$[V_s + V_p]_{max} < V_f^y < [V_s + V_c + V_p]_{max} \quad (6\text{-}2)$$

(iii) Ductile Flexure;

$$V_f^y < [V_s + V_p]_{max} \quad (6\text{-}3)$$

where V_f^y = flexural strength at first yielding.

In order to evaluate column responses in detail, strength variation with deformation and interaction between flexure and shear should be considered. For this purpose, this section presents a methodology to combine flexure and shear responses and application examples. The methodology can cover all three failure modes mentioned above and has been implemented into a Fortran computer program ENVELOPE, through which a response envelope can be generated. The present section also demonstrates that the proposed truss modeling technique can be used to generate not only a monotonic response envelope but also cyclic responses for cyclic loading of reinforced concrete members. The technique for cyclic response is defined as CIST (Cyclic Inelastic Strut-and-Tie) modeling in this study and the general purpose nonlinear inelastic computer program, DRAIN-2DX *(Prakash, et al., 1992a,b)*, is used for analysis purposes. To begin with, it is important to understand that there is a strength reduction in shear due to several sources which are described in what follows.

6.2 Strength Reduction in Shear

It is considered that strengths of the three shear mechanisms (V_s, V_c and V_p) are limited by interaction with the flexural mechanism (V_f), the energy consumed by cyclic loading and/or stresses in critical diagonal struts.

6.2.1 Interaction between Flexure and Shear

When combining the previously mentioned mechanism responses, it is important to consider the interaction between flexure and shear and in particular which of the two

mechanisms to govern the column response at any given deformation. Two important issues need to be addressed: i) the loss of V_c due to yielding of the longitudinal reinforcing steel; and ii) the loss of V_p and V_s due to the decay in M_c resulting from cyclic loading.

When longitudinal reinforcing steel yields, it is assumed that the initial bond strength is destroyed which may be the source of anchorage of tension ties in a series of differential trusses for concrete mechanism (V_c). Therefore, as steel yielding penetrates along the longitudinal steel, the effective region for V_c mechanism will be reduced resulting in loss of V_c. Paulay *(1971a,b)* showed tensile stress distribution over the longitudinal reinforcing steel when lateral deformation is imposed on the tested reinforced concrete coupling beams as depicted in figure 6-1(a). This phenomenon can also be observed from the plastic analysis of reinforced concrete columns using the strut-and-tie model. Assuming a quadratic idealization for the nonlinear distribution of tensile stress along the longitudinal steel, the probable reduction factor for concrete mechanism (V_c) due to flexural yielding may be estimated by

$$r(f) = \left(\frac{M_y}{M_{\max}}\right)^2 = \left(\frac{V_f^y}{V_f^{\max}}\right)^2 \leq 1 \qquad \text{(6-4)}$$

in which V_f^y = flexural strength at first yielding, $V_f^{\max}$ = maximum flexural strength. It is implied from this equation that the semi-ductile shear failure mode is likely to emerge only in columns with good confinement, without which the increment rate of the flexural strength cannot be maintained to make $r(f)$ small enough to cause a further loss of V_c.

When cyclic loading is applied, the eccentric concrete stress block will decay and the centroid of the concrete stress block will move toward to the center of the column section as depicted in figure 6-1(b). At the final stage, when only the residual stress exists in which $M_c = 0$, the flexural lever arm will be $jd = 0.5D$ where D is column section overall depth. Then, the reduced lever arm jd will cause to limit the strength of a corner-to-corner arch mechanism (V_p).

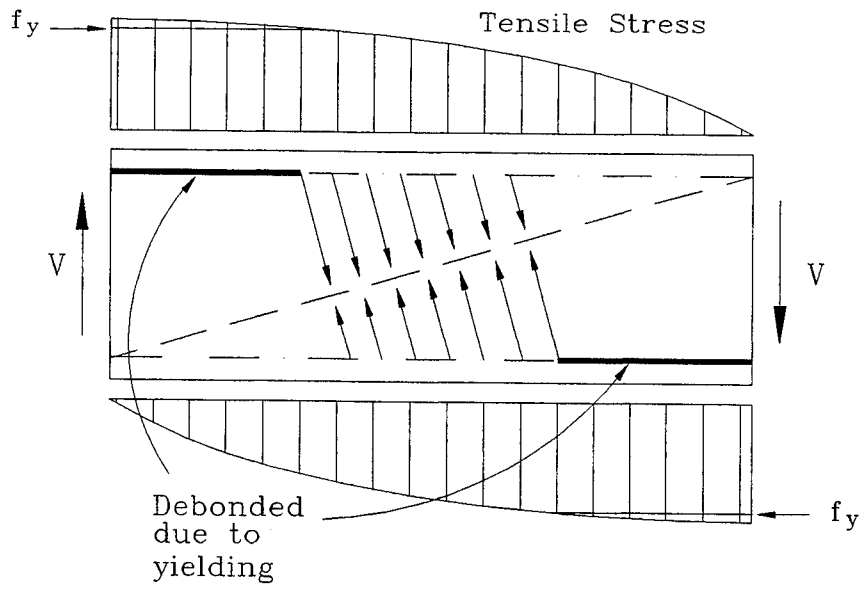

(a) Tensile stress distribution over longitudinal steel

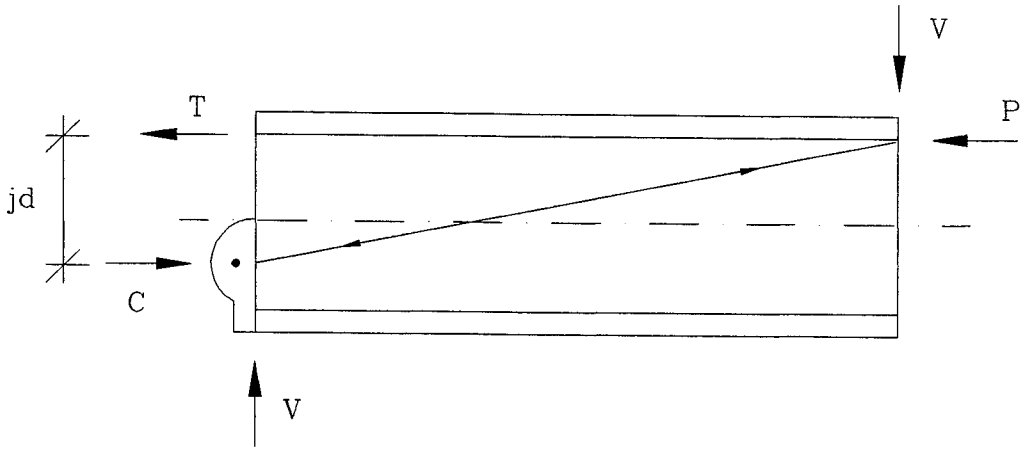

(b) Effect of cyclic loading on flexural lever arm

Figure 6-1. Factors causing degradation of shear strength.

6.2.2 Energy Consideration due to Cyclic Loading

The concept of energy consumption is utilized to evaluate the cyclic loading effect on the strength of transverse steel truss mechanism (V_s). This topic is extensively discussed elsewhere *(Kim, 1996; Dutta and Mander, 1998; Mander, et al., 1998)*.

6.2.3 Strength Limited by Stresses in Diagonal Struts

The expressions for strengths of three shear mechanisms (V_s, V_c and V_p) have been derived on the assumption that the diagonal strut members behave linear-elastically. However, since tensile stresses are generated in the direction perpendicular to the diagonal struts, it is expected that the compressive strengths of diagonal struts are subjected to the corresponding crack width and accordingly, in some stage, the strengths of those three shear mechanisms become limited by the strengths of diagonal struts.

Based on the experimental observation on various concrete panel elements, Vecchio and Collins *(1986)* suggested an upper limit of compressive stresses in the direction of diagonal cracks when subjected to shear. The limit is, in terms of the principal tensile strain,

$$\frac{f_{cd}^{max}}{f_c'} = \frac{1}{0.8 + 170\,\varepsilon_1} \leq 1 \qquad (6\text{-}5)$$

Application of this limit to the expressions of V_s, V_c and V_p derived from the analysis of two-point Gauss truss model is straightforward. Rearranging equations (2-25), (4-38) and (5-15) for V_s, V_c and V_p mechanisms, respectively, after substituting equation (6-5) into them, the strength limit of each mechanism due to stresses in critical diagonal struts is obtained as

$$V_s \leq \frac{f_c' A_v \left(\frac{b_{ws}}{b_w}\right) \cot\theta}{2\left(0.8 + 170\,\varepsilon_1^{avg}\right)\left\{1 + (1 - x_1)^2 \cot^2\theta\right\}} \qquad (6\text{-}6)$$

$$r(f)\,V_c \le \frac{f_c' A_v \left(\frac{b_{wc}}{b_w}\right) \tan\theta \,(1-\tan^2\theta)}{2\left(0.8+170\,\varepsilon_1^{avg}\right)\left\{(1-\tan^2\theta)^2(1-x_1)^2+\tan^2\theta\right\}} \tag{6-7}$$

$$V_p \le \frac{f_c' A_v \left(\frac{b_{wp}}{b_w}\right)\left(1.5\frac{D}{jd}-1\right)}{2\left(0.8+170\,\varepsilon_1^{avg}\right)\cot\alpha} \tag{6-8}$$

in which $x_1 = 0.2113249$. Note that the longer diagonal strut $(EA)_{d2}$ in figures 2-8 and 4-9 is the more critical for V_s and V_c mechanisms.

6.3 Calculation of Combined Responses

This subsection presents a summary of the solution strategy for the individual strength mechanisms discussed through the foregoing sections in order to obtain a complete force-deformation response envelope of a reinforced concrete member by combining flexure and shear responses.

6.3.1 Step-by-Step Procedures for Combined Response Envelopes

Since procedures for flexure only analysis are readily available elsewhere *(Mander, et al., 1984, 1988a,b; Chang and Mander, 1994a,b)*, detailed derivation procedures for equations are not included herein. However, reference can be made to subsections 2.2 and 3.3. Even for shear-only analysis, the present subsection does not include every single equation for the sake of brief presentation. Detailed equations should be referred to relevant parts of this report.

Part I Preliminary Calculation for Constants

Step 1 Calculate moments and curvatures at cracking and first yielding, respectively: M_{cr}, ϕ_{cr}, M_y and ϕ_y'.

Step 2 Calculate effective elastic flexural rigidities before and after cracking: EI_{un} and EI_{cr}. For this, elasticity and equations (2-29) and (2-34) are utilized.

$$EI_{un} = \frac{M_y L_c^2}{3 \Delta_y'} \tag{6-9}$$

for fixed-fixed ends,

$$EI_{cr} = \frac{1}{12} \xi^{-1} E_s A_{st} L^2 \tan^2\alpha \tag{6-10}$$

for fixed-pinned ends,

$$EI_{cr} = \frac{1}{3} \xi^{-1} E_s A_{st} L^2 \tan^2\alpha \tag{6-11}$$

where $L_c = M/V_f$, Δ_y' = flexural displacement at first yielding, ξ = 0.5704 for fixed-fixed ends, ξ = 1.5704 for fixed-pinned ends, L = column length and α = corner-to-corner diagonal angle (rad).

Step 3 Calculate the crack angle θ using equation (2-69). Note that the corner-to-corner angle α is used as a crack angle to calculate the shear strength of a cantilever.

$$\theta = \tan^{-1}\left(\frac{\rho_v n + \zeta \frac{\rho_v}{\rho_t}\frac{A_v}{A_g}}{1 + \rho_v n}\right)^{\frac{1}{4}} \tag{6-12}$$

Step 4 Determine the ratio of the effective column width for each shear mechanism using equation (1-8). For this purpose, mechanism strengths are recommended as per equations (1-1) to (1-4).

$$\frac{b_{ws}}{b_w} = \frac{V_s}{V_u} \; ; \; \frac{b_{wc}}{b_w} = \frac{V_c}{V_u} \; ; \; \frac{b_{wp}}{b_w} = \frac{V_p}{V_u} \tag{6-13}$$

$$V_u = V_s + V_c + V_p \tag{6-14}$$

$$V_s = A_{sh} f_{yh} \frac{jd}{s} \cot\theta \tag{6-15}$$

$$V_c = 0.1\sqrt{f'_c}\,A_v \cot\theta \tag{6-16}$$

$$V_p = P_o \tan\alpha \tag{6-17}$$

Note that mechanism strengths in equations (6-15) to (6-17) are suggested for initial values.

Part II Flexure Only Analysis

Step 1 Choose a curvature ϕ at the column critical section.

Step 2 Calculate moment M and corresponding flexural lateral strength V_f.

Step 3 Calculate column flexural displacement Δ_f and drift angle Θ_f. For this equations (3-39) to (3-42) and figure 3-3 are utilized.

$$\Delta_{fe} = \frac{M L_c^2}{3 EI_{un}} + \frac{L_c^2}{6 M^2}\left(M - M_{cr}\right)^2\left(M_{cr} + 2M\right)\left(\frac{1}{EI_{cr}} - \frac{1}{EI_{un}}\right) \tag{6-18}$$

$$\Delta_{fp} = \Theta_p\left(L_c - 0.25 L_{pc}\right) \tag{6-19}$$

$$\Theta_p = \phi_p\left(L_{pc}/3 + L_{py}\right) \tag{6-20}$$

$$\phi_p = \phi - \phi_{cr} - \left(\phi'_y - \phi_{cr}\right)\left(\frac{M - M_{cr}}{M_y - M_{cr}}\right) \tag{6-21}$$

$$L_{pc} = \left(1 - \frac{M_y}{M_{\max}}\right) L_c \geq 0 \tag{6-22}$$

$$L_{py} = 32\sqrt{d_b} \tag{6-23}$$

$$\Delta_f = \Delta_{fe} + \Delta_{fp} \tag{6-24}$$

$$\Theta_f = \Delta_f / L_c \tag{6-25}$$

where Δ_{fe} = elastic flexural displacement and Δ_{fp} =plastic flexural displacement.

Part III **Shear Only Analysis**

Step 1 Choose a column shear rotation angle Θ_s.

Step 2 Calculate transverse tie strain ε_T, stress f_T and mechanism strength V_s using equations (3-33), (3-27) and (3-34), respectively. Repeat this step until converged.

$$\varepsilon_T = \frac{\Theta_s \cot\theta}{1 + \dfrac{2\,\rho_v n\, T^*(\theta)}{\left(\dfrac{b_{ws}}{b_w}\right)}\left(\left(1+\left(\dfrac{\varepsilon_T}{\varepsilon_y^*}\right)^{20}\right)^{-0.05} + \left(\dfrac{1+sign\left(\varepsilon_T-\varepsilon_y^*\right)}{2E_s\,\varepsilon_T}\right)\left(f_{su}-E_s\,\varepsilon_y^*\right)\left(1-\left|\dfrac{\varepsilon_{su}-\varepsilon_T}{\varepsilon_{su}-\varepsilon_y^*}\right|^p\right)\right)} \tag{6-26}$$

$$f_T = \frac{E_s\,\varepsilon_T}{\left[1+\left(\dfrac{\varepsilon_T}{\varepsilon_y^*}\right)^{20}\right]^{0.05}} + \left(\frac{1+sign\left(\varepsilon_T-\varepsilon_y^*\right)}{2}\right)\left(f_{su}-E_s\,\varepsilon_y^*\right)\left[1-\left|\frac{\varepsilon_{su}-\varepsilon_T}{\varepsilon_{su}-\varepsilon_y^*}\right|^p\right] \tag{6-27}$$

$$V_s = A_{sh} f_T \frac{jd}{s}\cot\theta \tag{6-28}$$

in which

$$T^*(\theta) = \left[1+x_1^2\cot^2\theta\right]^2 + \left[1+(1-x_1)^2\cot^2\theta\right]^2 \;;$$

$$x = 0.2113249 \;;$$

$$\varepsilon_y^* = \frac{f_y - E_{sh}\,\varepsilon_{sh}}{E_s - E_{sh}} \;;$$

$$p = E_{sh}\left(\frac{\varepsilon_{su} - \varepsilon_{sh}}{f_{su} - f_y}\right) ;$$

$$sign\left(\varepsilon_T - \varepsilon_y^*\right) = -1 \text{ for } \varepsilon_T < \varepsilon_y^* \text{ ; and } sign\left(\varepsilon_T - \varepsilon_y^*\right) = 1 \text{ for } \varepsilon_T \geq \varepsilon_y^* .$$

Step 3 Calculate concrete average principal strain ε_1^{avg}, stress f_1^{avg} and mechanism strength V_c using equations (4-44), (4-4) and (4-42), respectively. Repeat this step until converged.

$$\varepsilon_1^{avg} = \frac{\Theta_s \cot\theta \cos^2\theta}{1 + \dfrac{2\,T(\theta)\cos^4\theta \cot^4\theta}{\left(\dfrac{b_{wc}}{b_w}\right)\left\{1 + \left(\dfrac{E_c}{E_{sec}} - 1\right)\left(\dfrac{\varepsilon_1^{avg}}{\varepsilon_t'}\right)^r\right\}}} \tag{6-29}$$

$$f_1^{avg} = \frac{f_t' r \left(\dfrac{\varepsilon_1^{avg}}{\varepsilon_t'}\right)}{r - 1 + \left(\dfrac{\varepsilon_1^{avg}}{\varepsilon_t'}\right)^r} \tag{6-30}$$

$$V_c = f_1^{avg} A_v \cot\theta \left(1 - 2\sin^2\theta\right) \tag{6-31}$$

in which

$$T(\theta) = \left[\left(1 - \tan^2\theta\right)^2 x_1^2 + \tan^2\theta\right]^2 + \left[\left(1 - \tan^2\theta\right)^2 \left(1 - x_1\right)^2 + \tan^2\theta\right]^2 ;$$

$$E_{sec} = \frac{f_t'}{\varepsilon_t'} \text{ ; and}$$

$$r = \frac{E_c}{E_c - E_{sec}} .$$

Step 4 Calculate column rotational stiffness due to axial load transfer mechanism, rotational angle at incipient rocking and mechanism strength V_p using equations (5-5), (5-12) and (5-14).

$$K_{p\Theta} = 0.5\, E_c\, A_v \left(\frac{b_{wp}}{b_w}\right)\left(1.5\,\frac{D}{jd} - 1\right)\sin^2\alpha \qquad (6\text{-}32)$$

for a column with fixed-fixed ends,

$$\Theta_{pr} = \frac{\tan\alpha}{1 + \left(\frac{500}{\psi}\right)\sin^2\alpha \left(\frac{A_v}{A_g}\right)\left(\frac{b_{wp}}{b_w}\right)\left(1.5\,\frac{D}{jd} - 1\right)} \qquad (6\text{-}33)$$

for a column with fixed-pinned ends,

$$\Theta_{pr} = \frac{\tan\alpha}{1 + \left(\frac{1000}{\psi}\right)\sin^2\alpha \left(\frac{A_v}{A_g}\right)\left(\frac{b_{wp}}{b_w}\right)\left(1.5\,\frac{D}{jd} - 1\right)} \qquad (6\text{-}34)$$

$$V_p = K_{p\Theta}\,\Theta_s \left[Q + \frac{1 - Q}{\left[1 + \left(\frac{\Theta_s}{\Theta_{pr}}\right)^{20}\right]^{0.05}}\right] \qquad (6\text{-}35)$$

where $$Q = \frac{-\Theta_{pr}}{\tan\alpha - \Theta_{pr}}\,.$$

Step 5 Adjust mechanism strengths limited by stresses in diagonal struts using equations (6-6), (6-7) and (6-8).

$$V_s \le \frac{f_c'\, A_v \left(\frac{b_{ws}}{b_w}\right)\cot\theta}{2\left(0.8 + 170\,\varepsilon_1^{avg}\right)\left\{1 + \left(1 - x_1\right)^2\cot^2\theta\right\}} \qquad (6\text{-}36)$$

$$r(f)\,V_c \le \frac{f_c'\, A_v \left(\frac{b_{wc}}{b_w}\right)\tan\theta\,\left(1 - \tan^2\theta\right)}{2\left(0.8 + 170\,\varepsilon_1^{avg}\right)\left\{\left(1 - \tan^2\theta\right)^2\left(1 - x_1\right)^2 + \tan^2\theta\right\}} \qquad (6\text{-}37)$$

$$V_p \leq \frac{f_c' A_v \left(\frac{b_{wp}}{b_w}\right)\left(1.5\frac{D}{jd} - 1\right)}{2\left(0.8 + 170\,\varepsilon_1^{avg}\right)\cot\alpha} \tag{6-38}$$

Step 6 Calculate column shear strength V_u using equation (1-6) with consideration of reduction factor $r(f)$ in equation (6-4).

$$V_u = V_s + r(f)\,V_c + V_p \tag{6-39}$$

Part IV **Combination of Responses in Shear and Flexure**

Step 1 Adjust Θ_f or Θ_s so that $V_f = V_u$, in which the lesser of V_f and V_u should be the base strength.

Step 2 Calculate reduction factor $r(f)$ using equation (6-4). If $r(f)$ changes from the value in the previous step, go to **Step III.5**.

$$r(f) = \left(\frac{M_y}{M_{max}}\right)^2 = \left(\frac{V_f^y}{V_f^{max}}\right)^2 \leq 1 \tag{6-40}$$

in which V_f^y = flexural strength at first yielding, V_f^{max} = maximum flexural strength.

Step 3 Calculate combined column strength and corresponding deformation referring to equations (1-5) and (1-6).

$$V = V_u = V_f \tag{6-41}$$

$$\Theta = \Theta_f + \Theta_s \tag{6-42}$$

where Θ = column total drift angle (rad).

Step 4 Plot V vs. Θ.

Step 5 Go to **Step II.1** for next deformation level until the prescribed column maximum deformation is reached.

6.3.2 Solution Algorithm and Computer Program ENVELOPE

Almost all steps in step-by-step procedures for combined response envelopes presented in the previous subsection are straightforward to follow. The only step requiring further explanation is **Step IV.1**. Adjustment of flexural (Θ_f) or shear (Θ_s) deformation for the given base strength, which is the lesser of V_f and V_u, involves a few cases to consider as shown in figure 6-2, in which notation $i+1$ denotes a state that a step of increment in deformation is imposed after step i.

The first ($V_u^{i+1} > V_u^i$) and second ($V_u^{i+1} < V_u^i$ and $\partial V_u / \partial \Theta_s > 0$) cases in the figure can be considered together. Both cases are pertaining to the elastic shear behavior before diagonal cracks in concrete advanced. There can be two subcases to consider:

(i) if $V_u^{i+1} > V_f^{i+1}$, then find Θ_s^{i+1} for $V_u^{i+1} = V_f^{i+1}$.

(ii) if $V_u^{i+1} < V_f^{i+1}$, then find Θ_f^{i+1} for $V_f^{i+1} = V_u^{i+1}$.

in which Θ_s^{i+1} and Θ_f^{i+1} are respectively shear and flexural deformation at step $i+1$.

The third case ($V_u^{i+1} < V_u^i$ and $\partial V_u / \partial \Theta_s < 0$) in the figure is pertaining to the state after concrete ruptures to form diagonal cracks. This state involves unloading in flexure and the corresponding flexural displacement can be found as

$$\Theta_f^{i+1} = \Theta_f^i + \left(V_u^{i+1} - V_u^i\right) / K_{fe} \qquad \text{(6-43)}$$

where K_{fe} = effective elastic flexural stiffness for drift angle after cracking.

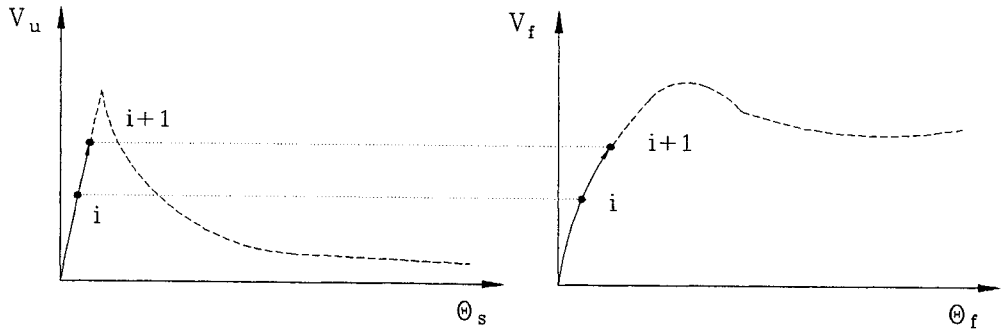

(a) $V_u^{i+1} > V_u^i$

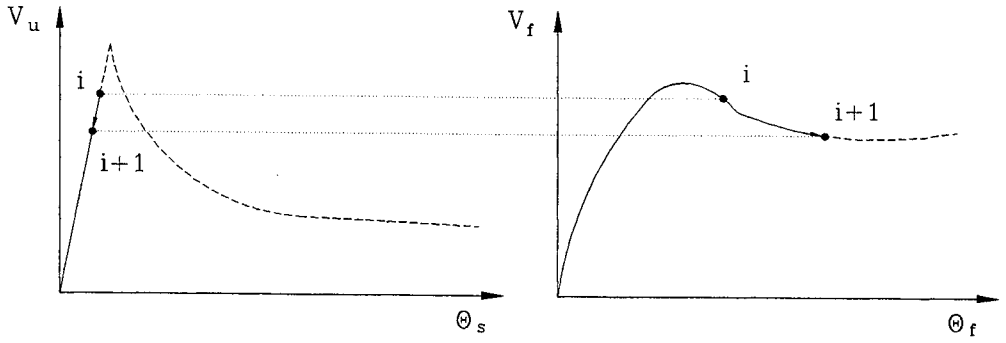

(b) $V_u^{i+1} < V_u^i$ and $\partial V_u / \partial \Theta_s > 0$

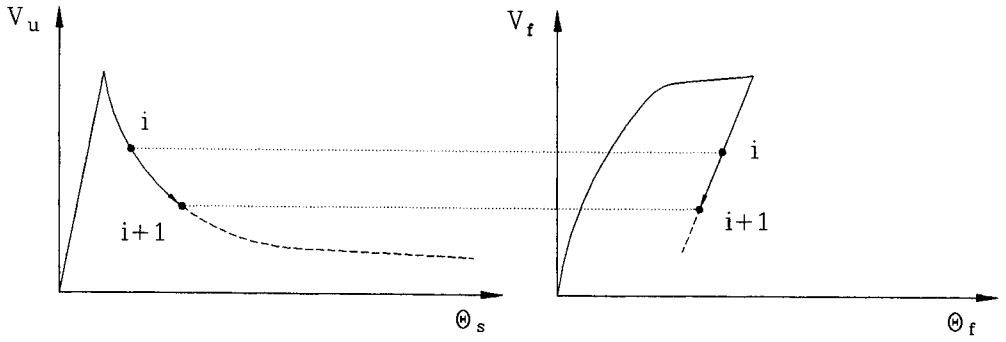

(c) $V_u^{i+1} < V_u^i$ and $\partial V_u / \partial \Theta_s < 0$

Figure 6-2. Combination of responses in shear and flexure.

In order to find Θ_s^{i+1} or Θ_f^{i+1} in cases 1 and 2, a root finding numerical scheme, the secant method, which is a modified conventional Newton's method *(Hornbeck, 1975)*, is used. Application of the numerical scheme to each solution is as follows:

(i) if $V_u^{i+1} > V_f^{i+1}$, then find Θ_s^{i+1} for $V_u^{i+1} = V_f^{i+1}$:

$$\Delta V^{i+1} = V_f^{i+1} - V_u^{i+1} \tag{6-44}$$

$$d\Theta_s^{i+1} = \frac{\Delta V^{i+1}}{\dfrac{V_u^{i+1} - V_u^i}{d\Theta_s^i}} \tag{6-45}$$

$$\Theta_s^{i+1} = \Theta_s^i + d\Theta_s^{i+1} \tag{6-46}$$

(ii) if $V_u^{i+1} < V_f^{i+1}$, then find Θ_f^{i+1} for $V_f^{i+1} = V_u^{i+1}$:

$$\Delta V^{i+1} = V_u^{i+1} - V_f^{i+1} \tag{6-47}$$

$$d\Theta_f^{i+1} = \frac{\Delta V^{i+1}}{\dfrac{V_f^{i+1} - V_f^i}{d\Theta_f^i}} \tag{6-48}$$

$$\Theta_f^{i+1} = \Theta_f^i + d\Theta_f^{i+1} \tag{6-49}$$

Repeat this operation until ΔV^{i+1} (difference between V_f^{i+1} and V_u^{i+1}) becomes small.

The constitutive laws used for materials are the Tsai's equation for concrete in compression and the modified Menegotto-Pinto equation for longitudinal reinforcement *(Chang and Mander, 1994a)*. For concrete in tension and transverse hoop reinforcement, Popovics and modified Menegotto-Pinto equations are respectively used as discussed in the foregoing sections. For transverse hoop reinforcement, the effect of steel embedment in the cracked concrete is

considered by using the average stress-average strain relationship as suggested by Hsu *(1993)*. Note that the concept of Gauss-Legendre numerical integration scheme is utilized for not only shear analysis but also flexural analysis. For shear analysis algorithm, the analysis results of two-point Gauss truss model are used while 2nd- to 6th-order Gauss quadratures can be selectively used for the moment-curvature analysis algorithm.

6.4 Application Examples

Examples presented herein are to demonstrate the application of the truss modeling technique to various reinforced concrete elements. For this, computer programs "envelope" and DRAIN-2DX are used to produce monotonic response envelopes and cyclic responses, respectively. However, it should be noted that the strength decay due to the cyclic loading effect cannot be simulated in the current version of both computer programs.

6.4.1 Response Envelopes Calculated by ENVELOPE

The selected examples include two rectangular sections and three circular sections ranged from a thin-webbed coupling beam to a large-section-webbed column-cap beam subassemblage which respectively represent the brittle shear-critical and ductile failure modes. The examples are:

- Coupling Beam Specimen 312 *(Paulay, 1971a,b)*
- Circular Column C5A *(Priestley, et al., 1994a,b)*
- Rectangular Column R5A *(Priestley, et al., 1994a,b)*
- Retrofitted Prototype Pier Subassemblage *(Mander, et al., 1996a)*
- Retrofitted 1/3 Scale Model Pier *(Mander, et al., 1996b)*

Material and geometrical properties of above specimens for input data are presented in Table 6-1 and parameter values calculated by ENVELOPE for the analysis are presented in Table 6-2.

Table 6-1. Input data of ENVELOPE for worked examples to obtain shear-flexure combined response envelopes.

Items	Coupling Beam 312[a]	Circular Column C5A	Rectangular Column R5A	Prototype Pier	Model Pier
Geometry					
b_w *(mm)*	152	-	406.4	-	-
D *(mm)*	787	609.6	609.6	838	279
L *(mm)*	1016	2438	1828.8	1791	1320
Cover (mm)	48	20.3	20.3	51	16
End Condition	F-F	F-F	F-F	F-P	F-F
Section Type	Rectangular	Circular	Rectangular	Circular	Circular
P_o *(kN)*	1.0	591.9	507.3	343+0.824V	59
Concrete					
f_c' *(MPa)*	35.2	35.87	32.42	44.8	56.6
r_{cc}	3.27	4.3	4.33	4.045	4.55
K_e	1.13	-	1.045	-	-
ε_t'	0.0002	0.0002	0.0002	0.0002	0.0002
Longitudinal Steel					
Diameter (mm)	23.4	19	19	28.6	9.5
Number of Bars	8	26	22	16	16
Number of Layers	2	-	8	-	-
f_y *(MPa)*	316	469	469	407	474
ε_{sh}	0.015	0.015	0.015	0.005	0.005
E_{sh}/E_s	0.02	0.02	0.02	0.02	0.02
f_{su} *(MPa)*	474	703.5	703.5	421	750
ε_{su}	0.15	0.15	0.15	0.19	0.12
Transverse Hoop					
Diameter (mm)	12.8	6.35	6.35	12.7	4.8
Spacing (mm)	102	127	127	305	102
f_y *(MPa)*	285	324.2	324.2	476	268
ε_{sh}	0.02	0.02	0.02	0.02	0.02
E_{sh}/E_s	0.015	0.015	0.015	0.014	0.03
f_{su} *(MPa)*	427	486.3	486.3	586	408
ε_{su}	0.15	0.15	0.15	0.15	0.14

Note:

1. Modulus of Elasticity for Steel E_s = **200000** ***MPa*** is used.
2. Concrete Tensile Stress at Peak f_t' = **0.33** $\sqrt{f_c'}$ ***(MPa)*** is used.

Table 6-2. Parameter values calculated by ENVELOPE for analysis.

Parameters	Coupling Beam 312	Circular Column C5A	Rectangular Column R5A	Prototype Pier	Model Pier Avg. Col.
Geometry					
A_g (mm^2)	119624	291863	247741	551541	61136
A_v (mm^2)	97584	248602	218322	410891	46072
jd (mm)	642	537.2	537.2	682	227.9
Concrete					
E_c (MPa)	27885	28148	26760	13387[a]	35360
f'_t (MPa)	1.978	1.996	1.898	2.231	2.508
f'_{lx}/f'_{lco}	0.00348	-	0.00635	-	-
f'_{ly}/f'_{lco}	0.0546	-	0.00994	-	-
K_e	-	1.045	-	1.054	1.031
Steel					
E_s/E_c	7.17	7.11	7.47	6.36	5.66
ε_{yL}	0.00158	0.00235	0.00235	0.00204	0.00237
ε_{yT}	0.00143	0.00162	0.00162	0.00238	0.00134
A_{st} (mm^2)	3440.4	7410.6	6270.5	10278.8	1134.1
ρ_t	0.0288	0.0254	0.0253	0.0186	0.0186
Shear					
θ (deg)	37.5	21.3	23.1	27.9	24.3
A_{sh} (mm^2)	257.4	43.8	63.3	185.5	27.1
ρ_v	0.0166	0.000886	0.00123	0.00115	0.00146
Flexure					
M_n $(kN-m)$	361.3	852.3	809.5	1409.5	61.5
M_{cr} $(kN-m)$	38.5	130.2	128.6	160	7.5
M_y $(kN-m)$	335	647.1	625.4	1003	44.8
K_{un} (kN/mm)	1195	86	205	136	18
K_{cr} (kN/mm)	474	52	104	106	9

[a]About $0.4\,E_c$ is assumed to account for the pre-existing cracked status.

Coupling Beam Specimen 312

The schematic test setup shown by Paulay *(1971a,b)* and the section of coupling beam specimen 312 are presented in figure 6-3. The material models used for analysis are shown in figure 6-4 as an example for all specimens discussed hereafter. The coupling beam had a thin web and hence, the effect of concrete tensile strength mechanism (V_c) is expected to be minimal. The theoretical response of the coupling beam is expected to be governed by the transverse hoop steel truss mechanism (V_s). Note that even though there is no externally applied axial load, a small axial load is provided for data input in order to avoid any possible numerical error in V_p mechanism.

The analysis results are presented in figure 6-5. The "shear-only" response has been calculated assuming a rigid flexural response (no flexural flexibility) while the "flexure-only" response has been calculated assuming a rigid shear response (no shear flexibility). The experimental response has been constructed by picking several representative data points from the reported experimental results. Note that the response is governed by the transverse hoop steel mechanism (V_s) and the contribution of V_c mechanism is minimal, as expected. Also note that the strength of shear mechanism is governed by the strength of diagonal struts from the shear rotation of 0.007 rad.

Circular (C5A) and Rectangular (R5A) Columns

These columns were tested by Priestley, et al. *(1994a,b)* to study the shear failure mode of non-seismically designed reinforced concrete bridge columns and the effectiveness of full-height steel jackets for enhancing the seismic shear strength. Column sections and test setup are presented in figure 6-6. It is noted that the test setup was designed to provide the fixed-fixed end condition in which the same magnitude of moment is expected to be generated at top and bottom ends of columns.

Analysis results of columns before the seismic retrofit is practiced are presented in

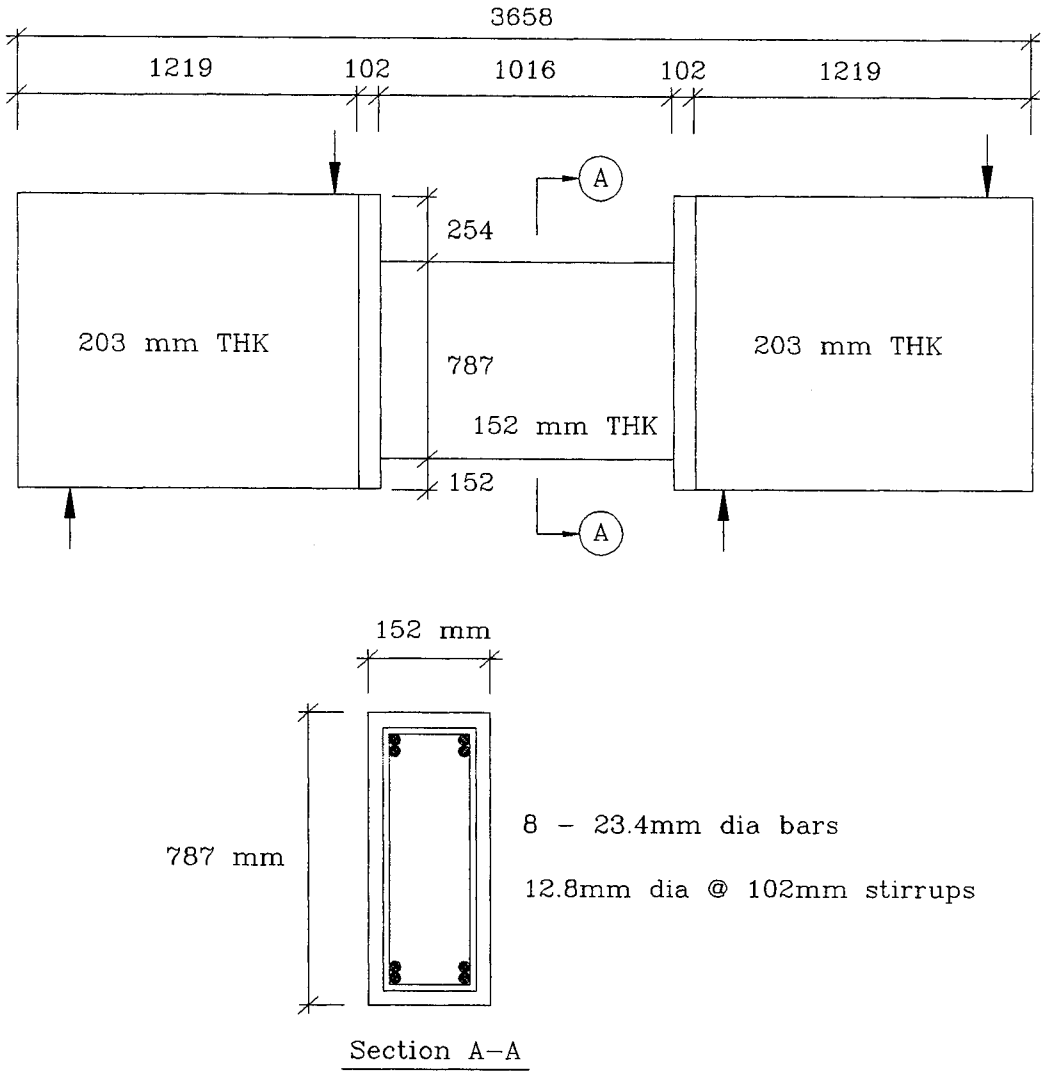

Figure 6-3. Test setup and section of coupling beam specimen 312 tested by Paulay *(1971a,b)*.

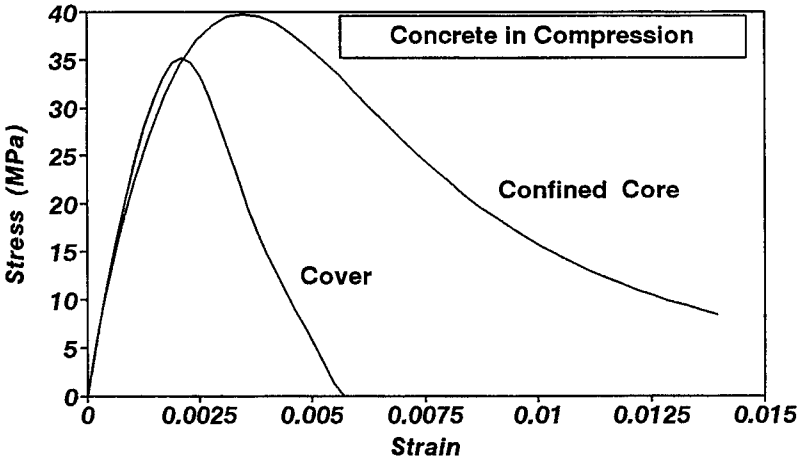

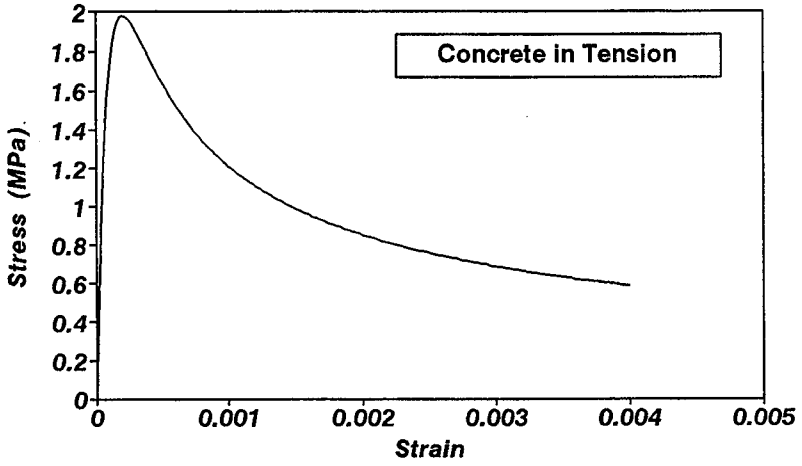

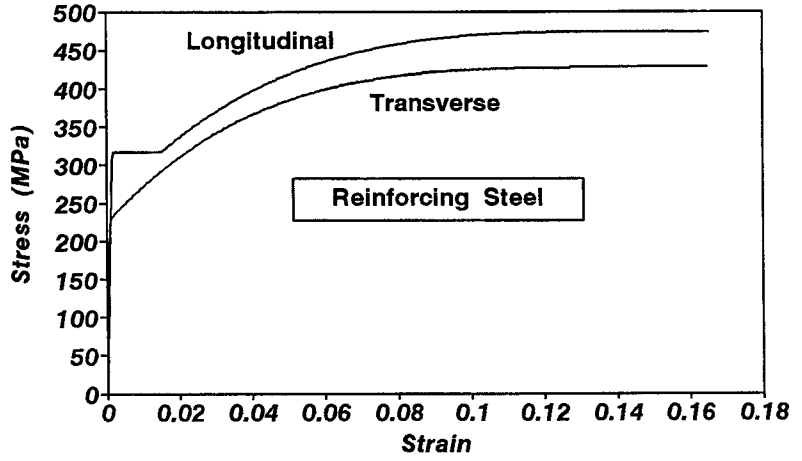

Figure 6-4. Material properties assumed for the analysis of coupling beam specimen 312 tested by Paulay *(1971a,b)*.

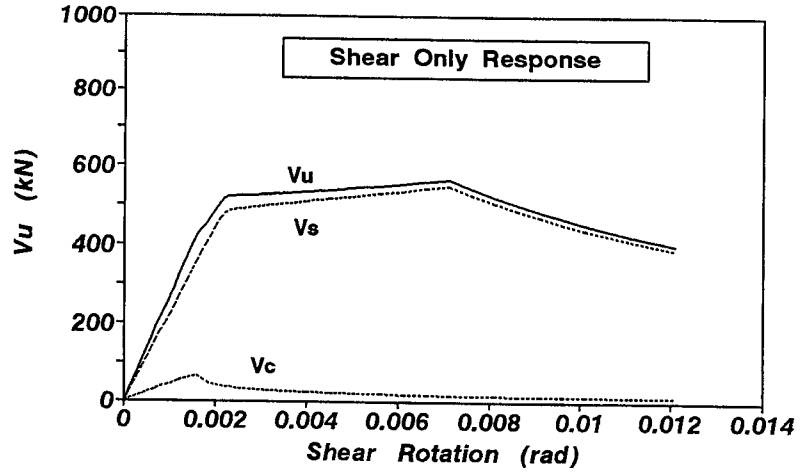

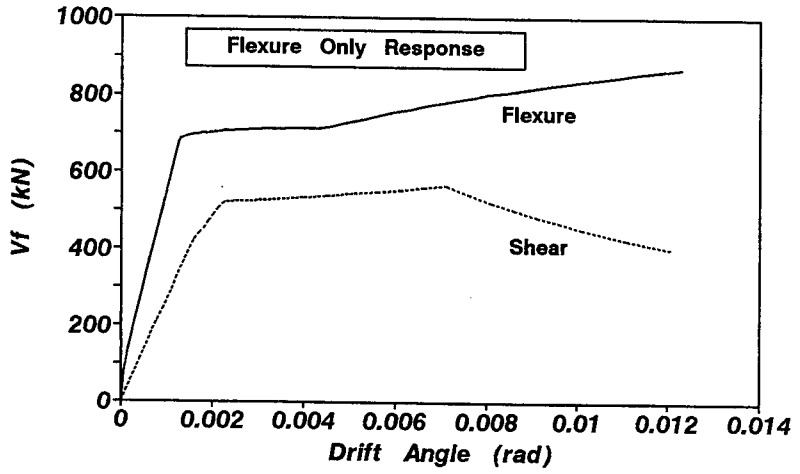

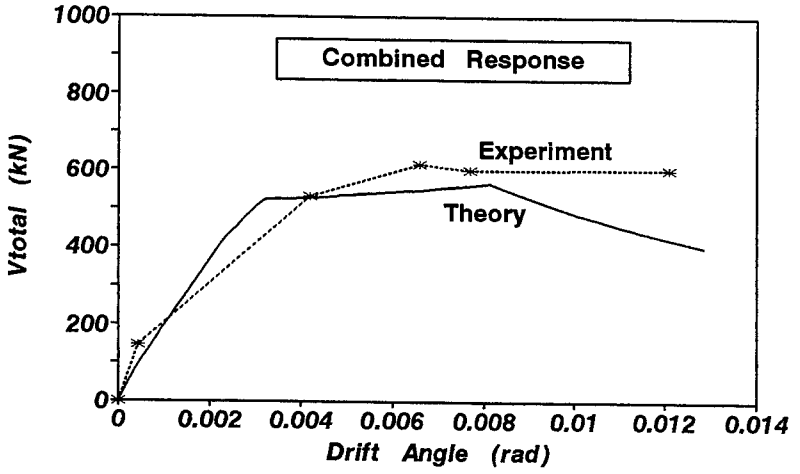

Figure 6-5. Combination of shear and flexural responses for coupling beam specimen 312 tested by Paulay *(1971a,b)*.

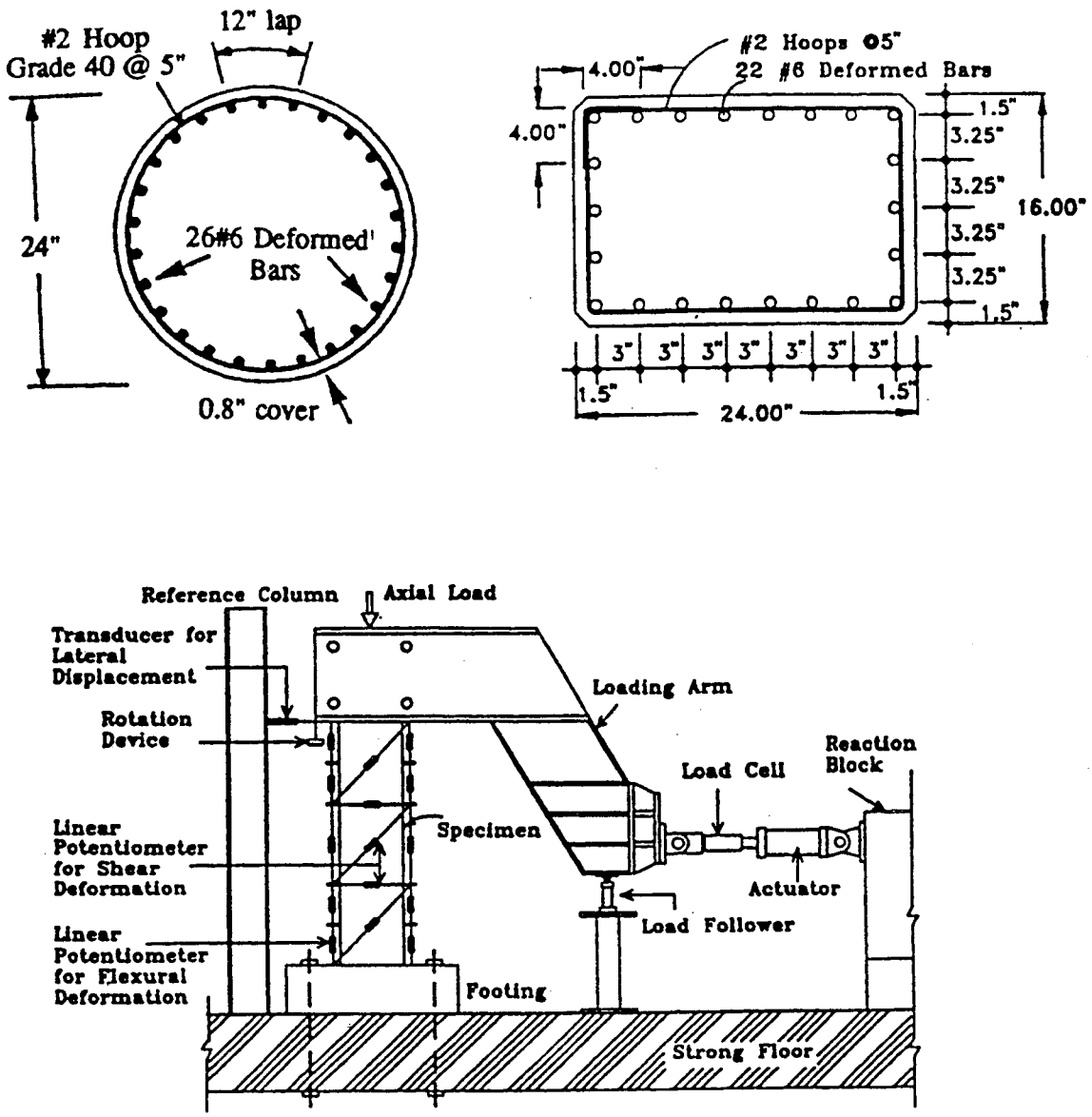

Figure 6-6. Section and test setup for circular (C5A) and rectangular (R5A) columns tested by Priestley, et al. *(1994a,b)*. (Note 1 inch = 25.4 mm).

figures 6-7 and 6-8 for C5A and R5A, respectively. The brittle shear failure mode is predicted for the columns as shown in experimental results. Note that the predicted response of C5A fits the experimental observation for displacement while the strength is overestimated by about 15%. For R5A, the theoretical strength fits the experimental one while displacement is less predicted. These deviations may be due to the imperfect boundary condition when modeling. In analysis, fixed-fixed ends are assumed to be perfectly rigid while the actual experimental setup implies some imperfection.

Retrofitted Prototype Pier Subassemblage

The experimental study was performed by Mander, et al. *(1996a)* to investigate the seismic performance of a full-scale prototype cap beam - circular column bridge pier subassemblage and its retrofit. The pre-retrofitted pier subassemblage was tested under quasi-static cyclic loading and the failure mode was attributed to the loss of anchorage and joint strength. The cap beam and joint were repaired and retrofitted by applying concrete jacketing with prestressing but the column was left without retrofitting. Column reinforcement and test setup of the retrofitted prototype subassemblage are presented in figure 6-9. Test of the retrofitted pier subassemblage showed a semi-ductile shear-critical failure mode of its column due to the effect of cyclic loading.

Analysis results for the retrofitted pier column are presented in figure 6-10. In order to account for the pre-existing cracked status resulting from the previous experiment over the pre-retrofitted pier subassemblage, the flexural rigidity of the column has been reduced to about $0.4EI$. The effect of cap beam flexibility, discussed in subsection 3.3, has also been considered for the theoretical response. The comparison between theoretical response and experimental observation shows good agreement. The column ultimately failed at 5% to 5.4% drift angle with diagonal crack opening and subsequent fracture of transverse hoop steel. This failure mode is attributed to the effect of cyclic loading which is not accounted for in the current version of ENVELOPE.

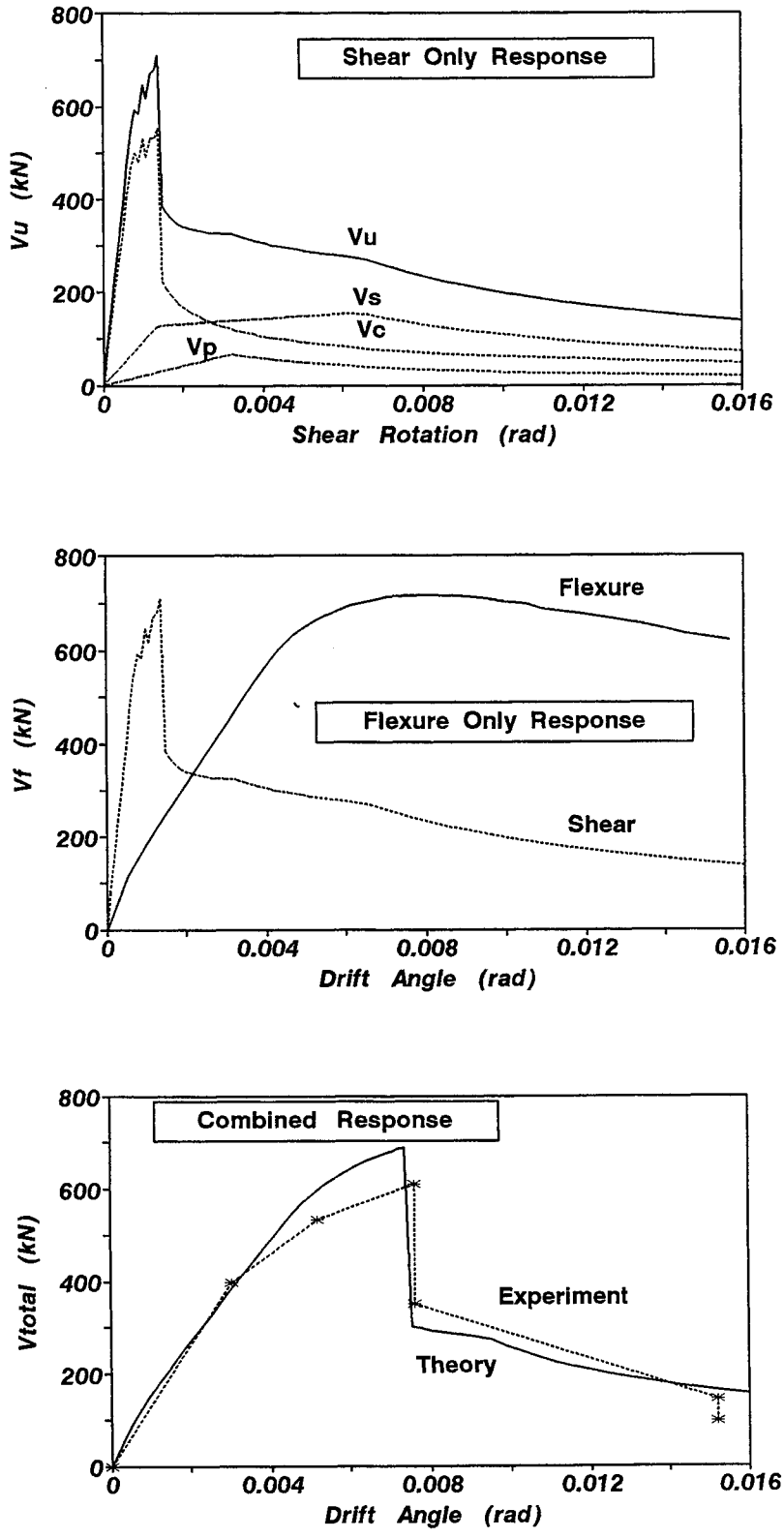

Figure 6-7. Combination of shear and flexural responses for circular column C5A tested by Priestley, et al. *(1994a,b)*.

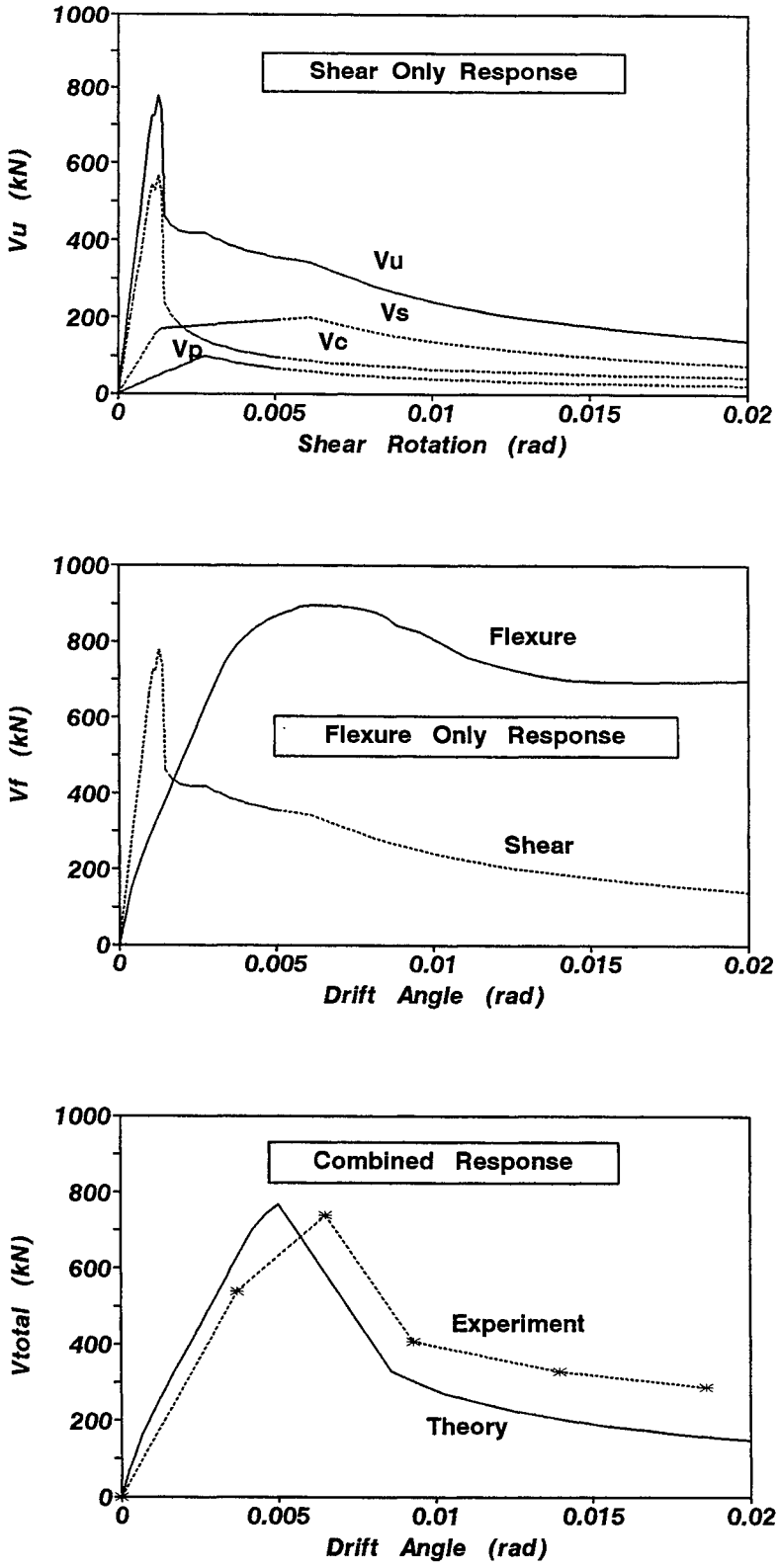

Figure 6-8. Combination of shear and flexural responses for rectangular column R5A tested by Priestley, et al. *(1994a,b)*.

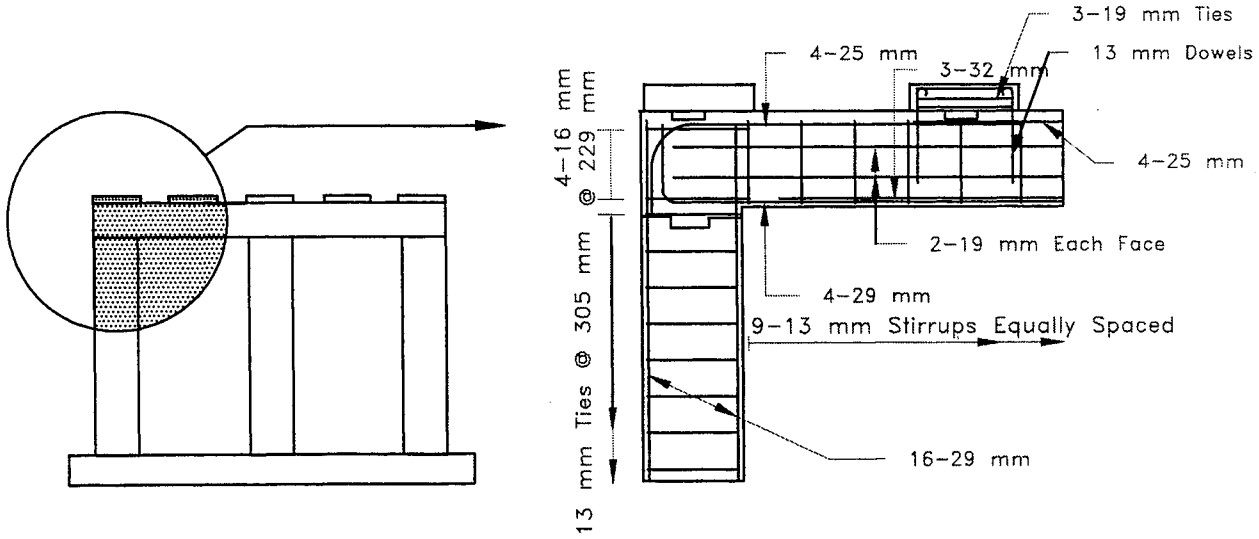

(a) Details of pier subassemblage

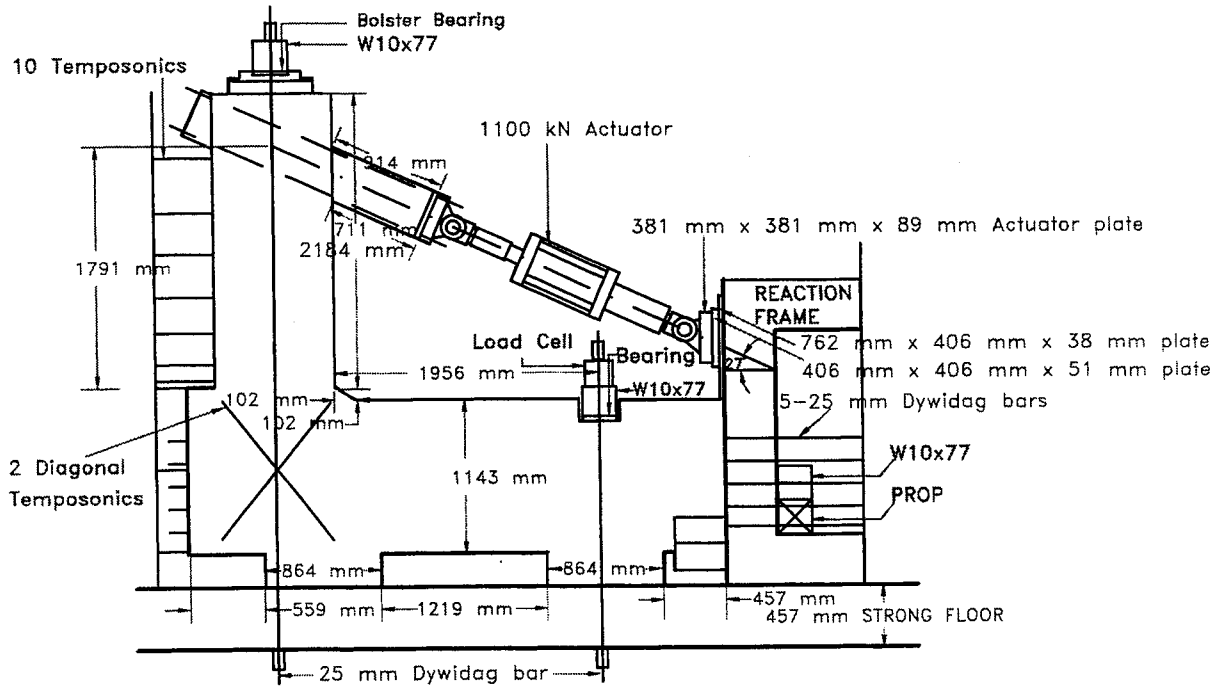

(b) Test setup

Figure 6-9. Retrofitted prototype pier subassemblage tested by Mander, et al. *(1996a)*.

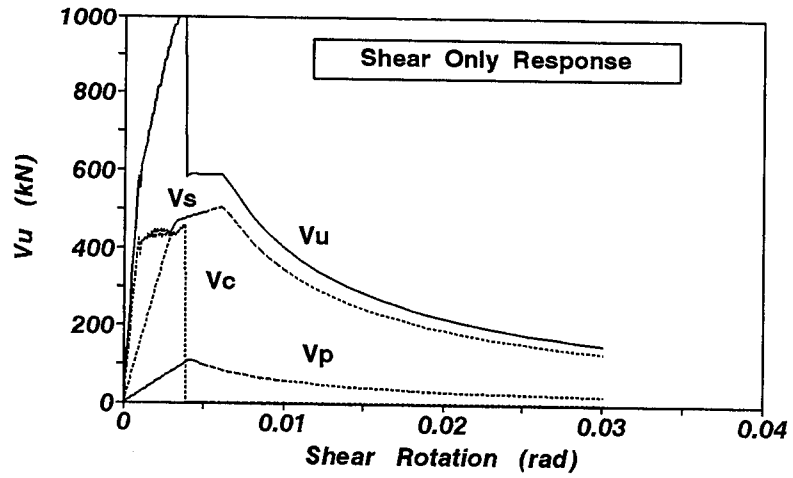

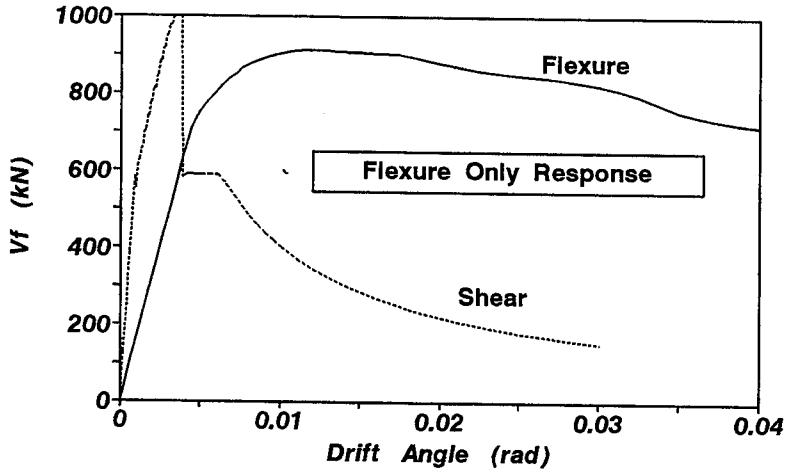

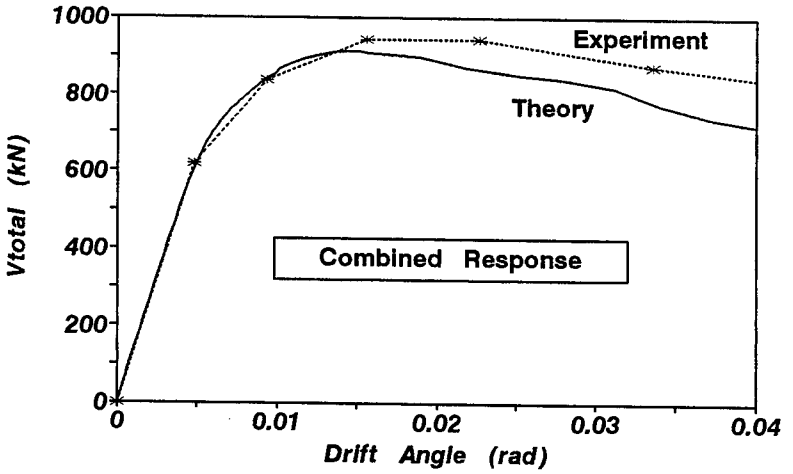

Figure 6-10. Combination of shear and flexural responses for retrofitted prototype cap beam-column subassemblage tested by Mander, et al. *(1996a)*.

Retrofitted 1/3 Scale Model Pier

The experimental study was performed by Mander, et al. *(1996b)* to investigate the seismic performance of a whole pier consisting of cap beam, three circular columns and foundation beam. The 1/3 scale model pier was constructed and tested under quasi-static cyclic loading to be damaged at joints , anchorage and lap-splice zones. The cap beam and joints were repaired and retrofitted by prestressed concrete jacketing as used for the companion prototype pier subassemblage *(Mander, et al., 1996a)* but columns were left without retrofitting. Column reinforcement detail and test setup for retrofitted model pier are presented in figure 6-11. For the purpose of comparison between theory and experiment, an average column is used for analysis and the strength of the whole pier is obtained by summing three average columns. The central column is used as the average one.

The theoretical prediction of the combined response is presented in figure 6-12. The theoretical prediction of the elastic stiffness shows a better fit to the experimental one than in the companion prototype subassemblage, which implies a less flexibility of cap beam and foundation beam, and a better anchorage of column longitudinal reinforcement. The theoretical response shows a ductile behavior of the retrofitted model pier, while the model pier failed at 3.1% to 4.7% drift angle due to the cyclic loading effect. Again, consideration of the strength decay due to cyclic loading is not available in the current version of ENVELOPE.

6.4.2 CIST Modeling

As described earlier in this section, CIST is an acronym for Cyclic Inelastic Strut-and-Tie modeling technique. This modeling technique utilizes the 2nd-order Gauss quadrature in determining the geometrical details of a mathematical model for reinforced concrete structural components. For the model analysis in this study, the general purpose nonlinear inelastic computer program, DRAIN-2DX *(Prakash, et al., 1992a,b)*, is used. The behavior of individual CIST elements available in DRAIN-2DX are depicted in figure 6-13. Reinforcement is modeled by a bilinear spring element and concrete in either compression or tension is modeled by a

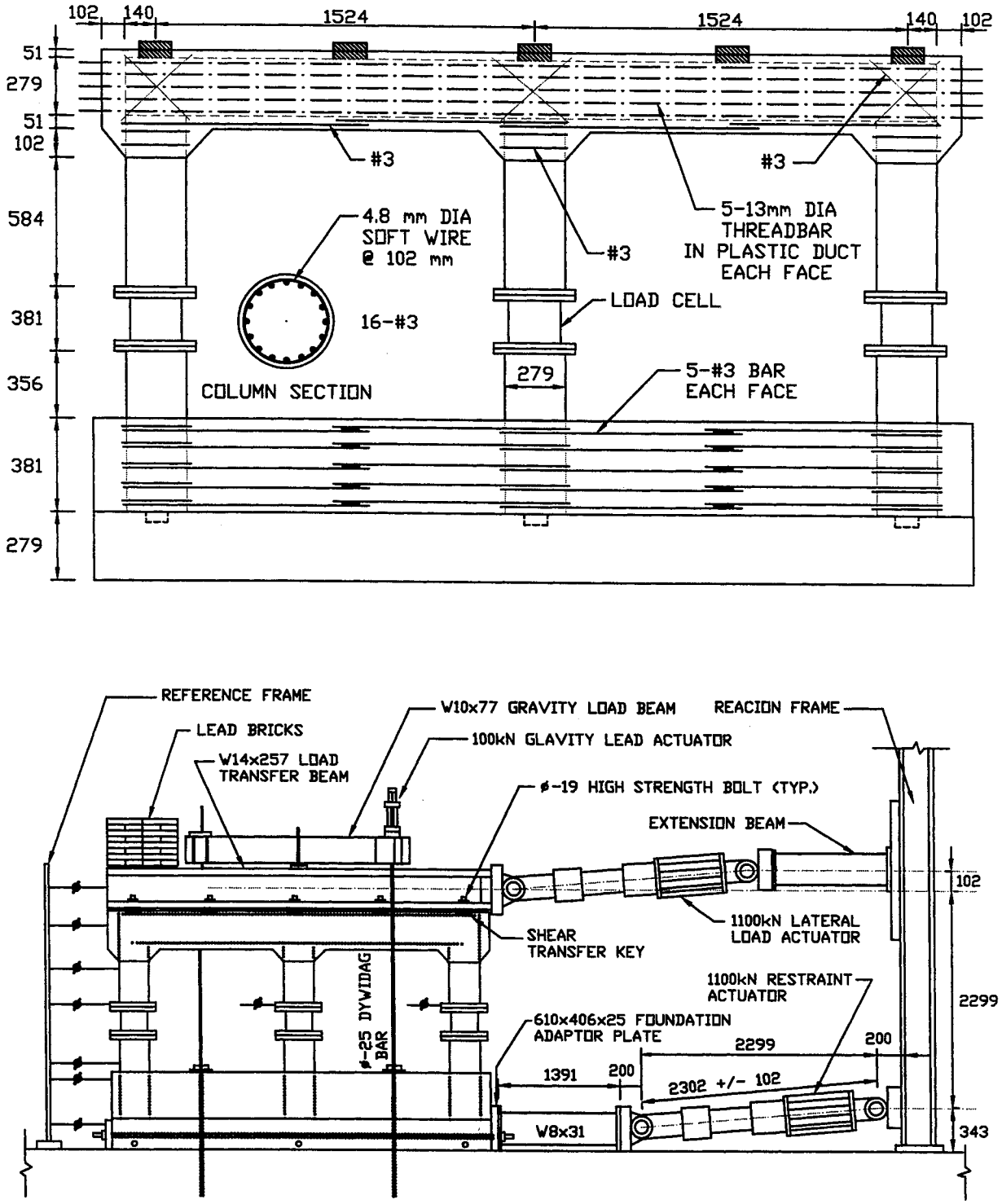

Figure 6-11. Reinforcement detail and test setup of the retrofitted 1/3 scale model pier tested by Mander, et al. *(1996b)*.

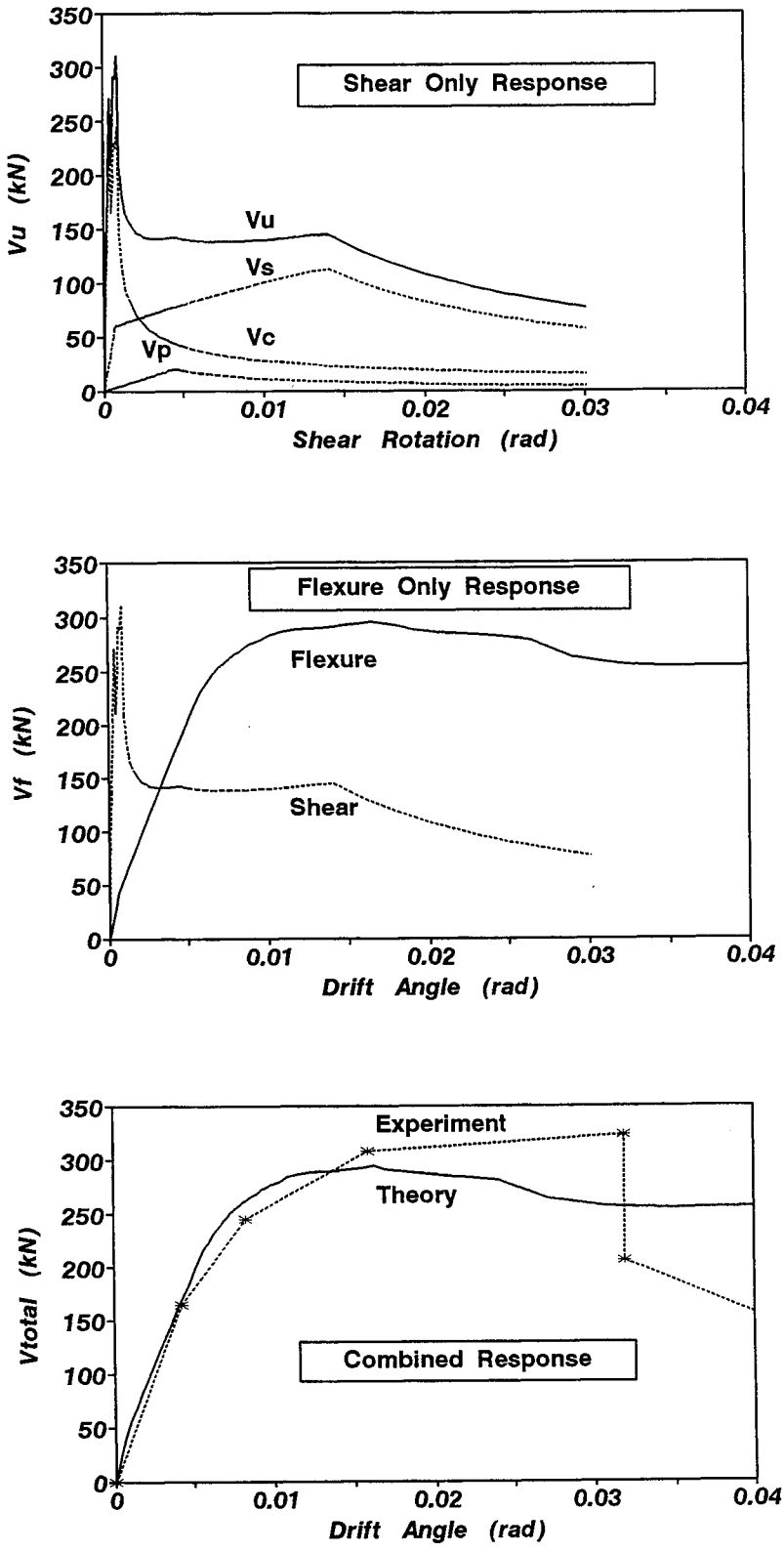

Figure 6-12. Combination of shear and flexural responses for retrofitted 1/3 scale model pier tested by Mander, et al. *(1996b)*.

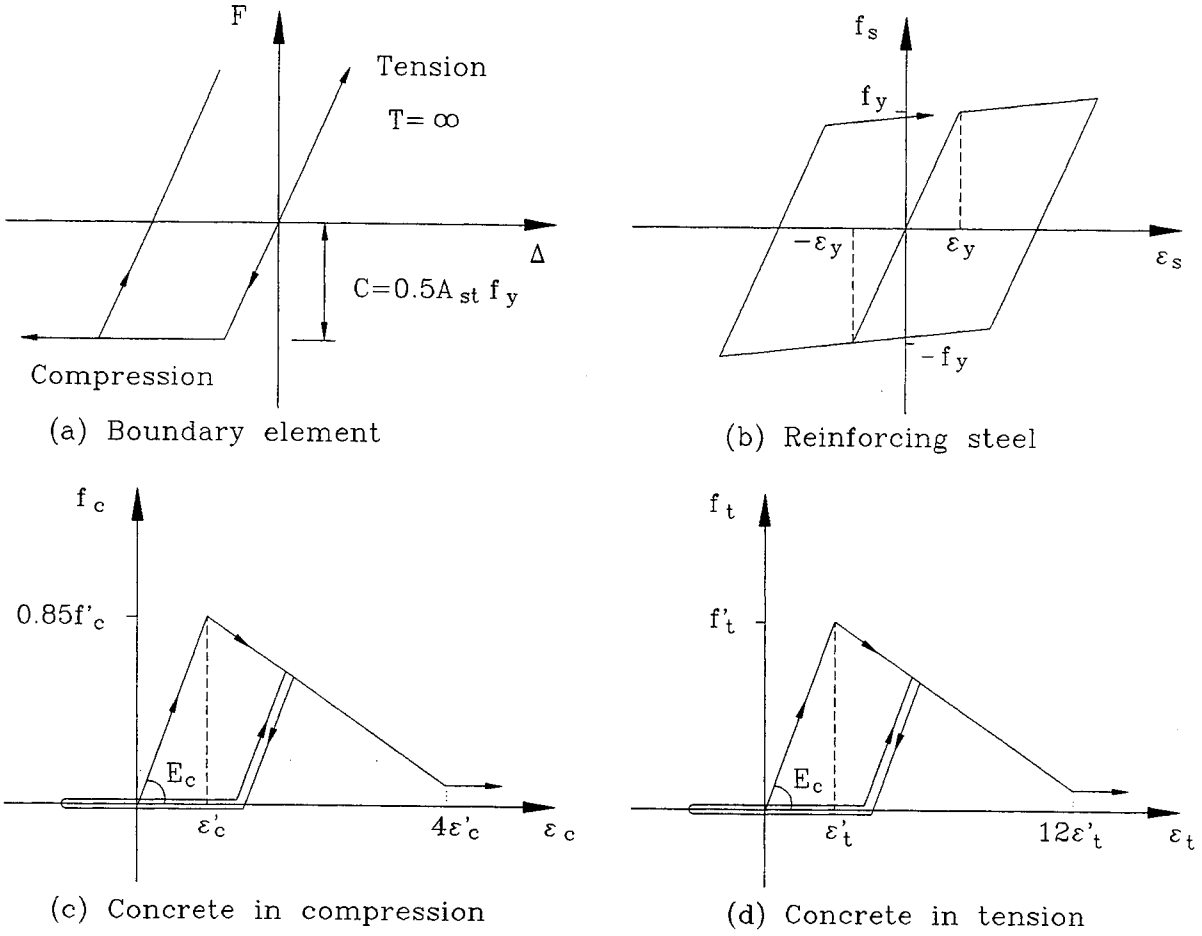

Figure 6-13. Behavior of individual CIST elements available in DRAIN-2DX.

trilinear uni-directional spring element. These individual CIST elements may be put together to form a truss member to obtain a desirable behavior. Two examples are presented in this subsection: coupling beam specimen 312 *(Paulay, 1971a,b)* and pre-retrofitted prototype cap beam - column subassemblage *(Mander, et al., 1996a)*. The necessary parameter values are available in Tables 6-1 and 6-2.

The CIST model of the coupling beam specimen 312 is shown in figure 6-14(a). It is noted that concrete tensile ties are arranged in parallel to the transverse steel ties. Boundary elements are provided in the longitudinal direction at both ends of the CIST model to simulate yielding in flexural compression at critical sections. The analysis result for a series of cyclic loading is presented in figure 6-15. The comparison shows a good agreement between theory and experiment.

The CIST model of the pre-retrofitted prototype cap beam - column subassemblage is presented in figure 6-14 (b). The specimen consists of a part of rectangular cap beam and a part of exterior circular column of the original pier. Since the beam-column joint is expected to be vulnerable, the CIST modeling technique is applied to all three structural components: column, joint and cap beam. The axial load is assumed to be applied by a half at each corner of the column end. Boundary elements are also provided in the column longitudinal direction at locations of pedestal corner. The boundary element behaves axially rigidly in compression and very soft in tension to emulate uplifting. A longitudinal truss member consists of three CIST elements which are steel, concrete in compression and concrete in tension. A transverse truss member consists of two CIST elements which are steel and concrete in tension. A diagonal truss member consists of a single CIST element, concrete in compression. These elements are dimensioned as explained through the foregoing sections.

The behavioral components to be compared to the experimental observation are the overall force-displacement, force-joint shear strain and force-joint diagonal displacements. Although many of these quantities are readily obtainable from the DRAIN-2DX analysis results, the joint shear strain should be calculated considering elasticity theory. Consider a joint panel

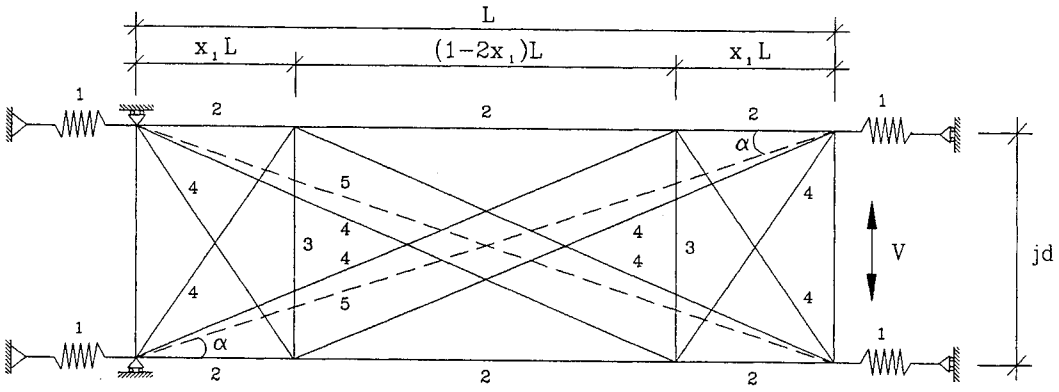

(a) Coupling beam specimen 312

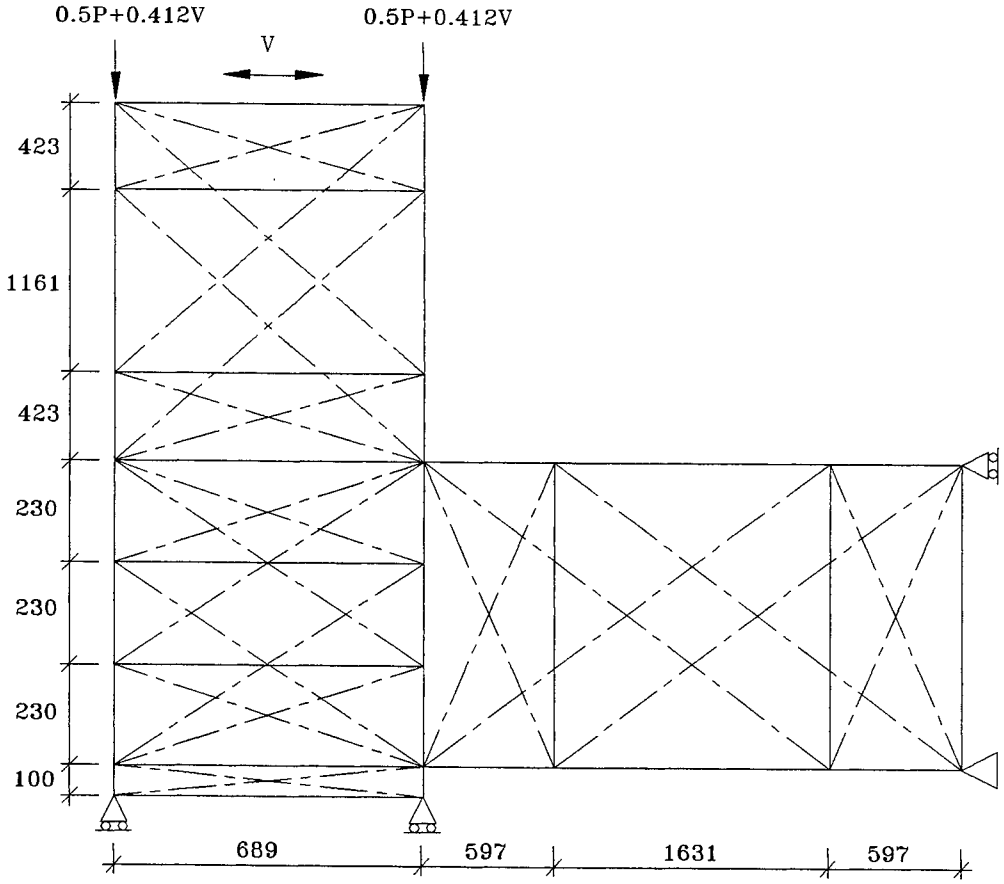

(b) Pre−retrofitted prototype pier subassemblage

Figure 6-14. CIST models for DRAIN-2DX analysis.

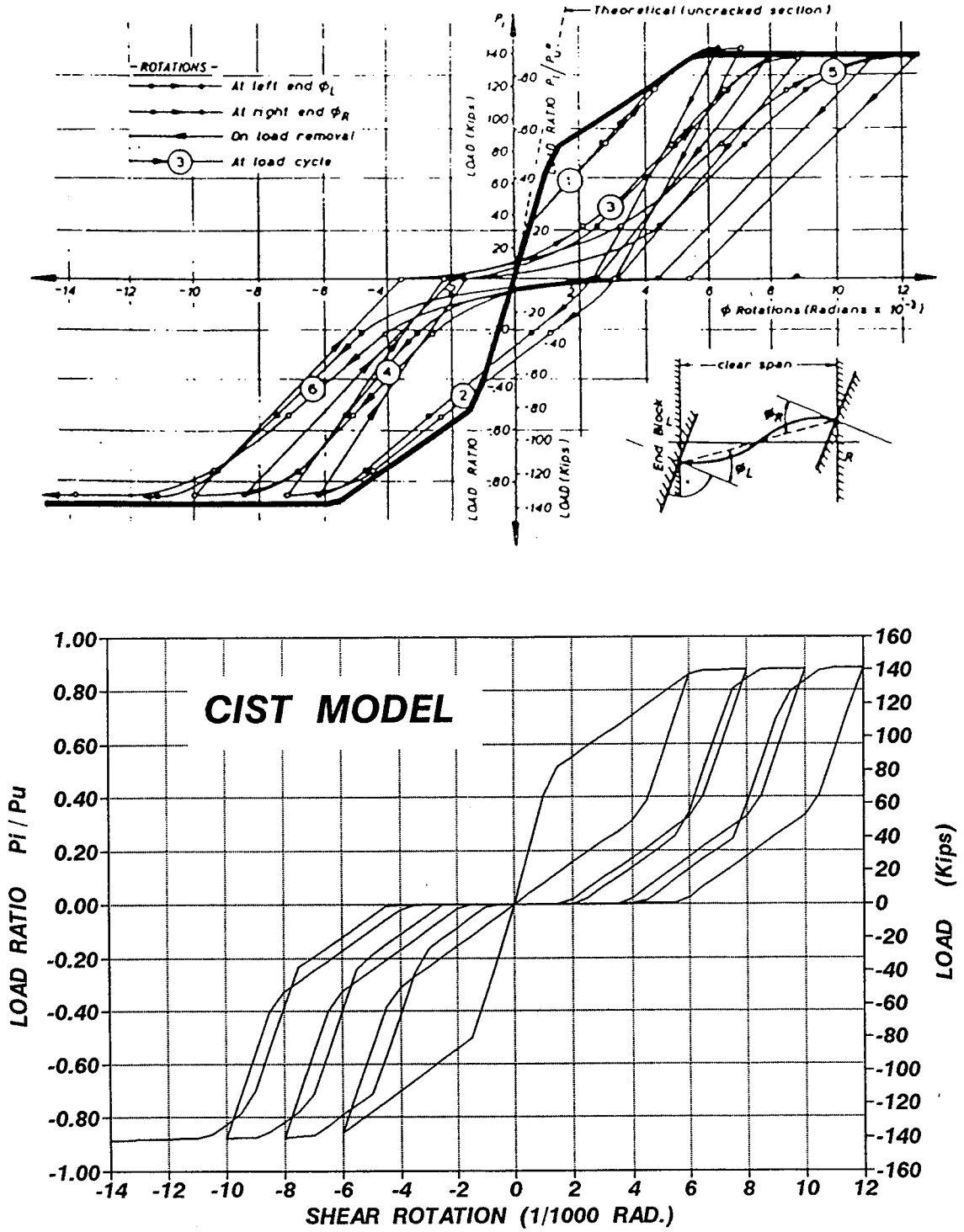

Figure 6-15. Comparison of responses between experiment and CIST model analysis for coupling beam 312 tested by Paulay *(1971a,b)*.

1-2-3-4 and its action for closing and opening moments as shown in figure 6-16. Then, total displacement components in x and y direction due to the axial deformation of diagonals $\overline{1-3}$ and $\overline{2-4}$ are

$$\Sigma\Delta_x = (\Delta_{1-3} - \Delta_{2-4}) \cos\alpha \tag{6-50}$$

$$\Sigma\Delta_y = (\Delta_{1-3} - \Delta_{2-4}) \sin\alpha \tag{6-51}$$

The shear strain due to $\Sigma\Delta_x$ only and $\Sigma\Delta_y$ only are respectively

$$\gamma_x = \frac{\Sigma\Delta_x}{l_y} = (\Delta_{1-3} - \Delta_{2-4}) \frac{\cos\alpha}{l_y} \tag{6-52}$$

$$\gamma_y = \frac{\Sigma\Delta_y}{l_x} = (\Delta_{1-3} - \Delta_{2-4}) \frac{\sin\alpha}{l_x} \tag{6-53}$$

Then, the shear strain of joint panel 1-2-3-4 can be obtained by averaging γ_x and γ_y, thus

$$\gamma = \frac{1}{2}(\gamma_x + \gamma_y) = \frac{1}{2}(\Delta_{1-3} - \Delta_{2-4})\left(\frac{\cos\alpha}{l_y} + \frac{\sin\alpha}{l_x}\right) \tag{6-54}$$

In the given example, $\alpha = 45°$ and $l_x = l_y = 689\ mm$. Thus the joint shear strain is calculated by

$$\gamma = \frac{\Delta_{1-3} - \Delta_{2-4}}{689\sqrt{2}} \tag{6-55}$$

where joint diagonal displacement Δ_{1-3} and Δ_{2-4} are positive in tension and negative in compression, and are given by the DRAIN-2DX analysis results.

Analysis results are compared to the experimental observation in figures 6-17 and 6-18 and a good agreement between two is obtained with the exception of diagonal displacement measured by T11 in figure 6-18. This deviation may be attributed to the loss of anchorage in longitudinal reinforcement at inner side of the column. If the anchorage had been perfect, the diagonal joint displacement would have been much larger than the experimentally observed one in the direction. As mentioned previously, the loss of anchorage is not accounted for in the

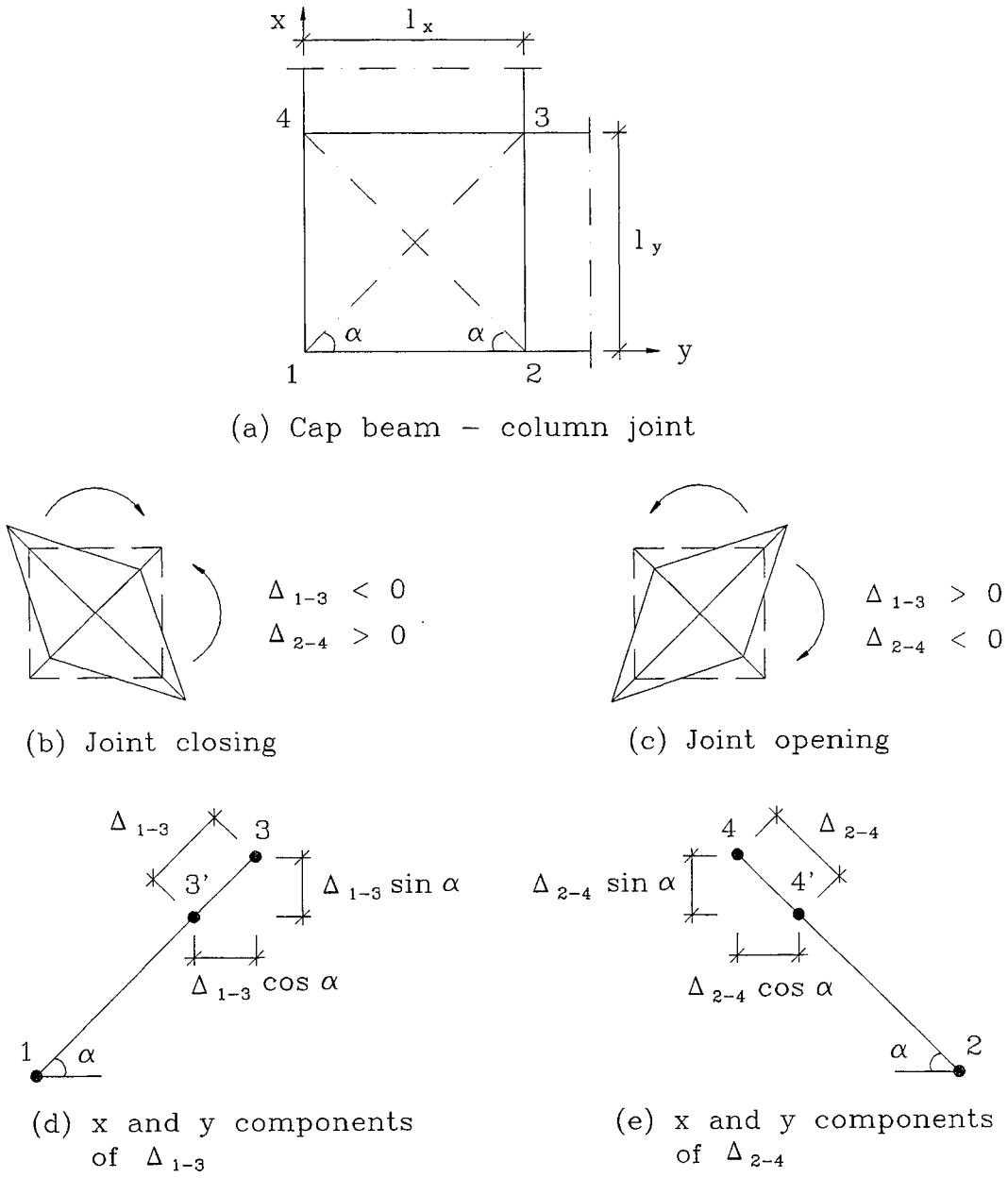

Figure 6-16. Calculation of joint shear strain using measured displacement components.

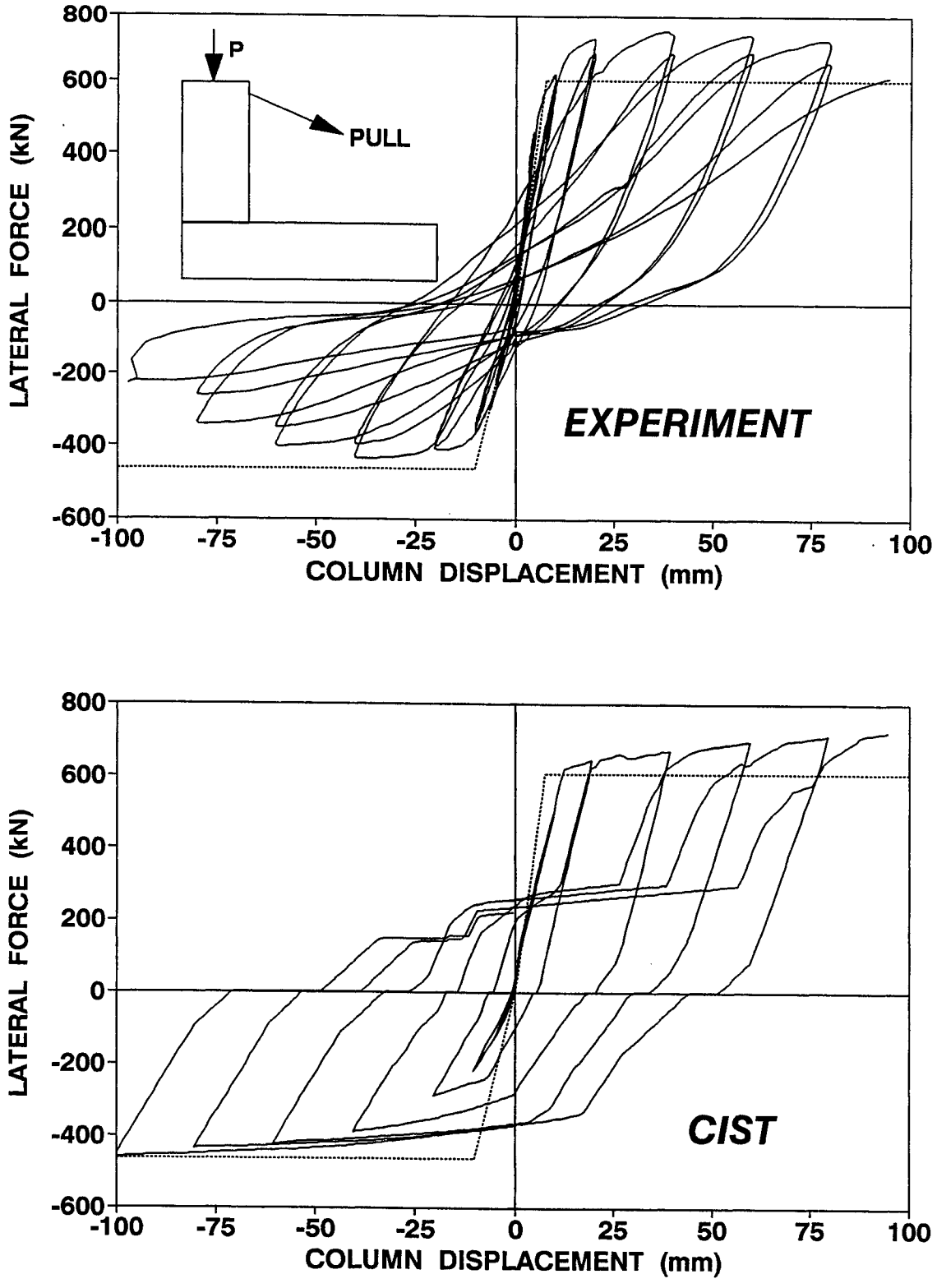

Figure 6-17. Overall response of pre-retrofitted prototype pier subassemblage tested by Mander, et al. *(1996a)*.

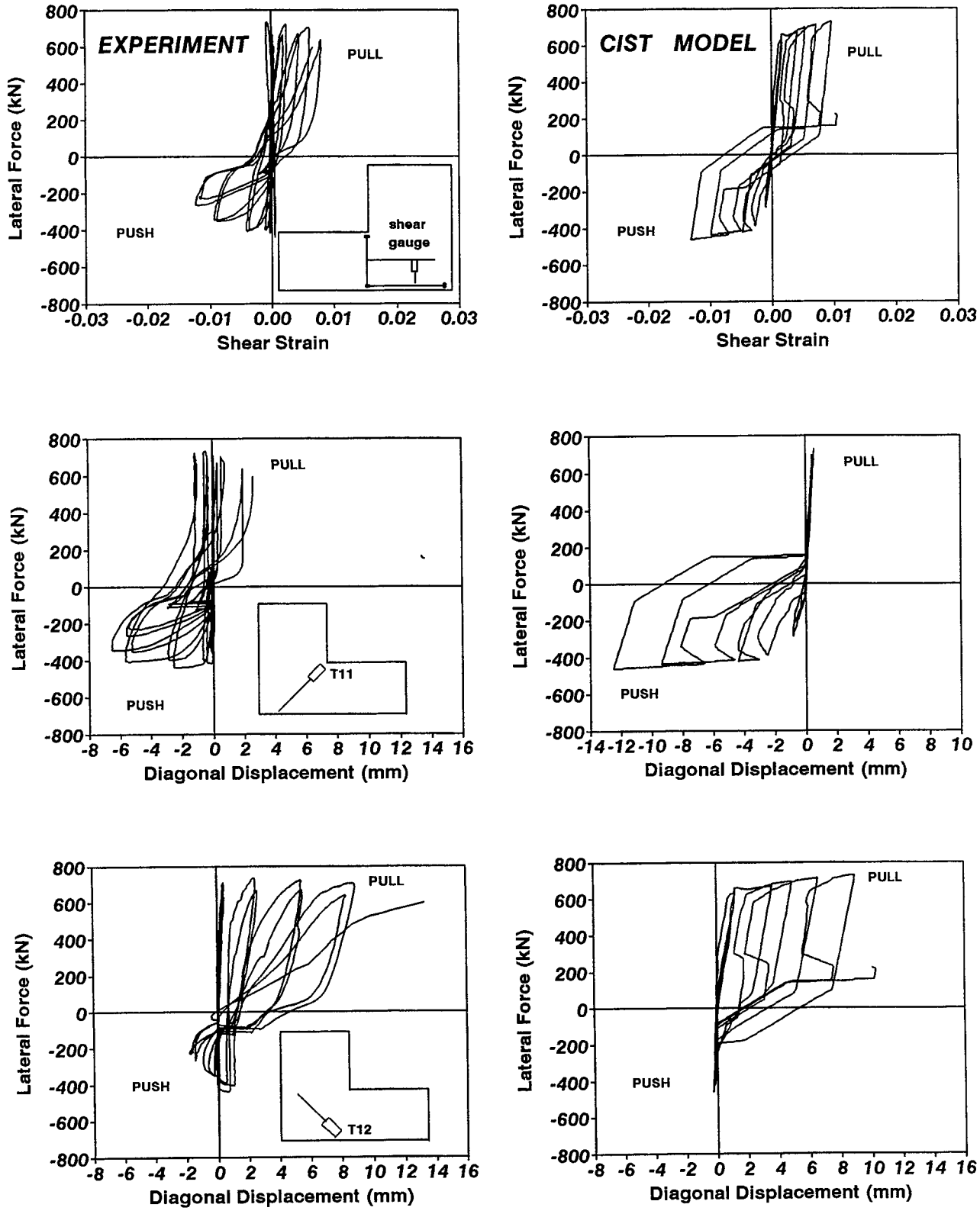

Figure 6-18. Joint behavior of pre-retrofitted prototype pier subassemblage tested by Mander, et al. *(1996a)*.

current version of modeling technique.

6.5 Conclusion

This section has presented the combination of the three mechanisms of shear resistance (V_s, V_c and V_p described separately in Sections 2-5) with flexural strength and deformation behavior to give the overall flexure-shear interactive response. Of particular concern is the degradation in shear strength due to the loss of bond strength in the longitudinal bars that arises from flexural yield, as well as crushing strength limitation of the diagonal struts. Both of these phenomena are implicitly dependent on ductility amplitude.

Examples have been presented that demonstrate the entire approach. Two methods have been used. The first is based on the force-deformation equations presented in the foregoing sections, while the second is a computational approach based on the CIST method. The foregoing theory is used to size the struts and ties and to provide the appropriate strength and deformation capacities.

Both methods have advantages and disadvantages. The first method, although straight-forward in principle, is cumbersome to implement due to the considerable bookkeeping necessary owing to the large number of equations that are employed. It is therefore desirable to use a computer program (such as the program ENVELOPE developed for this study) to automate the analysis. The second method, which is computational, has the distinct advantage of tracking cyclic loading behavior. However, the implementation is limited by the ability of the strut and tie models resident in the computer program that are used to represent the constitutive relations of the constituent materials - concrete and steel. For example in the DRAIN-2DX computer code, it is not possible to model strength decay due to cyclic loading, nor the beneficial effects of aggregate interlock. These are the primary factors that lead to differences in the predicted and observed hysteresis loops. If improved constitutive models were used to more faithfully represent concrete and steel behavior (under cyclic loading), then the overall predictions should also markedly improve.

SECTION 7
SUMMARY, CONCLUSIONS AND RECOMMENDATIONS

7.1 Summary

This report has been concerned with development of the comprehensive analysis methods to set up relationships between force and deformation of reinforced concrete beam/columns subjected to both shear and flexure with a particular emphasis on the three principal shear resisting mechanisms - that is, V_s, V_c and V_p in terms of both stiffness and strength. The proposed analysis methods enable structural engineers to quantitatively as well as qualitatively understand the flow of forces at any instance of column deformation. For this purpose, two truss mechanisms have been investigated: constant angle truss and variable angle truss. As a result of the investigation, some pragmatic truss models based on simple numerical integration requirements have been proposed suitable for hand (design office) analysis. Alternatively, more sophisticated truss models can be easily incorporated with comprehensive computational modeling-based techniques using the static options of general inelastic structural analysis programs such as DRAIN-2DX. Even though the proposed analysis method may make the load transferring mechanism in reinforced concrete structures quite transparent and comprehensive, it lacks the capability to account for the effect of cyclic loading. As a supplemental option, the evolving energy-based damage analysis has also been introduced and extended. The study on the proposed truss models and energy-based damage modeling have produced some findings and conclusions summarized in what follows.

7.2 Conclusions

7.2.1 Truss Mechanism due to Transverse Steel Contribution

1. Numerical integration schemes have been introduced for the solution of the variable angle truss behavior. Either the constant angle modeling or variable angle modeling is satisfactory for determining shear stiffness over the length of beam-columns.

2. The numerical integration schemes have been implemented into truss models for physical simplification while maintaining reasonable accuracy. Among them, two-point and three-point Gauss truss models have been extensively studied. Two-point Gauss truss model provides a simple and sufficiently accurate tool to determine the post-cracking stiffness and deformation in shear and flexure. However, using the three-point Gauss truss model, a more realistic distribution of tensile strain in the transverse ties can be captured. This can be an important factor when modeling the nonlinear (post-yield) behavior of columns which are lightly reinforced transversely and may eventually lead to premature failure at mid-member height due to corner-to-corner diagonal cracking.

3. A mathematical expression for crack angle calculation has been derived by energy minimization of external work done by shear as well as flexural behavior and gives very favorable agreement with crack angles observed experimentally and reported in the literature for a wide range of tests by many different investigators.

4. The piece-wise linear elastic analysis method using the idealized linear model for concrete diagonal struts and bilinear model for longitudinal chords and transverse ties offers a simple and comprehensive analysis tool for shear and flexure. The analysis method can be advanced by implementing a nonlinear material model for reinforcing steel and be used to build the column lateral force and deformation relationship. All approaches can be implemented by either hand-analysis or using computerized cyclic non-linear force-deformation (CIST) analysis.

5. This study shows that the effective section area of the transverse shear reinforcement for circular columns is affected by diameter of column section, crack angle and transverse hoop spacing. This indicates that the widely accepted constant $\pi/2$ used for the calculation of shear strength of circular columns due to the transverse steel should be corrected. Thus the constant should range between 2 through $4/\pi$.

7.2.2 Effect of Concrete Tensile Strength

1. A variable angle truss model is used for the concrete only mechanism from which concrete principal tensile strain and stress profiles along the diagonal crack plane have been obtained. The average values of principal tensile strain and stress can be obtained by integrating those profiles within the effective region of the column length. The effective region has been defined by consideration of flexural cracking at the critical section.

2. The solution of the variable angle truss model has been achieved by numerous numerical integration schemes in a way similar to the transverse steel truss mechanism. Among them, the two-point Gauss quadrature and the simplified truss model with inclined ties have been extensively investigated. Using the Gauss two-point truss model with inclined ties, the concrete average principal tensile strain and stress as well as column shear force and deformation relationship have been obtained.

3. The Gauss two-point truss model with inclined ties for concrete only mechanism (V_c) can be converted to the one with perpendicular ties for the convenience in CIST modeling. However, the conversion may cause the V_c mechanism stiffness to vary in a range of 0.7-1.75 of the original one.

7.2.3 Effect of Axial Load (Arch Action)

1. The mean section area of the corner-to-corner diagonal strut has been determined based on the postulated compression field. The arch action mechanism for column axial load transfer appears to be unrelated to the crack angle.

2. The strength of the compressive arch action mechanism is governed by the amplitude of applied column axial load and load transfer capacity of the diagonal strut. The column shear resistance increases up to the moment of incipient rocking by axial deformation of the diagonal strut and then, decreases with rocking.

7.2.4 Combination of Responses and CIST Modeling

1. Using the proposed advanced inelastic truss models, the force flow and interaction between shear and flexure are explained and traced. Three response limits for beam-columns subjected to lateral loading are defined: (i) brittle shear-critical; (ii) semi-ductile shear-critical; and (iii) ductile flexure.

2. The shear strength of reinforced concrete structural members are subjected to the interaction between flexure and shear, and the compressive strength of diagonal struts. For this, reduction factors are considered.

3. The calculation methodology of individual mechanism strengths and their combination for a given deformation are summarized in step-by-step procedure and the corresponding solution algorithm for numerical process is discussed. The entire combination procedure has been implemented into a Fortran computer program ENVELOPE.

4. The CIST modeling technique can utilize the concept of Gaussian quadrature (numerical integration) schemes (particularly 2nd-order Gauss quadrature in this study) to determine the mathematical model geometry. For the model analysis, the general purpose nonlinear inelastic computer program, DRAIN-2DX, has been successfully employed.

5. The analysis results in comparison to the experimental observation reported by various researchers show good agreement. However, the present CIST analysis methodology shows a limitation in predicting the gradual loss of anchorage and strength decay due to the effect of cyclic loading.

7.3 Research Recommendations

1. Certain equations derived in the present shear study are rather complex. There may be merit in studying more simplified ways of implementing inelastic truss models suitable for

routine design office use.

2. Conversely, the proposed CIST truss models should be incorporated with the existing advanced column analysis programs such as UB-COLA *(Chang and Mander, 1994a)*.

3. The shear-flexure theory presented herein is based on a monotonic lateral load analysis, whereas the CIST method of analysis is capable of reversed loading. Both approaches, however, do not account for the strength deterioration expected as a result of cyclic loading. Research is needed to extend the present shear-flexure and CIST analysis methodologies to account for damage that occurs as a result of reversed cyclic loading. Recent work by Kim *(1996)* has started in this direction and an energy-based approach shows promise.

4. Advanced analysis programs such as UB-COLA may capture all the non-linear features of a column, but this is only for a single element. In this research, it has been demonstrated that non-linear finite element analysis using inelastic truss models (CIST analysis) is a promising way of looking at large structures. However, the force-deformation models used herein lack the ability to accommodate strength degradation under cyclic loading. Therefore, it is recommended that investigation using comprehensive CIST based macro-elements which include strength degradation based on energy considerations be pursued with vigor. It is considered that this could perhaps lead to some significant breakthrough in our understanding of structural concrete behavior.

SECTION 8

REFERENCES

_____AASHTO (1994), *AASHTO LRFD Bridge Design Specifications*, 1st ed., American Association of State Highway and Transportation Officials, Washington, D.C.

_____ACI Committee 209 (1982), *Prediction of Creep, Shrinkage and Temperature Effects in Concrete Structures,* ACI 209R-82, American Concrete Institute, Detroit, Michigan.

_____ACI Committee 318 (1995), *Building Code Requirements for Reinforcement Concrete and Commentary*, ACI 318-95, American Concrete Institute, Detroit.

Ang, B.G. (1985), *Seismic Shear Strength of Circular Bridge Piers*, Ph.D. Dissertation, Department of Civil Engineering, University of Canterbury, Christchurch, New Zealand, 407 pp.

Ang, B.G., Priestley, M.J.N, and Paulay, T. (1989), "Seismic Shear Strength of Circular Reinforced Concrete Columns", ACI Structural Journal, Title no. 86-S6, Jan.-Feb., pp. 45-59.

Barnard, P.R. (1964), "Research into the Complete Stress-Strain Curve for Concrete", *Magazine of Concrete Research,* Vol. 16, No. 49, December, pp. 203-210.

Bažant, Z.P. and Oh, B.H. (1983), "Crack Band Theory for Fracture of Concrete", Materiaux et Constructions, Paris, France, 16(3), pp.155-177.

Carreira, D.J. and Chu, K.H. (1986), "Stress-Strain Relationship for Reinforced Concrete in Tension", *ACI Journal*, Vol. 83, No. 1, January-February, pp. 21-28.

Chai, Y.H., Priestley, M.J.N. and Seible, F. (1990), "Retrofit of Bridge Columns for Enhanced Seismic Performance", *Proceedings* of the First U.S.-Japan Workshop on Seismic Retrofit of Bridges, Public Works Research Institute, Tsukuba, Japan, pp. 321-340.

Chai, Y.H., Priestley, M.J.N, and Seible, F. (1991), "Seismic Retrofit of Circular Bridge Columns for Enhanced Flexural Performance", ACI Structural Journal, V. 88, No. 5, Sept.-Oct., pp.572-584.

Chang, G.A. and Mander, J.B. (1994a), *Seismic Energy Based Fatigue Damage Analysis of Bridge Columns, Part I: Evaluation of Seismic Capacity*, Technical Report NCEER-94-0006, National Center for Earthquake Engineering Research, State University of New York at Buffalo, New York.

Chang, G.A. and Mander, J.B. (1994b), *Seismic Energy Based Fatigue Damage Analysis of*

Bridge Columns, Part II: Evaluation of Seismic Demand, Technical Report NCEER-94-0013, National Center for Earthquake Engineering Research, State University of New York at Buffalo, New York.

Chapra, S.C. and Canale, R.P. (1988), *Numerical Methods for Engineers*, 2nd Edition, McGraw-Hill, Inc.

Collins, M.P. and Mitchell, D. (1991), *Prestressed Concrete Structures*, Prentice-Hall, Inc.

Dilger, W. (1966), "Veränderlichkeit der Biege- und Schubsteifigkeit bei Stahlbetontragwerken und ihr Einfluß auf Schnittkraftverteilung und Traglast bei statisch unbestimmter Lagerung", Deutscher Ausschuss für Stahlbeton, Heft 179, Berline, Germany.

Dutta, A. and Mander, J.B. (1998), *Capacity Design and Fatigue Analysis of Confined Concrete Columns*, Technical Report MCEER-98-0007, Multidisciplinary Center for Earthquake Engineering Research, State Universty of New York at Buffalo, New York.

Hornbeck, R.W. (1975), *Numerical Methods,* Quantum Publishers, Inc.

Hsu, T.T.C. (1993), *Unified Theory of Reinforced Concrete*, CRC Press, Inc.

Hsu, T.T.C. (1996), "Toward A Unified Nomenclature for Reinforced-Concrete Theory", ASCE Journal of Structural Engineering, Vol. 122, No. 3, March, pp.275-283.

Kim, J.H. (1996), *Seismic Evaluation of Shear-Critical Reinforced Concrete Columns and Their Connections*, Ph.D. Dissertation, Department of Civil Engineering, State University of New York at Buffalo, New York.

MacGregor, J.G. (1992), *Reinforced Concrete: Mechanics and Design,* Prentice-Hall, Inc.

Malvar, L.J. (1992), "Bond of Reinforcement Under Controlled Confinement", ACI Materials Journal, V. 89, No. 6, Nov.-Dec., pp. 593-601,

Mander, J.B., Priestley, M.J.N., and Park, R. (1984), *Seismic Design of Bridge Piers*, Research Report No. 84-2, University of Canterbury, New Zealand.

Mander, J.B., Priestley, M.J.N., and Park, R. (1988a), "Theoretical Stress-Strain Model for Confined Concrete", ASCE Journal of Structural Engineering, Vol. 114, no. 8, August, pp. 1804-1826.

Mander, J.B., Priestley, M.J.N., and Park, R. (1988b), "Observed Stress-Strain Behavior of Confined Concrete", ASCE Journal of Structural Engineering, Vol. 114, no. 8, August, pp. 1827-1849.

Mander, J.B. and Cheng, C.-T. (1995), "Renewable Hinge Detailing for Bridge Columns",

Proceedings of Pacific Conference on Earthquake Engineering, Australia, November 20-22, pp. 197-206.

Mander, J.B., Mahmoodzadegan, B., Bhadra, S, and Chen, S.S. (1996a), *Seismic Evaluation of A 30-Year Old Non-Ductile Highway Bridge Pier and Its Retrofit*, Technical Report NCEER-96-0008, National Center for Earthquake Engineering Research, State University of New York at Buffalo, New York.

Mander, J.B., Kim, J.H. and Ligozio, C.A. (1996b), *Seismic Performance of A Model Reinforced Concrete Bridge Pier Before and After Retrofit*, Technical Report NCEER-96-0009, National Center for Earthquake Engineering Research, State University of New York at Buffalo, New York.

Mander, J.B., Dutta, A. and Kim, J.H. (1998), *Fatigue Analysis of Unconfined Concrete Columns*, Technical Report MCEER-98-0009, Multidisciplinary Center for Earthquake Engineering Research, State University of New York at Buffalo, New York.

Menegotto, M. and Pinto, P.E. (1973), "Method of Analysis for Cyclically Loaded R.C. Plane Frames Including Changes in Geometry and Non-Elastic Behavior of Elements under Combined Normal Force and Bending", IABSE Symposium on *Resistance and Ultimate Deformability of Structures Acted on by Well-Defined Repeated Loads*, Lisboa.

Morcos, S.S. and Bjorhovde, R. (1995), "Fracture Modeling of Concrete and Steel", ASCE Journal of Structural Engineering, Vol. 121, No. 7, July, pp. 1125-1133.

Mörsch, E. (1908), *Der Eisenbeton. Seine Theorie und Anwendung*, Wittwer, Stuttgart, Germany.

Pang, X.B.D. and Hsu, T.T.C. (1996), "Fixed Angle Softened Truss Model for Reinforced Concrete", ACI Structural Journal, Title no. 93-S18, Mar.-Apr., pp.197-207.

Park, R. and Paulay, T. (1975), *Reinforced Concrete Structures*, John Wiley and Sons, Inc., New York.

Paulay, T. (1971a), "Coupling Beams of Reinforced Concrete Shear Walls", *Journal of the Structural Division, ASCE*, Vol. 97, ST3, March, pp. 843-862.

Paulay, T. (1971b), "Simulated Seismic Loading of Spandrel Beams", *Journal of the Structural Division, ASCE*, Vol. 97, ST9, September, pp. 2407-2419.

Petersson, P.E. (1980), "Fracture Energy of Concrete: Practical performance and experimental results", Cement and Concrete Research., 10, pp.91-101.

Popovics, S. (1973), "A Numerical Approach to the Complete Stress-Strain Curve of Concrete", *Cement and Concrete Research,* Vol. 3, No. 4, September, pp. 583-599.

Prakash, V., Powell, G.H., and Filippou, F.C. (1992a), *DRAIN-2DX: Base Program User Guide*, Department of Civil Engineering, University of California at Berkeley, California.

Prakash, V., Powell, G.H., Campbell, S.D., and Filippou, F.C. (1992b), *DRAIN-2DX: Preliminary Element User Guide*, Department of Civil Engineering, University of California at Berkeley, California.

Priestley, M.J.N., Park, R., and Potangaroa, R.T. (1981), "Ductility of Spirally-Confined Concrete Columns", ASCE Journal of the Structural Division, Vol. 107, No. ST1, January, pp. 181-202.

Priestley, M.J.N., Seible, F., Xiao, Y. and Verma, R. (1994a), "Steel Jacket Retrofitting of Reinforced Concrete Bridge Columns for Enhanced Shear Strength - Part 1: Theoretical Considerations and Test Design", *ACI Structural Journal*, Vol. 91, No. 4, July-August, pp. 394-405.

Priestley, M.J.N., Seible, F., Xiao, Y. and Verma, R. (1994b), "Steel Jacket Retrofitting of Reinforced Concrete Bridge Columns for Enhanced Shear Strength - Part 2: Test Results and Comparison with Theory", *ACI Structural Journal*, Vol. 91, No. 5, September-October, pp. 537-551.

Priestley, M.J.N., Verma, R., and Xiao, Y. (1994c), "Seismic Shear Strength of Reinforced Concrete Columns", *Journal of Structural Engineering*, Vol. 120, No. 8, ASCE, August, pp. 2310-2329.

Ritter, W. (1899), *Die Bauweise Hennebique (Construction Techniques of Hennebique)*, Schweizerische Bazeitung, Zürich, Feb.

Rots, J.G., Nauta, P., Kusters, G.M.A., and Blaauwendraad, J. (1985), "Smeared crack approach and fracture localization in concrete", Heron, Delft, Netherlands, 30(1), pp. 1-48.

Schlaich, J., Schäfer, K. and Jennewein, M. (1987), "Toward a Consistent Design of Structural Concrete", *PCI Journal*, Vol. 32, No. 3, May-June, pp. 74-150.

Vecchio, F.J. and Collins, M.P. (1986), "The Modified Compression-Field Theory for Reinforced Concrete Elements Subjected to Shear", *ACI Journal*, Vol. 83, No. 2, March-April, pp. 219-231.

Watanabe, F. and Ichinose, T. (1992), "Strength and Ductility Design of R.C. Members Subjected to Combined Bending and Shear", *Proceedings of Workshop on Concrete Shear in Earthquake*, Edited by T.T.C. Hsu and S.T. Mau, University of Houston, Texas, pp. 429-438.

Wong, Y.L. (1990), *Squat Circular Bridge Piers under Multi-Directional Seismic Attack*, Ph.D. Dissertation, Department of Civil Engineering, University of Canterbury, Christchurch, New Zealand.

Yankelevsky, D.Z. and Reinhardt, H.W. (1987), "Response of Plain Concrete to Cyclic Tension", *ACI Materials Journal*, Vol. 84, No. 5, September-October, pp. 365-373.

Multidisciplinary Center for Earthquake Engineering Research
List of Technical Reports

The Multidisciplinary Center for Earthquake Engineering Research (MCEER) publishes technical reports on a variety of subjects related to earthquake engineering written by authors funded through MCEER. These reports are available from both MCEER Publications and the National Technical Information Service (NTIS). Requests for reports should be directed to MCEER Publications, Multidisciplinary Center for Earthquake Engineering Research, State University of New York at Buffalo, Red Jacket Quadrangle, Buffalo, New York 14261. Reports can also be requested through NTIS, 5285 Port Royal Road, Springfield, Virginia 22161. NTIS accession numbers are shown in parenthesis, if available.

NCEER-87-0001 "First-Year Program in Research, Education and Technology Transfer," 3/5/87, (PB88-134275, A04, MF-A01).

NCEER-87-0002 "Experimental Evaluation of Instantaneous Optimal Algorithms for Structural Control," by R.C. Lin, T.T. Soong and A.M. Reinhorn, 4/20/87, (PB88-134341, A04, MF-A01).

NCEER-87-0003 "Experimentation Using the Earthquake Simulation Facilities at University at Buffalo," by A.M. Reinhorn and R.L. Ketter, to be published.

NCEER-87-0004 "The System Characteristics and Performance of a Shaking Table," by J.S. Hwang, K.C. Chang and G.C. Lee, 6/1/87, (PB88-134259, A03, MF-A01). This report is available only through NTIS (see address given above).

NCEER-87-0005 "A Finite Element Formulation for Nonlinear Viscoplastic Material Using a Q Model," by O. Gyebi and G. Dasgupta, 11/2/87, (PB88-213764, A08, MF-A01).

NCEER-87-0006 "Symbolic Manipulation Program (SMP) - Algebraic Codes for Two and Three Dimensional Finite Element Formulations," by X. Lee and G. Dasgupta, 11/9/87, (PB88-218522, A05, MF-A01).

NCEER-87-0007 "Instantaneous Optimal Control Laws for Tall Buildings Under Seismic Excitations," by J.N. Yang, A. Akbarpour and P. Ghaemmaghami, 6/10/87, (PB88-134333, A06, MF-A01). This report is only available through NTIS (see address given above).

NCEER-87-0008 "IDARC: Inelastic Damage Analysis of Reinforced Concrete Frame - Shear-Wall Structures," by Y.J. Park, A.M. Reinhorn and S.K. Kunnath, 7/20/87, (PB88-134325, A09, MF-A01). This report is only available through NTIS (see address given above).

NCEER-87-0009 "Liquefaction Potential for New York State: A Preliminary Report on Sites in Manhattan and Buffalo," by M. Budhu, V. Vijayakumar, R.F. Giese and L. Baumgras, 8/31/87, (PB88-163704, A03, MF-A01). This report is available only through NTIS (see address given above).

NCEER-87-0010 "Vertical and Torsional Vibration of Foundations in Inhomogeneous Media," by A.S. Veletsos and K.W. Dotson, 6/1/87, (PB88-134291, A03, MF-A01). This report is only available through NTIS (see address given above).

NCEER-87-0011 "Seismic Probabilistic Risk Assessment and Seismic Margins Studies for Nuclear Power Plants," by Howard H.M. Hwang, 6/15/87, (PB88-134267, A03, MF-A01). This report is only available through NTIS (see address given above).

NCEER-87-0012 "Parametric Studies of Frequency Response of Secondary Systems Under Ground-Acceleration Excitations," by Y. Yong and Y.K. Lin, 6/10/87, (PB88-134309, A03, MF-A01). This report is only available through NTIS (see address given above).

NCEER-87-0013 "Frequency Response of Secondary Systems Under Seismic Excitation," by J.A. HoLung, J. Cai and Y.K. Lin, 7/31/87, (PB88-134317, A05, MF-A01). This report is only available through NTIS (see address given above).

NCEER-87-0014 "Modelling Earthquake Ground Motions in Seismically Active Regions Using Parametric Time Series Methods," by G.W. Ellis and A.S. Cakmak, 8/25/87, (PB88-134283, A08, MF-A01). This report is only available through NTIS (see address given above).

NCEER-87-0015 "Detection and Assessment of Seismic Structural Damage," by E. DiPasquale and A.S. Cakmak, 8/25/87, (PB88-163712, A05, MF-A01). This report is only available through NTIS (see address given above).

NCEER-87-0016 "Pipeline Experiment at Parkfield, California," by J. Isenberg and E. Richardson, 9/15/87, (PB88-163720, A03, MF-A01). This report is available only through NTIS (see address given above).

NCEER-87-0017 "Digital Simulation of Seismic Ground Motion," by M. Shinozuka, G. Deodatis and T. Harada, 8/31/87, (PB88-155197, A04, MF-A01). This report is available only through NTIS (see address given above).

NCEER-87-0018 "Practical Considerations for Structural Control: System Uncertainty, System Time Delay and Truncation of Small Control Forces," J.N. Yang and A. Akbarpour, 8/10/87, (PB88-163738, A08, MF-A01). This report is only available through NTIS (see address given above).

NCEER-87-0019 "Modal Analysis of Nonclassically Damped Structural Systems Using Canonical Transformation," by J.N. Yang, S. Sarkani and F.X. Long, 9/27/87, (PB88-187851, A04, MF-A01).

NCEER-87-0020 "A Nonstationary Solution in Random Vibration Theory," by J.R. Red-Horse and P.D. Spanos, 11/3/87, (PB88-163746, A03, MF-A01).

NCEER-87-0021 "Horizontal Impedances for Radially Inhomogeneous Viscoelastic Soil Layers," by A.S. Veletsos and K.W. Dotson, 10/15/87, (PB88-150859, A04, MF-A01).

NCEER-87-0022 "Seismic Damage Assessment of Reinforced Concrete Members," by Y.S. Chung, C. Meyer and M. Shinozuka, 10/9/87, (PB88-150867, A05, MF-A01). This report is available only through NTIS (see address given above).

NCEER-87-0023 "Active Structural Control in Civil Engineering," by T.T. Soong, 11/11/87, (PB88-187778, A03, MF-A01).

NCEER-87-0024 "Vertical and Torsional Impedances for Radially Inhomogeneous Viscoelastic Soil Layers," by K.W. Dotson and A.S. Veletsos, 12/87, (PB88-187786, A03, MF-A01).

NCEER-87-0025 "Proceedings from the Symposium on Seismic Hazards, Ground Motions, Soil-Liquefaction and Engineering Practice in Eastern North America," October 20-22, 1987, edited by K.H. Jacob, 12/87, (PB88-188115, A23, MF-A01). This report is available only through NTIS (see address given above).

NCEER-87-0026 "Report on the Whittier-Narrows, California, Earthquake of October 1, 1987," by J. Pantelic and A. Reinhorn, 11/87, (PB88-187752, A03, MF-A01). This report is available only through NTIS (see address given above).

NCEER-87-0027 "Design of a Modular Program for Transient Nonlinear Analysis of Large 3-D Building Structures," by S. Srivastav and J.F. Abel, 12/30/87, (PB88-187950, A05, MF-A01). This report is only available through NTIS (see address given above).

NCEER-87-0028 "Second-Year Program in Research, Education and Technology Transfer," 3/8/88, (PB88-219480, A04, MF-A01).

NCEER-88-0001 "Workshop on Seismic Computer Analysis and Design of Buildings With Interactive Graphics," by W. McGuire, J.F. Abel and C.H. Conley, 1/18/88, (PB88-187760, A03, MF-A01). This report is only available through NTIS (see address given above).

NCEER-88-0002 "Optimal Control of Nonlinear Flexible Structures," by J.N. Yang, F.X. Long and D. Wong, 1/22/88, (PB88-213772, A06, MF-A01).

NCEER-88-0003 "Substructuring Techniques in the Time Domain for Primary-Secondary Structural Systems," by G.D. Manolis and G. Juhn, 2/10/88, (PB88-213780, A04, MF-A01).

NCEER-88-0004 "Iterative Seismic Analysis of Primary-Secondary Systems," by A. Singhal, L.D. Lutes and P.D. Spanos, 2/23/88, (PB88-213798, A04, MF-A01).

NCEER-88-0005 "Stochastic Finite Element Expansion for Random Media," by P.D. Spanos and R. Ghanem, 3/14/88, (PB88-213806, A03, MF-A01).

NCEER-88-0006 "Combining Structural Optimization and Structural Control," by F.Y. Cheng and C.P. Pantelides, 1/10/88, (PB88-213814, A05, MF-A01).

NCEER-88-0007 "Seismic Performance Assessment of Code-Designed Structures," by H.H-M. Hwang, J-W. Jaw and H-J. Shau, 3/20/88, (PB88-219423, A04, MF-A01). This report is only available through NTIS (see address given above).

NCEER-88-0008 "Reliability Analysis of Code-Designed Structures Under Natural Hazards," by H.H-M. Hwang, H. Ushiba and M. Shinozuka, 2/29/88, (PB88-229471, A07, MF-A01). This report is only available through NTIS (see address given above).

NCEER-88-0009 "Seismic Fragility Analysis of Shear Wall Structures," by J-W Jaw and H.H-M. Hwang, 4/30/88, (PB89-102867, A04, MF-A01).

NCEER-88-0010 "Base Isolation of a Multi-Story Building Under a Harmonic Ground Motion - A Comparison of Performances of Various Systems," by F-G Fan, G. Ahmadi and I.G. Tadjbakhsh, 5/18/88, (PB89-122238, A06, MF-A01). This report is only available through NTIS (see address given above).

NCEER-88-0011 "Seismic Floor Response Spectra for a Combined System by Green's Functions," by F.M. Lavelle, L.A. Bergman and P.D. Spanos, 5/1/88, (PB89-102875, A03, MF-A01).

NCEER-88-0012 "A New Solution Technique for Randomly Excited Hysteretic Structures," by G.Q. Cai and Y.K. Lin, 5/16/88, (PB89-102883, A03, MF-A01).

NCEER-88-0013 "A Study of Radiation Damping and Soil-Structure Interaction Effects in the Centrifuge," by K. Weissman, supervised by J.H. Prevost, 5/24/88, (PB89-144703, A06, MF-A01).

NCEER-88-0014 "Parameter Identification and Implementation of a Kinematic Plasticity Model for Frictional Soils," by J.H. Prevost and D.V. Griffiths, to be published.

NCEER-88-0015 "Two- and Three- Dimensional Dynamic Finite Element Analyses of the Long Valley Dam," by D.V. Griffiths and J.H. Prevost, 6/17/88, (PB89-144711, A04, MF-A01).

NCEER-88-0016 "Damage Assessment of Reinforced Concrete Structures in Eastern United States," by A.M. Reinhorn, M.J. Seidel, S.K. Kunnath and Y.J. Park, 6/15/88, (PB89-122220, A04, MF-A01). This report is only available through NTIS (see address given above).

NCEER-88-0017 "Dynamic Compliance of Vertically Loaded Strip Foundations in Multilayered Viscoelastic Soils," by S. Ahmad and A.S.M. Israil, 6/17/88, (PB89-102891, A04, MF-A01).

NCEER-88-0018 "An Experimental Study of Seismic Structural Response With Added Viscoelastic Dampers," by R.C. Lin, Z. Liang, T.T. Soong and R.H. Zhang, 6/30/88, (PB89-122212, A05, MF-A01). This report is available only through NTIS (see address given above).

NCEER-88-0019 "Experimental Investigation of Primary - Secondary System Interaction," by G.D. Manolis, G. Juhn and A.M. Reinhorn, 5/27/88, (PB89-122204, A04, MF-A01).

NCEER-88-0020 "A Response Spectrum Approach For Analysis of Nonclassically Damped Structures," by J.N. Yang, S. Sarkani and F.X. Long, 4/22/88, (PB89-102909, A04, MF-A01).

NCEER-88-0021 "Seismic Interaction of Structures and Soils: Stochastic Approach," by A.S. Veletsos and A.M. Prasad, 7/21/88, (PB89-122196, A04, MF-A01). This report is only available through NTIS (see address given above).

NCEER-88-0022 "Identification of the Serviceability Limit State and Detection of Seismic Structural Damage," by E. DiPasquale and A.S. Cakmak, 6/15/88, (PB89-122188, A05, MF-A01). This report is available only through NTIS (see address given above).

NCEER-88-0023 "Multi-Hazard Risk Analysis: Case of a Simple Offshore Structure," by B.K. Bhartia and E.H. Vanmarcke, 7/21/88, (PB89-145213, A05, MF-A01).

NCEER-88-0024 "Automated Seismic Design of Reinforced Concrete Buildings," by Y.S. Chung, C. Meyer and M. Shinozuka, 7/5/88, (PB89-122170, A06, MF-A01). This report is available only through NTIS (see address given above).

NCEER-88-0025 "Experimental Study of Active Control of MDOF Structures Under Seismic Excitations," by L.L. Chung, R.C. Lin, T.T. Soong and A.M. Reinhorn, 7/10/88, (PB89-122600, A04, MF-A01).

NCEER-88-0026 "Earthquake Simulation Tests of a Low-Rise Metal Structure," by J.S. Hwang, K.C. Chang, G.C. Lee and R.L. Ketter, 8/1/88, (PB89-102917, A04, MF-A01).

NCEER-88-0027 "Systems Study of Urban Response and Reconstruction Due to Catastrophic Earthquakes," by F. Kozin and H.K. Zhou, 9/22/88, (PB90-162348, A04, MF-A01).

NCEER-88-0028 "Seismic Fragility Analysis of Plane Frame Structures," by H.H-M. Hwang and Y.K. Low, 7/31/88, (PB89-131445, A06, MF-A01).

NCEER-88-0029 "Response Analysis of Stochastic Structures," by A. Kardara, C. Bucher and M. Shinozuka, 9/22/88, (PB89-174429, A04, MF-A01).

NCEER-88-0030 "Nonnormal Accelerations Due to Yielding in a Primary Structure," by D.C.K. Chen and L.D. Lutes, 9/19/88, (PB89-131437, A04, MF-A01).

NCEER-88-0031 "Design Approaches for Soil-Structure Interaction," by A.S. Veletsos, A.M. Prasad and Y. Tang, 12/30/88, (PB89-174437, A03, MF-A01). This report is available only through NTIS (see address given above).

NCEER-88-0032 "A Re-evaluation of Design Spectra for Seismic Damage Control," by C.J. Turkstra and A.G. Tallin, 11/7/88, (PB89-145221, A05, MF-A01).

NCEER-88-0033 "The Behavior and Design of Noncontact Lap Splices Subjected to Repeated Inelastic Tensile Loading," by V.E. Sagan, P. Gergely and R.N. White, 12/8/88, (PB89-163737, A08, MF-A01).

NCEER-88-0034 "Seismic Response of Pile Foundations," by S.M. Mamoon, P.K. Banerjee and S. Ahmad, 11/1/88, (PB89-145239, A04, MF-A01).

NCEER-88-0035 "Modeling of R/C Building Structures With Flexible Floor Diaphragms (IDARC2)," by A.M. Reinhorn, S.K. Kunnath and N. Panahshahi, 9/7/88, (PB89-207153, A07, MF-A01).

NCEER-88-0036 "Solution of the Dam-Reservoir Interaction Problem Using a Combination of FEM, BEM with Particular Integrals, Modal Analysis, and Substructuring," by C-S. Tsai, G.C. Lee and R.L. Ketter, 12/31/88, (PB89-207146, A04, MF-A01).

NCEER-88-0037 "Optimal Placement of Actuators for Structural Control," by F.Y. Cheng and C.P. Pantelides, 8/15/88, (PB89-162846, A05, MF-A01).

NCEER-88-0038 "Teflon Bearings in Aseismic Base Isolation: Experimental Studies and Mathematical Modeling," by A. Mokha, M.C. Constantinou and A.M. Reinhorn, 12/5/88, (PB89-218457, A10, MF-A01). This report is available only through NTIS (see address given above).

NCEER-88-0039 "Seismic Behavior of Flat Slab High-Rise Buildings in the New York City Area," by P. Weidlinger and M. Ettouney, 10/15/88, (PB90-145681, A04, MF-A01).

NCEER-88-0040 "Evaluation of the Earthquake Resistance of Existing Buildings in New York City," by P. Weidlinger and M. Ettouney, 10/15/88, to be published.

NCEER-88-0041 "Small-Scale Modeling Techniques for Reinforced Concrete Structures Subjected to Seismic Loads," by W. Kim, A. El-Attar and R.N. White, 11/22/88, (PB89-189625, A05, MF-A01).

NCEER-88-0042 "Modeling Strong Ground Motion from Multiple Event Earthquakes," by G.W. Ellis and A.S. Cakmak, 10/15/88, (PB89-174445, A03, MF-A01).

NCEER-88-0043 "Nonstationary Models of Seismic Ground Acceleration," by M. Grigoriu, S.E. Ruiz and E. Rosenblueth, 7/15/88, (PB89-189617, A04, MF-A01).

NCEER-88-0044 "SARCF User's Guide: Seismic Analysis of Reinforced Concrete Frames," by Y.S. Chung, C. Meyer and M. Shinozuka, 11/9/88, (PB89-174452, A08, MF-A01).

NCEER-88-0045 "First Expert Panel Meeting on Disaster Research and Planning," edited by J. Pantelic and J. Stoyle, 9/15/88, (PB89-174460, A05, MF-A01).

NCEER-88-0046 "Preliminary Studies of the Effect of Degrading Infill Walls on the Nonlinear Seismic Response of Steel Frames," by C.Z. Chrysostomou, P. Gergely and J.F. Abel, 12/19/88, (PB89-208383, A05, MF-A01).

NCEER-88-0047 "Reinforced Concrete Frame Component Testing Facility - Design, Construction, Instrumentation and Operation," by S.P. Pessiki, C. Conley, T. Bond, P. Gergely and R.N. White, 12/16/88, (PB89-174478, A04, MF-A01).

NCEER-89-0001 "Effects of Protective Cushion and Soil Compliancy on the Response of Equipment Within a Seismically Excited Building," by J.A. HoLung, 2/16/89, (PB89-207179, A04, MF-A01).

NCEER-89-0002 "Statistical Evaluation of Response Modification Factors for Reinforced Concrete Structures," by H.H-M. Hwang and J-W. Jaw, 2/17/89, (PB89-207187, A05, MF-A01).

NCEER-89-0003 "Hysteretic Columns Under Random Excitation," by G-Q. Cai and Y.K. Lin, 1/9/89, (PB89-196513, A03, MF-A01).

NCEER-89-0004 "Experimental Study of 'Elephant Foot Bulge' Instability of Thin-Walled Metal Tanks," by Z-H. Jia and R.L. Ketter, 2/22/89, (PB89-207195, A03, MF-A01).

NCEER-89-0005 "Experiment on Performance of Buried Pipelines Across San Andreas Fault," by J. Isenberg, E. Richardson and T.D. O'Rourke, 3/10/89, (PB89-218440, A04, MF-A01). This report is available only through NTIS (see address given above).

NCEER-89-0006 "A Knowledge-Based Approach to Structural Design of Earthquake-Resistant Buildings," by M. Subramani, P. Gergely, C.H. Conley, J.F. Abel and A.H. Zaghw, 1/15/89, (PB89-218465, A06, MF-A01).

NCEER-89-0007 "Liquefaction Hazards and Their Effects on Buried Pipelines," by T.D. O'Rourke and P.A. Lane, 2/1/89, (PB89-218481, A09, MF-A01).

NCEER-89-0008 "Fundamentals of System Identification in Structural Dynamics," by H. Imai, C-B. Yun, O. Maruyama and M. Shinozuka, 1/26/89, (PB89-207211, A04, MF-A01).

NCEER-89-0009 "Effects of the 1985 Michoacan Earthquake on Water Systems and Other Buried Lifelines in Mexico," by A.G. Ayala and M.J. O'Rourke, 3/8/89, (PB89-207229, A06, MF-A01).

NCEER-89-R010 "NCEER Bibliography of Earthquake Education Materials," by K.E.K. Ross, Second Revision, 9/1/89, (PB90-125352, A05, MF-A01). This report is replaced by NCEER-92-0018.

NCEER-89-0011 "Inelastic Three-Dimensional Response Analysis of Reinforced Concrete Building Structures (IDARC-3D), Part I - Modeling," by S.K. Kunnath and A.M. Reinhorn, 4/17/89, (PB90-114612, A07, MF-A01). This report is available only through NTIS (see address given above).

NCEER-89-0012 "Recommended Modifications to ATC-14," by C.D. Poland and J.O. Malley, 4/12/89, (PB90-108648, A15, MF-A01).

NCEER-89-0013 "Repair and Strengthening of Beam-to-Column Connections Subjected to Earthquake Loading," by M. Corazao and A.J. Durrani, 2/28/89, (PB90-109885, A06, MF-A01).

NCEER-89-0014 "Program EXKAL2 for Identification of Structural Dynamic Systems," by O. Maruyama, C-B. Yun, M. Hoshiya and M. Shinozuka, 5/19/89, (PB90-109877, A09, MF-A01).

NCEER-89-0015 "Response of Frames With Bolted Semi-Rigid Connections, Part I - Experimental Study and Analytical Predictions," by P.J. DiCorso, A.M. Reinhorn, J.R. Dickerson, J.B. Radziminski and W.L. Harper, 6/1/89, to be published.

NCEER-89-0016 "ARMA Monte Carlo Simulation in Probabilistic Structural Analysis," by P.D. Spanos and M.P. Mignolet, 7/10/89, (PB90-109893, A03, MF-A01).

NCEER-89-P017 "Preliminary Proceedings from the Conference on Disaster Preparedness - The Place of Earthquake Education in Our Schools," Edited by K.E.K. Ross, 6/23/89, (PB90-108606, A03, MF-A01).

NCEER-89-0017 "Proceedings from the Conference on Disaster Preparedness - The Place of Earthquake Education in Our Schools," Edited by K.E.K. Ross, 12/31/89, (PB90-207895, A012, MF-A02). This report is available only through NTIS (see address given above).

NCEER-89-0018 "Multidimensional Models of Hysteretic Material Behavior for Vibration Analysis of Shape Memory Energy Absorbing Devices, by E.J. Graesser and F.A. Cozzarelli, 6/7/89, (PB90-164146, A04, MF-A01).

NCEER-89-0019 "Nonlinear Dynamic Analysis of Three-Dimensional Base Isolated Structures (3D-BASIS)," by S. Nagarajaiah, A.M. Reinhorn and M.C. Constantinou, 8/3/89, (PB90-161936, A06, MF-A01). This report has been replaced by NCEER-93-0011.

NCEER-89-0020 "Structural Control Considering Time-Rate of Control Forces and Control Rate Constraints," by F.Y. Cheng and C.P. Pantelides, 8/3/89, (PB90-120445, A04, MF-A01).

NCEER-89-0021 "Subsurface Conditions of Memphis and Shelby County," by K.W. Ng, T-S. Chang and H-H.M. Hwang, 7/26/89, (PB90-120437, A03, MF-A01).

NCEER-89-0022 "Seismic Wave Propagation Effects on Straight Jointed Buried Pipelines," by K. Elhmadi and M.J. O'Rourke, 8/24/89, (PB90-162322, A10, MF-A02).

NCEER-89-0023 "Workshop on Serviceability Analysis of Water Delivery Systems," edited by M. Grigoriu, 3/6/89, (PB90-127424, A03, MF-A01).

NCEER-89-0024 "Shaking Table Study of a 1/5 Scale Steel Frame Composed of Tapered Members," by K.C. Chang, J.S. Hwang and G.C. Lee, 9/18/89, (PB90-160169, A04, MF-A01).

NCEER-89-0025 "DYNA1D: A Computer Program for Nonlinear Seismic Site Response Analysis - Technical Documentation," by Jean H. Prevost, 9/14/89, (PB90-161944, A07, MF-A01). This report is available only through NTIS (see address given above).

NCEER-89-0026 "1:4 Scale Model Studies of Active Tendon Systems and Active Mass Dampers for Aseismic Protection," by A.M. Reinhorn, T.T. Soong, R.C. Lin, Y.P. Yang, Y. Fukao, H. Abe and M. Nakai, 9/15/89, (PB90-173246, A10, MF-A02). This report is available only through NTIS (see address given above).

NCEER-89-0027 "Scattering of Waves by Inclusions in a Nonhomogeneous Elastic Half Space Solved by Boundary Element Methods," by P.K. Hadley, A. Askar and A.S. Cakmak, 6/15/89, (PB90-145699, A07, MF-A01).

NCEER-89-0028 "Statistical Evaluation of Deflection Amplification Factors for Reinforced Concrete Structures," by H.H.M. Hwang, J-W. Jaw and A.L. Ch'ng, 8/31/89, (PB90-164633, A05, MF-A01).

NCEER-89-0029 "Bedrock Accelerations in Memphis Area Due to Large New Madrid Earthquakes," by H.H.M. Hwang, C.H.S. Chen and G. Yu, 11/7/89, (PB90-162330, A04, MF-A01).

NCEER-89-0030 "Seismic Behavior and Response Sensitivity of Secondary Structural Systems," by Y.Q. Chen and T.T. Soong, 10/23/89, (PB90-164658, A08, MF-A01).

NCEER-89-0031 "Random Vibration and Reliability Analysis of Primary-Secondary Structural Systems," by Y. Ibrahim, M. Grigoriu and T.T. Soong, 11/10/89, (PB90-161951, A04, MF-A01).

NCEER-89-0032 "Proceedings from the Second U.S. - Japan Workshop on Liquefaction, Large Ground Deformation and Their Effects on Lifelines, September 26-29, 1989," Edited by T.D. O'Rourke and M. Hamada, 12/1/89, (PB90-209388, A22, MF-A03).

NCEER-89-0033 "Deterministic Model for Seismic Damage Evaluation of Reinforced Concrete Structures," by J.M. Bracci, A.M. Reinhorn, J.B. Mander and S.K. Kunnath, 9/27/89, (PB91-108803, A06, MF-A01).

NCEER-89-0034 "On the Relation Between Local and Global Damage Indices," by E. DiPasquale and A.S. Cakmak, 8/15/89, (PB90-173865, A05, MF-A01).

NCEER-89-0035 "Cyclic Undrained Behavior of Nonplastic and Low Plasticity Silts," by A.J. Walker and H.E. Stewart, 7/26/89, (PB90-183518, A10, MF-A01).

NCEER-89-0036 "Liquefaction Potential of Surficial Deposits in the City of Buffalo, New York," by M. Budhu, R. Giese and L. Baumgrass, 1/17/89, (PB90-208455, A04, MF-A01).

NCEER-89-0037 "A Deterministic Assessment of Effects of Ground Motion Incoherence," by A.S. Veletsos and Y. Tang, 7/15/89, (PB90-164294, A03, MF-A01).

NCEER-89-0038 "Workshop on Ground Motion Parameters for Seismic Hazard Mapping," July 17-18, 1989, edited by R.V. Whitman, 12/1/89, (PB90-173923, A04, MF-A01).

NCEER-89-0039 "Seismic Effects on Elevated Transit Lines of the New York City Transit Authority," by C.J. Costantino, C.A. Miller and E. Heymsfield, 12/26/89, (PB90-207887, A06, MF-A01).

NCEER-89-0040 "Centrifugal Modeling of Dynamic Soil-Structure Interaction," by K. Weissman, Supervised by J.H. Prevost, 5/10/89, (PB90-207879, A07, MF-A01).

NCEER-89-0041 "Linearized Identification of Buildings With Cores for Seismic Vulnerability Assessment," by I-K. Ho and A.E. Aktan, 11/1/89, (PB90-251943, A07, MF-A01).

NCEER-90-0001 "Geotechnical and Lifeline Aspects of the October 17, 1989 Loma Prieta Earthquake in San Francisco," by T.D. O'Rourke, H.E. Stewart, F.T. Blackburn and T.S. Dickerman, 1/90, (PB90-208596, A05, MF-A01).

NCEER-90-0002 "Nonnormal Secondary Response Due to Yielding in a Primary Structure," by D.C.K. Chen and L.D. Lutes, 2/28/90, (PB90-251976, A07, MF-A01).

NCEER-90-0003 "Earthquake Education Materials for Grades K-12," by K.E.K. Ross, 4/16/90, (PB91-251984, A05, MF-A05). This report has been replaced by NCEER-92-0018.

NCEER-90-0004 "Catalog of Strong Motion Stations in Eastern North America," by R.W. Busby, 4/3/90, (PB90-251984, A05, MF-A01).

NCEER-90-0005 "NCEER Strong-Motion Data Base: A User Manual for the GeoBase Release (Version 1.0 for the Sun3)," by P. Friberg and K. Jacob, 3/31/90 (PB90-258062, A04, MF-A01).

NCEER-90-0006 "Seismic Hazard Along a Crude Oil Pipeline in the Event of an 1811-1812 Type New Madrid Earthquake," by H.H.M. Hwang and C-H.S. Chen, 4/16/90, (PB90-258054, A04, MF-A01).

NCEER-90-0007 "Site-Specific Response Spectra for Memphis Sheahan Pumping Station," by H.H.M. Hwang and C.S. Lee, 5/15/90, (PB91-108811, A05, MF-A01).

NCEER-90-0008 "Pilot Study on Seismic Vulnerability of Crude Oil Transmission Systems," by T. Ariman, R. Dobry, M. Grigoriu, F. Kozin, M. O'Rourke, T. O'Rourke and M. Shinozuka, 5/25/90, (PB91-108837, A06, MF-A01).

NCEER-90-0009 "A Program to Generate Site Dependent Time Histories: EQGEN," by G.W. Ellis, M. Srinivasan and A.S. Cakmak, 1/30/90, (PB91-108829, A04, MF-A01).

NCEER-90-0010 "Active Isolation for Seismic Protection of Operating Rooms," by M.E. Talbott, Supervised by M. Shinozuka, 6/8/9, (PB91-110205, A05, MF-A01).

NCEER-90-0011 "Program LINEARID for Identification of Linear Structural Dynamic Systems," by C-B. Yun and M. Shinozuka, 6/25/90, (PB91-110312, A08, MF-A01).

NCEER-90-0012 "Two-Dimensional Two-Phase Elasto-Plastic Seismic Response of Earth Dams," by A.N. Yiagos, Supervised by J.H. Prevost, 6/20/90, (PB91-110197, A13, MF-A02).

NCEER-90-0013 "Secondary Systems in Base-Isolated Structures: Experimental Investigation, Stochastic Response and Stochastic Sensitivity," by G.D. Manolis, G. Juhn, M.C. Constantinou and A.M. Reinhorn, 7/1/90, (PB91-110320, A08, MF-A01).

NCEER-90-0014 "Seismic Behavior of Lightly-Reinforced Concrete Column and Beam-Column Joint Details," by S.P. Pessiki, C.H. Conley, P. Gergely and R.N. White, 8/22/90, (PB91-108795, A11, MF-A02).

NCEER-90-0015 "Two Hybrid Control Systems for Building Structures Under Strong Earthquakes," by J.N. Yang and A. Danielians, 6/29/90, (PB91-125393, A04, MF-A01).

NCEER-90-0016 "Instantaneous Optimal Control with Acceleration and Velocity Feedback," by J.N. Yang and Z. Li, 6/29/90, (PB91-125401, A03, MF-A01).

NCEER-90-0017 "Reconnaissance Report on the Northern Iran Earthquake of June 21, 1990," by M. Mehrain, 10/4/90, (PB91-125377, A03, MF-A01).

NCEER-90-0018 "Evaluation of Liquefaction Potential in Memphis and Shelby County," by T.S. Chang, P.S. Tang, C.S. Lee and H. Hwang, 8/10/90, (PB91-125427, A09, MF-A01).

NCEER-90-0019 "Experimental and Analytical Study of a Combined Sliding Disc Bearing and Helical Steel Spring Isolation System," by M.C. Constantinou, A.S. Mokha and A.M. Reinhorn, 10/4/90, (PB91-125385, A06, MF-A01). This report is available only through NTIS (see address given above).

NCEER-90-0020 "Experimental Study and Analytical Prediction of Earthquake Response of a Sliding Isolation System with a Spherical Surface," by A.S. Mokha, M.C. Constantinou and A.M. Reinhorn, 10/11/90, (PB91-125419, A05, MF-A01).

NCEER-90-0021 "Dynamic Interaction Factors for Floating Pile Groups," by G. Gazetas, K. Fan, A. Kaynia and E. Kausel, 9/10/90, (PB91-170381, A05, MF-A01).

NCEER-90-0022 "Evaluation of Seismic Damage Indices for Reinforced Concrete Structures," by S. Rodriguez-Gomez and A.S. Cakmak, 9/30/90, PB91-171322, A06, MF-A01).

NCEER-90-0023 "Study of Site Response at a Selected Memphis Site," by H. Desai, S. Ahmad, E.S. Gazetas and M.R. Oh, 10/11/90, (PB91-196857, A03, MF-A01).

NCEER-90-0024 "A User's Guide to Strongmo: Version 1.0 of NCEER's Strong-Motion Data Access Tool for PCs and Terminals," by P.A. Friberg and C.A.T. Susch, 11/15/90, (PB91-171272, A03, MF-A01).

NCEER-90-0025 "A Three-Dimensional Analytical Study of Spatial Variability of Seismic Ground Motions," by L-L. Hong and A.H.-S. Ang, 10/30/90, (PB91-170399, A09, MF-A01).

NCEER-90-0026 "MUMOID User's Guide - A Program for the Identification of Modal Parameters," by S. Rodriguez-Gomez and E. DiPasquale, 9/30/90, (PB91-171298, A04, MF-A01).

NCEER-90-0027 "SARCF-II User's Guide - Seismic Analysis of Reinforced Concrete Frames," by S. Rodriguez-Gomez, Y.S. Chung and C. Meyer, 9/30/90, (PB91-171280, A05, MF-A01).

NCEER-90-0028 "Viscous Dampers: Testing, Modeling and Application in Vibration and Seismic Isolation," by N. Makris and M.C. Constantinou, 12/20/90 (PB91-190561, A06, MF-A01).

NCEER-90-0029 "Soil Effects on Earthquake Ground Motions in the Memphis Area," by H. Hwang, C.S. Lee, K.W. Ng and T.S. Chang, 8/2/90, (PB91-190751, A05, MF-A01).

NCEER-91-0001 "Proceedings from the Third Japan-U.S. Workshop on Earthquake Resistant Design of Lifeline Facilities and Countermeasures for Soil Liquefaction, December 17-19, 1990," edited by T.D. O'Rourke and M. Hamada, 2/1/91, (PB91-179259, A99, MF-A04).

NCEER-91-0002 "Physical Space Solutions of Non-Proportionally Damped Systems," by M. Tong, Z. Liang and G.C. Lee, 1/15/91, (PB91-179242, A04, MF-A01).

NCEER-91-0003 "Seismic Response of Single Piles and Pile Groups," by K. Fan and G. Gazetas, 1/10/91, (PB92-174994, A04, MF-A01).

NCEER-91-0004 "Damping of Structures: Part 1 - Theory of Complex Damping," by Z. Liang and G. Lee, 10/10/91, (PB92-197235, A12, MF-A03).

NCEER-91-0005 "3D-BASIS - Nonlinear Dynamic Analysis of Three Dimensional Base Isolated Structures: Part II," by S. Nagarajaiah, A.M. Reinhorn and M.C. Constantinou, 2/28/91, (PB91-190553, A07, MF-A01). This report has been replaced by NCEER-93-0011.

NCEER-91-0006 "A Multidimensional Hysteretic Model for Plasticity Deforming Metals in Energy Absorbing Devices," by E.J. Graesser and F.A. Cozzarelli, 4/9/91, (PB92-108364, A04, MF-A01).

NCEER-91-0007 "A Framework for Customizable Knowledge-Based Expert Systems with an Application to a KBES for Evaluating the Seismic Resistance of Existing Buildings," by E.G. Ibarra-Anaya and S.J. Fenves, 4/9/91, (PB91-210930, A08, MF-A01).

NCEER-91-0008 "Nonlinear Analysis of Steel Frames with Semi-Rigid Connections Using the Capacity Spectrum Method," by G.G. Deierlein, S-H. Hsieh, Y-J. Shen and J.F. Abel, 7/2/91, (PB92-113828, A05, MF-A01).

NCEER-91-0009 "Earthquake Education Materials for Grades K-12," by K.E.K. Ross, 4/30/91, (PB91-212142, A06, MF-A01). This report has been replaced by NCEER-92-0018.

NCEER-91-0010 "Phase Wave Velocities and Displacement Phase Differences in a Harmonically Oscillating Pile," by N. Makris and G. Gazetas, 7/8/91, (PB92-108356, A04, MF-A01).

NCEER-91-0011 "Dynamic Characteristics of a Full-Size Five-Story Steel Structure and a 2/5 Scale Model," by K.C. Chang, G.C. Yao, G.C. Lee, D.S. Hao and Y.C. Yeh," 7/2/91, (PB93-116648, A06, MF-A02).

NCEER-91-0012 "Seismic Response of a 2/5 Scale Steel Structure with Added Viscoelastic Dampers," by K.C. Chang, T.T. Soong, S-T. Oh and M.L. Lai, 5/17/91, (PB92-110816, A05, MF-A01).

NCEER-91-0013 "Earthquake Response of Retaining Walls; Full-Scale Testing and Computational Modeling," by S. Alampalli and A-W.M. Elgamal, 6/20/91, to be published.

NCEER-91-0014 "3D-BASIS-M: Nonlinear Dynamic Analysis of Multiple Building Base Isolated Structures," by P.C. Tsopelas, S. Nagarajaiah, M.C. Constantinou and A.M. Reinhorn, 5/28/91, (PB92-113885, A09, MF-A02).

NCEER-91-0015 "Evaluation of SEAOC Design Requirements for Sliding Isolated Structures," by D. Theodossiou and M.C. Constantinou, 6/10/91, (PB92-114602, A11, MF-A03).

NCEER-91-0016 "Closed-Loop Modal Testing of a 27-Story Reinforced Concrete Flat Plate-Core Building," by H.R. Somaprasad, T. Toksoy, H. Yoshiyuki and A.E. Aktan, 7/15/91, (PB92-129980, A07, MF-A02).

NCEER-91-0017 "Shake Table Test of a 1/6 Scale Two-Story Lightly Reinforced Concrete Building," by A.G. El-Attar, R.N. White and P. Gergely, 2/28/91, (PB92-222447, A06, MF-A02).

NCEER-91-0018 "Shake Table Test of a 1/8 Scale Three-Story Lightly Reinforced Concrete Building," by A.G. El-Attar, R.N. White and P. Gergely, 2/28/91, (PB93-116630, A08, MF-A02).

NCEER-91-0019 "Transfer Functions for Rigid Rectangular Foundations," by A.S. Veletsos, A.M. Prasad and W.H. Wu, 7/31/91, to be published.

NCEER-91-0020 "Hybrid Control of Seismic-Excited Nonlinear and Inelastic Structural Systems," by J.N. Yang, Z. Li and A. Danielians, 8/1/91, (PB92-143171, A06, MF-A02).

NCEER-91-0021 "The NCEER-91 Earthquake Catalog: Improved Intensity-Based Magnitudes and Recurrence Relations for U.S. Earthquakes East of New Madrid," by L. Seeber and J.G. Armbruster, 8/28/91, (PB92-176742, A06, MF-A02).

NCEER-91-0022 "Proceedings from the Implementation of Earthquake Planning and Education in Schools: The Need for Change - The Roles of the Changemakers," by K.E.K. Ross and F. Winslow, 7/23/91, (PB92-129998, A12, MF-A03).

NCEER-91-0023 "A Study of Reliability-Based Criteria for Seismic Design of Reinforced Concrete Frame Buildings," by H.H.M. Hwang and H-M. Hsu, 8/10/91, (PB92-140235, A09, MF-A02).

NCEER-91-0024 "Experimental Verification of a Number of Structural System Identification Algorithms," by R.G. Ghanem, H. Gavin and M. Shinozuka, 9/18/91, (PB92-176577, A18, MF-A04).

NCEER-91-0025 "Probabilistic Evaluation of Liquefaction Potential," by H.H.M. Hwang and C.S. Lee," 11/25/91, (PB92-143429, A05, MF-A01).

NCEER-91-0026 "Instantaneous Optimal Control for Linear, Nonlinear and Hysteretic Structures - Stable Controllers," by J.N. Yang and Z. Li, 11/15/91, (PB92-163807, A04, MF-A01).

NCEER-91-0027 "Experimental and Theoretical Study of a Sliding Isolation System for Bridges," by M.C. Constantinou, A. Kartoum, A.M. Reinhorn and P. Bradford, 11/15/91, (PB92-176973, A10, MF-A03).

NCEER-92-0001 "Case Studies of Liquefaction and Lifeline Performance During Past Earthquakes, Volume 1: Japanese Case Studies," Edited by M. Hamada and T. O'Rourke, 2/17/92, (PB92-197243, A18, MF-A04).

NCEER-92-0002 "Case Studies of Liquefaction and Lifeline Performance During Past Earthquakes, Volume 2: United States Case Studies," Edited by T. O'Rourke and M. Hamada, 2/17/92, (PB92-197250, A20, MF-A04).

NCEER-92-0003 "Issues in Earthquake Education," Edited by K. Ross, 2/3/92, (PB92-222389, A07, MF-A02).

NCEER-92-0004 "Proceedings from the First U.S. - Japan Workshop on Earthquake Protective Systems for Bridges," Edited by I.G. Buckle, 2/4/92, (PB94-142239, A99, MF-A06).

NCEER-92-0005 "Seismic Ground Motion from a Haskell-Type Source in a Multiple-Layered Half-Space," A.P. Theoharis, G. Deodatis and M. Shinozuka, 1/2/92, to be published.

NCEER-92-0006 "Proceedings from the Site Effects Workshop," Edited by R. Whitman, 2/29/92, (PB92-197201, A04, MF-A01).

NCEER-92-0007 "Engineering Evaluation of Permanent Ground Deformations Due to Seismically-Induced Liquefaction," by M.H. Baziar, R. Dobry and A-W.M. Elgamal, 3/24/92, (PB92-222421, A13, MF-A03).

NCEER-92-0008 "A Procedure for the Seismic Evaluation of Buildings in the Central and Eastern United States," by C.D. Poland and J.O. Malley, 4/2/92, (PB92-222439, A20, MF-A04).

NCEER-92-0009 "Experimental and Analytical Study of a Hybrid Isolation System Using Friction Controllable Sliding Bearings," by M.Q. Feng, S. Fujii and M. Shinozuka, 5/15/92, (PB93-150282, A06, MF-A02).

NCEER-92-0010 "Seismic Resistance of Slab-Column Connections in Existing Non-Ductile Flat-Plate Buildings," by A.J. Durrani and Y. Du, 5/18/92, (PB93-116812, A06, MF-A02).

NCEER-92-0011 "The Hysteretic and Dynamic Behavior of Brick Masonry Walls Upgraded by Ferrocement Coatings Under Cyclic Loading and Strong Simulated Ground Motion," by H. Lee and S.P. Prawel, 5/11/92, to be published.

NCEER-92-0012 "Study of Wire Rope Systems for Seismic Protection of Equipment in Buildings," by G.F. Demetriades, M.C. Constantinou and A.M. Reinhorn, 5/20/92, (PB93-116655, A08, MF-A02).

NCEER-92-0013 "Shape Memory Structural Dampers: Material Properties, Design and Seismic Testing," by P.R. Witting and F.A. Cozzarelli, 5/26/92, (PB93-116663, A05, MF-A01).

NCEER-92-0014 "Longitudinal Permanent Ground Deformation Effects on Buried Continuous Pipelines," by M.J. O'Rourke, and C. Nordberg, 6/15/92, (PB93-116671, A08, MF-A02).

NCEER-92-0015 "A Simulation Method for Stationary Gaussian Random Functions Based on the Sampling Theorem," by M. Grigoriu and S. Balopoulou, 6/11/92, (PB93-127496, A05, MF-A01).

NCEER-92-0016 "Gravity-Load-Designed Reinforced Concrete Buildings: Seismic Evaluation of Existing Construction and Detailing Strategies for Improved Seismic Resistance," by G.W. Hoffmann, S.K. Kunnath, A.M. Reinhorn and J.B. Mander, 7/15/92, (PB94-142007, A08, MF-A02).

NCEER-92-0017 "Observations on Water System and Pipeline Performance in the Limón Area of Costa Rica Due to the April 22, 1991 Earthquake," by M. O'Rourke and D. Ballantyne, 6/30/92, (PB93-126811, A06, MF-A02).

NCEER-92-0018 "Fourth Edition of Earthquake Education Materials for Grades K-12," Edited by K.E.K. Ross, 8/10/92, (PB93-114023, A07, MF-A02).

NCEER-92-0019 "Proceedings from the Fourth Japan-U.S. Workshop on Earthquake Resistant Design of Lifeline Facilities and Countermeasures for Soil Liquefaction," Edited by M. Hamada and T.D. O'Rourke, 8/12/92, (PB93-163939, A99, MF-E11).

NCEER-92-0020 "Active Bracing System: A Full Scale Implementation of Active Control," by A.M. Reinhorn, T.T. Soong, R.C. Lin, M.A. Riley, Y.P. Wang, S. Aizawa and M. Higashino, 8/14/92, (PB93-127512, A06, MF-A02).

NCEER-92-0021 "Empirical Analysis of Horizontal Ground Displacement Generated by Liquefaction-Induced Lateral Spreads," by S.F. Bartlett and T.L. Youd, 8/17/92, (PB93-188241, A06, MF-A02).

NCEER-92-0022 "IDARC Version 3.0: Inelastic Damage Analysis of Reinforced Concrete Structures," by S.K. Kunnath, A.M. Reinhorn and R.F. Lobo, 8/31/92, (PB93-227502, A07, MF-A02).

NCEER-92-0023 "A Semi-Empirical Analysis of Strong-Motion Peaks in Terms of Seismic Source, Propagation Path and Local Site Conditions, by M. Kamiyama, M.J. O'Rourke and R. Flores-Berrones, 9/9/92, (PB93-150266, A08, MF-A02).

NCEER-92-0024 "Seismic Behavior of Reinforced Concrete Frame Structures with Nonductile Details, Part I: Summary of Experimental Findings of Full Scale Beam-Column Joint Tests," by A. Beres, R.N. White and P. Gergely, 9/30/92, (PB93-227783, A05, MF-A01).

NCEER-92-0025 "Experimental Results of Repaired and Retrofitted Beam-Column Joint Tests in Lightly Reinforced Concrete Frame Buildings," by A. Beres, S. El-Borgi, R.N. White and P. Gergely, 10/29/92, (PB93-227791, A05, MF-A01).

NCEER-92-0026 "A Generalization of Optimal Control Theory: Linear and Nonlinear Structures," by J.N. Yang, Z. Li and S. Vongchavalitkul, 11/2/92, (PB93-188621, A05, MF-A01).

NCEER-92-0027 "Seismic Resistance of Reinforced Concrete Frame Structures Designed Only for Gravity Loads: Part I - Design and Properties of a One-Third Scale Model Structure," by J.M. Bracci, A.M. Reinhorn and J.B. Mander, 12/1/92, (PB94-104502, A08, MF-A02).

NCEER-92-0028 "Seismic Resistance of Reinforced Concrete Frame Structures Designed Only for Gravity Loads: Part II - Experimental Performance of Subassemblages," by L.E. Aycardi, J.B. Mander and A.M. Reinhorn, 12/1/92, (PB94-104510, A08, MF-A02).

NCEER-92-0029 "Seismic Resistance of Reinforced Concrete Frame Structures Designed Only for Gravity Loads: Part III - Experimental Performance and Analytical Study of a Structural Model," by J.M. Bracci, A.M. Reinhorn and J.B. Mander, 12/1/92, (PB93-227528, A09, MF-A01).

NCEER-92-0030 "Evaluation of Seismic Retrofit of Reinforced Concrete Frame Structures: Part I - Experimental Performance of Retrofitted Subassemblages," by D. Choudhuri, J.B. Mander and A.M. Reinhorn, 12/8/92, (PB93-198307, A07, MF-A02).

NCEER-92-0031 "Evaluation of Seismic Retrofit of Reinforced Concrete Frame Structures: Part II - Experimental Performance and Analytical Study of a Retrofitted Structural Model," by J.M. Bracci, A.M. Reinhorn and J.B. Mander, 12/8/92, (PB93-198315, A09, MF-A03).

NCEER-92-0032 "Experimental and Analytical Investigation of Seismic Response of Structures with Supplemental Fluid Viscous Dampers," by M.C. Constantinou and M.D. Symans, 12/21/92, (PB93-191435, A10, MF-A03). This report is available only through NTIS (see address given above).

NCEER-92-0033 "Reconnaissance Report on the Cairo, Egypt Earthquake of October 12, 1992," by M. Khater, 12/23/92, (PB93-188621, A03, MF-A01).

NCEER-92-0034 "Low-Level Dynamic Characteristics of Four Tall Flat-Plate Buildings in New York City," by H. Gavin, S. Yuan, J. Grossman, E. Pekelis and K. Jacob, 12/28/92, (PB93-188217, A07, MF-A02).

NCEER-93-0001 "An Experimental Study on the Seismic Performance of Brick-Infilled Steel Frames With and Without Retrofit," by J.B. Mander, B. Nair, K. Wojtkowski and J. Ma, 1/29/93, (PB93-227510, A07, MF-A02).

NCEER-93-0002 "Social Accounting for Disaster Preparedness and Recovery Planning," by S. Cole, E. Pantoja and V. Razak, 2/22/93, (PB94-142114, A12, MF-A03).

NCEER-93-0003 "Assessment of 1991 NEHRP Provisions for Nonstructural Components and Recommended Revisions," by T.T. Soong, G. Chen, Z. Wu, R-H. Zhang and M. Grigoriu, 3/1/93, (PB93-188639, A06, MF-A02).

NCEER-93-0004 "Evaluation of Static and Response Spectrum Analysis Procedures of SEAOC/UBC for Seismic Isolated Structures," by C.W. Winters and M.C. Constantinou, 3/23/93, (PB93-198299, A10, MF-A03).

NCEER-93-0005 "Earthquakes in the Northeast - Are We Ignoring the Hazard? A Workshop on Earthquake Science and Safety for Educators," edited by K.E.K. Ross, 4/2/93, (PB94-103066, A09, MF-A02).

NCEER-93-0006 "Inelastic Response of Reinforced Concrete Structures with Viscoelastic Braces," by R.F. Lobo, J.M. Bracci, K.L. Shen, A.M. Reinhorn and T.T. Soong, 4/5/93, (PB93-227486, A05, MF-A02).

NCEER-93-0007 "Seismic Testing of Installation Methods for Computers and Data Processing Equipment," by K. Kosar, T.T. Soong, K.L. Shen, J.A. HoLung and Y.K. Lin, 4/12/93, (PB93-198299, A07, MF-A02).

NCEER-93-0008 "Retrofit of Reinforced Concrete Frames Using Added Dampers," by A. Reinhorn, M. Constantinou and C. Li, to be published.

NCEER-93-0009 "Seismic Behavior and Design Guidelines for Steel Frame Structures with Added Viscoelastic Dampers," by K.C. Chang, M.L. Lai, T.T. Soong, D.S. Hao and Y.C. Yeh, 5/1/93, (PB94-141959, A07, MF-A02).

NCEER-93-0010 "Seismic Performance of Shear-Critical Reinforced Concrete Bridge Piers," by J.B. Mander, S.M. Waheed, M.T.A. Chaudhary and S.S. Chen, 5/12/93, (PB93-227494, A08, MF-A02).

NCEER-93-0011 "3D-BASIS-TABS: Computer Program for Nonlinear Dynamic Analysis of Three Dimensional Base Isolated Structures," by S. Nagarajaiah, C. Li, A.M. Reinhorn and M.C. Constantinou, 8/2/93, (PB94-141819, A09, MF-A02).

NCEER-93-0012 "Effects of Hydrocarbon Spills from an Oil Pipeline Break on Ground Water," by O.J. Helweg and H.H.M. Hwang, 8/3/93, (PB94-141942, A06, MF-A02).

NCEER-93-0013 "Simplified Procedures for Seismic Design of Nonstructural Components and Assessment of Current Code Provisions," by M.P. Singh, L.E. Suarez, E.E. Matheu and G.O. Maldonado, 8/4/93, (PB94-141827, A09, MF-A02).

NCEER-93-0014 "An Energy Approach to Seismic Analysis and Design of Secondary Systems," by G. Chen and T.T. Soong, 8/6/93, (PB94-142767, A11, MF-A03).

NCEER-93-0015 "Proceedings from School Sites: Becoming Prepared for Earthquakes - Commemorating the Third Anniversary of the Loma Prieta Earthquake," Edited by F.E. Winslow and K.E.K. Ross, 8/16/93, (PB94-154275, A16, MF-A02).

NCEER-93-0016 "Reconnaissance Report of Damage to Historic Monuments in Cairo, Egypt Following the October 12, 1992 Dahshur Earthquake," by D. Sykora, D. Look, G. Croci, E. Karaesmen and E. Karaesmen, 8/19/93, (PB94-142221, A08, MF-A02).

NCEER-93-0017 "The Island of Guam Earthquake of August 8, 1993," by S.W. Swan and S.K. Harris, 9/30/93, (PB94-141843, A04, MF-A01).

NCEER-93-0018 "Engineering Aspects of the October 12, 1992 Egyptian Earthquake," by A.W. Elgamal, M. Amer, K. Adalier and A. Abul-Fadl, 10/7/93, (PB94-141983, A05, MF-A01).

NCEER-93-0019 "Development of an Earthquake Motion Simulator and its Application in Dynamic Centrifuge Testing," by I. Krstelj, Supervised by J.H. Prevost, 10/23/93, (PB94-181773, A-10, MF-A03).

NCEER-93-0020 "NCEER-Taisei Corporation Research Program on Sliding Seismic Isolation Systems for Bridges: Experimental and Analytical Study of a Friction Pendulum System (FPS)," by M.C. Constantinou, P. Tsopelas, Y-S. Kim and S. Okamoto, 11/1/93, (PB94-142775, A08, MF-A02).

NCEER-93-0021 "Finite Element Modeling of Elastomeric Seismic Isolation Bearings," by L.J. Billings, Supervised by R. Shepherd, 11/8/93, to be published.

NCEER-93-0022 "Seismic Vulnerability of Equipment in Critical Facilities: Life-Safety and Operational Consequences," by K. Porter, G.S. Johnson, M.M. Zadeh, C. Scawthorn and S. Eder, 11/24/93, (PB94-181765, A16, MF-A03).

NCEER-93-0023 "Hokkaido Nansei-oki, Japan Earthquake of July 12, 1993, by P.I. Yanev and C.R. Scawthorn, 12/23/93, (PB94-181500, A07, MF-A01).

NCEER-94-0001 "An Evaluation of Seismic Serviceability of Water Supply Networks with Application to the San Francisco Auxiliary Water Supply System," by I. Markov, Supervised by M. Grigoriu and T. O'Rourke, 1/21/94, (PB94-204013, A07, MF-A02).

NCEER-94-0002 "NCEER-Taisei Corporation Research Program on Sliding Seismic Isolation Systems for Bridges: Experimental and Analytical Study of Systems Consisting of Sliding Bearings, Rubber Restoring Force Devices and Fluid Dampers," Volumes I and II, by P. Tsopelas, S. Okamoto, M.C. Constantinou, D. Ozaki and S. Fujii, 2/4/94, (PB94-181740, A09, MF-A02 and PB94-181757, A12, MF-A03).

NCEER-94-0003 "A Markov Model for Local and Global Damage Indices in Seismic Analysis," by S. Rahman and M. Grigoriu, 2/18/94, (PB94-206000, A12, MF-A03).

NCEER-94-0004 "Proceedings from the NCEER Workshop on Seismic Response of Masonry Infills," edited by D.P. Abrams, 3/1/94, (PB94-180783, A07, MF-A02).

NCEER-94-0005 "The Northridge, California Earthquake of January 17, 1994: General Reconnaissance Report," edited by J.D. Goltz, 3/11/94, (PB193943, A10, MF-A03).

NCEER-94-0006 "Seismic Energy Based Fatigue Damage Analysis of Bridge Columns: Part I - Evaluation of Seismic Capacity," by G.A. Chang and J.B. Mander, 3/14/94, (PB94-219185, A11, MF-A03).

NCEER-94-0007 "Seismic Isolation of Multi-Story Frame Structures Using Spherical Sliding Isolation Systems," by T.M. Al-Hussaini, V.A. Zayas and M.C. Constantinou, 3/17/94, (PB193745, A09, MF-A02).

NCEER-94-0008 "The Northridge, California Earthquake of January 17, 1994: Performance of Highway Bridges," edited by I.G. Buckle, 3/24/94, (PB94-193851, A06, MF-A02).

NCEER-94-0009 "Proceedings of the Third U.S.-Japan Workshop on Earthquake Protective Systems for Bridges," edited by I.G. Buckle and I. Friedland, 3/31/94, (PB94-195815, A99, MF-A06).

NCEER-94-0010 "3D-BASIS-ME: Computer Program for Nonlinear Dynamic Analysis of Seismically Isolated Single and Multiple Structures and Liquid Storage Tanks," by P.C. Tsopelas, M.C. Constantinou and A.M. Reinhorn, 4/12/94, (PB94-204922, A09, MF-A02).

NCEER-94-0011 "The Northridge, California Earthquake of January 17, 1994: Performance of Gas Transmission Pipelines," by T.D. O'Rourke and M.C. Palmer, 5/16/94, (PB94-204989, A05, MF-A01).

NCEER-94-0012 "Feasibility Study of Replacement Procedures and Earthquake Performance Related to Gas Transmission Pipelines," by T.D. O'Rourke and M.C. Palmer, 5/25/94, (PB94-206638, A09, MF-A02).

NCEER-94-0013 "Seismic Energy Based Fatigue Damage Analysis of Bridge Columns: Part II - Evaluation of Seismic Demand," by G.A. Chang and J.B. Mander, 6/1/94, (PB95-18106, A08, MF-A02).

NCEER-94-0014 "NCEER-Taisei Corporation Research Program on Sliding Seismic Isolation Systems for Bridges: Experimental and Analytical Study of a System Consisting of Sliding Bearings and Fluid Restoring Force/Damping Devices," by P. Tsopelas and M.C. Constantinou, 6/13/94, (PB94-219144, A10, MF-A03).

NCEER-94-0015 "Generation of Hazard-Consistent Fragility Curves for Seismic Loss Estimation Studies," by H. Hwang and J-R. Huo, 6/14/94, (PB95-181996, A09, MF-A02).

NCEER-94-0016 "Seismic Study of Building Frames with Added Energy-Absorbing Devices," by W.S. Pong, C.S. Tsai and G.C. Lee, 6/20/94, (PB94-219136, A10, A03).

NCEER-94-0017 "Sliding Mode Control for Seismic-Excited Linear and Nonlinear Civil Engineering Structures," by J. Yang, J. Wu, A. Agrawal and Z. Li, 6/21/94, (PB95-138483, A06, MF-A02).

NCEER-94-0018 "3D-BASIS-TABS Version 2.0: Computer Program for Nonlinear Dynamic Analysis of Three Dimensional Base Isolated Structures," by A.M. Reinhorn, S. Nagarajaiah, M.C. Constantinou, P. Tsopelas and R. Li, 6/22/94, (PB95-182176, A08, MF-A02).

NCEER-94-0019 "Proceedings of the International Workshop on Civil Infrastructure Systems: Application of Intelligent Systems and Advanced Materials on Bridge Systems," Edited by G.C. Lee and K.C. Chang, 7/18/94, (PB95-252474, A20, MF-A04).

NCEER-94-0020 "Study of Seismic Isolation Systems for Computer Floors," by V. Lambrou and M.C. Constantinou, 7/19/94, (PB95-138533, A10, MF-A03).

NCEER-94-0021 "Proceedings of the U.S.-Italian Workshop on Guidelines for Seismic Evaluation and Rehabilitation of Unreinforced Masonry Buildings," Edited by D.P. Abrams and G.M. Calvi, 7/20/94, (PB95-138749, A13, MF-A03).

NCEER-94-0022 "NCEER-Taisei Corporation Research Program on Sliding Seismic Isolation Systems for Bridges: Experimental and Analytical Study of a System Consisting of Lubricated PTFE Sliding Bearings and Mild Steel Dampers," by P. Tsopelas and M.C. Constantinou, 7/22/94, (PB95-182184, A08, MF-A02).

NCEER-94-0023 "Development of Reliability-Based Design Criteria for Buildings Under Seismic Load," by Y.K. Wen, H. Hwang and M. Shinozuka, 8/1/94, (PB95-211934, A08, MF-A02).

NCEER-94-0024 "Experimental Verification of Acceleration Feedback Control Strategies for an Active Tendon System," by S.J. Dyke, B.F. Spencer, Jr., P. Quast, M.K. Sain, D.C. Kaspari, Jr. and T.T. Soong, 8/29/94, (PB95-212320, A05, MF-A01).

NCEER-94-0025 "Seismic Retrofitting Manual for Highway Bridges," Edited by I.G. Buckle and I.F. Friedland, published by the Federal Highway Administration (PB95-212676, A15, MF-A03).

NCEER-94-0026 "Proceedings from the Fifth U.S.-Japan Workshop on Earthquake Resistant Design of Lifeline Facilities and Countermeasures Against Soil Liquefaction," Edited by T.D. O'Rourke and M. Hamada, 11/7/94, (PB95-220802, A99, MF-E08).

NCEER-95-0001 "Experimental and Analytical Investigation of Seismic Retrofit of Structures with Supplemental Damping: Part 1 - Fluid Viscous Damping Devices," by A.M. Reinhorn, C. Li and M.C. Constantinou, 1/3/95, (PB95-266599, A09, MF-A02).

NCEER-95-0002 "Experimental and Analytical Study of Low-Cycle Fatigue Behavior of Semi-Rigid Top-And-Seat Angle Connections," by G. Pekcan, J.B. Mander and S.S. Chen, 1/5/95, (PB95-220042, A07, MF-A02).

NCEER-95-0003 "NCEER-ATC Joint Study on Fragility of Buildings," by T. Anagnos, C. Rojahn and A.S. Kiremidjian, 1/20/95, (PB95-220026, A06, MF-A02).

NCEER-95-0004 "Nonlinear Control Algorithms for Peak Response Reduction," by Z. Wu, T.T. Soong, V. Gattulli and R.C. Lin, 2/16/95, (PB95-220349, A05, MF-A01).

NCEER-95-0005 "Pipeline Replacement Feasibility Study: A Methodology for Minimizing Seismic and Corrosion Risks to Underground Natural Gas Pipelines," by R.T. Eguchi, H.A. Seligson and D.G. Honegger, 3/2/95, (PB95-252326, A06, MF-A02).

NCEER-95-0006 "Evaluation of Seismic Performance of an 11-Story Frame Building During the 1994 Northridge Earthquake," by F. Naeim, R. DiSulio, K. Benuska, A. Reinhorn and C. Li, to be published.

NCEER-95-0007 "Prioritization of Bridges for Seismic Retrofitting," by N. Basöz and A.S. Kiremidjian, 4/24/95, (PB95-252300, A08, MF-A02).

NCEER-95-0008 "Method for Developing Motion Damage Relationships for Reinforced Concrete Frames," by A. Singhal and A.S. Kiremidjian, 5/11/95, (PB95-266607, A06, MF-A02).

NCEER-95-0009 "Experimental and Analytical Investigation of Seismic Retrofit of Structures with Supplemental Damping: Part II - Friction Devices," by C. Li and A.M. Reinhorn, 7/6/95, (PB96-128087, A11, MF-A03).

NCEER-95-0010 "Experimental Performance and Analytical Study of a Non-Ductile Reinforced Concrete Frame Structure Retrofitted with Elastomeric Spring Dampers," by G. Pekcan, J.B. Mander and S.S. Chen, 7/14/95, (PB96-137161, A08, MF-A02).

NCEER-95-0011 "Development and Experimental Study of Semi-Active Fluid Damping Devices for Seismic Protection of Structures," by M.D. Symans and M.C. Constantinou, 8/3/95, (PB96-136940, A23, MF-A04).

NCEER-95-0012 "Real-Time Structural Parameter Modification (RSPM): Development of Innervated Structures," by Z. Liang, M. Tong and G.C. Lee, 4/11/95, (PB96-137153, A06, MF-A01).

NCEER-95-0013 "Experimental and Analytical Investigation of Seismic Retrofit of Structures with Supplemental Damping: Part III - Viscous Damping Walls," by A.M. Reinhorn and C. Li, 10/1/95, (PB96-176409, A11, MF-A03).

NCEER-95-0014 "Seismic Fragility Analysis of Equipment and Structures in a Memphis Electric Substation," by J-R. Huo and H.H.M. Hwang, (PB96-128087, A09, MF-A02), 8/10/95.

NCEER-95-0015 "The Hanshin-Awaji Earthquake of January 17, 1995: Performance of Lifelines," Edited by M. Shinozuka, 11/3/95, (PB96-176383, A15, MF-A03).

NCEER-95-0016 "Highway Culvert Performance During Earthquakes," by T.L. Youd and C.J. Beckman, available as NCEER-96-0015.

NCEER-95-0017 "The Hanshin-Awaji Earthquake of January 17, 1995: Performance of Highway Bridges," Edited by I.G. Buckle, 12/1/95, to be published.

NCEER-95-0018 "Modeling of Masonry Infill Panels for Structural Analysis," by A.M. Reinhorn, A. Madan, R.E. Valles, Y. Reichmann and J.B. Mander, 12/8/95.

NCEER-95-0019 "Optimal Polynomial Control for Linear and Nonlinear Structures," by A.K. Agrawal and J.N. Yang, 12/11/95, (PB96-168737, A07, MF-A02).

NCEER-95-0020 "Retrofit of Non-Ductile Reinforced Concrete Frames Using Friction Dampers," by R.S. Rao, P. Gergely and R.N. White, 12/22/95, (PB97-133508, A10, MF-A02).

NCEER-95-0021 "Parametric Results for Seismic Response of Pile-Supported Bridge Bents," by G. Mylonakis, A. Nikolaou and G. Gazetas, 12/22/95, (PB97-100242, A12, MF-A03).

NCEER-95-0022 "Kinematic Bending Moments in Seismically Stressed Piles," by A. Nikolaou, G. Mylonakis and G. Gazetas, 12/23/95.

NCEER-96-0001 "Dynamic Response of Unreinforced Masonry Buildings with Flexible Diaphragms," by A.C. Costley and D.P. Abrams," 10/10/96.

NCEER-96-0002 "State of the Art Review: Foundations and Retaining Structures," by I. Po Lam, to be published.

NCEER-96-0003 "Ductility of Rectangular Reinforced Concrete Bridge Columns with Moderate Confinement," by N. Wehbe, M. Saiidi, D. Sanders and B. Douglas, 11/7/96, (PB97-133557, A06, MF-A02).

NCEER-96-0004 "Proceedings of the Long-Span Bridge Seismic Research Workshop," edited by I.G. Buckle and I.M. Friedland, to be published.

NCEER-96-0005 "Establish Representative Pier Types for Comprehensive Study: Eastern United States," by J. Kulicki and Z. Prucz, 5/28/96, (PB98-119217, A07, MF-A02).

NCEER-96-0006 "Establish Representative Pier Types for Comprehensive Study: Western United States," by R. Imbsen, R.A. Schamber and T.A. Osterkamp, 5/28/96, (PB98-118607, A07, MF-A02).

NCEER-96-0007 "Nonlinear Control Techniques for Dynamical Systems with Uncertain Parameters," by R.G. Ghanem and M.I. Bujakov, 5/27/96, (PB97-100259, A17, MF-A03).

NCEER-96-0008 "Seismic Evaluation of a 30-Year Old Non-Ductile Highway Bridge Pier and Its Retrofit," by J.B. Mander, B. Mahmoodzadegan, S. Bhadra and S.S. Chen, 5/31/96.

NCEER-96-0009 "Seismic Performance of a Model Reinforced Concrete Bridge Pier Before and After Retrofit," by J.B. Mander, J.H. Kim and C.A. Ligozio, 5/31/96.

NCEER-96-0010 "IDARC2D Version 4.0: A Computer Program for the Inelastic Damage Analysis of Buildings," by R.E. Valles, A.M. Reinhorn, S.K. Kunnath, C. Li and A. Madan, 6/3/96, (PB97-100234, A17, MF-A03).

NCEER-96-0011 "Estimation of the Economic Impact of Multiple Lifeline Disruption: Memphis Light, Gas and Water Division Case Study," by S.E. Chang, H.A. Seligson and R.T. Eguchi, 8/16/96, (PB97-133490, A11, MF-A03).

NCEER-96-0012 "Proceedings from the Sixth Japan-U.S. Workshop on Earthquake Resistant Design of Lifeline Facilities and Countermeasures Against Soil Liquefaction, Edited by M. Hamada and T. O'Rourke, 9/11/96, (PB97-133581, A99, MF-A06).

NCEER-96-0013 "Chemical Hazards, Mitigation and Preparedness in Areas of High Seismic Risk: A Methodology for Estimating the Risk of Post-Earthquake Hazardous Materials Release," by H.A. Seligson, R.T. Eguchi, K.J. Tierney and K. Richmond, 11/7/96.

NCEER-96-0014 "Response of Steel Bridge Bearings to Reversed Cyclic Loading," by J.B. Mander, D-K. Kim, S.S. Chen and G.J. Premus, 11/13/96, (PB97-140735, A12, MF-A03).

NCEER-96-0015 "Highway Culvert Performance During Past Earthquakes," by T.L. Youd and C.J. Beckman, 11/25/96, (PB97-133532, A06, MF-A01).

NCEER-97-0001 "Evaluation, Prevention and Mitigation of Pounding Effects in Building Structures," by R.E. Valles and A.M. Reinhorn, 2/20/97, (PB97-159552, A14, MF-A03).

NCEER-97-0002 "Seismic Design Criteria for Bridges and Other Highway Structures," by C. Rojahn, R. Mayes, D.G. Anderson, J. Clark, J.H. Hom, R.V. Nutt and M.J. O'Rourke, 4/30/97, (PB97-194658, A06, MF-A03).

NCEER-97-0003 "Proceedings of the U.S.-Italian Workshop on Seismic Evaluation and Retrofit," Edited by D.P. Abrams and G.M. Calvi, 3/19/97, (PB97-194666, A13, MF-A03).

NCEER-97-0004 "Investigation of Seismic Response of Buildings with Linear and Nonlinear Fluid Viscous Dampers," by A.A. Seleemah and M.C. Constantinou, 5/21/97, (PB98-109002, A15, MF-A03).

NCEER-97-0005 "Proceedings of the Workshop on Earthquake Engineering Frontiers in Transportation Facilities," edited by G.C. Lee and I.M. Friedland, 8/29/97, (PB98-128911, A25, MR-A04).

NCEER-97-0006 "Cumulative Seismic Damage of Reinforced Concrete Bridge Piers," by S.K. Kunnath, A. El-Bahy, A. Taylor and W. Stone, 9/2/97, (PB98-108814, A11, MF-A03).

NCEER-97-0007 "Structural Details to Accommodate Seismic Movements of Highway Bridges and Retaining Walls," by R.A. Imbsen, R.A. Schamber, E. Thorkildsen, A. Kartoum, B.T. Martin, T.N. Rosser and J.M. Kulicki, 9/3/97.

NCEER-97-0008 "A Method for Earthquake Motion-Damage Relationships with Application to Reinforced Concrete Frames," by A. Singhal and A.S. Kiremidjian, 9/10/97, (PB98-108988, A13, MF-A03).

NCEER-97-0009 "Seismic Analysis and Design of Bridge Abutments Considering Sliding and Rotation," by K. Fishman and R. Richards, Jr., 9/15/97, (PB98-108897, A06, MF-A02).

NCEER-97-0010 "Proceedings of the FHWA/NCEER Workshop on the National Representation of Seismic Ground Motion for New and Existing Highway Facilities," edited by I.M. Friedland, M.S. Power and R.L. Mayes, 9/22/97.

NCEER-97-0011 "Seismic Analysis for Design or Retrofit of Gravity Bridge Abutments," by K.L. Fishman, R. Richards, Jr. and R.C. Divito, 10/2/97, (PB98-128937, A08, MF-A02).

NCEER-97-0012 "Evaluation of Simplified Methods of Analysis for Yielding Structures," by P. Tsopelas, M.C. Constantinou, C.A. Kircher and A.S. Whittaker, 10/31/97, (PB98-128929, A10, MF-A03).

NCEER-97-0013 "Seismic Design of Bridge Columns Based on Control and Repairability of Damage," by C-T. Cheng and J.B. Mander, 12/8/97.

NCEER-97-0014 "Seismic Resistance of Bridge Piers Based on Damage Avoidance Design," by J.B. Mander and C-T. Cheng, 12/10/97.

NCEER-97-0015 "Seismic Response of Nominally Symmetric Systems with Strength Uncertainty," by S. Balopoulou and M. Grigoriu, 12/23/97, (PB98-153422, A11, MF-A03).

NCEER-97-0016 "Evaluation of Seismic Retrofit Methods for Reinforced Concrete Bridge Columns," by T.J. Wipf, F.W. Klaiber and F.M. Russo, 12/28/97.

NCEER-97-0017 "Seismic Fragility of Existing Conventional Reinforced Concrete Highway Bridges," by C.L. Mullen and A.S. Cakmak, 12/30/97, (PB98-153406, A08, MF-A02).

NCEER-97-0018 "Loss Asssessment of Memphis Buildings," edited by D.P. Abrams and M. Shinozuka, 12/31/97.

NCEER-97-0019 "Seismic Evaluation of Frames with Infill Walls Using Quasi-static Experiments," by K.M. Mosalam, R.N. White and P. Gergely, 12/31/97, (PB98-153455, A07, MF-A02).

NCEER-97-0020 "Seismic Evaluation of Frames with Infill Walls Using Pseudo-dynamic Experiments," by K.M. Mosalam, R.N. White and P. Gergely, 12/31/97.

NCEER-97-0021 "Computational Strategies for Frames with Infill Walls: Discrete and Smeared Crack Analyses and Seismic Fragility," by K.M. Mosalam, R.N. White and P. Gergely, 12/31/97, (PB98-153414, A10, MF-A02).

NCEER-97-0022 "Proceedings of the NCEER Workshop on Evaluation of Liquefaction Resistance of Soils," edited by T.L. Youd and I.M. Idriss, 12/31/97.

MCEER-98-0001 "Extraction of Nonlinear Hysteretic Properties of Seismically Isolated Bridges from Quick-Release Field Tests," by Q. Chen, B.M. Douglas, E.M. Maragakis and I.G. Buckle, 5/26/98.

MCEER-98-0002 "Methodologies for Evaluating the Importance of Highway Bridges," by A. Thomas, S. Eshenaur and J. Kulicki, 5/29/98.

MCEER-98-0003 "Capacity Design of Bridge Piers and the Analysis of Overstrength," by J.B. Mander, A. Dutta and P. Goel, 6/1/98.

MCEER-98-0004 "Evaluation of Bridge Damage Data from the Loma Prieta and Northridge, California Earthquakes," by N. Basoz and A. Kiremidjian, 6/2/98.

MCEER-98-0005 "Screening Guide for Rapid Assessment of Liquefaction Hazard at Highway Bridge Sites,"by T. L. Youd, 6/16/98.

MCEER-98-0006 "Structural Steel and Steel/Concrete Interface Details for Bridges," by P. Ritchie, N. Kauhl and J. Kulicki, 7/13/98.

MCEER-98-0007 "Capacity Design and Fatigue Analysis of Confined Concrete Columns," by A. Dutta and J.B. Mander, 7/14/98.

MCEER-98-0008 "Proceedings of the Workshop on Performance Criteria for Telecommunication Services Under Earthquake Conditions," edited by A.J. Schiff, 7/15/98.

MCEER-98-0009 "Fatigue Analysis of Unconfined Concrete Columns," by J.B. Mander, A. Dutta and J.H. Kim, 9/12/98.

MCEER-98-0010 "Centrifuge Modeling of Cyclic Lateral Response of Pile-Cap Systems and Seat-Type Abutments in Dry Sands," by A.D. Gadre and R. Dobry, 10/2/98.

MCEER-98-0011 "IDARC-BRIDGE: A Computational Platform for Seismic Damage Assessment of Bridge Structures," by A.M. Reinhorn, V. Simeonov, G. Mylonakis and Y. Reichman, 10/2/98.

MCEER-98-0012 "Experimental Investigation of the Dynamic Response of Two Bridges Before and After Retrofitting with Elastomeric Bearings," by D.A. Wendichansky, S.S. Chen and J.B. Mander, 10/2/98.

MCEER-98-0013 "Design Procedures for Hinge Restrainers and Hinge Sear Width for Multiple-Frame Bridges," by R. Des Roches and G.L. Fenves, 11/3/98.

MCEER-98-0014 "Response Modification Factors for Seismically Isolated Bridges," by M.C. Constantinou and J.K. Quarshie, 11/3/98.

MCEER-98-0015 "Proceedings of the U.S.-Italy Workshop on Seismic Protective Systems for Bridges," edited by I.M. Friedland and M.C. Constantinou, 11/3/98.

MCEER-98-0016 "Appropriate Seismic Reliability for Critical Equipment Systems: Recommendations Based on Regional Analysis of Financial and Life Loss," by K. Porter, C. Scawthorn, C. Taylor and N. Blais, 11/10/98.

MCEER-98-0017 "Proceedings of the U.S. Japan Joint Seminar on Civil Infrastructure Systems Research," edited by M. Shinozuka and A. Rose, 11/12/98.

MCEER-98-0018 "Modeling of Pile Footings and Drilled Shafts for Seismic Design," by I. PoLam, M. Kapuskar and D. Chaudhuri, 12/21/98.

MCEER-99-0001 "Seismic Evaluation of a Masonry Infilled Reinforced Concrete Frame by Pseudodynamic Testing," by S.G. Buonopane and R.N. White, 2/16/99.

MCEER-99-0002 "Response History Analysis of Structures with Seismic Isolation and Energy Dissipation Systems: Verification Examples for Program SAP2000," by J. Scheller and M.C. Constantinou, 2/22/99.

MCEER-99-0003 "Experimental Study on the Seismic Design and Retrofit of Bridge Columns Including Axial Load Effects," by A. Dutta, T. Kokorina and J.B. Mander, 2/22/99.

MCEER-99-0004 "Experimental Study of Bridge Elastomeric and Other Isolation and Energy Dissipation Systems with Emphasis on Uplift Prevention and High Velocity Near-source Seismic Excitation," by A. Kasalanati and M. C. Constantinou, 2/26/99.

MCEER-99-0005 "Truss Modeling of Reinforced Concrete Shear-flexure Behavior," by J.H. Kim and J.B. Mander, 3/8/99.